STRESS STRAIN BEHAVIOUR OF A COHESIVE SOIL DEPOSITED UNDER WATER

by

Kenneth Been

Balliol College, Oxford

A thesis submitted to the University of Oxford

for the degree of

Doctor of Philosophy

Trinity Term 1980

Department of Engineering Science

Parks Road

Oxford

CONTENTS

Table of Contents 1

List of Tables, Figures and Plates 5

Acknowledgements 8

Abstract 9

CHAPTER 1 INTRODUCTION 10

1.1 Suspensions of Soil in Water 13

1.2 Consolidation of Soil 14

1.3 The Transition from a Suspension to a Soil 14

1.4 A Review of Previous Work 16

1.4.1 Settling of Solid Suspensions in Water 17

1.4.2 Soil Consolidation Theory 18

1.4.3 Experimental Studies 19

1.5 A Method of Studying Effective Stress Behaviour in Soils with High Void Ratios 21

1.6 Outline of This Thesis 23

CHAPTER 2 EQUIPMENT 24

2.1 X-ray Density Measurement 26

2.1.1 Background 26

2.1.2 Some Previous Use of X- and Gamma-rays for Density Measurement 30

2.1.3 An X-ray and Scintillation Counter Technique 32

2.1.4 X-ray Source 35

2.1.5 Scintillation Counter 37

Crystal and Photomultiplier 39

Counter Electronics 40

Choice of Operating Conditions 45

2.1.6 Geometry and Collimation of the System 56

2.1.7 The Laboratory 62

2.1.8 Calibration 64

2.1.9 Performance 70

Variation of Radiation Energy and Intensity 70

Choice of Time Constant 78
Accuracy 82
2.2 Pressure Measurement 86
2.2.1 Requirements of the Method 86
Pore Water Pressure 86
Total Stress 87
2.2.2 Pressure Transducers 87
2.2.3 Pore Water Pressure Transducer Housing 88
2.2.4 Total Stress on the Column Base 92
2.2.5 Total Stress on the Side of the Column 92
2.2.6 Electronics 94
2.2.7 Calibration 94
2.2.8 Accuracy 95
2.2.9 Use of Standpipes 95

CHAPTER 3 EXPERIMENTAL PROCEDURES 96

3.1 Equipment Preparation 98
3.1.1 Column Assembly 98
3.1.2 X-ray Apparatus 98
3.1.3 Pressure Transducers 99
3.1.4 Standpipes 99
3.2 Soil Preparation 99
3.2.1 Batch Weighing 101
3.2.2 Stirring Procedure 101
3.3 An Experiment 102
3.4 Data Collection and Validation 103
3.5 Experiments Performed 104

CHAPTER 4 EXPERIMENTAL OBSERVATIONS 106

4.1 Suspension Settling Behaviour 109
4.2 Density Structures During Settling 111
4.3 Segregation of Particles During Settling 117
4.4 Stress Distribution in a Settling Sediment 118
4.5 Intermediate Phase and Soil Behaviour 122
4.5.1 Surface Settlement 127
4.5.2 Density 130
4.5.3 Pore Water Pressure 137
4.5.4 Effective Stress Development 144

4.5.5 Permeability 151
4.6 Total Stress Measurement 159
4.7 Horizontal Stress 161

CHAPTER 5 A QUALITATIVE DISCUSSION OF THE EXPERIMENTAL RESULTS 163

5.1 Phases of Settling and Consolidation 165
5.1.1 Suspensions 165
5.1.2 Intermediate Phase 167
5.1.3 Soil 168
5.2 A Comparison with other Studies 169

CHAPTER 6 SOME EXISTING THEORIES OF SEDIMENTATION AND CONSOLIDATION 171

6.1 Hindered Settling 173
6.2 Soil Consolidation 177
6.2.1 The Governing Equation 177
6.2.2 A Self Weight Consolidation Solution 179
The Linear Soil Model 179
Solution for Dredged Fill, Surface Drain 181
6.3 Comparison Between Hindered Settling Theory and Consolidation Theory 184
6.4 Application to the Present Experimental Work 187
6.4.1 Settling of Suspensions 187
6.4.2 Consolidation Theory 188

CHAPTER 7 COMPARISON OF A MODIFIED LINEAR CONSOLIDATION THEORY WITH EXPERIMENTAL RESULTS 191

7.1 Derivation and Solution of the Modified Consolidation Equations 193
7.1.1 Void Ratio Distribution 197
7.1.2 Pore Water Pressure Distribution 203
7.1.3 Degree of Settlement 206
7.1.4 Transformation to Space Coordinates 207
7.2 Determination of the Coefficient of Consolidation 209
7.2.1 Choice of Soil Parameters and Initial Conditions 210

Initial Conditions, e_i and z_1 210
Parameters, e_o and Beta 212
Void Ratio / Effective Stress Relationships 214
7.2.2 C_f from Settlement Curves 216
7.2.3 C_f from Pore Pressure Distributions 225
7.2.4 Calculation of C_f from Soil Properties 228
7.2.5 Comparison of C_f found by Three Methods 230
7.3 Density Profiles Compared 232
7.4 Discussion 240

CHAPTER 8 IN CONCLUSION 242

8.1 Conclusions 243
8.1.1 Experimental Techniques and Procedures 243
8.1.2 Stages of Soil Sedimentation 243
8.1.3 Theoretical Considerations 246
8.2 Contribution of This Thesis 247
8.3 Application of the Results to Practical Problems 248
8.4 Recommendations for Further Work 249

References 253

LIST OF TABLES, FIGURES AND PLATES

Figure	1.1	Stages of Soil Formation	15
	1.2	Diagram of Settling Experiment	22
Figure	2.1	Mass Absorption Coefficients	29
	2.2	Energy Distribution of X-rays from Source	36
	2.3	Scintillation Detector	38
	2.4	Spectral Response of "Super S-11" Photocathode	41
	2.5	Gain Curve of Photomultiplier	42
	2.6	Diagram of Counting Installation	44
	2.7	Energy Distribution of X-rays Reaching Detector	47
	2.8	Pulse Energy Distribution Reaching Photocathode	49
	2.9	Proportion of Pulses with Higher than a Certain Energy	50
	2.10	Photocathode Charge vs Apparent Energy Dissipation	52
	2.11	Photocathode Threshold vs EHT for Discriminator	54
	2.12	Calculated Count Rate vs EHT Curve	55
	2.13	Layout of Density Apparatus	57
	2.14	Collimation Geometry of System	58
Plate	2.15	Collimators	59
Plate	2.16	X-ray Density Apparatus	61
Plate	2.17	X-ray Beam at Detector (Prints from Radiographs)	63
Figure	2.18	Density Calibration Curves	67
	2.19	Count Rate vs EHT. X-ray Voltage Varying	71
	2.20	Count Rate vs EHT. Effect of Filter on Beam	72
	2.21	Count Rate vs EHT. Discriminator Threshold Varying	73
	2.22	Count Rate vs X-ray Voltage	75
	2.23	Count Rate vs Anode Current	76
	2.24	Photomultiplier Saturation at High Count Rates	79
	2.25	Error in Count Rate, 95% Confidence Limit	81
	2.26	Typical Recorded Density Profile	83
	2.27	Pore Water Pressure Transducer Housings	89
Plate	2.28	Pore Water Pressure Transducer and Housing	90
Figure	2.29	Total Stress Transducer Mountings	93

Plate	3.1	Lower Portion of Column and Instrumentation	100
Table	3.1	Experiment Details	105
Figure	4.1	Particle Size Distribution. River Parrett Silt	108
	4.2	Height of Suspension Water Interface. Expts 1-5	110
	4.3	Density Profiles. Experiment 6	112
	4.4	Height / Time Plot. Experiment 6	113
	4.5	Density Profiles. Experiment 7	114
	4.6	Height / Time Plot. Experiment 7	115
	4.7	Density Profiles. Experiment 8	116
	4.8	Particle Size Distribution at End of Experiment 7	119
	4.9	Particle Size Distribution at End of Experiment 8	120
	4.10	Particle Size Distribution at end of Experiment 9	121
	4.11 - 13	Density and Stress Distribution. Experiment 7	123 - 5
	4.14	Initial Density and Stress Distribution. Expt 8	126
	4.15	Surface Settlement. Expts 10 - 15	128
	4.16	Surface Settlement (Log Time). Expts 10 - 15	129
	4.17 - 22	Density Profiles. Expts 10 - 15	131 - 6
	4.23 - 28	Pore Water Pressure. Expts 10 - 15	138 - 43
	4.29 - 34	Void Ratio / Effective Stress. Expts 10 - 15	145 - 50
	4.35 - 40	Permeability / Void Ratio. Expts 10 - 15	153 - 8
	4.41	Total Stress on Column Base.	160
	4.42	Horizontal Stress at 300 mm Height	162
Figure	6.1	Typical Kynch Plot of Constant Concentration Lines	176
	6.2	Dredged Fill, Boundary Conditions	182
Figure	7.1	Effective Stress / Void Ratio Relationship	195
	7.2	Permeability / Void Ratio Relationship	196
	7.3	Isochrones of Void Ratio	198
	7.4	Boundary Conditions Solution Must Satisfy	200
	7.5	Definition of the Modified Problem	200
	7.6	Isochrones of Void Ratio, $z_o = 1.5\ z_1$	202
	7.7	Modified Excess Pore Pressures	204
	7.8	Isochrones of Pore Pressure, $z_o = 1.5\ z_1$	205
	7.9	Degree of Surface Settlement, $z_o = 1.5\ z_1$	208
Table	7.1	Experimental Data for Calculations	211

Figure	7.10	Soil Parameter Trends	213
	7.11	Assumed Final Effective Stress / Void Ratio Relationships	215
	7.12 - 17	Settlement Curves. Expts 10 - 15	217 - 22
Table	7.2	Coefficient of Consolidation from Settlement Curves	223
Table	7.3	Coefficient of Consolidation from Pore Pressures	223
Figure	7.18	Permeability, Back Analysed from Settlement C_f	224
	7.19 - 20	Normalised Excess Pore Pressure Isochrones. Expts 11 and 15	226 - 7
Table	7.4	Calculated Coefficient of Consolidation	229
Figure	7.21	Comparison of Coefficients of Consolidation	231
	7.22 - 27	Comparison of Density Profiles. Expts 10 - 15	234 - 39
Figure	8.1	The Intermediate Phase and Soil	245
	8.2	Constant Rate of Sedimentation Device	250

ACKNOWLEDGEMENTS

My sincere thanks are due to Dr. G.C. Sills, who first interested me in this topic, for her supervision and guidance throughout this study. Nothing would have been possible without her.

The Rhodes Trust provided the generous financial assistance which made my stay in Oxford possible and enjoyable.

Dr. R. Parker, of the Institute of Oceanographic Sciences, provided valuable advice early in the study, showed interest all along and lent some important items of equipment.

Help from the staff and technicians of the Engineering Laboratory was always forthcoming. I am especially indebted to members of the Soil Mechanics group, in particular;

Mr. R. Sawala who made most of the experimental apparatus

Mr. S. Oldham who looked after the electronics

Dr. G. Austin and Dr. K. Lee for their advice and help throughout on matters both large and small.

Finally, I must mention Fiona who has been a very understanding companion these last three years, and who also did most of the typing.

ABSTRACT

Stress Strain Behaviour of a Cohesive Soil Deposited under Water.

Kenneth Been

Balliol College

A thesis submitted to the University of Oxford for the degree of Doctor of Philosophy.

Trinity Term 1980

A dilute suspension of soil particles in water will normally flocculate and settle under gravity to form a bed of consolidating soil. The essential difference between the suspension and the soil is that effective stresses exist in the soil. This thesis is concerned with the effective stress behaviour during the sedimentation and consolidation processes.

Chapters two and three are a description of the equipment and experimental procedures used to determine void ratio changes, pore pressures and effective stresses during this soil formation process. The density measuring technique developed, using an X-ray source and a scintillation counter, is described in some detail. An experiment consists of monitoring the sedimentation, from an initially uniform suspension, of an inorganic clayey silt in a 102 mm I.D. column.

Experimental results are presented and discussed in the next two chapters. Some novel aspects of stress/strain behaviour (in one-dimensional consolidation) are revealed. In particular an intermediate zone is identified, which has properties between those of a suspension and a soil in the traditional sense. This zone does have effective stresses, but the effective stress/void ratio relationship is not unique.

Theoretical consideration of settling suspensions and soil consolidation is covered in chapter six, forming an introduction to the next chapter, where a large strain soil consolidation theory is modified and applied to the intermediate zone. Differences between the theory and experimental results largely reflect the inaccuracies resulting from the simplifying assumptions necessary to keep the mathematics simple. The expulsion of pore water, rather than soil compressibility, is the major factor in determining consolidation behaviour of the intermediate phase.

Finally, some recommendations are made as to how to continue the study and on applications to real problems such as dredging, pollution and land reclamation.

CHAPTER 1. INTRODUCTION

1.1 Suspensions of Soil in Water 13

1.2 Consolidation of Soil 14

1.3 The Transition from a Suspension to a Soil 14

1.4 A Review of Previous Work 16

1.4.1 Settling of Solid Suspensions in Water 17

1.4.2 Soil Consolidation Theory 18

1.4.3 Experimental Studies 19

1.5 A Method of Studying Effective Stress Behaviour in Soils with High Void Ratios 21

1.6 Outline of This Thesis 23

CHAPTER 1. INTRODUCTION

In some of his early work on consolidation, Terzaghi considered the behaviour of a mass of soil grains shaken up with water and allowed to settle. Subsequently, Terzaghi and other engineers have devoted their attention to the soil formed after the sedimentation process is complete and the soil is sufficiently strong as an engineering material. There is thus lack of knowledge amongst geotechnical engineers about the sedimentation process itself and the early stages of natural consolidation of soils deposited under water in this way. This thesis is a study of sedimentation and soil formation in a natural silt in order to gain a fundamental understanding of the process and the behaviour of soil at very low stresses.

In addition to fulfilling the need for an understanding of soil behaviour, the study has a number of direct applications in the modern world. Dredging harbours and shipping routes is an expensive operation but probably occurs more frequently than necessary. Echo-sounders respond to both the density and acoustic velocity gradients so that an echo-sounder survey could show the seabed as the top of a suspension which may be relatively dilute. This is unlikely to be a navigational hazard until considerable consolidation and strength increase has taken place and dredging of such watery material is inefficient. Land reclamation of areas under waste dredged material or mine tailings is becoming increasingly necessary for industrial and building purposes. Better understanding of the soil formation process could be of benefit to both dredging and land recovery technology.

Large scale sediment movement and deposition in estuaries, lakes

and offshore is of particular importance for environmental reasons. Chemical and radioactive pollutants borne by the sediment particles are deposited as the suspension settles. There is evidence that chemical conditions in the settled sediment quickly change and cause some pollutants to go into solution in the pore fluid rather than remaining on the mineral grains. The fluid is expelled during consolidation and the pollutant released back into circulation.

In this chapter the phases of soil formation are described and previous work on the subject is reviewed briefly. The final two sections outline the method and scope of the present study.

1.1 SUSPENSIONS OF SOIL IN WATER

A suspension may be considered as a mixture of soil particles in water where the dilution is such that the soil particles are widely spaced. The particles are supported by the fluid as they settle so that the pressure in the water phase is given by the total weight of the mixture. In soil mechanics terminology the pore water pressure is equal to the total stress and there are no effective stresses.

Stokes' law describes the idealised behaviour of a single particle by equating the fluid drag force to the gravitational force on the particle at the terminal settling velocity. In real suspensions, however, there is considerable particle interaction which affects the settling velocity but not the equality of water pressure and total stress.

Flocculation occurs in most natural soil suspensions and is very important in determining the suspension properties. (Flocs are clusters of particles plus enclosed water formed by chemical and electrostatic forces amongst particles and water.) In a dispersed suspension each solid particle settles at a velocity depending mainly on its size and density and settling behaviour shows segregation of particle sizes by differential settling velocities. In contrast, each floc consists of a variety of particle sizes so that larger particles can be trapped in a cluster with smaller ones and settle at similar velocities in flocculated suspensions. Environmental conditions such as ion concentrations (e.g. salinity), organic matter, mineral composition and shear rates all have an effect on flocculation and therefore the properties of a suspension.

1.2 CONSOLIDATION OF SOIL

A saturated soil is a matrix of soil particles with water filling the voids. Soil behaviour is that of a frictional material and is governed by effective stresses. Consolidation is a time dependent process of the water flowing out of the soil matrix and the soil properties changing as a result.

Settling of a soil suspension in water and consolidation of a soil are therefore similar processes in that they are both the movement of mineral grains and water relative to each other. The essential difference between settling and consolidation is the existence of effective stresses in soils. There is generally a unique virgin consolidation line for each soil which describes the relationship of the effective stress to the void ratio, but clearly there is no equivalent property of a suspension.

1.3 THE TRANSITION FROM A SUSPENSION TO A SOIL

A dilute suspension of soil, depicted in fig 1.1(a), if left to settle under gravity will after some time become a settled bed of soil (fig 1.1(c)). Soon after the initial state flocs will form and start to settle forming a boundary at the top of the dispersion between slightly murky water and soil flocs. (This interface will not occur in dispersed soil suspensions.) At the base of the column, settling brings the flocs close together and one may expect a soil to be formed as the particles come into contact. Because of interparticle forces and water layers around particles and flocs, however, the process of soil formation is more complex than this.

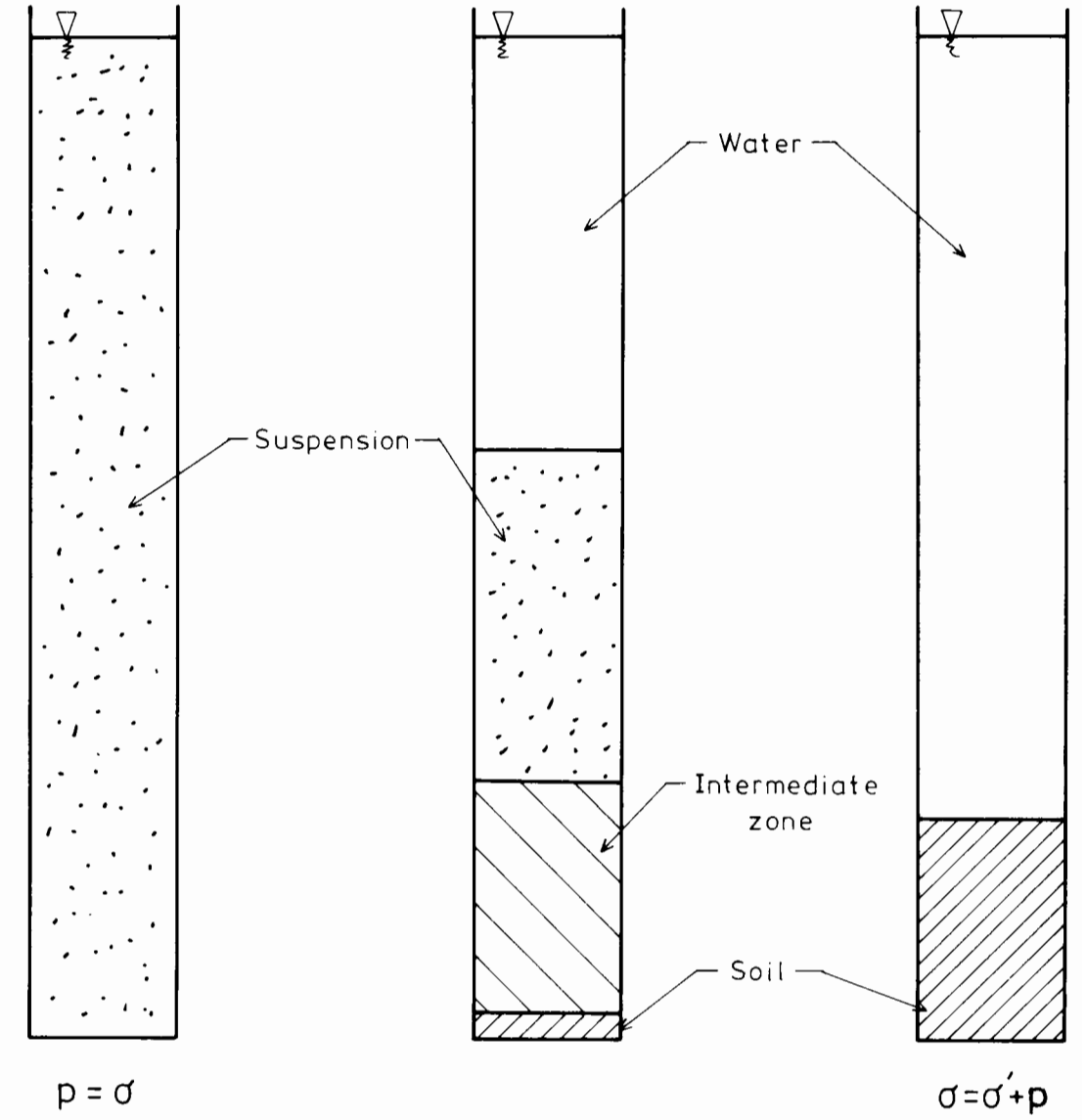


Fig 1.1. Stages of Soil Formation.

Effective stresses must develop before the mud can be called a soil, which means the mineral grains must be close and form some structure for the soil mass to behave as a frictional material. Each particle or floc will be surrounded by a boundary layer of water while in suspension which keeps the grains well apart. Before the mineral particles can become dense enough to be a soil, certain chemical and electrostatic forces between particles and flocs must be overcome and relatively large volumes of water have to be expelled. This water has to flow upwards (assuming no base drainage)through the soil forming above it, further affecting the rate of soil formation.

There will therefore be an intermediate phase as shown in fig 1.1(b) between the settled soil and the settling suspension. This intermediate region is where the mineral grains undergo a transition from a random suspension to a more ordered soil matrix, and changes in floc structure occur. During this transition the behaviour changes from being dominated by the water and water films around the particles to that of a soil, and the mud will not exhibit all the properties, particularly effective stress behaviour, of either a soil or a suspension.

1.4 A REVIEW OF PREVIOUS WORK

Published work on sedimentation and properties of recently deposited soils is divided on a theoretical basis between settling of suspensions and consolidation of soils, although some chemical engineers and sedimentologists have made attempts to explain "hindered settling" and "settling in compression" without consideration of effective stresses. There is also some purely experimental observation of very soft soils.

1.4.1 Settling of Solid Suspensions in Water

Several investigations have been carried out on the settling behaviour in a concentrated suspension based on Stokes' law, with the best agreement of experiments with equations of the form used by Richardson and Zaki (1954). Working with uniform spheres greater than 100 microns (fine sand size) they suggested a settling rate given by

$$v = u_{st} n^r \qquad (1.1)$$

where v = velocity of settling dispersion

u_{st} = Stokes' velocity (velocity at low concentration)

n = porosity of the suspension

r = a coefficient, approximately 4.65

The assumptions inherent in this type of analysis are a gross over simplification for a typical natural soil with large variations in particle shapes and sizes and complex flocculation behaviour. Michaels and Bolger (1962) in a study on flocculated kaolin suspensions, extended the Richardson and Zaki equation using flocs as the basic flow units. Floc volume concentration and the attractive forces between flocs determine the shear strength or viscosity of the suspension which is an important part of their analysis. Good agreement with experimental results was obtained.

The first step away from this traditional approach to settling was by Kynch (1952). Assuming that the speed of fall of particles in a suspension is determined by the local particle density only, his theory determines the settling process entirely from the continuity equations of the solid and liquid phases. This theory of so called hindered

settling is examined in more detail in chapter 6.

Hindered settling theory is clearly valid only if the concentration is such that flocs are not in contact. Tory and Shannon (1965) recognised that mechanical stress transmitted by particle contacts accounts for the slower settling rates encountered in "settling in compression", but continue to use Kynch's theory combined with empirical relationships to examine an extensive series of tests on calcium carbonate slurries settling in compression.

McRoberts and Nixon (1976) were the first in Geotechnical practice to investigate hindered settling theory. Relaxing Kynch's assumption of equi-sized particles on the basis that no segregation of particle sizes occurs at hindered settling concentrations, they modified Kynch's theory accordingly and combined it with the Richardson and Zaki equation (1.1). A comparison between the theory and observed settling modes was made for two natural silts and a fine sand using measurements of the suspension water interface. No attempt was made at using consolidation theory or stress measurement.

1.4.2 Soil Consolidation Theory

Terzaghi's theory of one-dimensional soil consolidation cannot be applied to a soft clay consolidating under its own weight. Large strains, stresses due to self-weight and variations in soil compressibility and permeability must be taken into account, as they have been by Gibson, England and Hussey (1967) in deriving a governing differential equation for one-dimensional consolidation.

Solutions of the Gibson, England and Hussey equations have been found for several cases by Lee (1979). In particular Lee has found analytic solutions (for a soil with linear effective stress/void ratio and permeability/void ratio relationships) taking account of the self-weight of the soil grains. These solutions differ from most numerical solutions for 'thick' strata and a layer increasing in thickness with time in that the weight of the soil is implicit in the theory rather than being approximated numerically. In chapter 6 this work is examined in more detail and it is modified for comparison with experimental results in chapter 7.

1.4.3 Experimental Studies

Several people have made field and laboratory observations of the properties of recently deposited mud.

Einsele, Overbeck, Schwarz and Unsold (1974) performed a study of different aspects of the mechanical behaviour of cohesive sediments which would be of interest to the sedimentologist but not necessarily the civil engineer. Their work did, however, include consolidation tests and measurement of shear strengths, moisture contents, pore pressures, erosion and slope stability followed by a brief discussion of the inapplicability of conventional soil mechanics theory to their very soft muds.

Owen (1970) reported a laboratory study of the formation of mud beds from suspensions in saline water and the subsequent consolidation and properties of the settled mud. Measurements were taken of the bed thickness at frequent intervals, shear strengths of the final mud and, when possible, density and shear strengths at certain

positions in the bed. Tests started with different water salinities, concentrations of suspension and heights of water column. His conclusions were empirical and no theoretical analysis was attempted.

In a report commissioned by the National Ports Council, Bishop and Vaughan (1972) review the engineering aspects of drainage and consolidation of fine-grained soils, particularly maintenance dredging spoil. This report discusses the problem in general terms drawing on the theory for soft normally consolidated soils to make recommendations, particularly about methods of accelerating consolidation. The object of their test program was to obtain basic data on engineering properties of a typical plastic clay derived from maintenance dredging and to obtain comparative data for the same material after treatment with a flocculant. Differences in behaviour of the treated and untreated material were not considered of engineering significance and the benefits of treatment with a flocculant were restricted to the initial sedimentation phase.

Field data from many normally consolidated strata, including recently deposited sediments, is collated and presented by Skempton (1970). Compression curves are drawn for overburden pressures as low as 1 kN/m^2 and it is shown that the void ratio of a normally consolidated stratum at a given overburden pressure depends on the nature and amount of clay minerals as indicated by the liquid limit of the soil.

A field study of fine-sediment behaviour in estuaries has been taking place since 1970 at The Institute of Oceanographic Sciences at Taunton, Kirby and Parker (1977) and Parker and Kirby (1977). Measurements are predominantly of turbidity and density profiles along with tidal data and current velocities, tracing the evolution of mobile

suspensions into static suspensions and their subsequent consolidation or erosion and redispersion.

1.5 A METHOD OF STUDYING EFFECTIVE STRESS BEHAVIOUR IN SOILS WITH HIGH VOID RATIOS

The study is restricted to one-dimensional consolidation for two reasons. Firstly the sedimentation process from suspension to consolidated soil must be continuous and secondly the simplest method of achieving very low stresses is to use the self-weight of the soil itself as the only loading. A test thus consists of placing a soil suspension in a 102 mm internal diameter clear acrylic column and monitoring the subsequent behaviour of the suspension, intermediate region and soil. Total stress, pore water pressure and void ratios are the measurements needed so that effective stresses and strains can be deduced.

Measurement of vertical total stress, except at the column base, is impossible without seriously disturbing the sediment, but non-destructive density measurement techniques are available. Calculation of a total stress at any point in a column of soil from the density profile is quite simple. Checks on total stresses found in this way are necessary (to assess wall friction effects, for example) and are relatively easily performed with a total stress cell in the base. Another advantage of density measurements is that the void ratio can be calculated directly from the density. Pore water pressure transducers or standpipes in the base and on the side of the column complete the required instrumentation. Fig 1.2 shows the experimental equipment schematically.

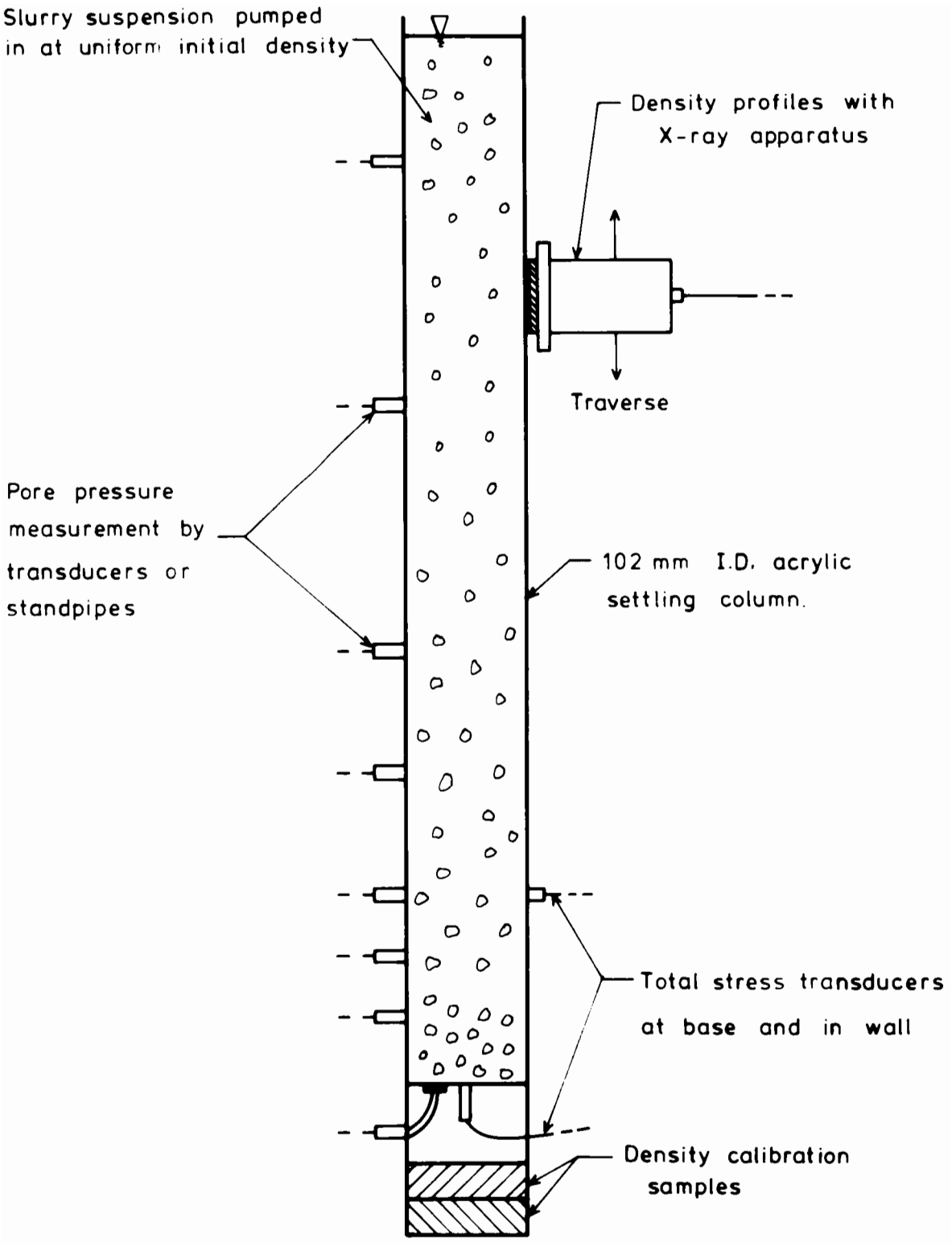


Fig 1.2. Diagram of Settling Experiment.

One dimensional consolidation theory ignores horizontal stresses, but since the horizontal and vertical stresses are likely to differ in a soil but not in a suspension, some form of horizontal total stress measurement is useful and is included in this study.

1.6 OUTLINE OF THIS THESIS

Chapter 2 is a detailed description of the equipment developed and used in this study. Much attention is devoted to the X-ray density measurement apparatus as this particular technique is new to geotechnics. The experimental procedure and series of tests is outlined in chapter 3. A naturally occurring silt was chosen for the study.

Experimental results are all presented in chapter 4 and discussed qualitatively in chapter 5 before an assessment of some theories is made in chapter 6. This chapter examines some existing theories in relation to the experimental results and compares consolidation and hindered settling theory analytically.

In chapter 7 modifications are made to the consolidation solutions of Lee (1979) and compared quantitatively to the experimental results. Finally, applications of the present work, recommendations for further work and conclusions are presented in chapter 8.

CHAPTER 2. EQUIPMENT

2.1 X-ray Density Measurement 26

2.1.1 Background 26
2.1.2 Some Previous Use of X- and Gamma-rays for Density Measurement 30
2.1.3 An X-ray and Scintillation Counter Technique 32
2.1.4 X-ray Source 35
2.1.5 Scintillation Counter 37
Crystal and Photomultiplier 39
Counter Electronics 40
Choice of Operating Conditions 45
2.1.6 Geometry and Collimation of the System 56
2.1.7 The Laboratory 62
2.1.8 Calibration 64
2.1.9 Performance 70
Variation of Radiation Energy and Intensity 70
Choice of Time Constant 78
Accuracy 82

2.2 Pressure Measurement 86

2.2.1 Requirements of the Method 86
Pore Water Pressure 86
Total Stress 87
2.2.2 Pressure Transducers 87
2.2.3 Pore Water Pressure Transducer Housing 88
2.2.4 Total Stress on the Column Base 92
2.2.5 Total Stress on the Side of the Column 92
2.2.6 Electronics 94
2.2.7 Calibration 94
2.2.8 Accuracy 95
2.2.9 Use of Standpipes 95

CHAPTER 2. EQUIPMENT.

Experimental work by Michaels and Bolger (1962) on flocculated kaolin suspensions gives a good indication of the size of container necessary for settling experiments. The container diameter (or wall) effect was negligible for the 48 mm to 65 mm containers used in their work. To allow for the possibility of different floc sizes and forces in other soils (and because they were readily available) 102 mm I.D. settling columns were used. Head room and handling problems limited the columns to a maximum length of 2 m.

The experimental equipment to measure density and pressure described in this chapter has thus been designed specifically for these columns. A prime consideration in the measurement techniques was that they disturb the settling and consolidation process as little as possible, hence the use of radiation density measurement and low compliance pressure transducers. Pressure measurements are made only at the base and sides of the columns because at extremely low shear strengths the edge effects would probably be less than the effect of an intrusive pressure probe.

2.1 X-RAY DENSITY MEASUREMENT

2.1.1 Background

The absorption of radiation as it passes through matter is a well known phenomenon. The general law governing this absorption (Kohl, Zentner and Lukens, 1961, ch 9) is that the fraction of the radiation absorbed in passing through a thin layer of matter is proportional to the thickness of the layer (Δx) and to an absorption coefficient (μ). Thus for a radiation intensity I,

$$\frac{\Delta I}{I} = -\mu \Delta x$$

For a finite path length x this may be integrated to give

$$I = I_0 e^{-\mu x} \qquad (2.1)$$

where I_0 and I are the incident and the transmitted intensities in the direction of travel of the radiation. Intensity may be measured in terms of radiant power (lumens or watts) or number of X-ray photons per unit time. In this equation μ is the linear absorption coefficient.

X-rays and Gamma-rays (which differ in origin but are otherwise identical in nature) fall into the electromagnetic spectrum where the important absorption processes are the photo-electric effect (true absorption), Compton scattering and Rayleigh scattering. Pair production only occurs at higher energies than are used in common soils

applications and need not be considered here. Scattering has the effect of altering the energy and/or the direction of the photons, so is strictly the attenuation rather than absorption of radiation. A further consequence of scattering is that the cross sectional area of the beam and absorber have an effect on the transmitted radiation. A distinction must thus be made between narrow and broad beam attenuation of radiation. Under ideal narrow beam conditions, where the linear absorption coefficient consists of the sum of the coefficients for each absorption process, the exponential relationship of equation 2.1 will hold, but in broad beam conditions scattered radiation will make a larger contribution to the transmitted radiation intensity and the equation must be modified by a build up factor.

The nature of the absorption processes makes the use of the more basic mass absorption coefficient convenient, where

$$\mu_m = \frac{\mu}{\rho}$$

and μ_m is the mass absorption coefficient

μ is the linear absorption coefficient

ρ is the density of the absorbing material

The total mass absorption coefficient includes the effect of photoelectric absorption and scattering. As such it is not a true absorption coefficient but refers to the attenuation of radiation per unit mass of absorber over a small cross-section. The narrow beam attenuation equation can now be written

$$I = I_0 e^{-\mu_m \gamma x} \qquad (2.2)$$

where γ is the bulk density of the absorbing material. In theory it is thus possible to calculate the bulk density from the incident and transmitted intensities if the mass absorption coefficient and path length are known. In practice difficulties frequently arise as the mass absorption coefficient is strongly dependent on the radiation energy and the atomic chemistry of the absorbing material. Fig 2.1 shows the variation of mass absorption coefficient with radiation energy for a number of common elements.

Mono-energetic radiation will be an advantage if the absorption law is to be used. Gamma rays are produced naturally by nuclear decay of radioisotopes, each isotope producing only discrete energies of radiation, so a source can be chosen (and selectively filtered if necessary) to produce a beam of known energy. In contrast X-rays from a typical X-ray tube have a wide distribution of energies with a maximum energy corresponding to the peak voltage in the tube. Intensity variations with time also occur for both X- and gamma-rays.

In addition to the absorption coefficient differences for radiation energy and chemical composition, it is important to realise that for saturated soils a change in bulk density is associated with a change in moisture content and hence also the ratios of the various atoms in a unit weight of soil; i.e. the absorption coefficient depends on the bulk density.

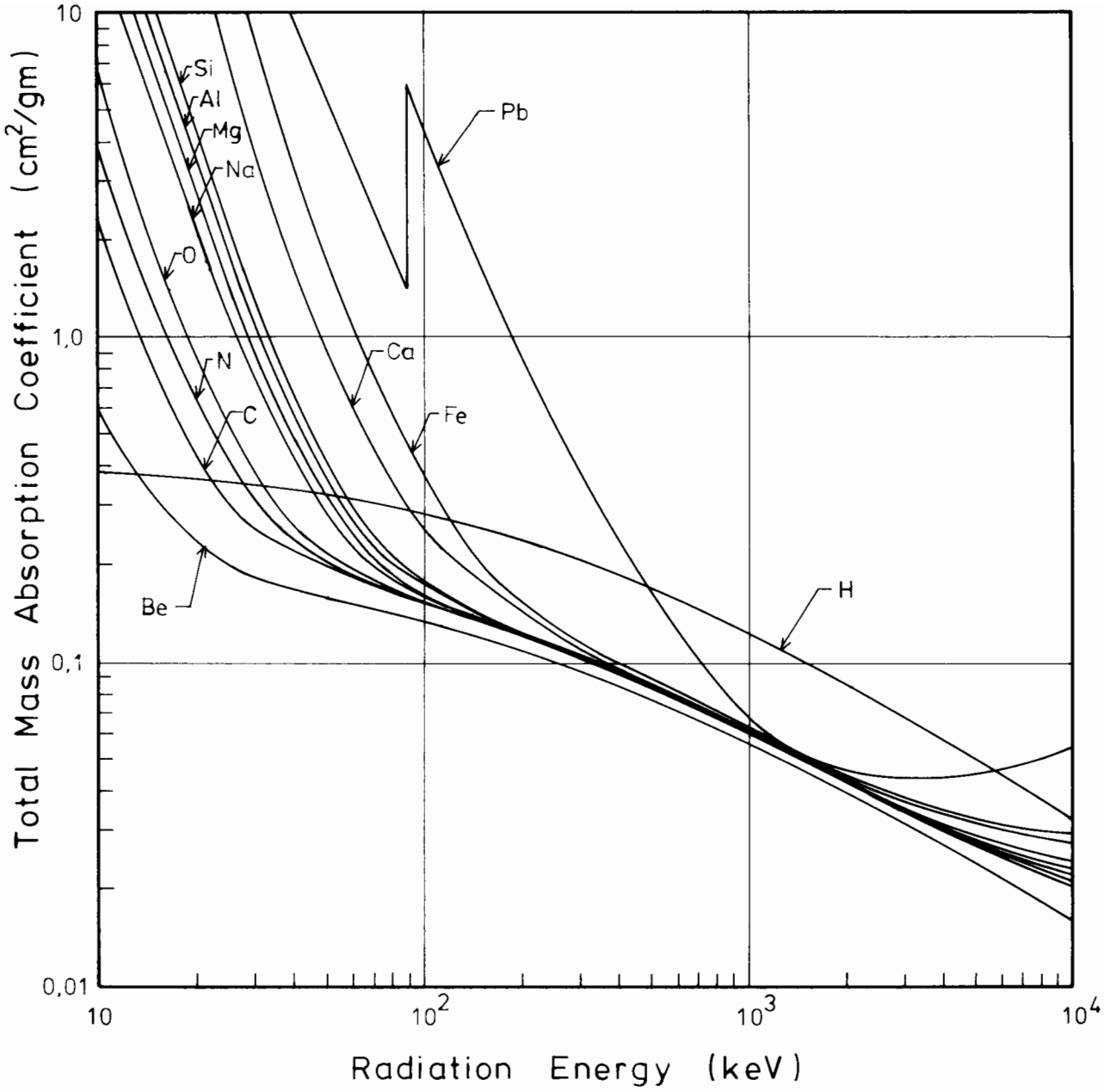


Fig 2.1 Mass Absorption Coefficients.

There are a number of possible ways of detecting X-rays and Gamma-rays, the choice of method depending largely on the radiation type and application. Kohl et al, (1961), chapter 3, give a detailed description of methods of detection. One group of detectors, including ionization chambers, Geiger-Muller counters and semi-conductor detectors, react to the ionization produced in them by radiation. In other detectors, excitation or molecular disassociation produces the measured effect. Photographic film for X-ray detection and scintillation counters for γ-ray applications, which are the most common methods for quantitative work in Geotechnics, fall into this category.

A further consideration if the relationship in equation 2.2 is to be used, is the position of the radiation source, absorbing material and detector in relation to one another. The detector must be exposed only to a narrow beam that has passed through the material and must be shielded from other scattered and direct radiation if the true transmitted intensity is to be found.

2.1.2 Some Previous Use of X- and Gamma-rays for Density Measurement.

The concept of using attenuation of a beam of radiation to measure a density, concentration or thickness of something is not new, although the use of X- and Gamma-rays for Geotechnical purposes only goes back to the 1950's.

At Cambridge both X- and Gamma-ray methods have been developed for the study of stress-strain behaviour of soils under static load conditions. Roscoe, Arthur and James (1963) describe the early use of X-rays with lead shot markers for obtaining shear and volumetric strain patterns within granular materials. A general account of how accurately the void ratio in granular materials can be measured using radiation attenuation, is given by O'Loughlin (1964), who gave consideration to the accuracy of absorption techniques, the effect of granularity and the statistical significance of the measurements. Sirwan (1965) used the density of X-ray films to detect changes in local voids ratios, but Coumoulos (1967) found that counting Gamma-rays passing through a soil sample was a more convenient and accurate method. The work at Cambridge was particularly fundamental and indicated many of the ways in which the radiological properties of soils differ from other materials and the difficulties in practice of applying radiation techniques and interpreting the results.

Calibration for accurate density measurement of a natural material is discussed by Preiss (1968) in a paper describing a Gamma-radiation method of measuring marine sediment densities in a core barrel. Liquid solutions of different densities (and chemicals) were used for calibration and allowances using the theoretical absorption law made for chemical composition, although the moisture content of the sediment was assumed to remain at 150%. It is possible to take account of moisture content change theoretically for the absorption coefficient, as per Maus, Rose and Nacci (1973). They used a similar method to Preiss to monitor one-dimensional consolidation tests, but calculated water contents during a test by the difference in count rate from the

final condition, for which the density was determined gravimetrically.

A.E.R.E. Harwell developed two successful field instruments to measure insitu densities using gamma radiation; a backscatter gauge (the detector is positioned so that only backscattered radiation is counted) and a transmission gauge built to I.O.S. (Taunton) specifications. Their performance is described by Parker, Sills and Paske (1975). Calibration was done empirically. Both instruments were used for profiling soft muds and suspensions so that the requirements were for a quick response to density changes as the instrument moved through the soil.

X-ray photographic methods of densitometry have been used other than at Cambridge. Krinitsky (1972) mentions many of the difficulties encountered when using X-radiography to measure density structures in dry soil loaded in models. After each load increment a radiograph was taken and the film density variation measured with a photodensimeter. Accuracy was achieved only by empirical corrections and extremely careful control of all processes.

The above techniques and papers are not an exhaustive list but serve to illustrate the basic practical aspects of non-destructive density measurement using X- and Gamma-radiation.

2.1.3 An X-ray and Scintillation Counter Technique

For the purposes of the present study a better performance,

with regard to spatial resolution and speed of measurement, was needed than any of the techniques of the previous section could provide. The ideal system of density measurement would have the following characteristics;

- a mono-energetic source of constant intensity.
- a source energy such that mass absorption coefficients at that energy do not vary with atomic number. This implies a source energy above about 300 keV, which also means less contrast for a change in density
- a detector that measures radiation intensity accurately and instantly
- a geometrical configuration that ensures that the relative positions of the source, sample and detector never change and that the detector only sees radiation that has passed through the sample.

The choice of a suitable radiation source is thus influenced both by the energy and intensity of the radiation. A gamma source, such as Caesium 137 which emits a single Gamma-ray of energy 0.66 MeV, could be chosen that satisfies the energy requirements although a lower energy source would give better contrast. However, nuclear decay is a random process so for a small, safe gamma source not requiring excessive shielding there is an inherent variation in emitted intensity over a short time period, as well as the long term effect of the exponential decay process, resulting in poor accuracy. Although it is possible to generate high energy X-rays (comparable to gamma sources) there is always a wide range of lower energies and shielding remains a problem. Below an energy of about 200 keV, high intensities of X-radiation can be produced without safety problems as shielding of this soft radiation

is relatively easy. As an empirical calibration of the intensity to density would be inevitable for the present purpose, the requirement of mono-energetic radiation above 300 keV was relaxed. Thus a 160 kV (maximum) constant potential X-ray source has been used.

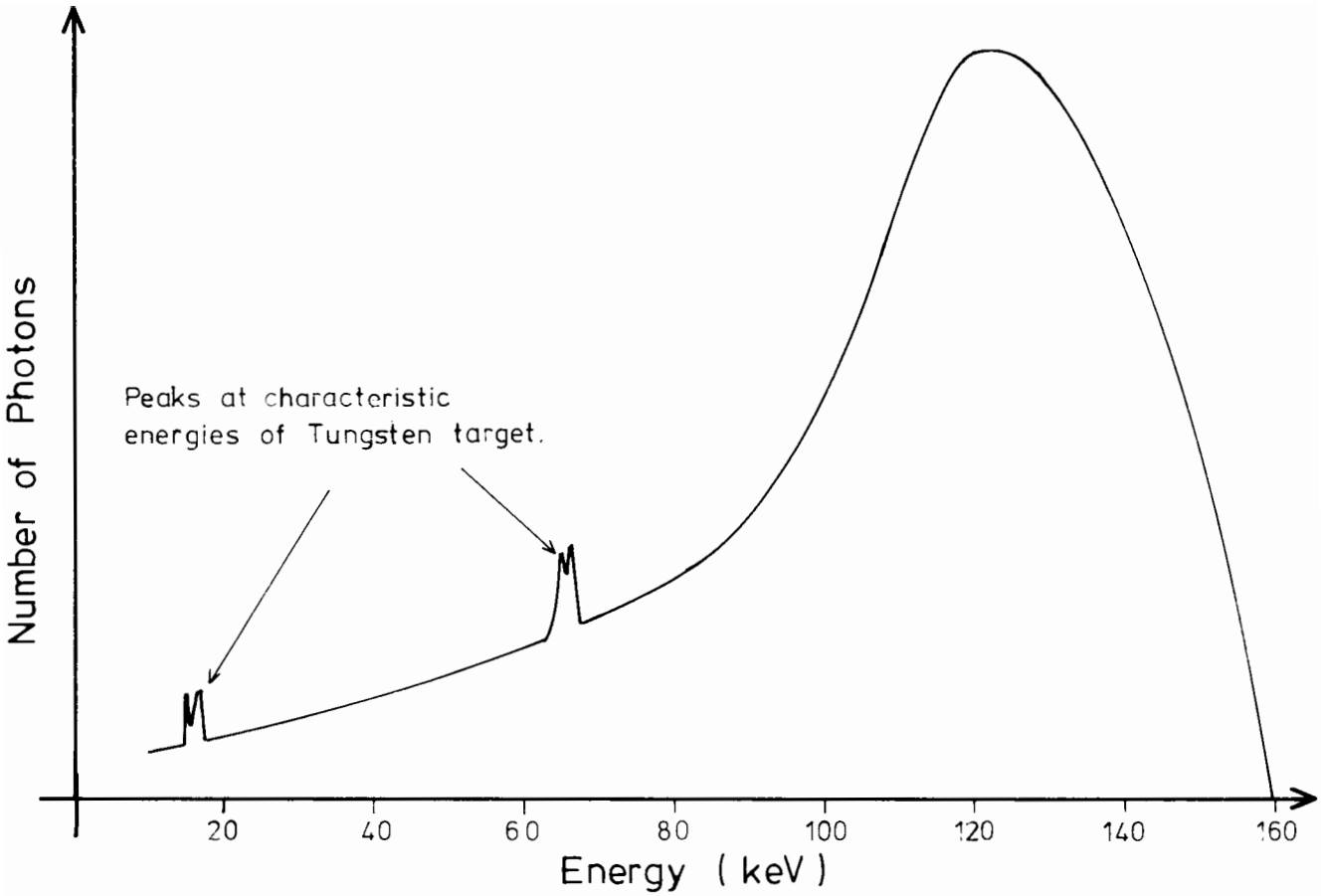
For geotechnical applications X-rays have in the past been detected by photographic film. This is a slow process, with exposure times of the order of many minutes rather than seconds, so that radiography is unsuitable for monitoring dynamic processes. Stringent control has to be kept on the processing of X-ray film because changes in chemical bath concentrations, temperatures, times and agitation all affect the film density significantly. A high quality photo-densimeter is also a necessity to detect small changes in film density. An alternative is a scintillation counter which does not have this limitation of being inherently slow, although time considerations are still important. Because X-rays are physically exactly the same as Gamma-rays, a gamma scintillation counter, suitably modified for lower energy X-rays, appears to be a suitable method of detection and was therefore used in this system.

The practical aspects of the X-ray and scintillation counter technique developed for the present study are described in the next sections. In order to achieve the performance and accuracy described in section 2.1.9 a great deal of careful experimentation, particularly on the scintillation counter, had to be carried out before a suitable combination of the variables in the source, counter and geometrical setup was achieved.

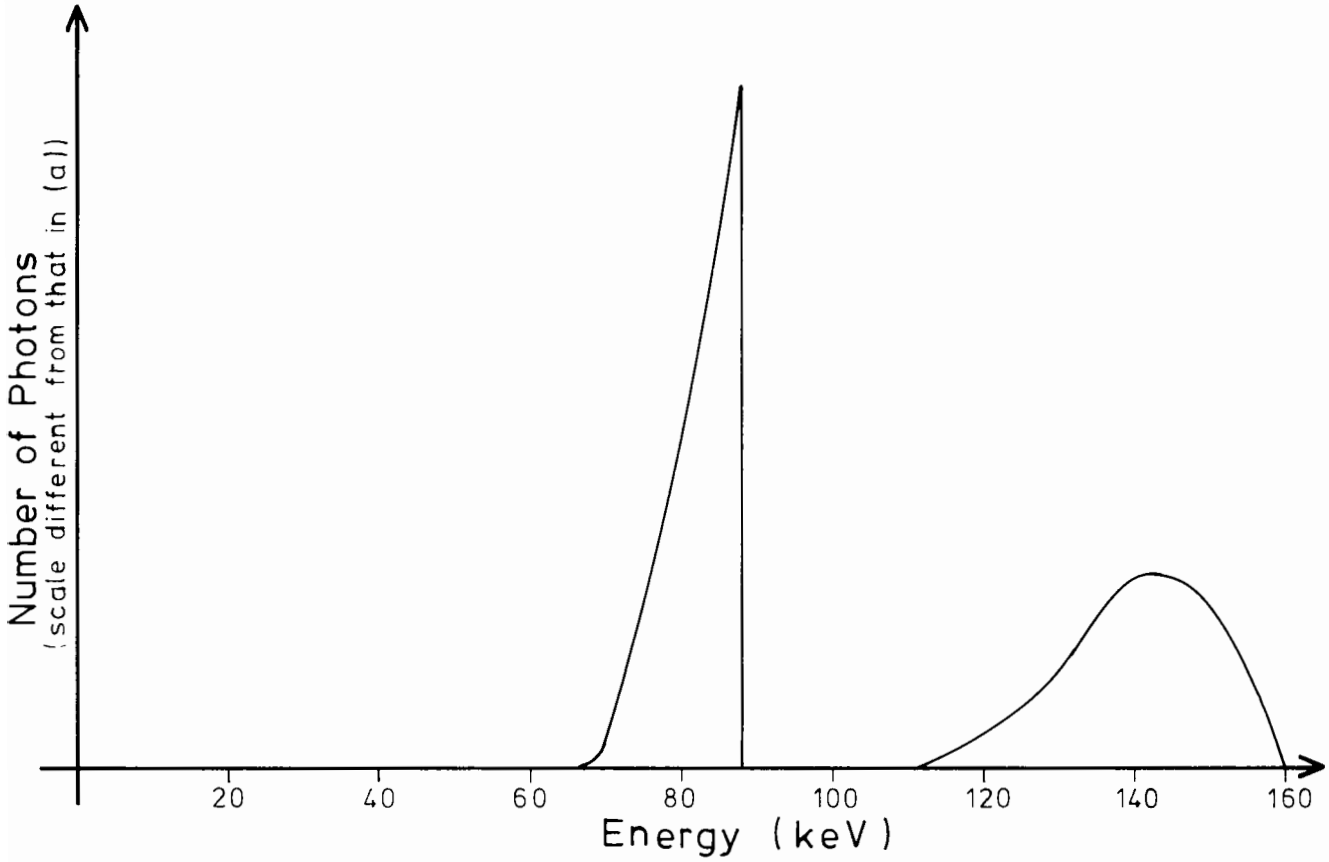
2.1.4 X-Ray Source

The X-rays are generated in a Philips MCN 161 X-ray tube, with a maximum operating tube voltage of 160 kV. This is part of an MG 160 constant potential industrial X-ray system, which features built in current and voltage regulation and low H.T. ripple. Maximum power is 3 kW on the standard (3 mm × 3 mm) focus and 650 W on fine focus (0.4 mm ×0.4 mm). Originally the system was installed with a recirculating water cooling unit which adversely affects the stability of the X-ray output. As the cooler draws a large current and only switches on intermittently, frequent electrical surges interfere with the stabilisation circuit and the temperature of the tungsten target fluctuates during operation. A continuous water to waste cooling system was subsequently installed and the X-ray output intensity fluctuates less than 1%. This is equivalent to tube voltage fluctuation of less than 0.5%

Although the regulated voltage and low H.T. ripple means the radiation output is relatively stable there is not a monochromatic beam of X-rays. In general the spectrum of X-rays will be quite wide with a maximum intensity occurring at an energy corresponding to approximately $^2/_3$ of the tube potential (Halmshaw, 1966) as in fig.2.2(a). Besides collimation of the beam of radiation (section 2.1.6) it was found that a 1.8 mm lead filter near the tube greatly enhanced the density measurement system. The effect of this filter on the energy distribution of fig 2.2(a) is to produce the distribution in fig 2.2(b). Although the total intensity of the beam is reduced by a factor of approximately 1000 in passing through the filter, the proportion of high energy photons is greatly increased because the absorption coefficient of lead is



(a) X-rays Direct from Tube.



(b) X-rays After Filtration by 1.8 mm Lead. (Narrow Beam Attenuation)

Fig 2.2. Energy Distribution of X-rays from Source.

strongly dependent on radiation energy (refer to fig 2.1). The lower energy rays are almost completely absorbed, but sufficient higher energy radiation is transmitted to provide a useful beam of X-rays.

The main advantage of the filter is that most of the photons in the filtered beam have a similar penetrating power. Below 70 keV, an energy difference of about 30 keV causes the mass absorption coefficients of soils to vary by an order of magnitude, but between 70 keV and 160 keV the variation is relatively small. Thus a small fluctuation in the energy distribution below 70 keV would have a substantial effect on the intensity of the attenuated radiation. A coincidental bonus is that the mass absorption coefficients of the various common elements in soils differ from one another significantly less as the energy increases, making calibration simpler. This aspect is discussed in section 2.1.8. The energy distribution after filtration is also more suitable for the scintillation counter used in this system which is sensitive to radiation energy as well as intensity.

2.1.5 Scintillation Counter

A scintillation counter is a combination of a phosphor, photo-multiplier tube and associated circuits for counting light emissions produced in the phosphor by the radiation. Figure 2.3 is a sketch of a scintillation detecter showing the important features. The phosphor, when subjected to radiation, emits light which in turn releases photoelectrons from the photocathode. These photoelectrons are accelerated through a potential difference of 100 Volts or more to a secondary

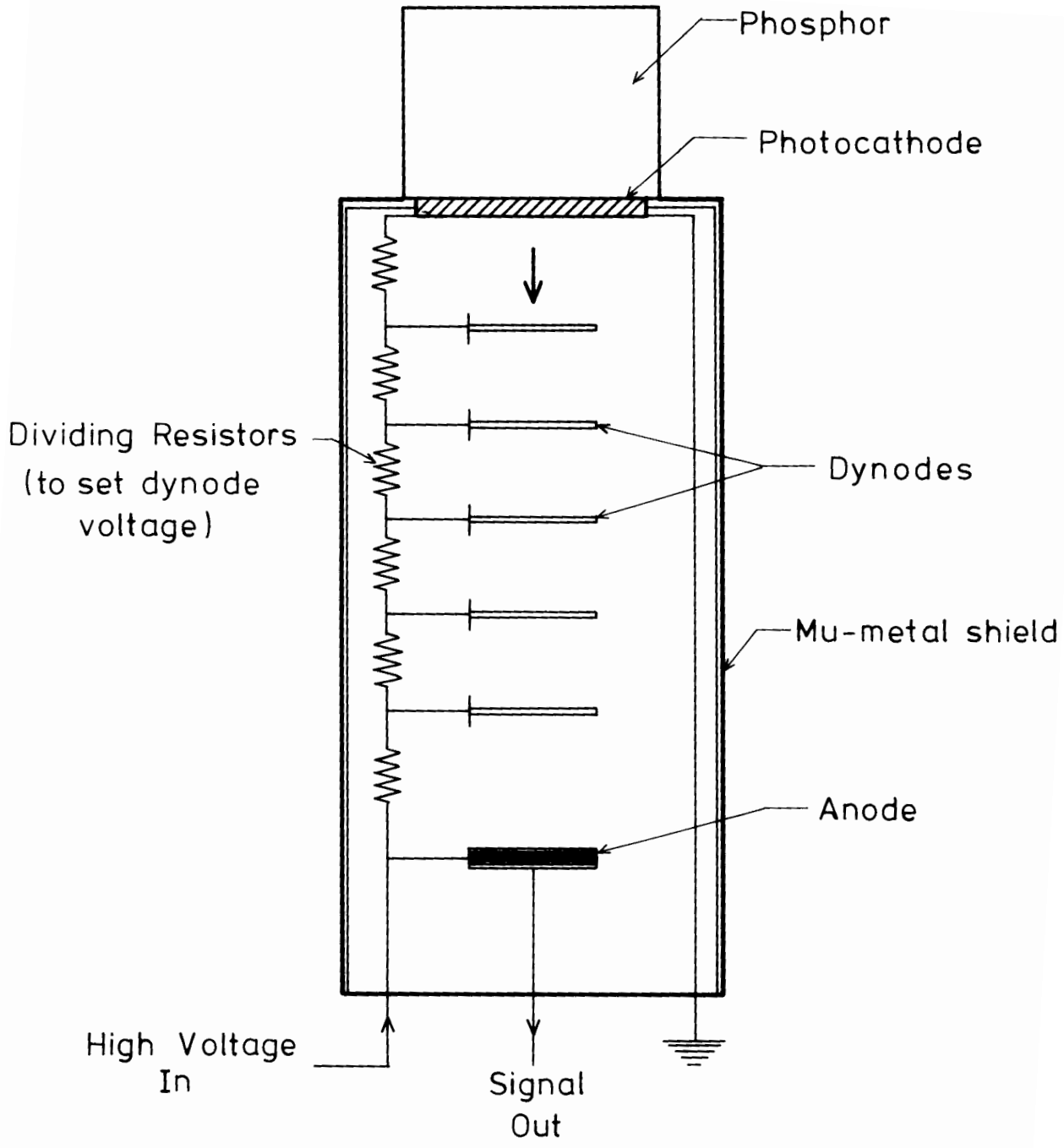


Fig 2.3. Scintillation Detector

electron emitter (dynode) where additional secondary electrons are released. This multiplication of secondary electrons continues through the chain of several dynodes until the anode is reached. An X-ray photon which interacts with the phosphor to produce sufficient light at the photocathode for photoelectric emission thus produces a detectable electronic pulse at the anode. The associated electronic circuits have the dual function of producing a high voltage across the photocathode-dynode-anode chain and of counting the anode pulses. A more detailed account of scintillation counters may be found in texts such as Kohl et al (1961), Sharpe (1964) and Pringle (1950).

Crystal and Photomultiplier

The phosphor and photomultiplier used in the present work was a special P-1065 assembly supplied by Rank Hilger, the choice being made on the basis of the successful Harwell transmission gauge, referred to in section 2.1.2.

The phosphor is a Thallium activated Sodium Iodide crystal, 75 mm in diameter and 5 mm thick. NaI(Tl) has a wavelength emission band from 3700 Å to 4600 Å with a peak at 4100 Å, a decay time of 0.25 micro-seconds and in this case an energy conversion efficiency of 12%. A useful property of the NaI(Tl) scintillation crystal is that the light emission is proportional to the energy lost by the photon in the crystal, although for energies below 100 keV the relationship is slightly non-linear, Iredale (1961). However the pulse distribution from the crystal does not correspond directly to the energy distribution of the incident

beam of radiation because not necessarily all the energy of the incident photons is lost in the crystal. There are two types of interaction of photons with the crystal; photoelectric absorption where the full energy of the X-ray is expended in the crystal and Compton scattering where only part of the energy is lost, although complete absorption can also take place by one or more Compton encounters followed by photo-electric absorption.

The crystal is protected by a 0.1 mm aluminium window and mounted directly on to a EMI 9708 R, 75 mm photomultiplier tube with a "Super" S - 11 (Cs_3Sb-O) photocathode, having a spectral response as in fig 2.4. Quantum efficiency of a photocathode is the number of photo-electrons emitted from the photocathode per incident photon of a particular wavelength and it may be seen that the "Super" S - 11 cathode has a peak response of 22 - 24%, coinciding with the emission band of the NaI(Tl) crystal. The photomultiplier is a chain of 9 venetian blind dynodes with CsSb secondary emitting surfaces enclosed in a mumetal screen. Fig 2.5 shows the gain / EHT supply voltage curve for this unit.

Counter Electronics

Harwell 2000 Series counting equipment to complete the system was lent by I.O.S. (Taunton) and the Nuclear Physics Department of Oxford University. This comprised a 1798 A Power Unit, a 95/2179-1/6 Scintillation Counter Adaptor and a 95/2134-2/6 Linear Ratemeter/Integrator. Although this series of fast scintillation counter electronics was out of date at this stage, it proved to be adequate while the density system was being developed and a suitably modified counter for this

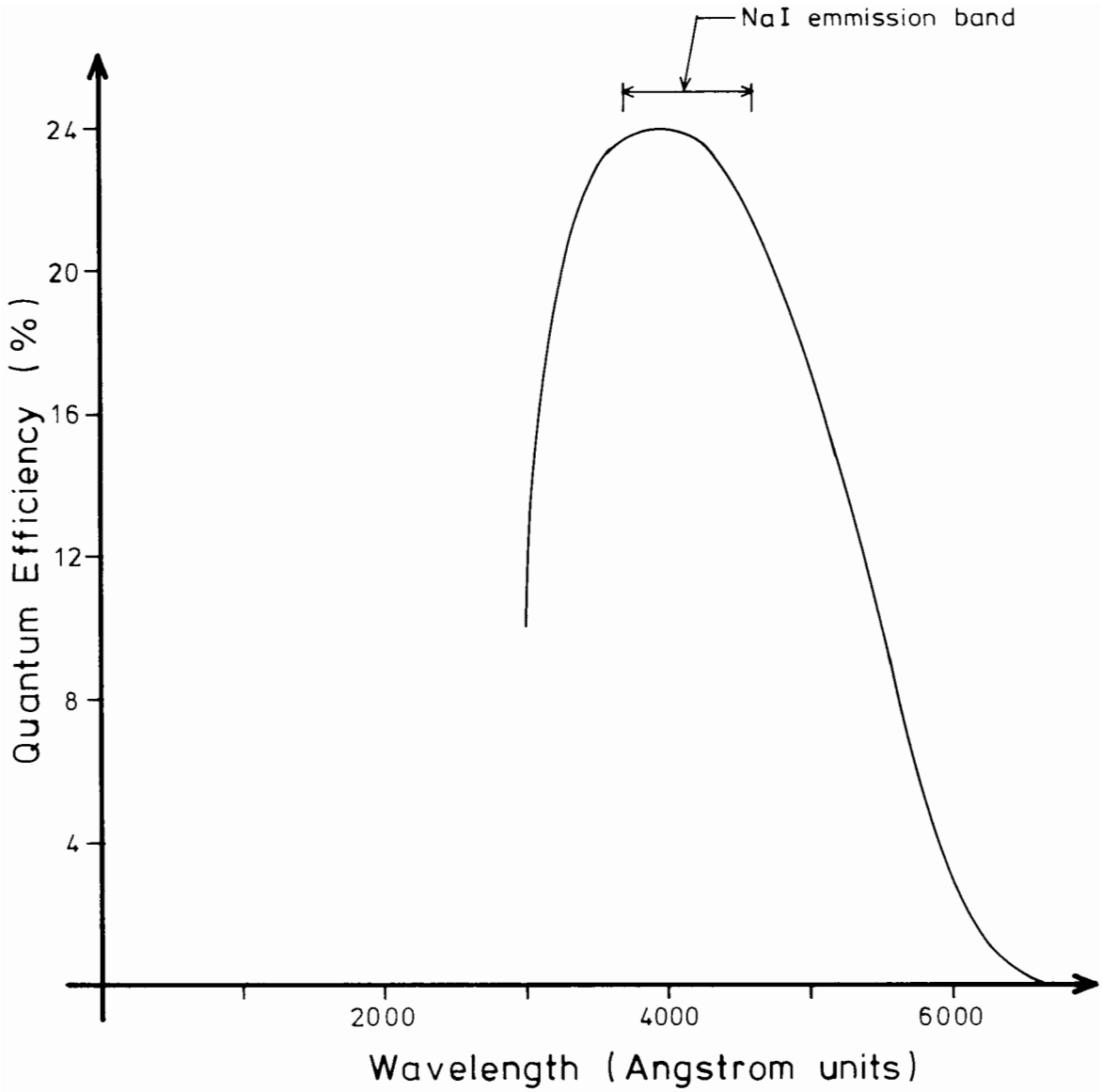


Fig 2.4. Spectral Response of "Super S-11" Photocathode.

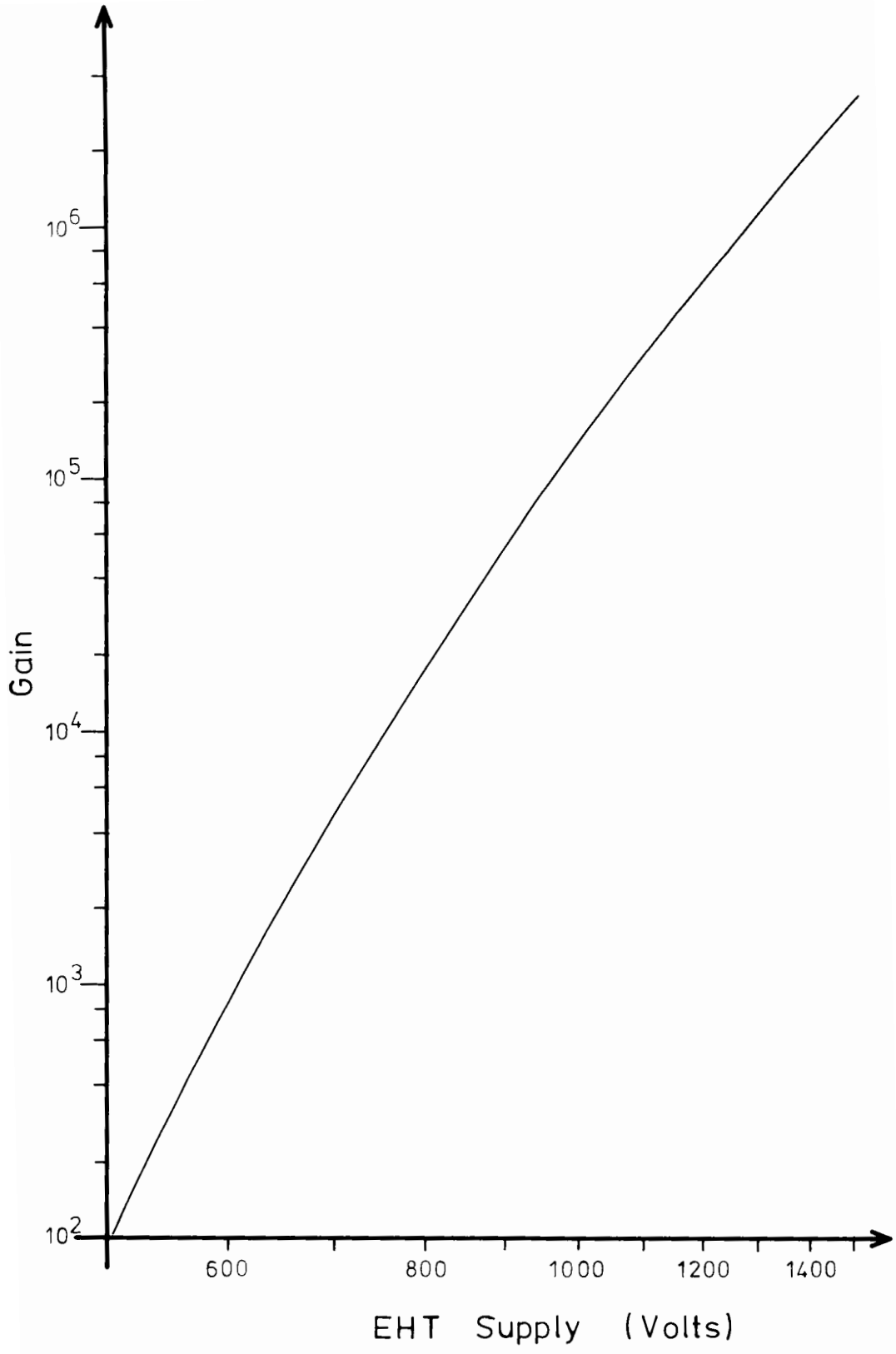


Fig 2.5. Gain Curve of Photomultiplier.

particular system is currently being designed and built on a follow-up research grant at Oxford. A schematic diagram of the whole counting installation is shown in fig 2.6.

The Scintillation Counter Adaptor provides an EHT supply for the photomultiplier and converts the output signal from the photomultiplier into a suitable form for analogue or digital recording. A helipot allows the stabilised EHT output to be set to any value from 400 V to 1400 V. Pulses from the photomultiplier anode return along the same line as the EHT supply before passing through a pulse shaper and low gain amplifier. If an analogue pulse record were required the signal would be tapped at this stage, but for digital counting, as in this instance, the pulse is amplified further before reaching a discriminator. When the discriminator circuit is triggered by the pulse, a digital pulse is generated in a separate circuit and fed to the Ratemeter. The discriminator is normally fixed at a threshold level equivalent to an input charge of about 2μμC, but this particular set had been modified to allow an increase in the threshold for elimination of pickup in field use. Dead time for the discriminator is 3.5 μs, which is significantly longer than the 0.25 μs decay time of the NaI(Tl) crystal and thus limits the maximum count rate before significant errors arise as a result of a second pulse being closer than 3.5 μs to the first. Too short a dead time is undesirable as one pulse might then trigger the discriminator twice.

There is an option of using the Linear Ratemeter as an Integrator (or total - count meter), but as this facility was not used it will not be included in this description. Output from the

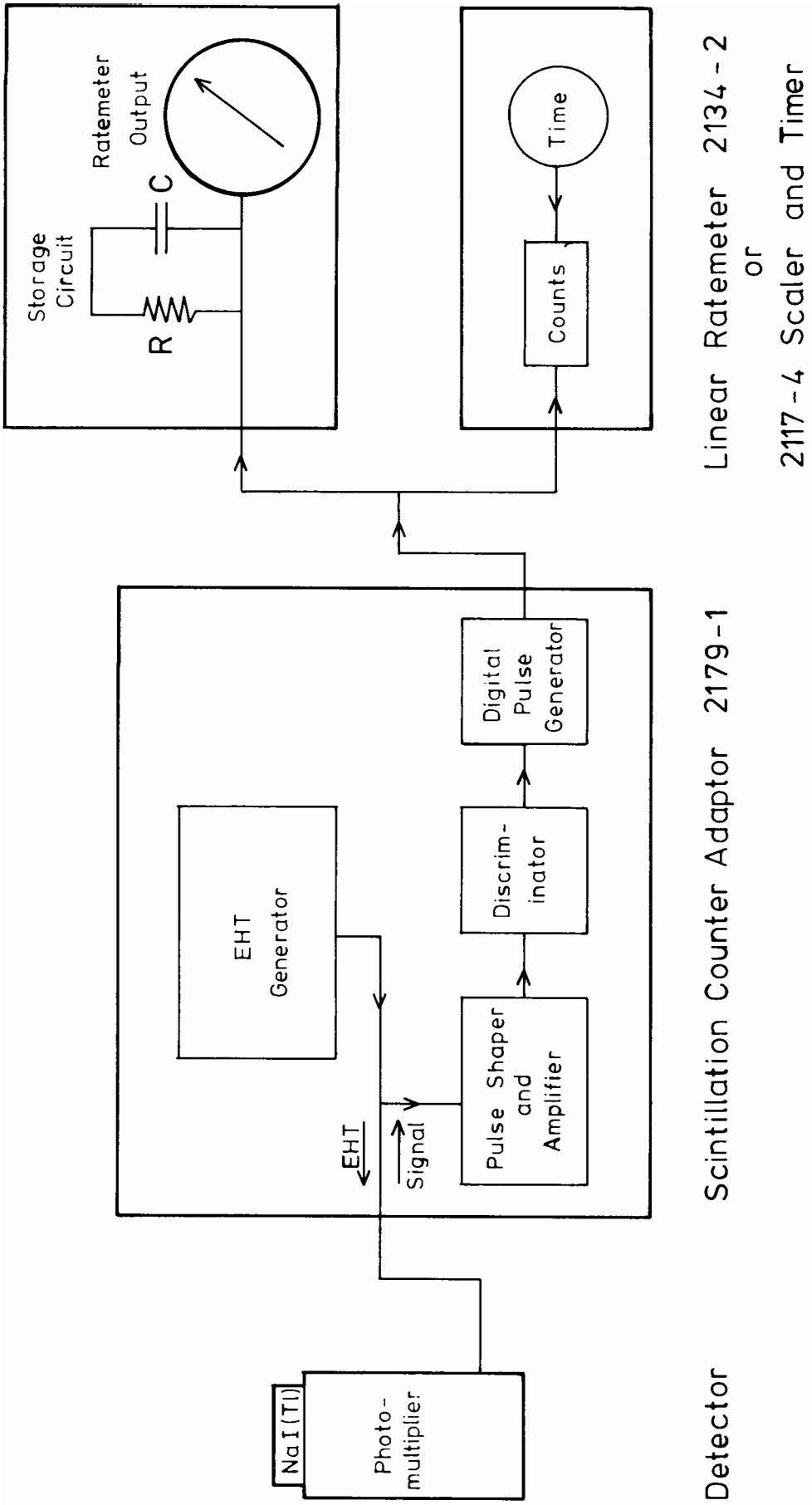


Fig 2.6. Diagram of Counting Installation.

ratemeter is an analogue voltage signal proportional to the counting rate of the digital pulses received from the scintillation counter adaptor. In this instance full scale output is 10 V but a back-off facility allows extension of the scale to 15 V. In the averaging section of the ratemeter circuit, which may be considered to contain a capacitor of C farads shunted by a resistance of R ohms (as depicted in fig 2.6), the values of R and C determine the speed with which the output current reflects changes in input pulse rate and also the precision of the output. The product, RC seconds, is called the time constant of the circuit (Kohl et al 1961, pp 129-132). Five time constants, from 0.2 to 125 seconds, are available on each of the ratemeter's nine ranges covering 0 to 1 and 0 to 10^4 counts per second.

On a few occasions when a total count over a certain period of time was required, a Harwell 2117-4 Scaler coupled with a 2236-1 Scaler / Timer was used. This simple digital pulse counting system has a counting specification far in excess of the output of the adaptor and could be used with confidence for calibration checks.

Choice of Operating Conditions

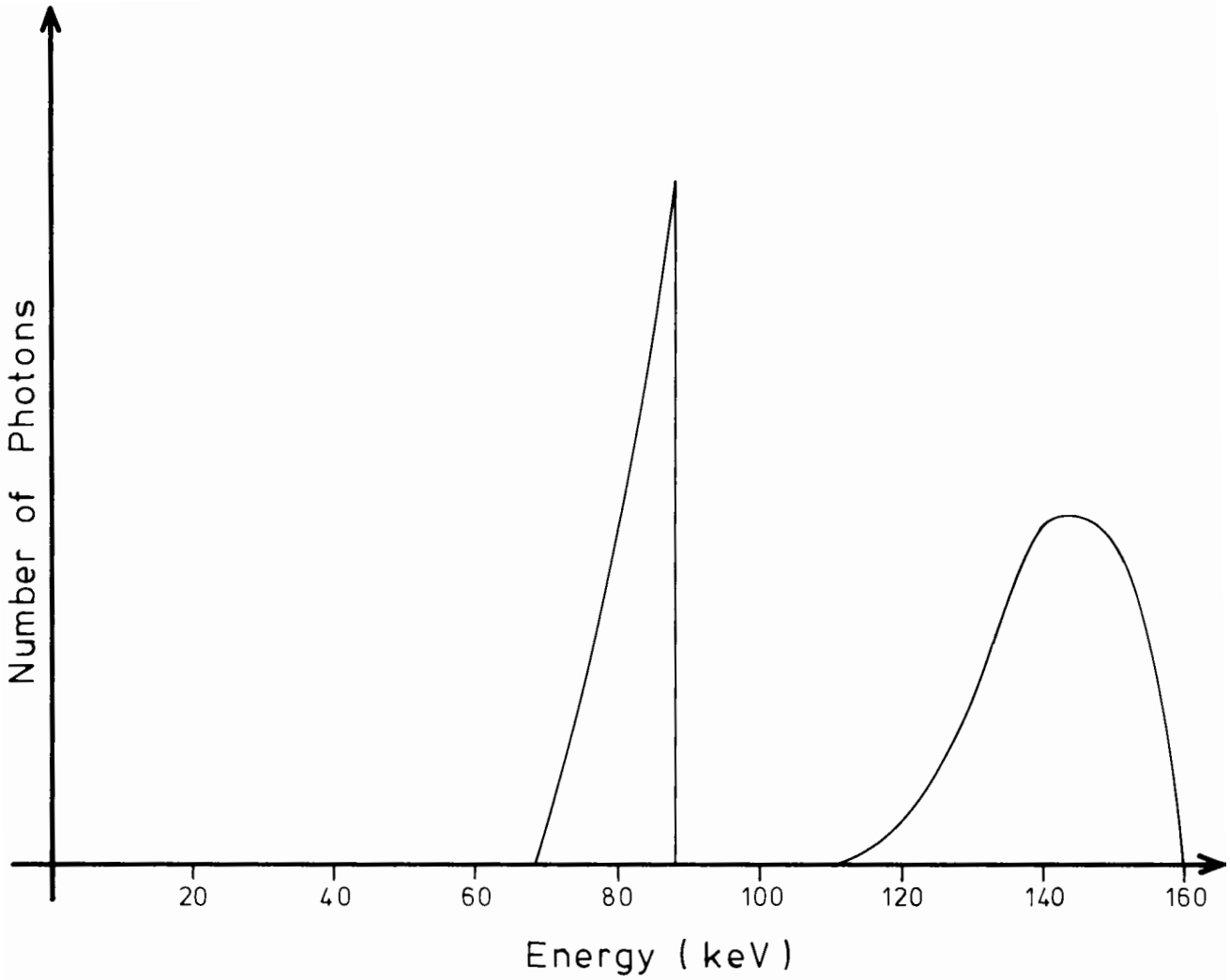
Count rate output from a scintillation counter depends (in addition to the intensity of radiation) on the energy distribution of the measured radiation, the type and efficiency of the various components of the counter and the preset values of discriminator threshold and EHT supply to the photomultiplier. This section illustrates this complex dependence by showing how a count rate versus EHT curve can be calculated, using the present equipment as an example.

Fig 2.7 shows the approximate energy distribution of the filtered beam of X-rays, after attenuation by the soil sample. Higher energy radiation is attenuated less than the lower energies in passing through the sample so the energy distribution reaching the detector is slightly different from figure 2.2(b). There is a further effect of absorption by the 0.1 mm aluminium window covering the crystal, but this attenuation is less than 1% for energies over 50 keV and is not considered here.

The next stage in the process is the conversion of the X-ray energy into light by the NaI(Tl) crystal. Efficiency depends on the absorption of X-radiation by the crystal and the overall energy conversion efficiency of NaI(Tl), given as 12% by the suppliers of this particular crystal.

Consideration must also be given to how much of the crystal light emission reaches the photocathode. Not all the light is emitted in the direction of the cathode and some light is absorbed by the crystal and by the glass separating the crystal and photocathode. This transmission efficiency would be difficult to determine analytically but considering the photocathode only covers 0.35 of the crystal surface area and allowing a 20% absorption loss (an approximate value from the catalogue), an average efficiency of approximately 30% seems reasonable in this case.

Light pulses that leave the crystal and actually reach the photocathode have a very different distribution from the incident X-rays, fig 2.7. Absorption processes in the crystal are complex and not all the energy from a particular X-ray is dissipated in the crystal. Clearly



Derived from fig 2.2(b) assuming

(a) Narrow beam attenuation $I = I_c e^{-\mu_m \gamma d}$ and no scattered radiation reaches detector.

(b) d = 100 mm, γ = 1.2 gm/cm^3

(c) μ_m = 0.143 cm^2/g for 145 keV

μ_m = 0.187 cm^2/g for 88 keV

Fig 2.7. Energy Distribution of X-rays Reaching Detector.

the energy of emitted light is reduced by the 12% energy conversion and 30% transmission efficiencies, but the 30% efficiency is only an estimated average value and a wide spread about the mean must be expected. Typical pulse height distributions from scintillation counters (see Sharpe, 1961, chapter 5) indicate that a distribution similar to that shown in fig 2.8 would be likely for the given incident X-ray distribution. (Photomultiplier resolution does also affect the final observed pulse height distribution). Energies plotted on the horizontal axis in fig 2.8 are the apparent energies that would have to be dissipated in the crystal, if the total efficiency was constant at 3.6%, to produce the light pulses at the photocathode, rather than the real energies dissipated. Integrating this distribution, fig 2.9, the proportion of light pulses reaching the photocathode with greater than a particular apparent dissipation energy, may be plotted.

The NaI crystal emits light with a wavelength distribution peak at 4100 Å, corresponding to an energy of 4.84×10^{-19} Joules per photon, calculated from the equation

$$E_\lambda = \frac{h\,c}{\lambda} \qquad (2.3)$$

where E_λ = energy of light photon

λ = wavelength of photon

c = speed of light, 3×10^{8} m/sec

h = Planck's constant, 6.62×10^{-34} Joule-sec.

Thus the apparent dissipation of energy E_x by an X-ray in the crystal

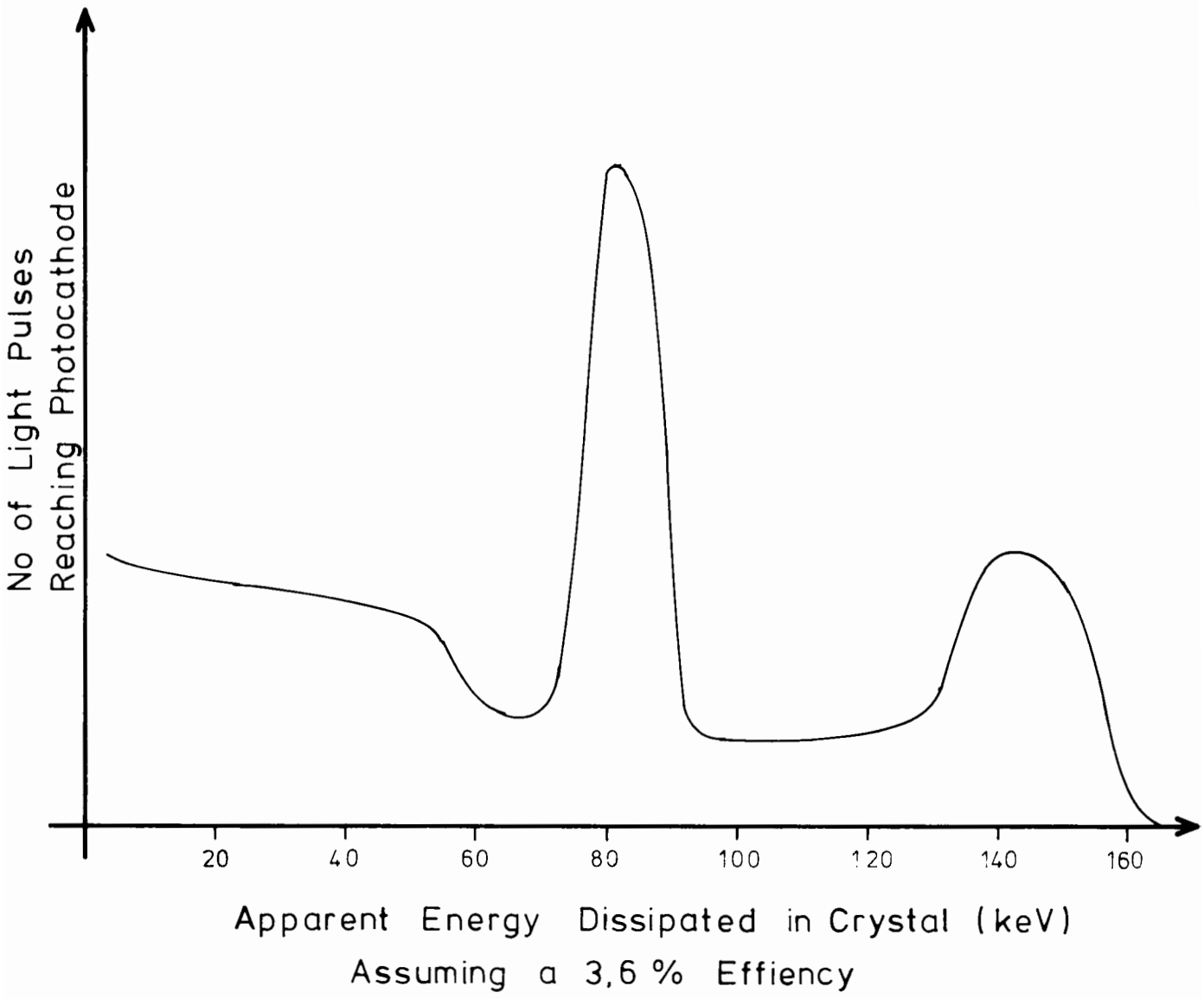


Fig 2.8. Pulse Energy Distribution Reaching Photocathode.

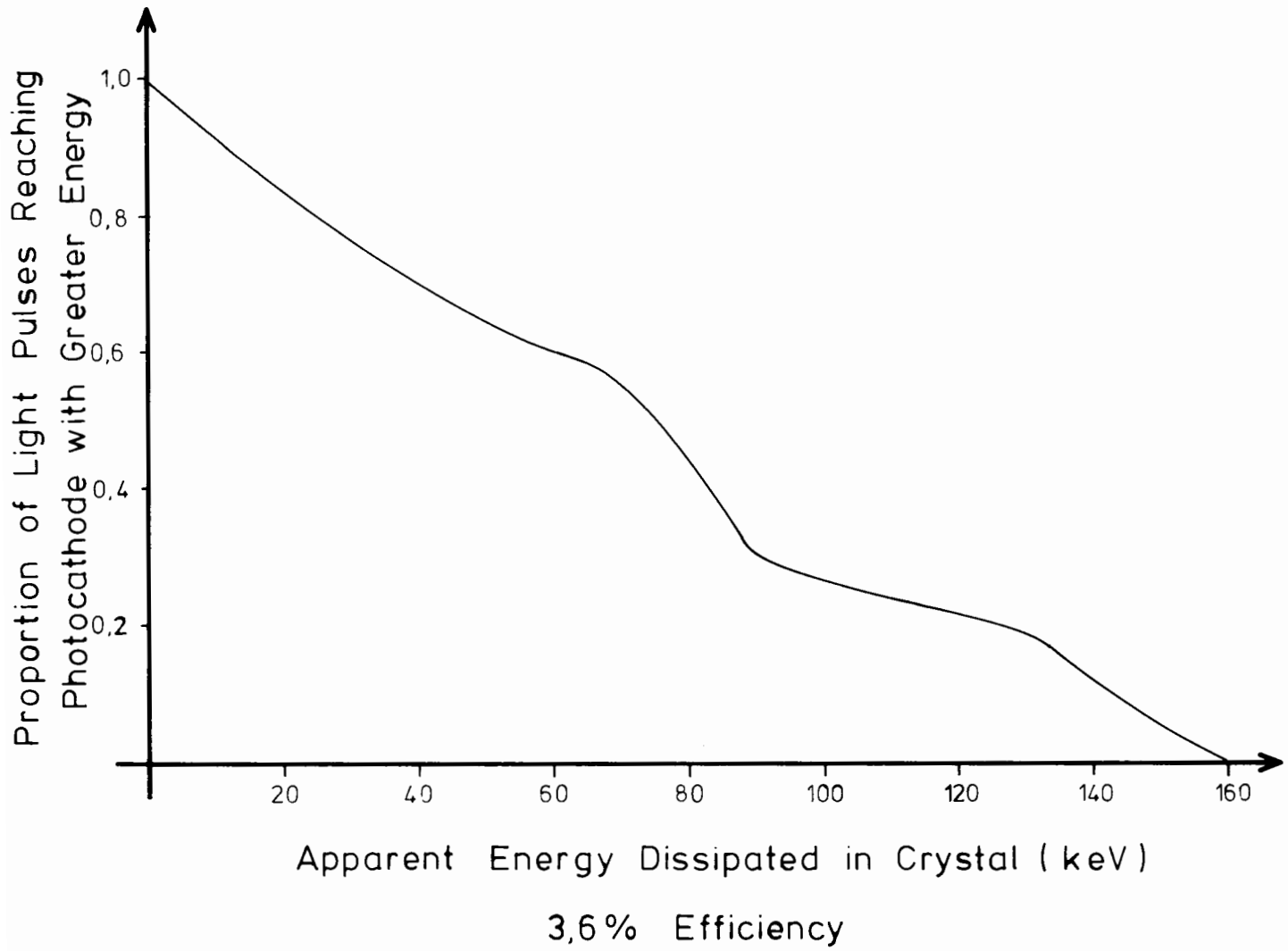


Fig 2.9. Proportion of Pulses with Higher than a Certain Energy.

causes N_{ph} photons of wavelength λ to reach the photocathode, where

$$N_{ph} = \frac{E_x}{E_\lambda} \eta \qquad (2.4)$$

and η is the average efficiency of conversion of X-ray energy to light at the photocathode (3.6% in this instance). By definition the quantum efficiency, $Q(\lambda)$, for a photocathode is the number of emitted photo-electrons per incident photon of wavelength λ, hence the electric charge from the cathode, C, is given by

$$C = N_{ph} e Q(\lambda) \qquad (2.5)$$

where e is the charge on an electron, 1.6×10^{-19} Coulombs. Using equations 2.3 to 2.5, the spectral response of the photocathode (fig2.4) and the spectral emission of NaI, the relationship between the apparent X-ray energy dissipated in the crystal and the photocathode output charge may be found. Assuming the crystal energy conversion efficiency is constant andthe NaI light emission has an average energy of 4.84×10^{-19} Joules for which the quantum efficiency is 20%, this relationship,shown in fig 2.10, is linear.

A pulse from the photocathode is amplified in the photo-multiplier before it reaches the counter electronics where it has to have an amplitude greater than the discriminator threshold to be counted. The amplification in the photomultiplier is strongly affected by the EHT voltage and can be found from the photomultiplier gain curve, fig 2.5. If the discriminator is set to a certain value of input charge, C_d, this will be equivalent to a threshold on the photocathode output charge,

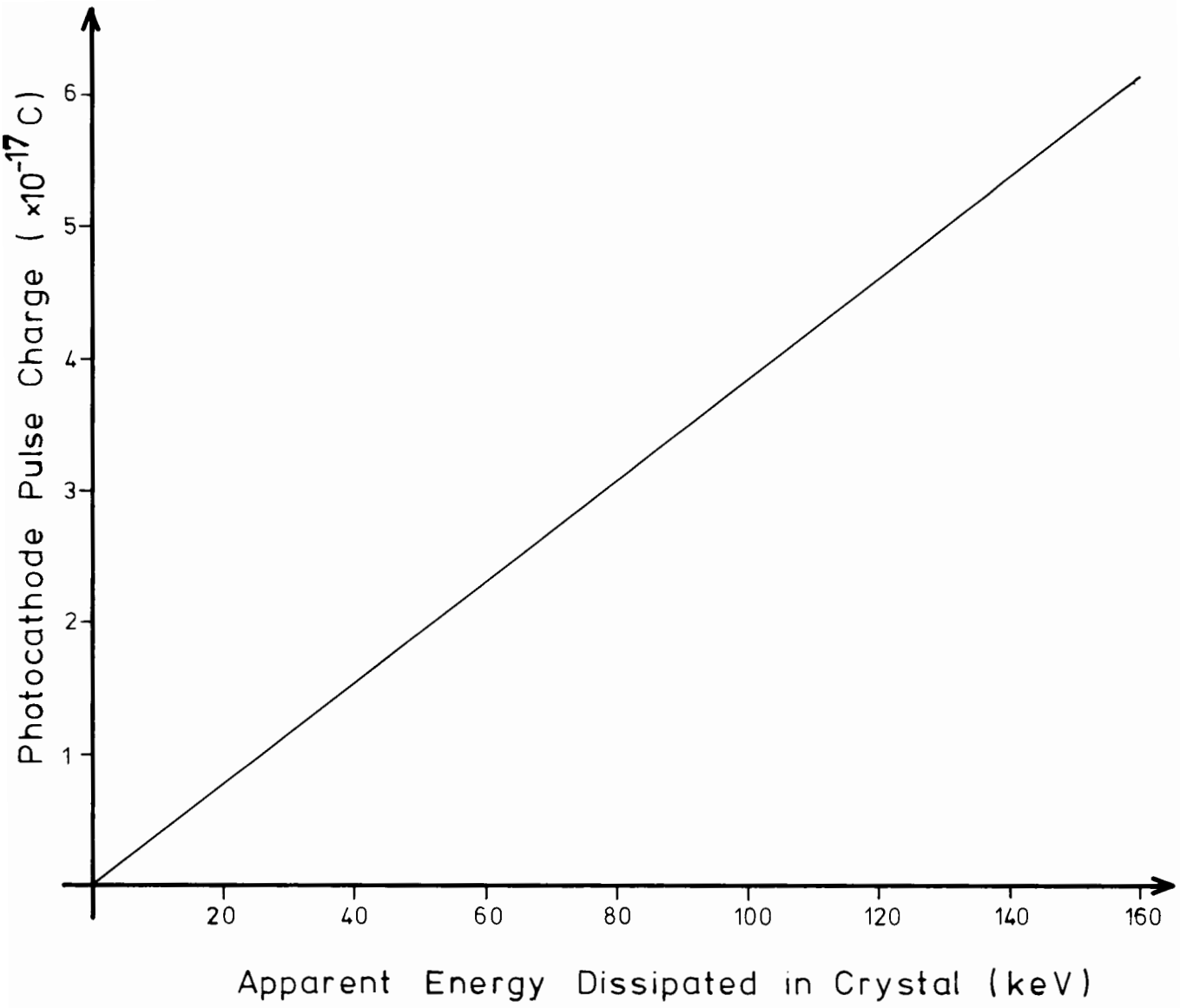


Fig 2.10. Photocathode Charge vs Apparent Energy Dissipation.

C_{th}, given by

$$C_{th} = \frac{C_d}{G} \qquad (2.6)$$

where G is the photomultiplier gain. In this instance, with a discriminator value of 2μμC and the gain curve in fig 2.5, the plot of threshold photocathode charge for varying EHT voltage is given in fig 2.11

A plot of count rate versus EHT can now be drawn, fig 2.12, for the scintillation counter described above subject to the given X-ray energy input. For a given EHT value the photocathode charge threshold is found from fig 2.11. Fig 2.10 then gives the apparent X-ray energy dissipation corresponding to this threshold. Finally the count rate is determined by reference to fig 2.9 which gives the number of pulses reaching the photocathode with more than the equivalent of this energy.

Clearly the best operating conditions for the scintillation counter will be on the count rate plateau in fig 2.12. Slight variations in EHT supply will not affect the count rate much, but equally important is the effect of a slight variation in the X-ray energy distribution, which is equivalent to moving along the EHT axis. Increasing the discriminator threshold will move the plateau to a higher value of EHT. The beneficial effect of the filter on the X-ray beam described in section 2.1.4 is now evident. A larger proportion of lower energy radiation would mean a steeper slope on the low energy section of the curve in fig 2.9, hence the derived count rate plateau would not be as flat.

Figures 2.19 to 2.21, which are discussed in section 2.1.9,

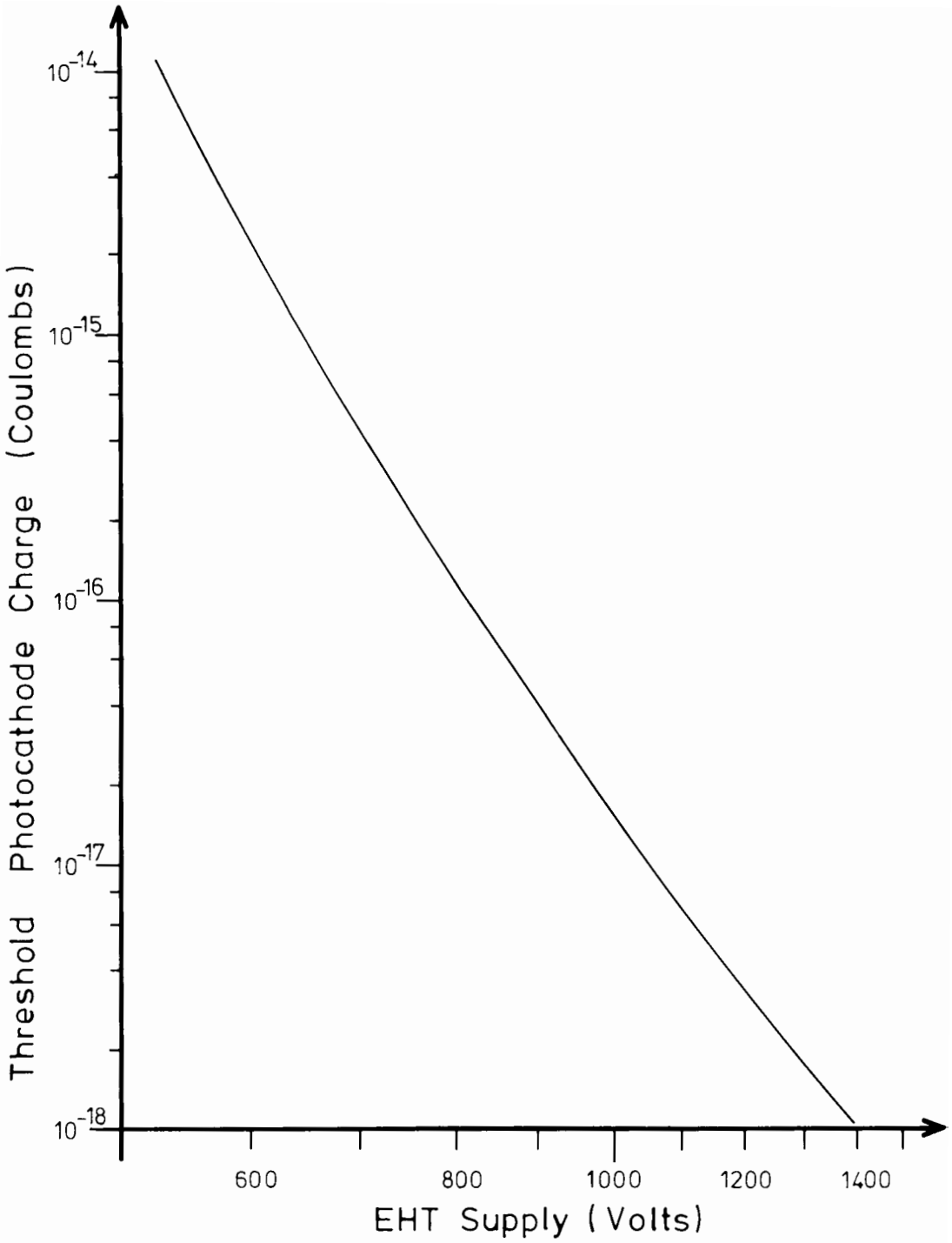


Fig 2.11. Photocathode Threshold vs EHT for 2μμC Discriminator.

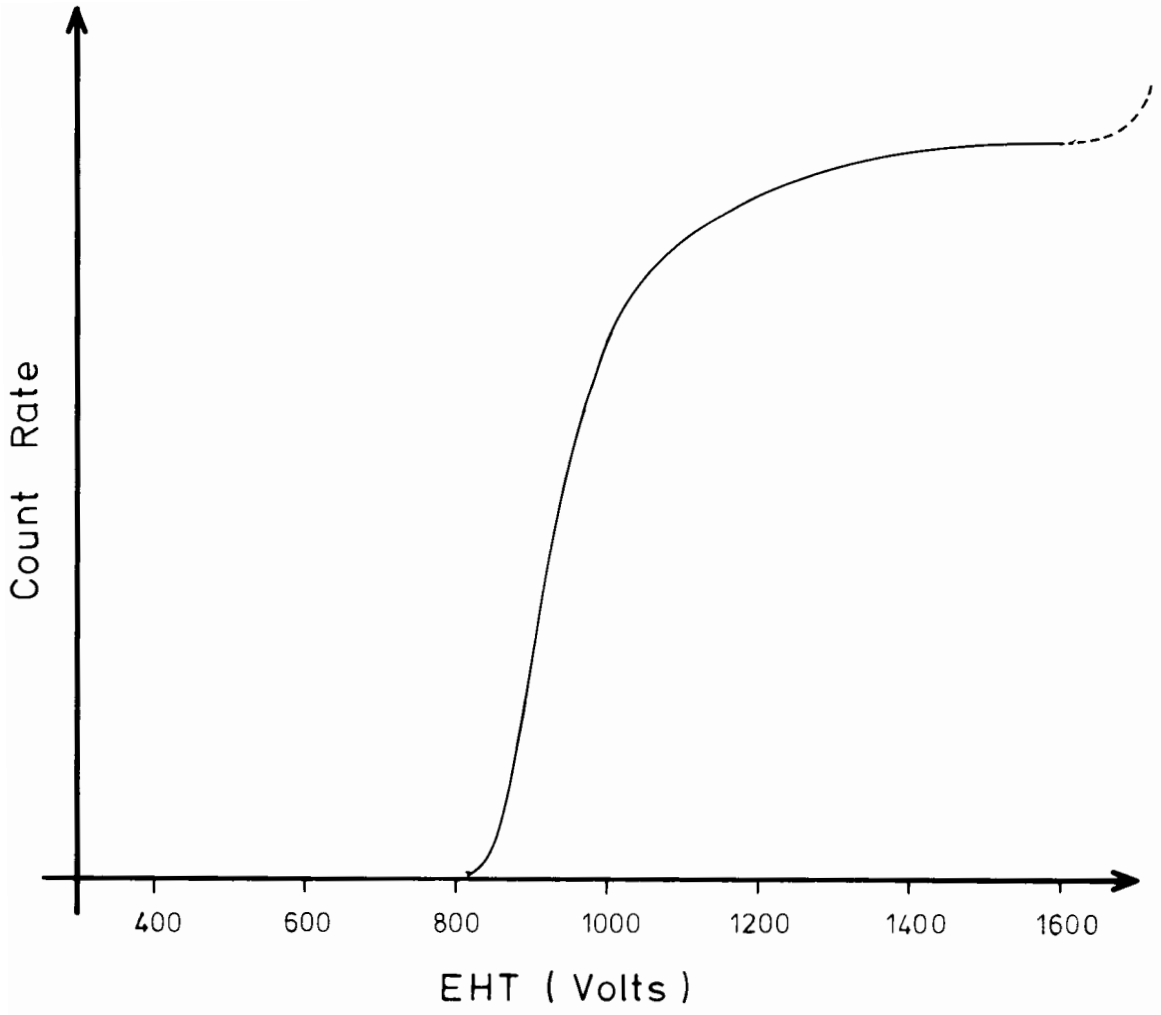


Fig 2.12. Calculated Count Rate vs EHT Curve.

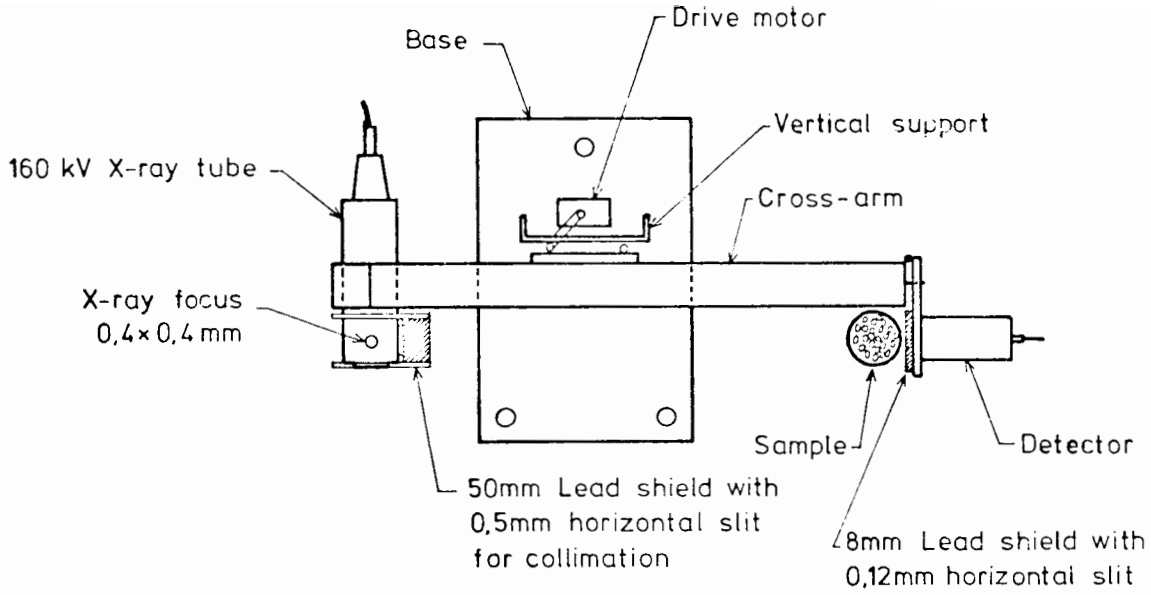
show the actual EHT/count rate curves obtained with this apparatus.

2.1.6 Geometry and Collimation of the System

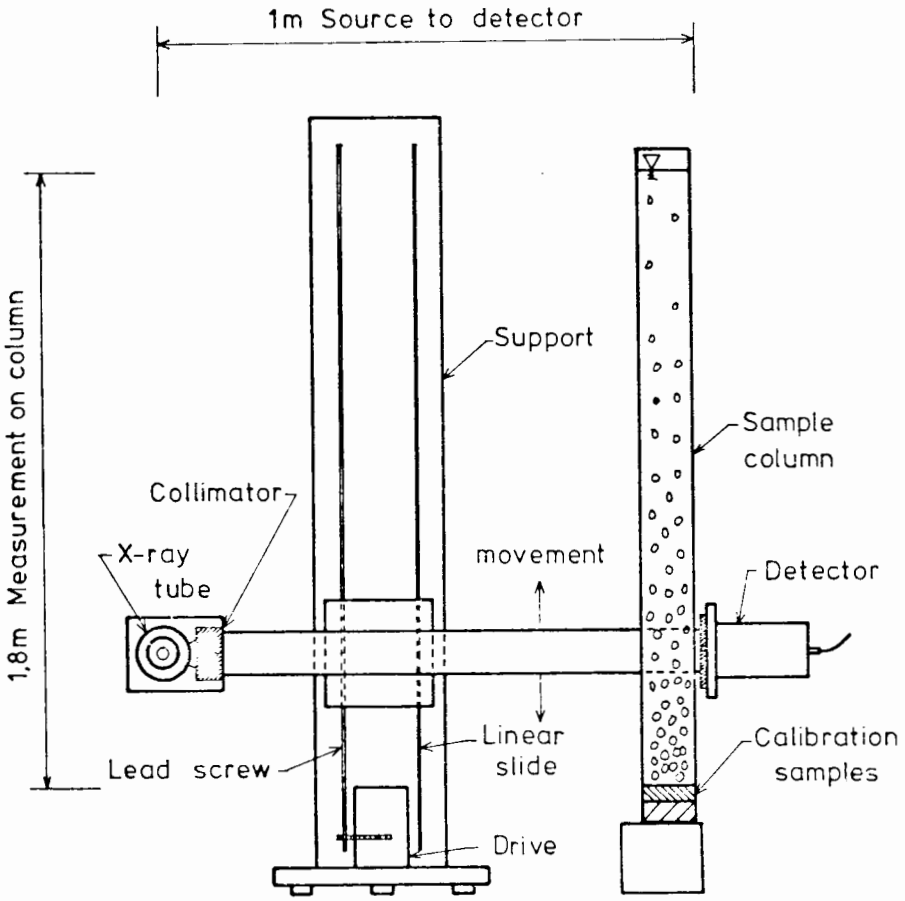
Good collimation of the radiation and ability to traverse a 2 m long settling column were the basic layout requirements of the density measuring system which is shown schematically in fig 2.13.

Collimation serves several purposes. Firstly by reducing to a minimum size the emergent beam from the source, there is less chance of radiation reflected from surrounding equipment reaching the detector. The equation for narrow beam attenuation, which is necessary to make a simple theoretical check on the experimental absorption, can only be applied to a system in which the collimation ensures that a negligible quantity of radiation scattered within the sample reaches the detector. Finally the spatial resolution of the density measurement is clearly determined by the degree of collimation.

Figure 2.14 shows the collimation geometry of the system, but one must bear in mind that the beam is collimated by slits, not circular holes, and is thus a narrow rectangle in section. At the X-ray source the collimator consists of two blocks of lead (with a small quantity of copper to harden it) machined from a 50 mm lead brick. These are bolted with two permanent 0.5 mm spacers to a dural framework rigidly fixed to the X-ray tube, Plate 2.15(a). A fixed safety collimator between this and the source limits the horizontal spread of the



(a) Plan



(b) Elevation

Fig 2.13. Layout of Density Apparatus.

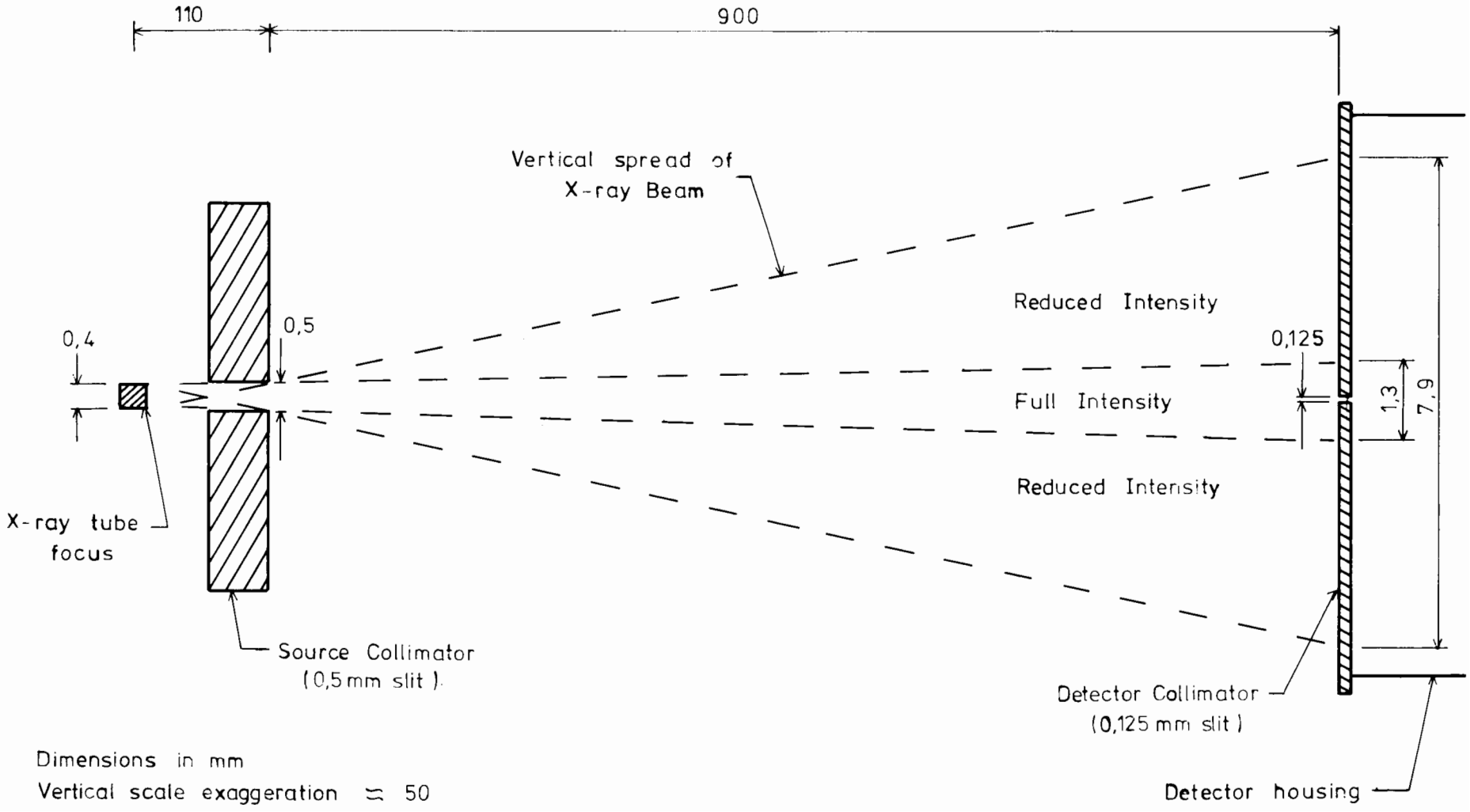
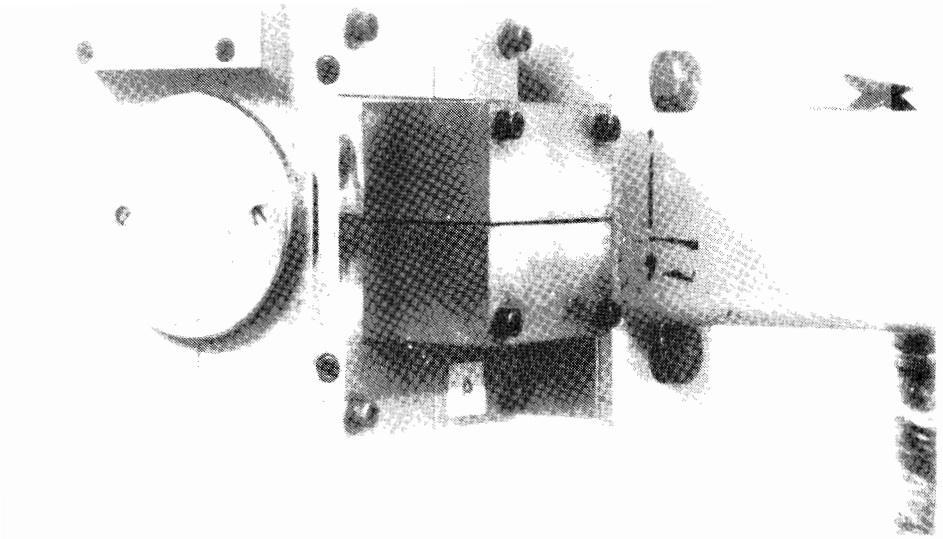
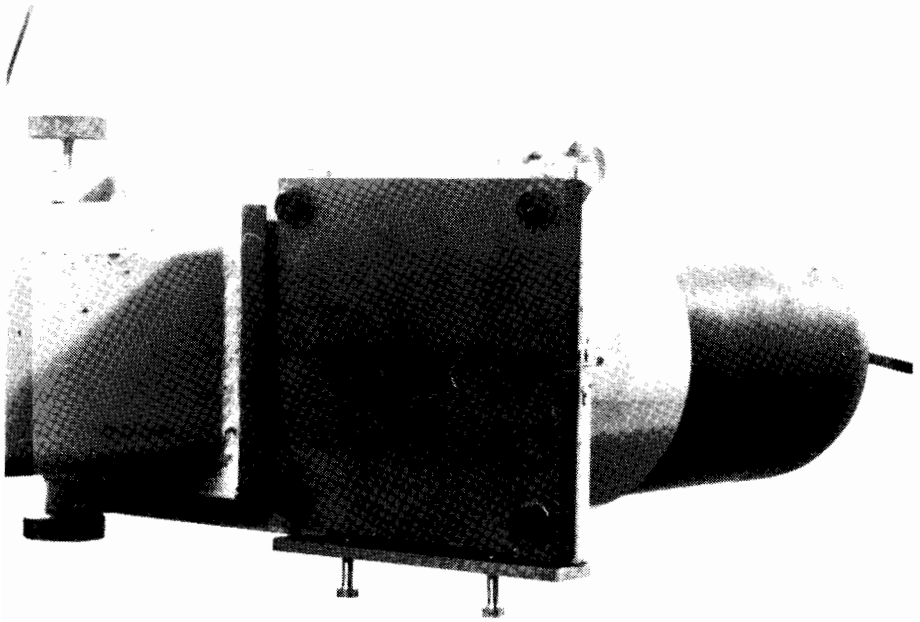


Fig 2.14. Collimation Geometry of System.



(a) Collimator at X-ray Tube



(b) Collimator at Detector

Plate 2.15. Collimators.

beam. Except for the aluminium window over the NaI(Tl) crystal, the scintillation detector is completely enclosed in a 3 mm layer of lead. Collimation in front of the window is again by machined lead blocks mounted to the detector holder, held 0.125 mm apart by two spacers, Plate 2.15(b). However the position of this slit can be adjusted by means of two screws on a plate below the lower block. Once the correct position is found the mounting bolts are tightened.

The X-ray tube, detector and collimators are mounted on a single arm to keep their relative positions fixed. This arm is part of a free standing rig, shown in plate 2.16. An electric driven lead screw moves the arm vertically up and down through a distance of 1.8 metres at speeds which can be set by a sliding potentiometer. Height of the arm relative to a datum is determined to the nearest millimetre with a potentiometer geared to the lead screw. Because the X-ray and rig were originally intended to be used mainly for strain measurements using heavy metal markers, the system is a modification of the design for that purpose and as such is not ideally suited to the present use, with a narrowly collimated beam and fixed horizontal position relative to a settling column.

In a detailed chapter on the theory of collimation for granular material, Sirwan (1965) shows that the source and detector should be placed as far apart as is compatible with an adequate counting rate and that the sample should be midway between source and counter, which was impractical in this case. Nevertheless, effects such as this become less important as the ideal conditions of narrow beam radiation are approached and would not significantly affect this system.

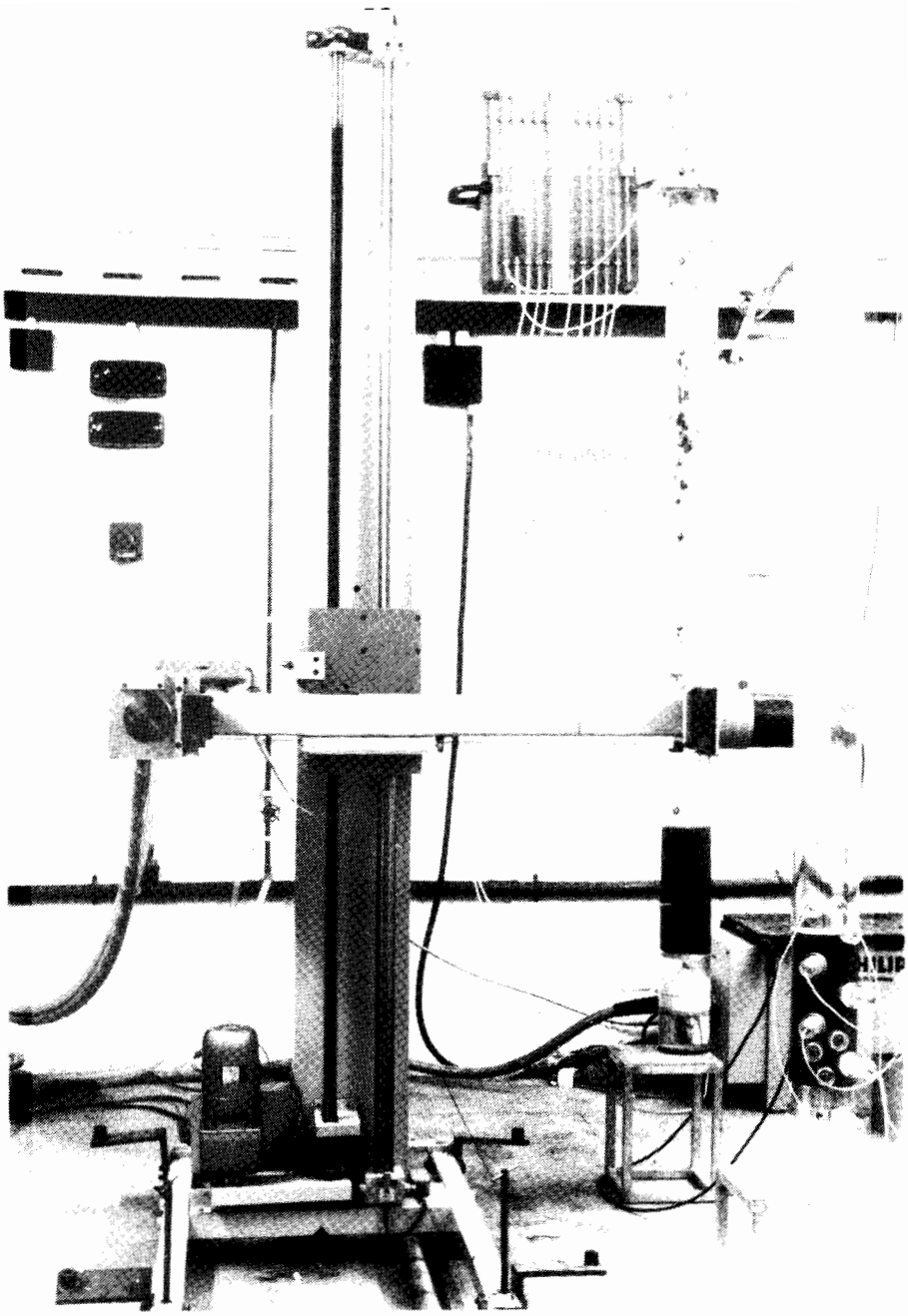
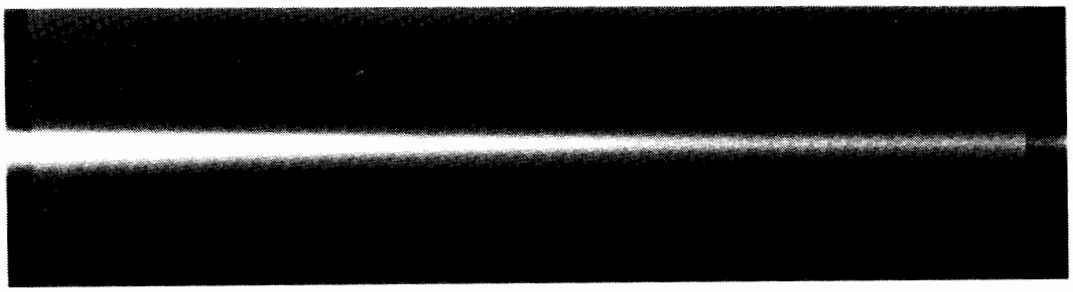


Plate 2.16. X-ray Density Apparatus.

Based on the collimation geometry of fig 2.14 and linear propogation, the cross section of the X-ray beam reaching the detector would be an 8 mm band of radiation but only a 1.3 mm wide band of maximum intensity radiation. This would not occur if the radiation were from a point source. Plate 2.17(a) shows the actual radiation beam that reaches the detector collimator. This is different from the calculated pattern which does not take into account a possible eccentricity of the source, intensity variations with angle of emergence and diffraction. The collimator for the detector must be accurately positioned to coincide with the narrow intense band shown in the photograph. This was done by trial and error and Plate 2.17(b) shows a photograph exposed behind the collimator with the ends protruding to check the alignment of the collimator slit.

2.1.7 The Laboratory

Exposure to X-rays can be extremely dangerous, so the room which contained the X-ray equipment had to be fully enclosed with lead shielding or concrete bricks to prevent radiation leaking, and also had interlocking safety systems so that the X-ray tube could only be operated from outside the room with the door shut. Besides the obvious disadvantage of not being able to see the equipment in action, all the controls and counting equipment were outside the shielded room. Long electrical leads were needed for this, resulting in more electrical noise pickup than might otherwise occur. The room was also not ventilated and considerable temperature variations occurred when the X-ray was on, before



(a) X-ray Beam Reaching Detector Collimator



(b) X-ray Beam Collimation at Detector

1. Higher contrast of print shows widening of the intense radiation band to right hand side which is not apparent on a radiograph.

2. Scintillation counter crystal spans central 75 mm of slit.

3. Slit is barely visible due to loss of definition in the photographic process.

4. Breaks in the slit near the ends are the 0.125 mm spacers between the lead blocks.

Plate 2.17. X-ray Beam at Detector.

(Prints from Radiographs)

the recycling water cooler was replaced with a water to waste system.

Electricity supply to the laboratory was not filtered in any way and spikes on the mains supply frequently triggered the counter, gave a spurious reading, or affected the X-ray generator stability. Fortunately such effects could usually be identified and data rejected accordingly. Installation of a separate earth to the building appeared to be of little value.

By far the most serious problem was pickup by the scintillation counter of high frequency signals from the welding bay next door to the laboratory. It was impossible to take density measurements during welding operations.

2.1.8 Calibration

For the geometrical arrangement detailed in section 2.1.6, equation 2.2 can be expressed in a slightly different way.

$$N = N_o e^{-\mu_m \gamma D} \qquad (2.7)$$

N_o = mean count rate with no sample in the settling column

N = mean count rate with sample present

μ_m = sample mass attenuation coefficient

γ = sample bulk density

D = sample diameter

The choice of an X-ray source and scintillation counter technique (section 2.1.3) means that an empirical calibration of count rate to density is required, and equation 2.7 suggests that a calibration curve of density against the logarithm of count rate might be informative.

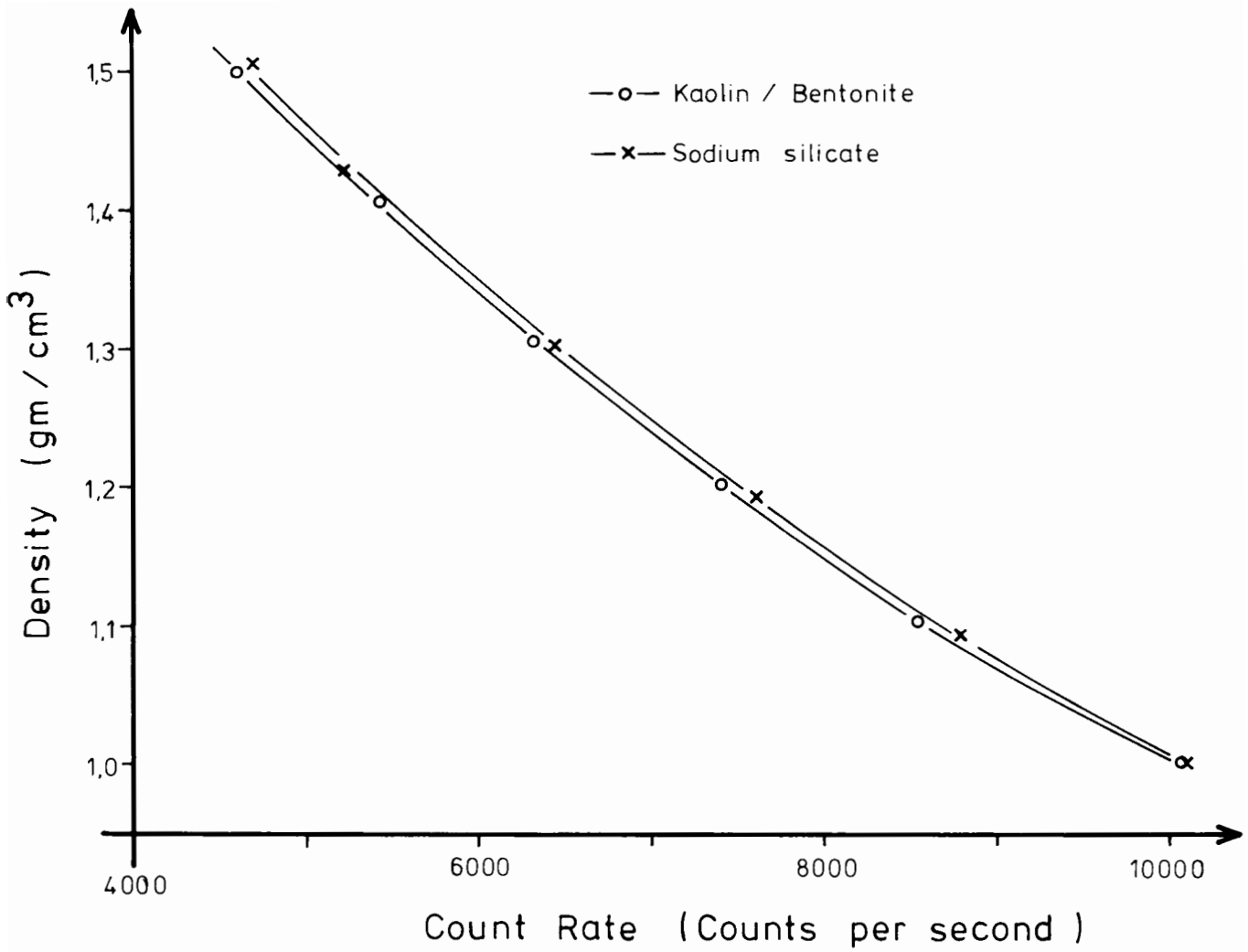
Calibration samples must be carefully chosen so that they have similar absorption qualities to the soil being used and must be such that known uniform densities from 1.0 to 1.5 gm/cm^3 can be permanently maintained. In addition the calibration specimen must be in a container of the same dimensions and material as the settling column. Variations in soil bulk density are associated with changes in moisture content, so aqueous solutions of Sodium Silicate were first used for calibration. Reference to figure 2.1 and the fact that soil minerals contain a large percentage of silicon, indicates that sodium silicate solutions in water would have similar absorption qualities to slurries of soil in water, although a sodium silicate solution at a certain density will not have the same water content as soil at that density.

Liquid solution calibration for a soil density device is, however, not entirely satisfactory. Krinitsky (1972) mentions an unevaluated effect on the absorption coefficient of high porosity in soils and the work of Coumoulos (1967) shows that the attenuation of X-rays by a multiphase material is not simply the sum of the effects of each individual phase. A soil that will remain at a constant density as low as 1.1 gm/cm^3 is needed. Tests with bentonite slurries showed that at a moisture content of 6, corresponding to a density of 1.1gm/cm^3, the mixture was too stiff and sticky to make a uniform sample. In

contrast, kaolin at a density of 1.5 gm/cm^3 is the correct consistency for a sample but consolidates if left undisturbed for a long time. Mixtures of kaolin and bentonite in the correct proportions to give the required properties were therefore used for calibration samples.

Five aqueous solutions of sodium silicate and five kaolin/bentonite slurries were made up at different densities and sealed in short sections of a settling column (102 mm I.D. acrylic tube). Sodium silicate solution densities were determined to ±0.0005 gm/cm^3 by weighing 3 samples at each density in 50 ml density bottles. Kaolin/bentonite slurry densities were measured to 0.001 gm/cm^3 by calculation from the average water contents of three samples at each density. The specific gravity of bentonite was taken as 2.73 and of kaolin as 2.60 after Makower et al (1937) and De Wit et al (1950). The table in figure 2.18 shows the relevant information about kaolin / bentonite calibration specimens. Two sodium silicate and one kaolin sample became suspect after a few months. Precipitates formed in sodium silicate solutions at 1.091 and 1.189 gm/cm^3, and the pure kaolin slurry at 1.501 gm/cm^3 consolidated to the extent that there was free water clearly visible in the container. Comparison with earlier calibration curves confirmed that a change in density had occurred in the kaolin.

Typical linear-linear and log-linear count rate versus density curves are shown in fig 2.18. Both methods of calibration give points remarkably close to a straight line on the log-linear axes. The implication of this from equation 2.7 is firstly that the assumption of narrow beam conditions is valid and secondly that the mass absorption



KAOLIN AND BENTONITE STANDARD DENSITY SLURRIES.			
Dry Weight Ratio Kaolin : Bentonite	S.G. of Solids G_s	Average Moisture Content	Density gm/cm^3
Tap water only			0.9984
1 : 1.66	2.68	5.9085	1.102
1 : 0.259	2.63	2.7178	1.202
1 : 0.091	2.61	1.6625	1.304
1 : 0.0296	2.60	1.1346	1.407
Kaolin only	2.60	0.8505	1.501

NOTE. G_s = 2.60 for Kaolin and G_s = 2.73 for Bentonite.

Slurry at 1.501 gm/cm^3 was unsuitable because of slow consolidation

Fig 2.18(a). Density Calibration Curves.

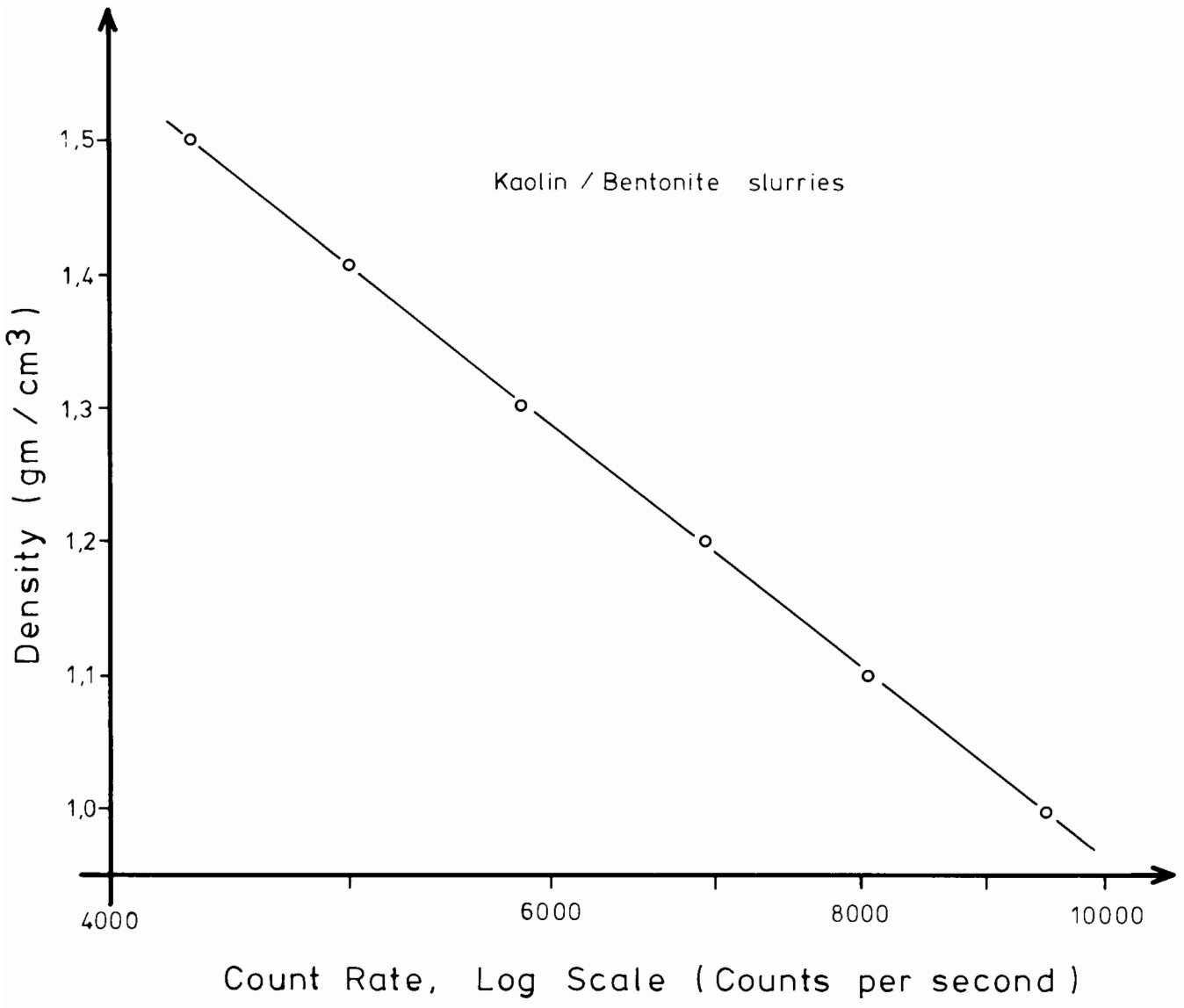


Fig 2.18(b). Density vs Log of Count Rate.

coefficients do not vary significantly as the bulk density changes, although it is possible that the two effects work in opposition and mask any deviations. Both lines have slightly different slopes as would be expected from different chemical and physical samples. Calculation of the mass absorption coefficient from these slopes gives a value of 0.15 cm^2/gm, which compares well with a value that might be predicted from the absorption coefficients in fig 2.1.

Regular calibration checks on the system with kaolin/bentonite mixes were performed. Although the slope of the line was consistent, the line was in a different position every time the X-ray tube was switched on. At least two calibration samples were therefore always placed at the bottom of a settling column to give reference points for the position of the line.

It remains to assess the effect on the absolute bulk density, rather than changes in density, determined for a soil using kaolin/bentonite mixtures for calibration. Maus et al. (1973) show that the chemistry of most sediment compounds is such that they have similar Compton attenuation qualities. For X-ray energies below about 100 keV photoelectric absorption in soils is also an important process and examination of the absorption coefficients of fig 2.1 indicates that variations in chemical composition are likely to have a greater effect at lower energies. The manner in which the lead filter over the X-ray source (section 2.1.4) aids calibration by absorbing most of the lower energy radiation is now evident. Checks on the absolute values of the density, by comparing load cell measured pressures with pressures calculated

by integrating density profiles of soil in the settling column, revealed no discrepancy within the accuracy of the density measurements.

If the checks had shown that densities in other soils are not being determined accurately using kaolin/bentonite mixtures, special calibration samples could be made simply by adding small quantities of bentonite to produce the right consistency in slurries of the particular soil. Soils containing heavy metals might well require such calibration.

2.1.9 Performance

Operation of the scintillation counter on a count rate plateau, see section 2.1.5, is essential if count rates are to be meaningful. Variables such as radiation energy and intensity and ratemeter time constants will also necessarily affect the performance of the equipment in terms of speed and accuracy, subject to a plateau existing for any condition.

Variation of Radiation Energy and Intensity

Figure 2.19 shows count rate against EHT supply curves for the apparatus. All the curves are similar to the curve in fig 2.12, which is a calculated curve for a 160 kV X-ray tube setting, and show that a good counting plateau exists for X-ray tube voltages between 100 kV and 160 kV. Removing the lead filter on the X-ray source and changing the discriminator threshold affects the plateau in the manner shown in

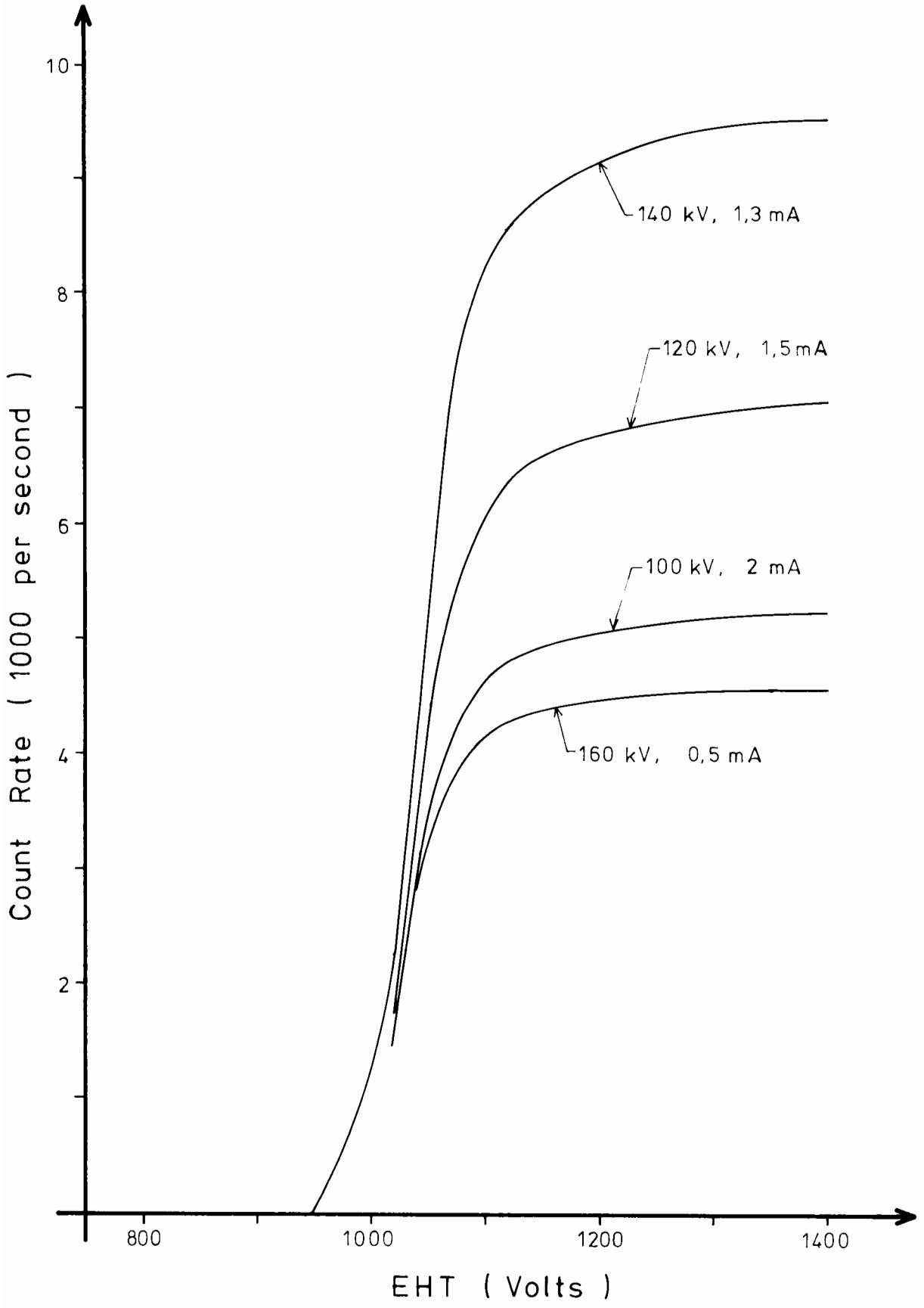


Fig 2.19. Count Rate vs EHT. X-ray Voltage Varying.

(Anode Current Adjusted Accordingly)

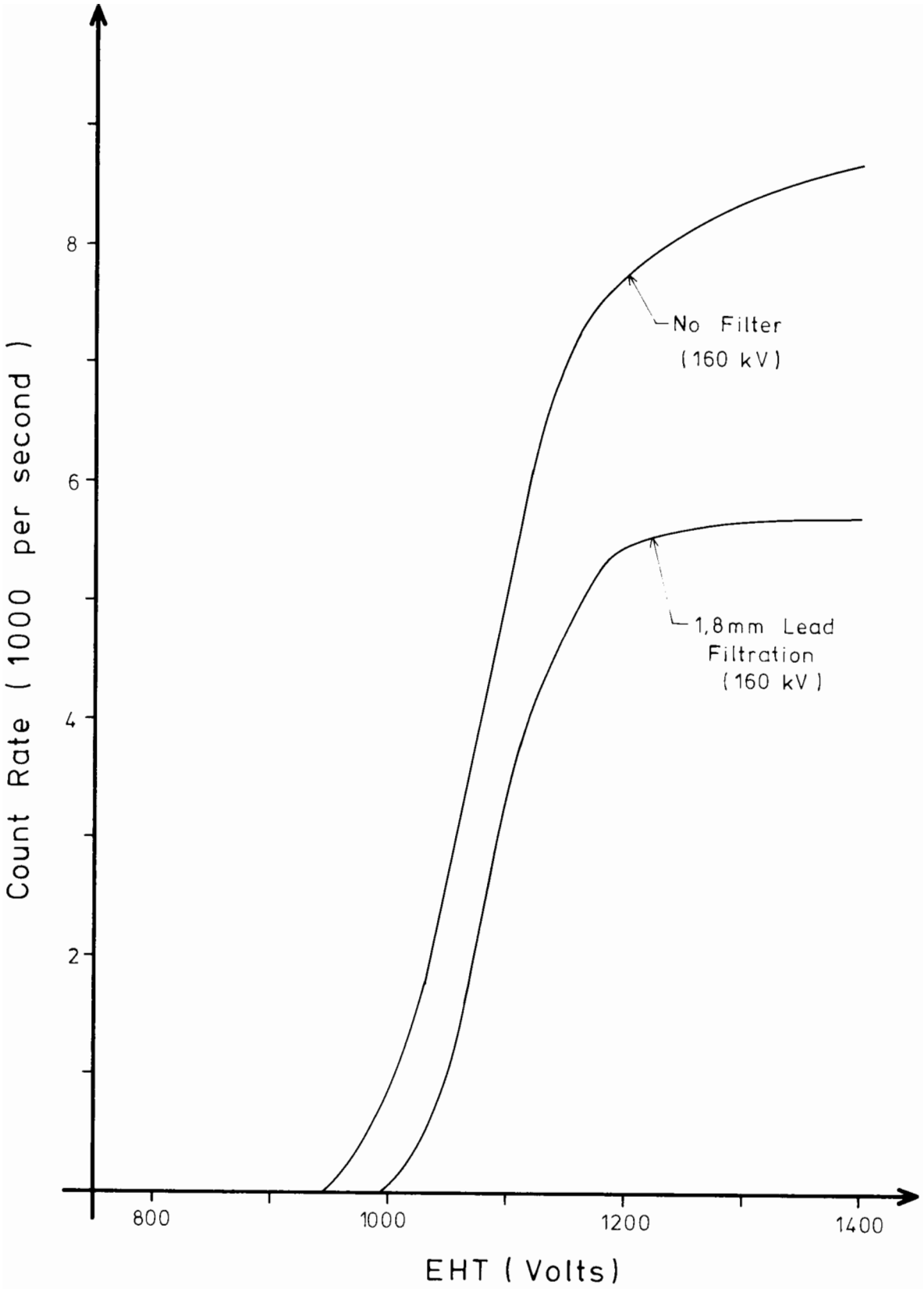


Fig 2.20. Count Rate vs EHT. Effect of Filter on Beam.

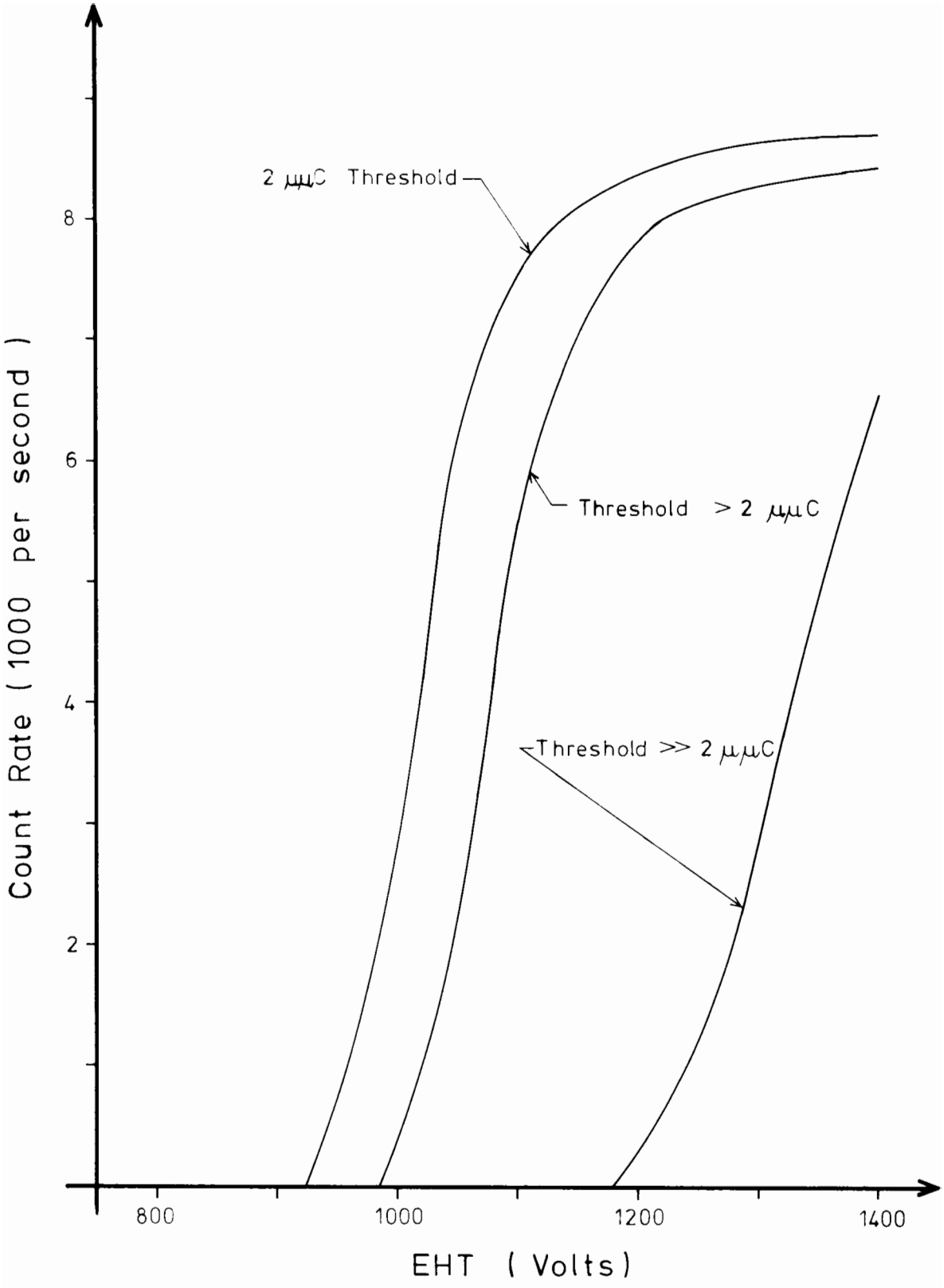


Fig 3.21. Count Rate vs EHT. Discriminator Threshold Varying.

fig 2.20 and fig 2.21 respectively. For the present equipment the optimum operating conditions for the scintillation counter are thus at an EHT of 1400 volts, the lowest setting of discriminator threshold and with a lead filter over the source. These settings are suitable over the range of X-ray energies being considered and therefore remained unchanged in all further work. Further tests with these values on samples of soil at different densities confirmed their suitability.

The effect of the X-ray tube voltage on the observed count rate is shown in fig 2.22. There is no obvious conclusion about optimum values to be drawn from this graph. Consideration given to mass absorption coefficient curves in the previous sections indicates that a higher X-ray tube potential difference would be best from the point of view of calibration and stability of count rate. On the basis of this an operating voltage of 160 kV was used.

Radiation intensity can be altered simply by the current regulator on the X-ray tube. Figure 2.23 shows how count rate varies with anode current at different voltages. Factors which affect the choice of a suitable maximum or minimum count rate are the statistics of counting and the capabilities of the scintillation counter. In this instance, the Harwell 2134-6 linear ratemeter which was used for analogue output had a maximum count rate capability of 15000 counts per second, but only 10000 counts/sec if the back bias was not used. Higher count rates could be determined with the 2117-4 Scaler.

If one assumes that the generation of X-rays is a random

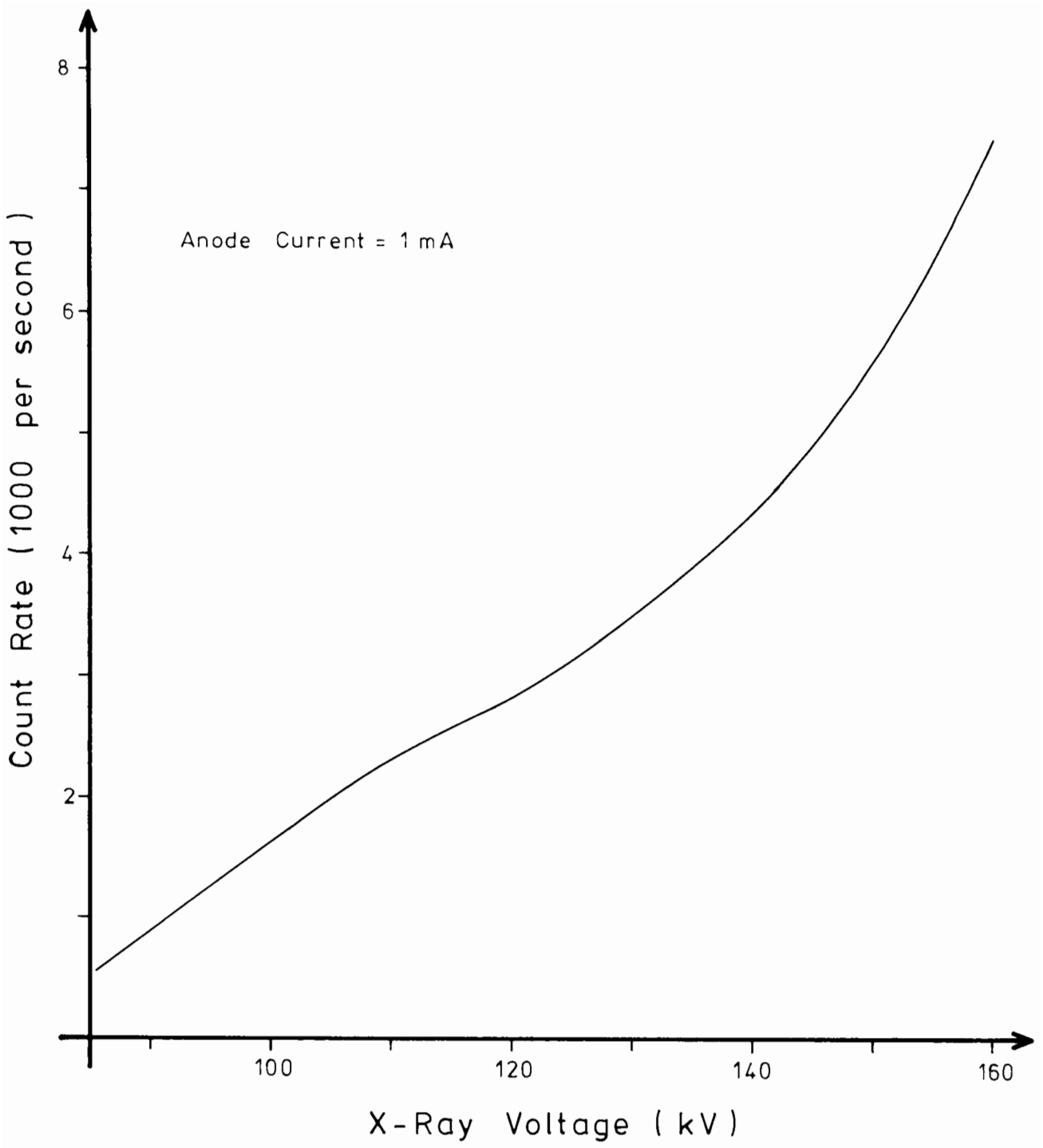


Fig 2.22. Count Rate vs X-ray Voltage.

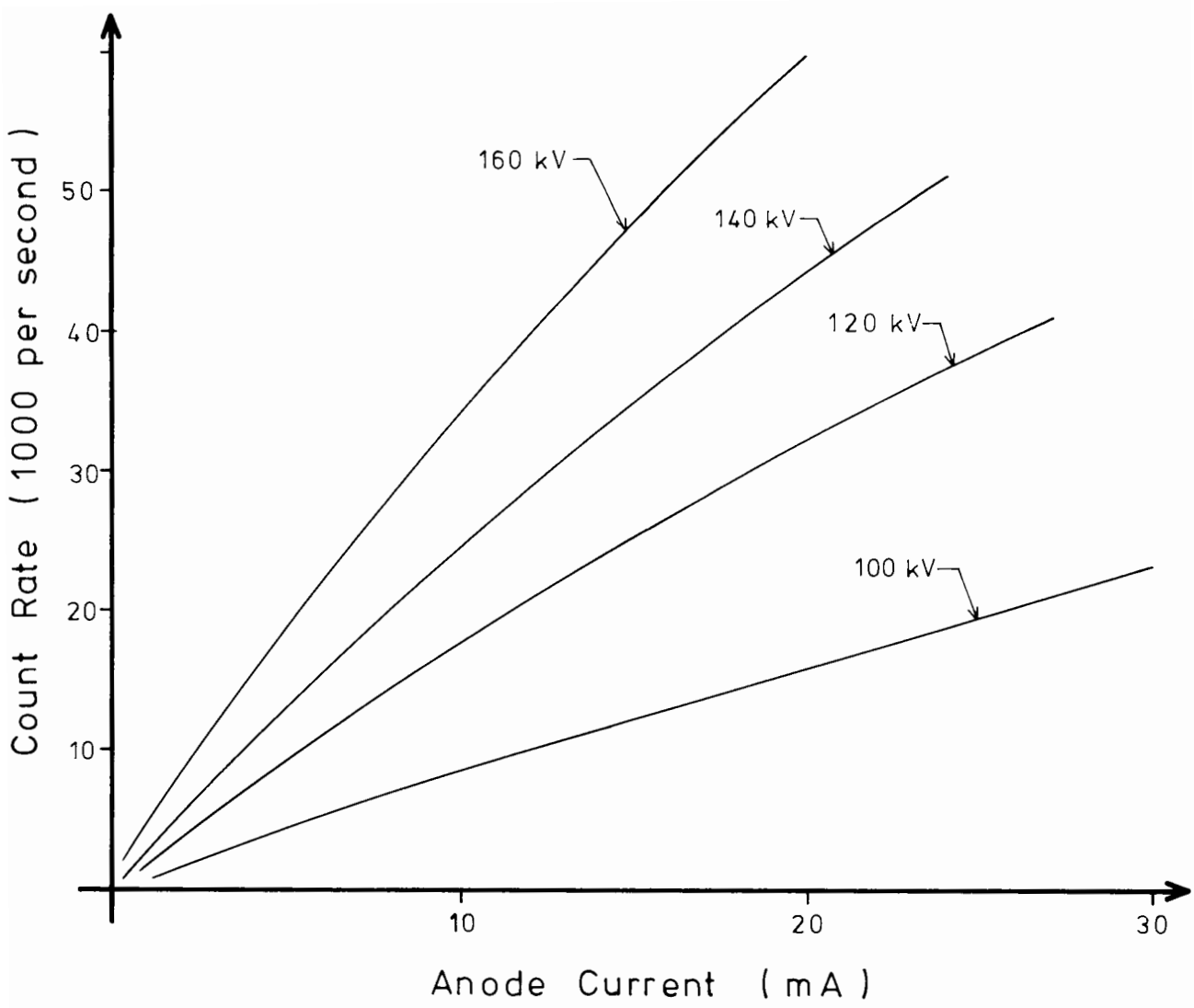


Fig 2.23. Count Rate vs Anode Current.

process, which is reasonable since X-ray photons are produced by electron collisions in the X-ray tube target, then errors in count rate determinations can be found using the normal distribution. The percentage error in the count rate will be inversely proportional to the square root of the total number of counts (Kohl et al, 1961, chapter 4), so a higher count rate will be advantageous if quick measurements are required.

There is an upper limit to the useful count rate determined by the recovery time (dead time) of the instrument. Kohl et al (1961) give the true mean count rate, N_t , as

$$N_t = \frac{N}{1 - Nt_r} \qquad (2.8)$$

where N = observed mean counting rate

t_r = instrument dead time

Equation 2.8 is valid if pulses are at random intervals, in which case the difference between the true and observed count rate will be taken into account by the calibration procedure anyway. This dead time loss is possibly another factor that contributes to the linearity of the calibration curves discussed in section 2.1.8. The non-linearity of the current/count rate curves in figure 2.23 is mainly due to counts lost in this way. For the present apparatus with a dead time of 3.5 μsec, about 3.4% of counts are lost at a count rate of 10000 per second.

In practice it was found that the count rate was limited by the photomultiplier tube characteristics. Large average currents

through the tube alter the efficiency and gain characteristics of the tube and a suitable count rate plateau could not be found for count rates over about 40000 per second. Typical examples of this behaviour of the photomultiplier are shown in figure 2.24.

An X-ray tube current corresponding to a maximum count rate of about 10000 counts per second was used in the present work, as it is sufficiently low for the photomultiplier operation to be stable and high enough to allow count rate determinations to be made quickly. This value is also high enough that variations in the background count rate (12 counts per second) would not significantly affect the accuracy of measurements. The calibration procedure does take account of the background count.

Choice of Time Constant

A time constant used for a density profiling system must be a compromise between a long time for accuracy in a constant density and a short time for a quick response to changes in density.

For variations in recorded ratemeter output for a constant density, the standard deviation, σ, for a single reading is given (Kohl et al, 1961) by

$$\sigma = \sqrt{\frac{N}{2RC}} \qquad (2.9)$$

N = mean count rate

RC = time constant

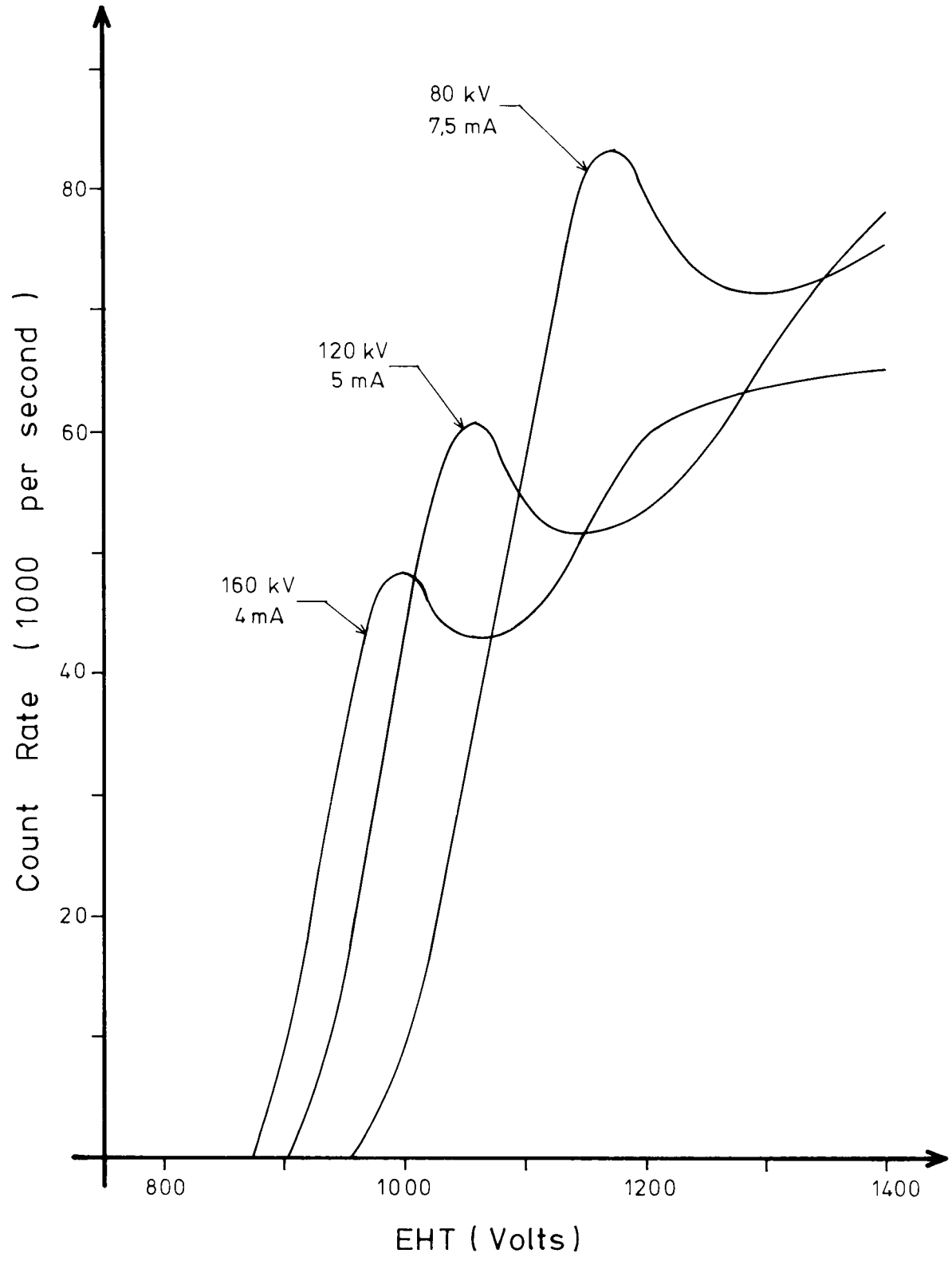


Fig 2.24. Photomultiplier Saturation at High Count Rates.

When the time of observation T is much greater than RC, the standard deviation as a proportion of the mean recorded rate is given by

$$\frac{\sigma(T)}{N} = \sqrt{\frac{1}{NT}} \qquad (2.10)$$

where NT represents the total number of counts measured in time T. Fig 2.25 is a graph of the percentage error within the 95% confidence limit (two standard deviations) against counts recorded based on equation 2.10.

When the input to the ratemeter is changed from N_1 to N_2 corresponding to a step change in density, the output mean count rate, N, is

$$N = N_2-(N_2-N_1)e^{-\frac{t}{RC}} \qquad (2.11)$$

From this the time taken for the meter to read to within one standard deviation of N_2 is given by

$$t = RC \ln\left(\frac{N_2-N_1}{\sqrt{N_2}}\right)\sqrt{2RC} \qquad (2.12)$$

For example if the count rate changes from 7000 to 8000 per second, the response time to one standard deviation will be 2.8 seconds for a 1 second time constant and 0.4 seconds for a 0.2 second time constant.

The minimum traverse speed of the arm with the X-ray and scintillation detector described in section 2.1.6 is approximately

Fig 2.25. Error in Count Rate, 95% Confidence Limit.

10 mm/second, which allows a complete profile to be plotted in under 4 minutes. Mud settling rates of over 2 mm/minute make this sort of profiling speed necessary. In order to register density changes within the space of a centimetre, a time constant of 0.2 seconds is desirable, but this results in unacceptably large deviations from the true density on the recorded ratemeter output. A time constant of 1 second was found to be a suitable balance between speed and accuracy for the present work. Distortion of the profile can be reduced by plotting density on an upwards as well as downwards traverse and also by halting the movement for a few seconds immediately after a step change in density. Hence applying the principles described by equations 2.9 to 2.12, a satisfactory density profile was derived from the plotted ratemeter output. A typical recorded profile and estimated density profile has been reproduced in fig 2.26

Accuracy

It is difficult to quantify the spatial resolution of the density measuring equipment described above, because of the complex, random nature of scattered radiation. An estimate can be made by considering the angle of acceptance of radiation by the collimator in front of the detector. The collimator is a 0.125 mm wide slit in 8 mm of lead. The side of the column furthest from the slit is approximately 120 mm away so that scattered radiation from that side of the column will only reach the detector directly if it is less than 1 mm above or below the slit. A conservative value for the resolution would therefore be ±1 mm along the settling column axis. There would be little advantage in

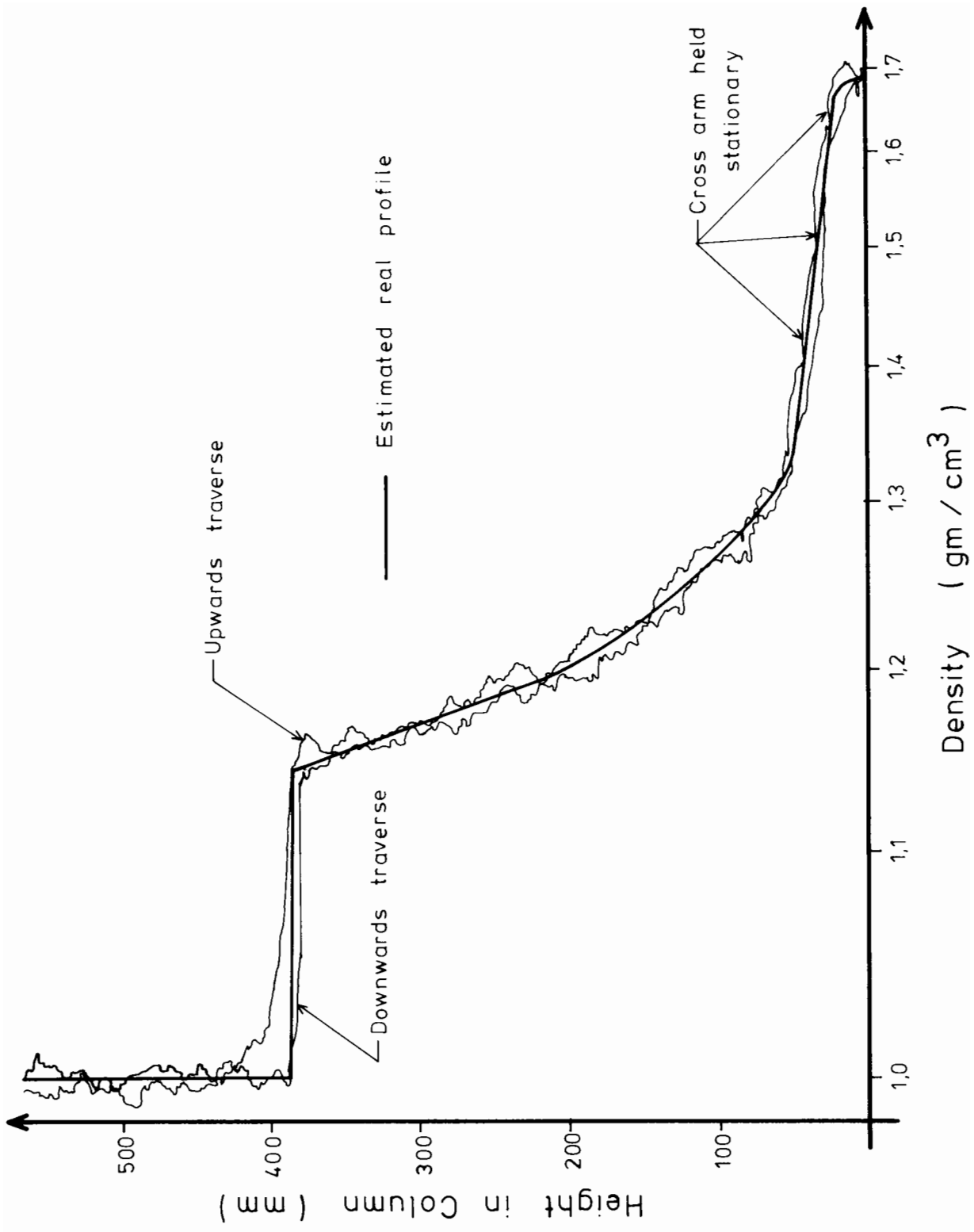


Fig 2.26. Typical Recorded Density Profile.

improving on this value for the present setup, as positioning of the cross-arm (± 0.5 mm) is only slightly more accurate and in most applications the arm is moving.

Any particular constant density can be determined to the desired degree of accuracy simply by taking a large enough count, provided the calibration is as accurate and the X-ray power drift is negligible. An estimate of the error for a certain total number of counts can be made from fig 2.25. By counting between 10^5 and 10^6 counts, errors in count rate are from 0.1% to 0.6%. From the calibration curves in fig 2.18, a 0.6% error in count rate is equivalent to a density error of 0.004gm/cm^3 over the range considered. The densities of the calibration samples (section 2.1.8) were determined to 0.001 gm/cm^3, which is a comparable order of magnitude. Greater precision is not warranted as densities measured to the fourth significant figure fluctuate with temperature variations.

Error estimations in the preceding paragraph are only valid if the mean X-ray intensity is constant while the measurement is made. Recordings of count rate in a constant density over periods of 1 hour show fluctuations in the mean count rate ± 0.7% about a constant average of the mean rates. Such fluctuations last for periods of a few minutes or less, while the average for any 20 minute period would be constant. This 0.7% fluctuation in mean count rate, which is equivalent to a density error of 0.005 gm/cm^3, is the limitation on the accuracy of the equipment for density measurement. From fig 2.22 this ± 0.7% fluctuation could be the result of a potential difference change of less than 0.2%

at the X-ray tube, giving an indication of how important stabilisation of the X-ray source is. This level of stability could not be achieved with a recirculating water cooler for the tube.

With the apparatus stationary and a counting time of 100 seconds, the overall accuracy of a density measurement will be ± 0.005 gm/cm^3 with a spatial resolution of ± 1 mm. However with a time constant of 1 second, plotting a density profile as described at the end of the previous sub-section, the density profile will be accurate to 0.01gm/cm^3 with a spatial resolution of 10 mm.

2.2 PRESSURE MEASUREMENT

Preliminary settling experiments with simple pore water pressure standpipes allowed an assessment of the requirements of the pore pressure measurement system. Although they were sufficiently accurate, standpipes were unsatisfactory for the settling experiments because they result in a flow of water into the soil as the pressure decreases. This effect is probably hardly noticable in dilute settling suspensions, but in soils and intermediate suspensions, where permeability is much lower, this flow could clearly have an effect on the consolidation process as well as the measured pressure.

Because the total stress distribution on the base is unlikely to be uniform, an experiment was carried out with pressure cells at the centre of the base and at radii of 18 mm and 36 mm. Over 7 days (the normal time scale for a settling test) the three transducer readings fell by 1.5%, 1.8% and 2.0% respectively and it was decided that just one pressure cell in the centre of the base would be adequate for future experiments.

2.2.1 Requirements of the Method

Pore Water Pressure

Accuracy of the order of 2 mm head of water is needed, with this resolution required excess to hydrostatic pressures of

up to 2 m of water. In order to avoid flow of water into or out of the soil through the porous stone, the system must have a very low compliance. Intrusions into the centre of the column would interfere with the settling process so measurements have to be made at the wall of the column.

For the most efficient use of transducers a system was devised in which individual transducers can be moved to a wide choice of positions during an experiment as the soil settles. Consideration must also be given to de-airing and sealing.

Total Stress

Similar accuracy to the pore pressure system is needed to be able to make the necessary comparisons with density measurements and pore pressures. A non-intrusive, low compliance device is also desirable in this case to minimise disturbance of the soil by the instrumentation.

2.2.2 Pressure Transducers

"Druck" model PDCR 22 Differential Pressure Transducers had the necessary specification and were used successfully in this instance. Full scale output is 50 mV (12 V exitation) for the 5p.s.i. range transducer. Combined linearity and hysteresis error is 0.06% of the best straight line, with reasonably small thermal zero and sensitivity shifts.

The transducer is a stiff silicon diaphragm mounted flush at

the end of a cylindrical housing containing the electronic circuits. The active diaphragm size varies between 2 mm and 5 mm square. Flush mounted diaphragms are essential in order to keep de-airing methods as simple as possible, particularly in low range transducers where vacuum de-airing would cause a 300% negative overload and is therefore unacceptable.

2.2.3 Pore Water Pressure Transducer Housing

Fig 2.27 and plate 2.28 show a transducer, housing and column mounting with a porous stone. There are six perspex parts to a housing and mounting assembly so that the transducer in its housing can be taken off the column mounting and moved to another position without the column draining or allowing air into the system.

Parts 1, 2 and 3 in fig 2.27 are the column mounting pieces. A sand and araldite mixture is cast into part 1 to form the porous interface before the piece is glued permanently to the settling column and filed flush with the inside wall. The water pressure line from the back of the porous stone is displaced from the centreline. Part 2 has a pressure line offset from the centreline by the same amount as part 1, and may be rotated to make or break the connection between the two lines. Two O-rings seal this connection, which is held by part 3, in either the open or shut condition.

The transducer is held between parts 4 and 6 which can then be

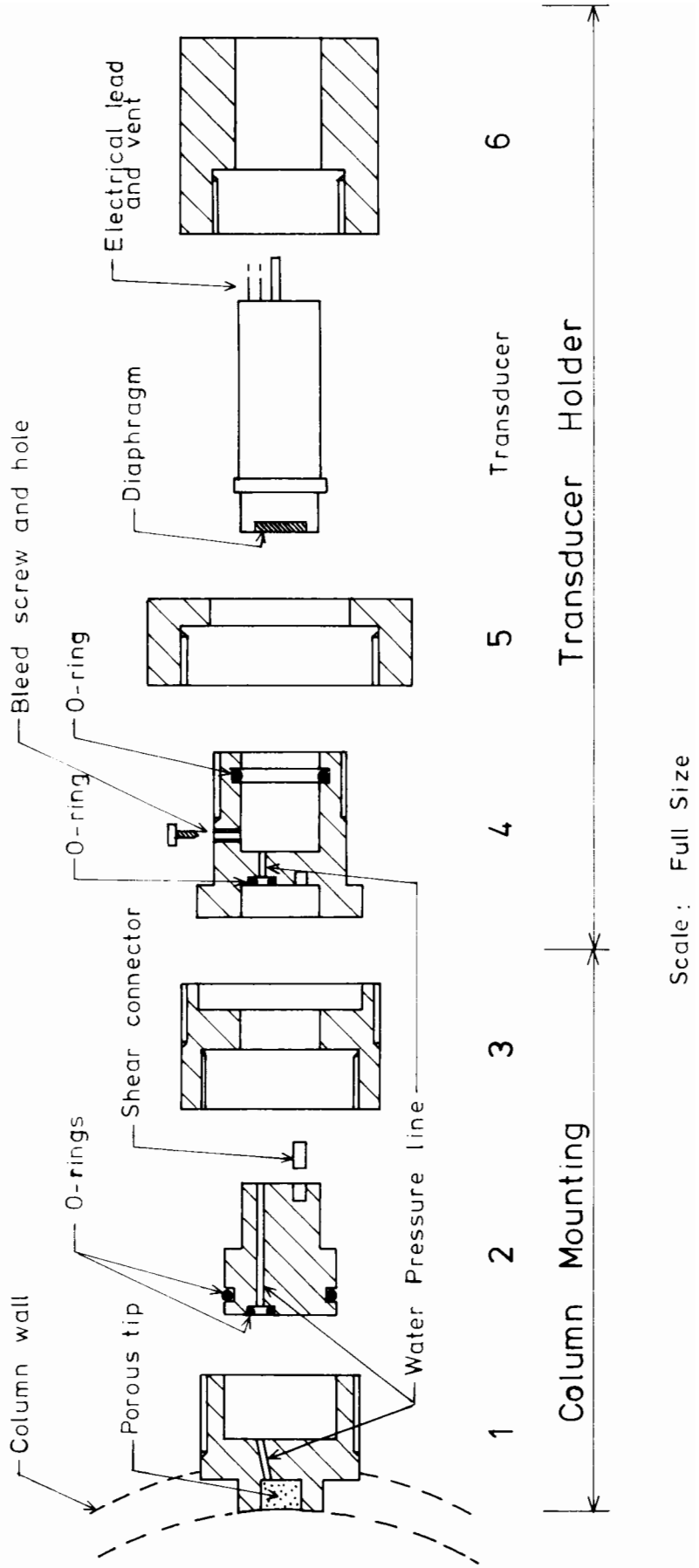


Fig 2.27. Pore Water Pressure Transducer Housings.

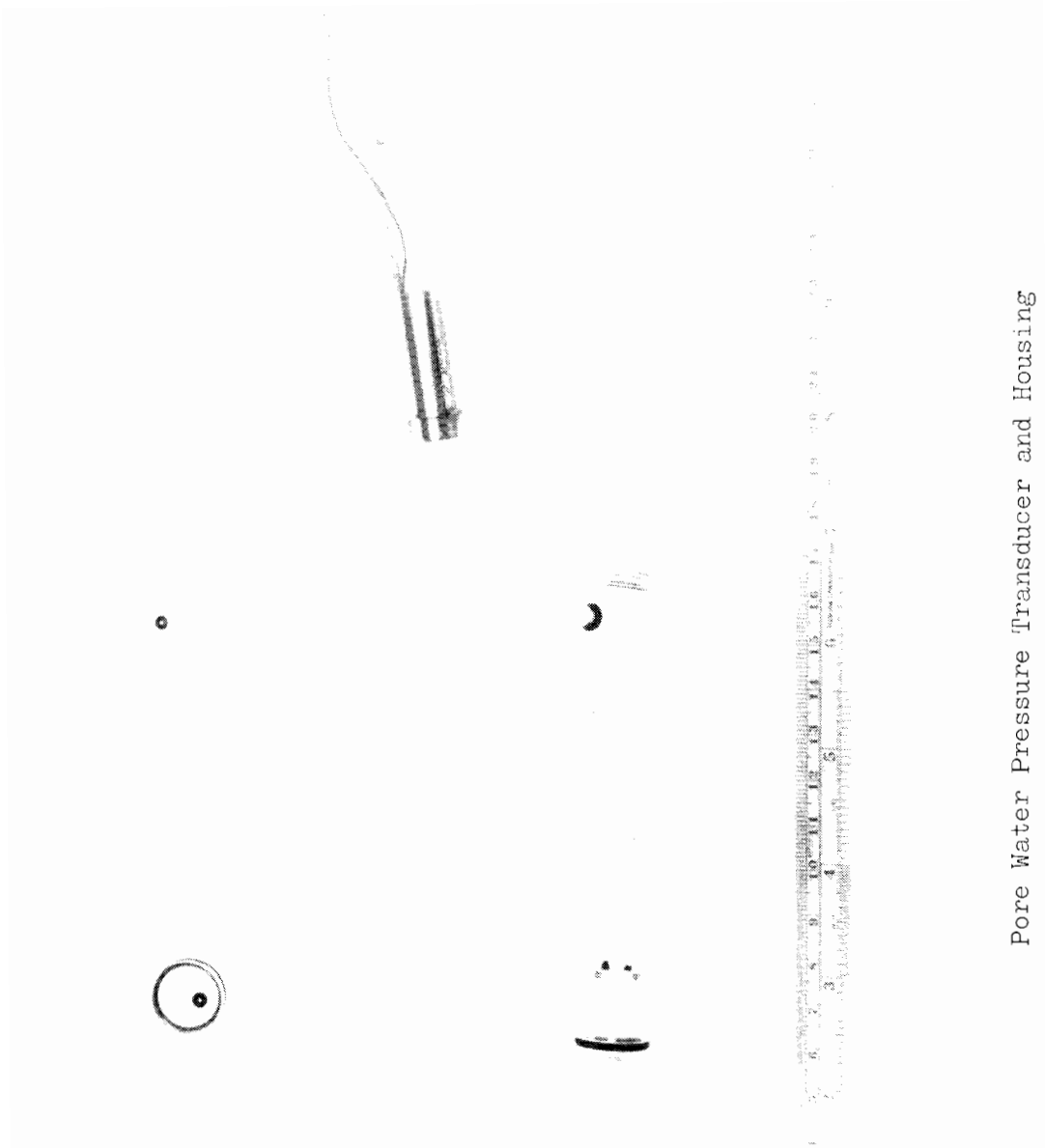


Plate 2.28. Pore Water Pressure Transducer and Housing.

fixed and sealed to the column mounting pieces with a locking ring (part 5). A shear connector between parts 2 and 4 ensures alignment of the pressure lines and is the means by which part 2 is rotated to switch the line on or off.

De-airing is achieved simply by bleeding water through the system, but difficulties can arise when moving transducers from one mounting to another. Both water lines from the transducer chamber and the settling column must be filled with water and have a water drop held by surface tension at the ends which are to be married up. As the locking ring is tightened, these two water drops are squeezed out from between parts 2 and 4 until the O-ring seals the connection. Occasionally the pressure on the transducer becomes too great during this operation and air can be drawn into the system as this pressure is allowed to dissipate. Fortunately bubbles are not difficult to see through the perspex walls so mistakes can be rectified.

Twenty one mounting positions for pore water pressure transducers were attached to a 2 metre long column at the following heights above the base (height in mm);

0	200	600
15	250	700
35	300	800
55	350	900
75	400	1000
100	450	1300
150	500	1600

Eight PDCR 22 transducers were available and were placed at suitable heights for pore pressure measurement during each settling experiment.

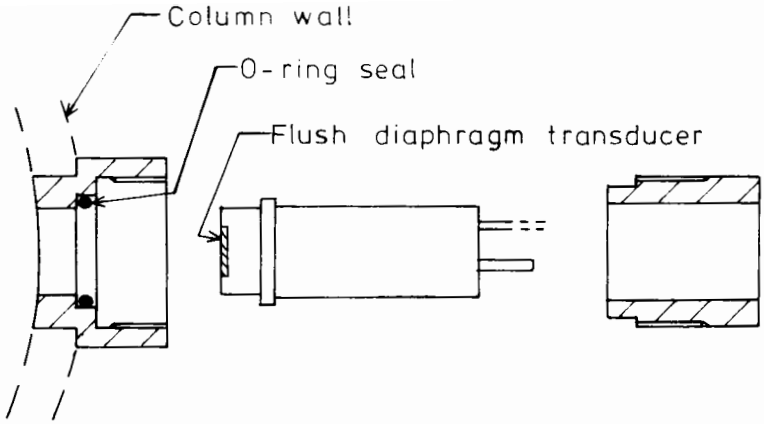
2.2.4 Total Stress on the Column Base

A column base was designed to seal the end of the column, house a total stress transducer flush with the base and also to provide a pore pressure port in the base. This base assembly is shown in section, with its three parts separated for clarity, in fig 2.29(a).

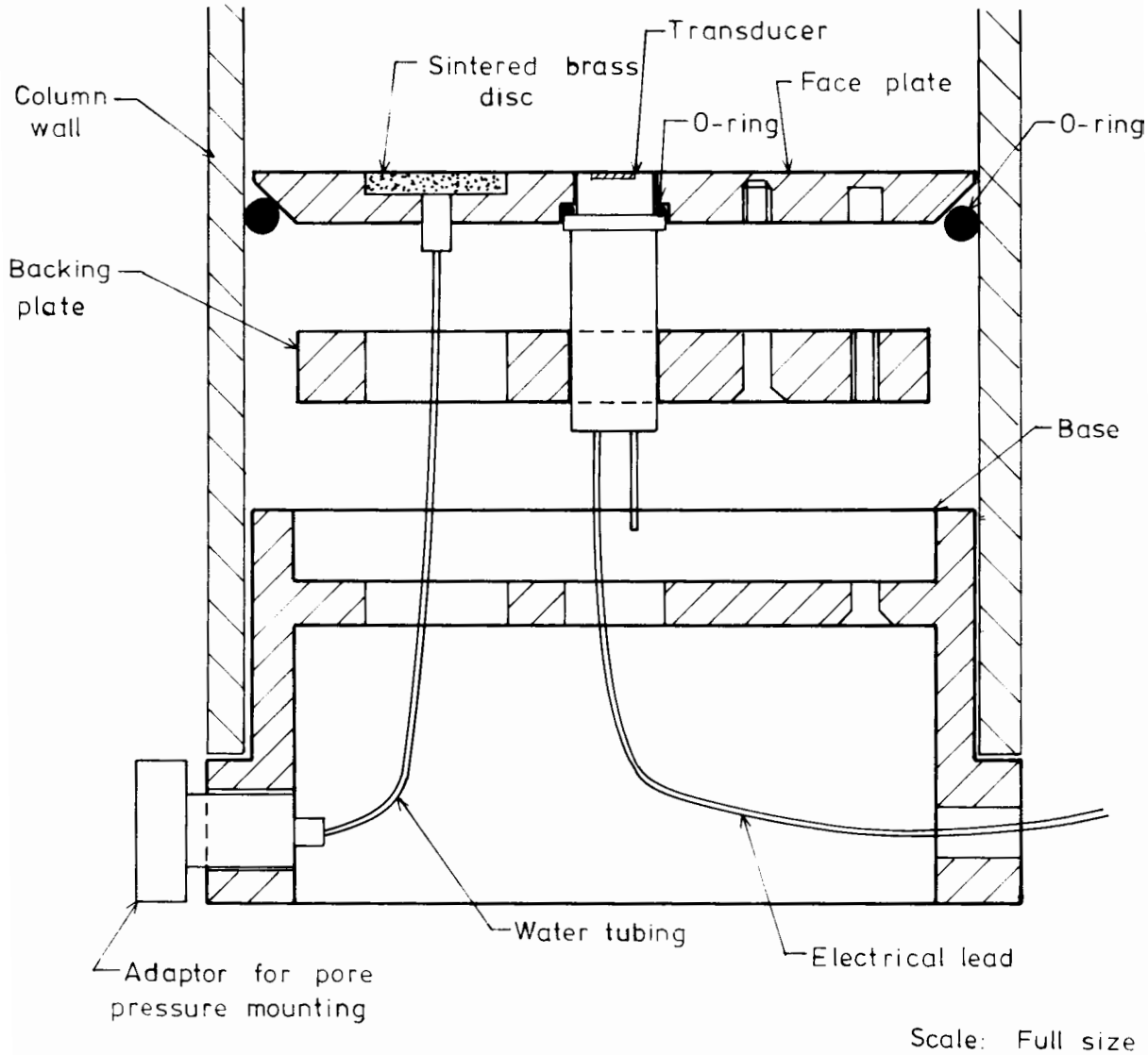
An O-ring pressed against the column wall by screwing the face plate down to the base seals the column. The pressure transducer is held with its diaphragm flush with the top of the face plate by a backing plate which also compresses the O-ring that seals around the transducer. A sintered brass disc is let into the face plate and a length of water tubing connects the back of the disc to a pore pressure transducer mounting on the side of the base.

2.2.5 Total Stress on the Side of the Column

One transducer only was mounted in the column wall, 300 mm above the base, to measure total stress. The mounting is simply two machined pieces of perspex. One piece is glued to the column and filed flush with the inside wall and the other piece, which holds the transducer, is screwed into the first until the diaphragm is just level with



(b) Transducer in Column Wall.



(a) Column Base.

Fig 2.29. Total Stress Transducer Mountings.

the inside wall and an O-ring is compressed sufficiently by the transducer flange to seal the hole. (Fig 2.29(b).

Clearly it is impossible to get a flat diaphragm flush with a round column wall. In this case the surface irregularities round the transducer are about 0.2 mm in either direction.

2.2.6 Electronics

All transducers were powered by a single stabilised power pack which maintained the excitation voltage between 11.998 and 12.002 Volts.

Readings of the transducer output were taken by a Solartron 7075 Digital Voltmeter and stored directly on paper tape by a data logging system built for general use in the laboratory.

2.2.7 Calibration

Because pressure measurements were required excess to comparatively high hydrostatic pressures and in units of water head, calibration of transducers was performed by raising and lowering the water level in the settling column (after de-airing) before each experiment. Water levels were measured to an accuracy of 1 mm each time a set of transducer readings was taken. Calibration curves were drawn for each transducer and used during experiments to convert electrical output to excess pore water pressure head or total stress.

2.2.8 Accuracy

Errors in the pressure measurement can arise from power supply drift, thermal drift of the transducers and calibration errors.

Power supply drift was less than 0.003 V in 12 V, an error of 0.025%. During calibration water levels could be measured to within 1 mm, whilst transducer mounting positions were accurate to about 0.1 mm. The least accurate transducer had a thermal zero drift of 0.04% full scale output per ^{o}C and a sensitivity drift of 0.03% per ^{o}C. Temperature variations in the X-ray room where experiments were performed were usually between 1 and 2 ^{o}C.

Estimations based on the above figures give a maximum error of 4 to 5 mm head of water in a depth of up to 2 m of water. The validity of this estimate was confirmed by taking transducer readings over a 24 hour period under a constant head of water. Variations in readings were about 50 μV which corresponds to a 3.5 mm change in water head.

2.2.9 Use of Standpipes

A few experiments were performed with standpipes instead of pressure transducers to measure pore pressures. This method was probably almost as accurate as the transducers, but the effect of water flow into the soil cannot be ignored so that results from these experiments were treated with due caution.

CHAPTER 3. EXPERIMENTAL PROCEDURES

3.1 Equipment Preparation 98

3.1.1 Column Assembly 98

3.1.2 X-ray Apparatus 98

3.1.3 Pressure Transducers 99

3.1.4 Standpipes 99

3.2 Soil Preparation 99

3.2.1 Batch Weighing 101

3.2.2 Stirring Procedure 101

3.3 An Experiment 102

3.4 Data Collection and Validation 103

3.5 Experiments Performed 104

CHAPTER 3. EXPERIMENTAL PROCEDURES

Having developed and set up the equipment to make measurements during settling, it is important that the methods used for handling the soil itself are suitable. The main requirement is that a fixed mass of soil is contained in a certain volume of slurry in a column, or alternatively that soil is introduced into a column of water at a uniform rate. This would present no great problem if dry soils were used, but it is essential that the soil is already wet before being introduced into the column because wetting is a complex time dependent process and clay properties are affected by desiccation and re-wetting. A constant rate of introduction of solid in a wet slurry form would require an extremely sensitive and sophisticated feedback system, but placing a given mass of soil at a uniform density is a simpler operation.

This chapter describes the experimental procedure, from soil and equipment preparation to data checking, for a series of experiments using a uniform density.

3.1 EQUIPMENT PREPARATION

3.1.1 Column Assembly

After cleaning, the column assembly including pore water pressure mountings, total stress transducers and sealing base is placed vertically in the X-ray laboratory. Vertical alignment of the column is extremely important as even small angles of tilt cause the displaced water to flow preferentially up one wall of the column during settling.

3.1.2 X-ray Apparatus

Calibration of the X-ray density apparatus before an experiment consists of a sweep trace directly on an X - Y recorder for each of six known densities to give a direct conversion of a count rate trace to a density profile. At least two density calibration samples are placed underneath the column so that the X-ray can be adjusted to the correct count rate and calibration checked before each profile is taken.

The X-ray and counter apparatus must be positioned relative to the column with care to ensure that the fixed geometry of the density system is maintained.

3.1.3 Pressure Transducers

Pore water pressure transducers are fixed to the column in suitable positions and de-aired by bleeding water through the mounting assemblies. After allowing time for water temperatures and electronics to stabilise, calibration of all transducers is performed by taking pressure readings at measured water levels in the column.

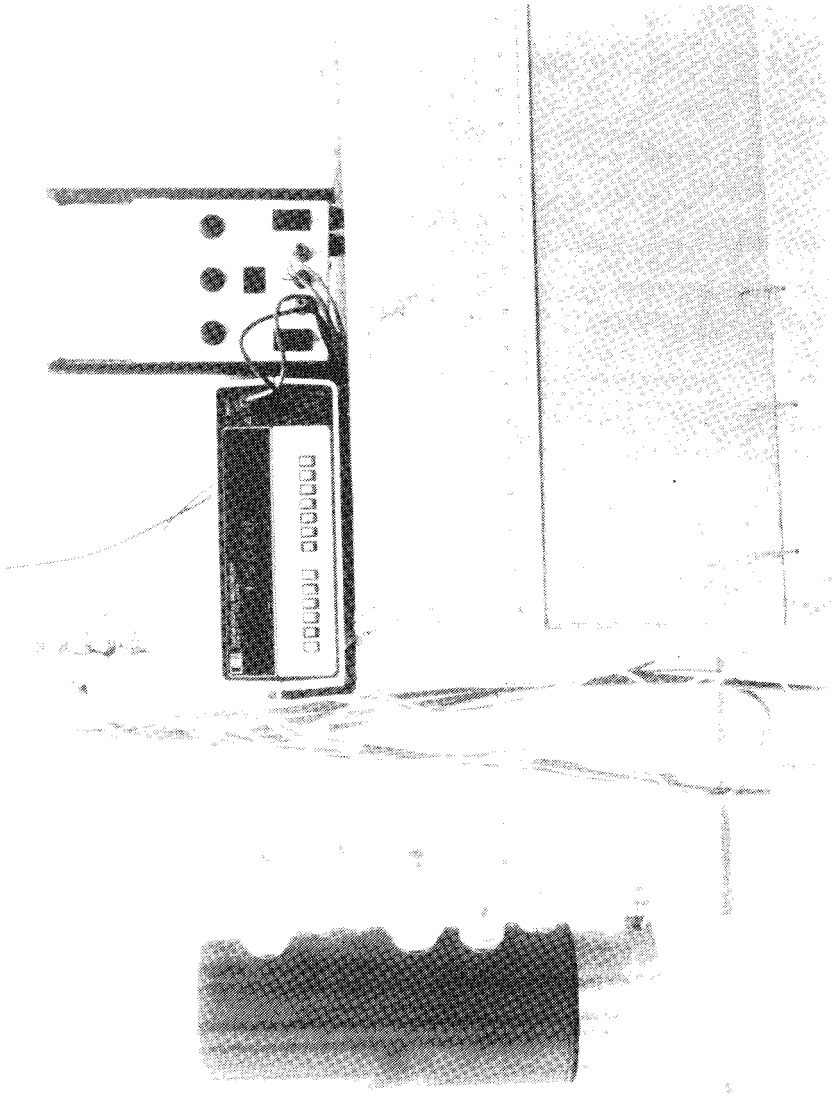
3.1.4 Standpipes

When standpipes are used instead of pore pressure cells, each standpipe must be filled with de-aired water and the open end blocked off until soil is put into the column. This ensures that during an experiment the water level in a standpipe is always falling so that water is flowing into the soil through the porous interface. Porous stones cannot therefore get clogged and standpipes always contain pure water.

Two settling columns (with mud in) are shown in plate 2.16 along with the X-ray density apparatus. Plate 3.1, an enlarged detail of the lower section of a column at the end of a test, shows calibration samples, the base, pressure transducers and the associated electronics.

3.2 SOIL PREPARATION

A single sample of silt from the River Parrett estuary was used



Lower Portion of Column and Instrumentation

Plate 3.1. Lower Portion of Column and Instrumention.

in these experiments. Approximately 10 kg was wet sieved and the material passing a 75 micron (BS 200) sieve was retained for experimental use. This sieved sample was a uniformly graded silt with a 30% clay fraction.

The soil is stored under water to ensure it remains wet and is stirred regularly.

3.2.1 Batch Weighing

For each settling experiment a certain mass of soil has to be transferred at a given density into a settling column.

A bin, with an overflow outlet to give a fixed water level, is weighed with water only and then with a soil slurry and water to the outlet level. This slurry is a representative batch from the sieved sample. The dry mass of soil can then be calculated and the appropriate slurry density is achieved, after allowing the slurry to settle, by siphoning off clear water to leave the correct volume.

3.2.2 Stirring Procedure

Because flocculation in a suspension is dependent on the initial state which is largely determined by how the slurry is stirred, it is essential to have a set stirring procedure.

The slurry of the correct average density is stirred for 5 minutes 12 to 16 hours before the soil is to be pumped into the column and then left

undisturbed. It is stirred again for 10 minutes immediately before being pumped. Stirring is by circulating the slurry with a centrifugal pump for the required time with manual stirring every 2 to 3 minutes to ensure that the soil is being circulated uniformly.

3.3 AN EXPERIMENT

This section describes the experimental procedure after the equipment and soil has been prepared.

During the 10 minute soil stirring period the pressure transducer zero points are checked. After stirring, while the column is still full of water, the pump delivery tube is inserted into the column taking care not to get air bubbles into the tube. The water is siphoned out of the column and slurry at the required density is pumped into the settling column to a certain depth, determined by the mass of solids required in the column.

Density profiles and pressure readings are taken at regular intervals while the mud in the column is settling and consolidating. Generally this was done every hour for the first 8 hours of an experiment and thereafter every 24 hours up to a week. Most experiments were terminated after a week but a few were continued for up to 4 months to assess long term consolidation behaviour.

Pore water pressure transducers are moved to different positions during an experiment depending on where measurements are needed. This

movement should be kept to a minimum, however, as it does involve the risk of air being drawn into the system.

3.4 DATA COLLECTION AND VALIDATION

Density profiles are plotted on an X - Y recorder, with one axis the ratemeter analogue signal corresponding to an averaged count rate and the other axis the height of the X-ray and counter arm as it moves up and down the column. Pressure readings are recorded on paper tape by a data logging system and can be initiated automatically or manually. If standpipes are being used the pore pressures are recorded by hand as water levels in the standpipes.

The procedure to obtain a set of readings is as follows:

-- After allowing the X-ray to warm up, check and adjust the anode current to give the correct count rates on the density calibration samples.
-- Traverse the X-ray up and down the column, recording the density profile both ways. Where density gradients are high, it is advantageous to stop the arm at approximately 15 mm intervals to get accurate densities.
-- At the top of the traverse the data logger is triggered to take pressure readings. Standpipe readings are taken after the X-ray is switched off.

Each set of readings is checked as soon as possible for errors due to equipment malfunctions, electrical interference or calibration. First the density profile is integrated and plotted as total stress and

compared with the total stress at the base estimated from the quantity of soil in the column and previous density profiles.

Pore water and total pressures are plotted on the same axes and compared to the integrated density profile. Transducers with air in the lines (after moving) give readings well above the total stress and can be picked out easily. The nature of the experiments means that the pore pressure at any point must necessarily be falling with time, so comparison with previous pressures is informative.

Besides being a check on data, this simple visual examination of data is very useful in assessing when the next reading should be taken, transducers moved or the experiment ended.

3.5 EXPERIMENTS PERFORMED.

During development of the measuring equipment and experimental procedures a number of experiments were performed without taking all the measurements described above or using different soil preparation and introduction procedures. The list of experiments in table 3.1 below is thus not comprehensive but does contain details of all experiments referred to in this work. Most quantitative analysis in the following chapters is based on the series of six experiments, numbers 10 to 15, in the table. Earlier experiments tended to be with slightly different soil sampling methods and have fewer recorded measurements.

Experiment no.	Mass of Soil kg	Initial Density gm/cm^3	Initial Height mm	Density Profiles	Transducers	Pore Pressure Standpipes	Duration hours	Comments
1	0.55	1.022	1929	*			43	
2	1.05	1.042	1910	*			119	
3	1.60	1.064	1920	*			23	For trends in a
4	1.93	1.077	1925	*			23	settling suspension
5	2.57	1.110	1791	*			23	
6	1.10	1.045	1867	*		*	25	
7	2.04	1.09	1742	*		*	79	
8	5.00	1.22	1748	*		*	2403	
9	1.06	1.045	1800	*			240	Dispersing agent added
10	0.51	1.02	1895	*	*		170	
11	1.17	1.05	1802	*	*		315	
12	1.19	1.05	1800	*		*	1853	Intermediate phase and
13	1.12	1.08	1123	*	*		144	soil behaviour
14	1.17	1.11	816	*	*		144	
15	1.23	1.146	643	*	*		848	

Table 3.1 Experiment Details.

CHAPTER 4. EXPERIMENTAL OBSERVATIONS

4.1	Suspension Settling Behaviour	109
4.2	Density Structures During Settling	111
4.3	Segregation of Particles During Settling	117
4.4	Stress Distribution in a Settling Sediment	118
4.5	Intermediate Phase and Soil Behaviour	122
	4.5.1 Surface Settlement	127
	4.5.2 Density	130
	4.5.3 Pore Water Pressure	137
	4.5.4 Effective Stress Development	144
	4.5.5 Permeability	151
4.6	Total Stress Measurement	159
4.7	Horizontal Stress	161

CHAPTER 4. EXPERIMENTAL OBSERVATIONS

A natural soil was used in this study although experimental results could be more difficult to analyse than for an artificial material. It was felt that any properties of the natural soil would in general be applicable to a wide variety of other similar soils, but that an idealised material may not exhibit certain naturally occurring phenomena and many observations would therefore be inappropriate. Mud from the River Parrett estuary was a convenient choice as field measurements on sediments in Bridgewater Bay have been made by the Institute of Oceanographic Sciences (Taunton).

The particle size distribution of the soil sample passing the 75 micron sieve, as described in chapter 3.2, is shown in fig 4.1. Approximately 30% of the sample is clay, it has a liquid limit of 53%, plastic limit of 25% and a plasticity index of 28%, classifying it as an inorganic clay of medium plasticity. This classification forms the largest single group of argillaceous sediments (Skempton, 1970), making the Parrett silt a suitable choice of material. The organic content is 1.8% and the specific gravity of the solid particles 2.66. Comparative values of the Atterberg limits were determined using sea water in place of distilled water, to see if these properties would be different in the natural saline environment of the soil. Values of 52% and 25% were found for the liquid and plastic limits respectively, indicating very little difference. Bishop and Vaughan (1972) came to a similar conclusion when adding flocculants to dredged spoil.

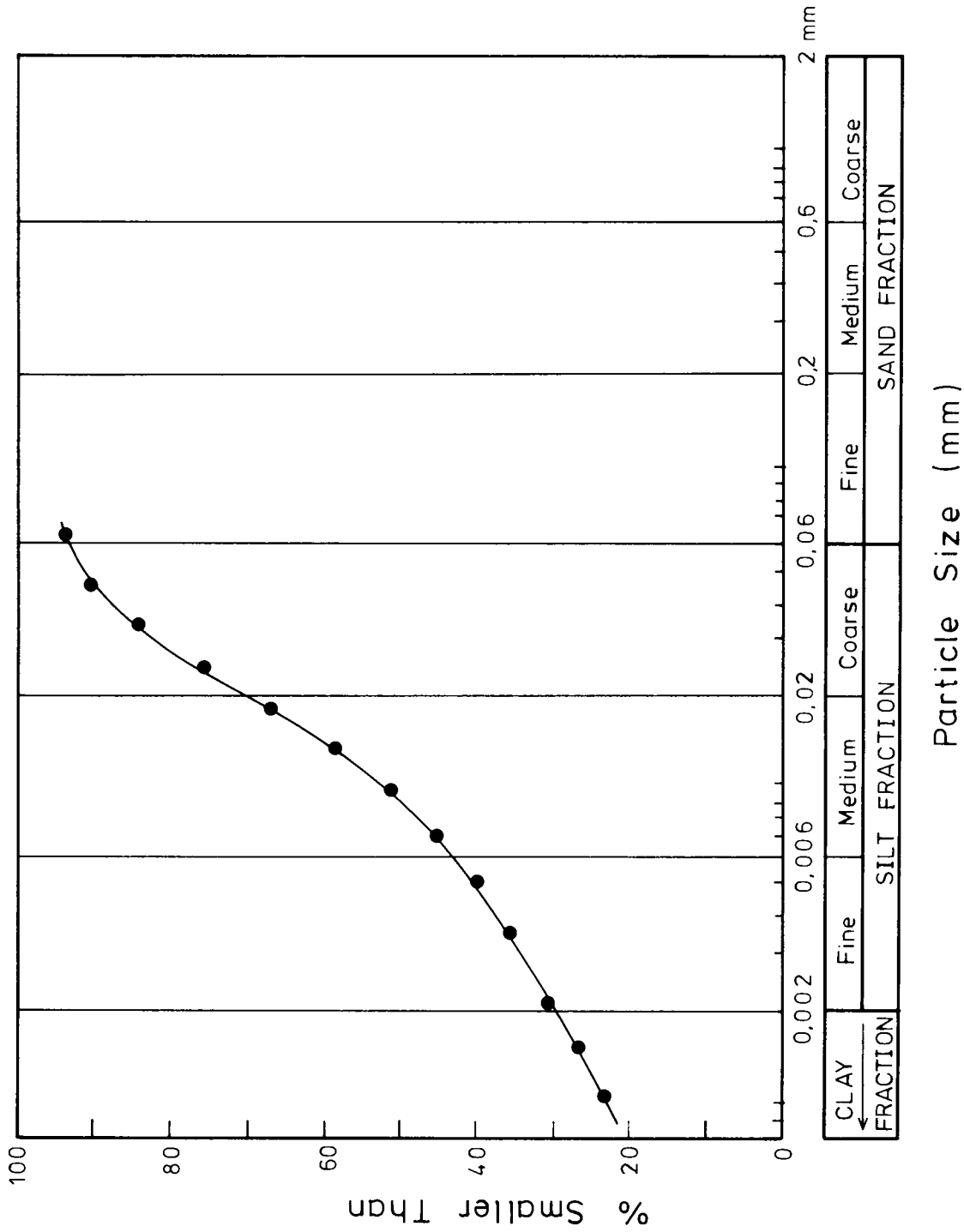


Fig 4.1. Particle Size Distribution.
River Parrett Silt Passing BS 200 Sieve.

4.1 SUSPENSION SETTLING BEHAVIOUR

In fig 4.2 the height/time relationship of the suspension/water interface during the suspension settling period is shown for experiments 1 to 5, each at a different initial density. Linearity of these early portions of the settling curve is not generally apparent. A more noticeable feature is that experiments 1 and 5, at the lower and upper densities, have significantly different settling rates to the tests at intermediate initial densities.

In general the appearance of a column of settling mud is uniform but, when the displaced water flows up preferential paths, channels appear in the mud. The visual appearance of this channelling is that of several pipes, 1 to 2 mm in diameter, rising almost vertically through the mud carrying water upwards relatively fast. This water flow entrains the surrounding soil particles and carries them upwards so that the soil is in a quick condition in a localised area around the channel. When a channel reaches the mud surface it appears as if a volcano is erupting there, with the soil deposited in a cone around the pipe outlet.

Channelling was observed in all these tests, the flatter portions at the end of the settling curves corresponding to the period after which channelling behaviour reached the mud/water interface. Fitch (1966) has suggested a mechanism where voids or bubbles of lower concentration may spontaneously segregate from the suspension and channel to the surface. This behaviour increases the flux of solids at a given concentration.

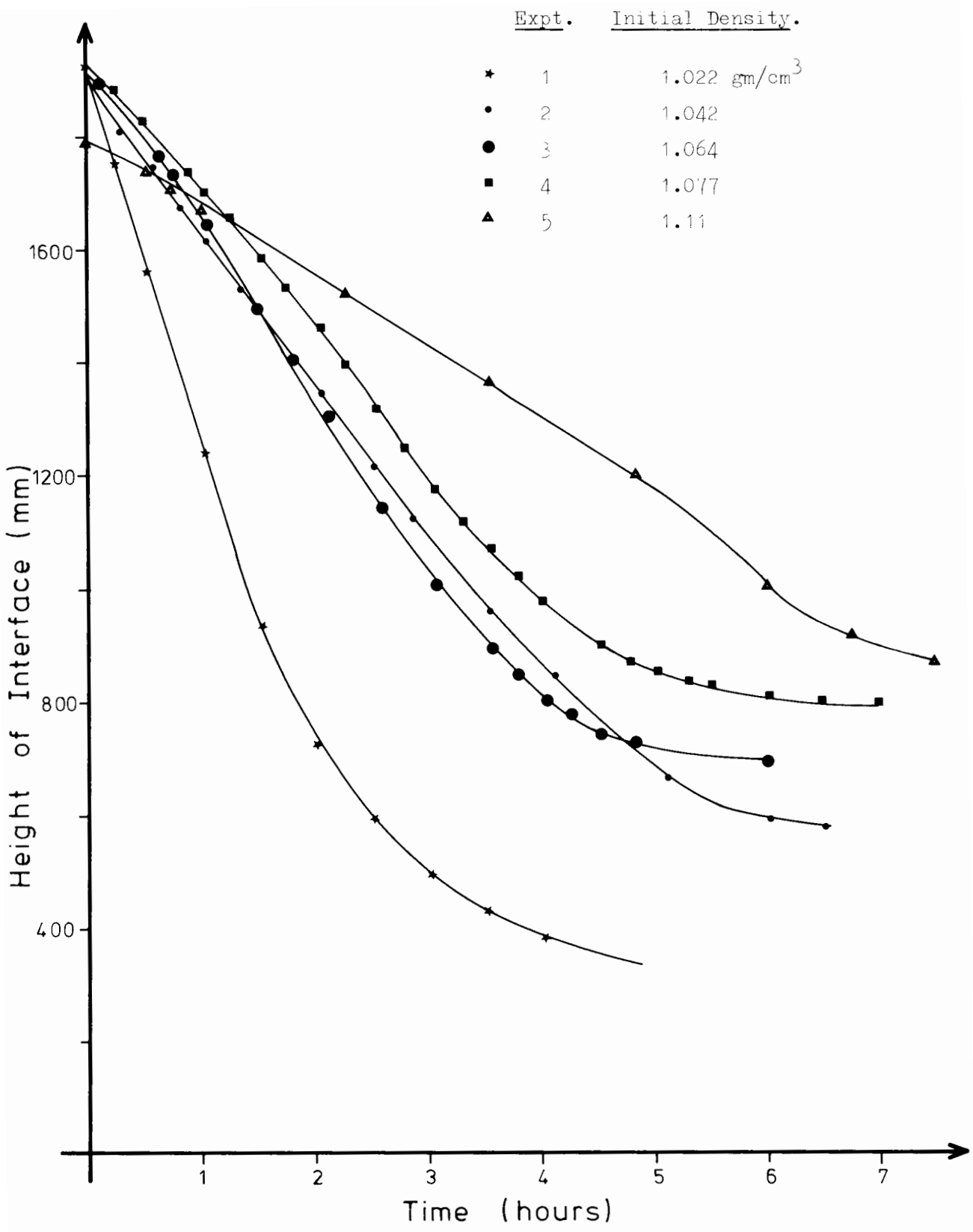


Fig 4.2. Height of Suspension Water Interface. Experiments 1-5.

4.2 DENSITY STRUCTURES DURING SETTLING

Sets of density profiles for three experiments (6,7 and 8 in Table 3.1) at different initial uniform densities are shown in figures 4.3, 4.5 and 4.7.

For the initial density of 1.045 gm/cm^3, fig 4.3, the suspension remains at the same density as it settles. A region with a density of about 1.13 gm/cm^3 rises from the base as the solids accumulate with a marked step in density between this region and the uniform suspension. Between 6 and 7 hours this step and the suspension water interface meet and the settling process slows down considerably. Figure 4.4, a graph of the height of a particular density against time for the same test, illustrates this more clearly. The graph has not been extended beyond the 9½ hour measurement as the next measured point on the graph is only at 24 hours (with the height 520 mm). The 1.0 gm/cm^3 line is the mud/clear water interface, 1.045 gm/cm^3 marks the bottom of the suspension and 1.11 gm/cm^3 the top of the rising denser region. This sharp change in density is represented by the shaded region. Channelling only occurs in this shaded region and about 50 mm below it. A relatively dense bed of soil develops quickly at the base of the column, which is clearly different from the zone of intermediate density. Density measurements in this area near the base were, however, not very precise when these experiments were performed and are not shown on the graph.

Profiles for a test at 1.09 gm/cm^3 initial density, fig 4.5, show similar features except that the density of the suspension decreases slightly in this case. Fig 4.6 shows the height/time graph of density lines for this test, with a few more than just the interface lines drawn,

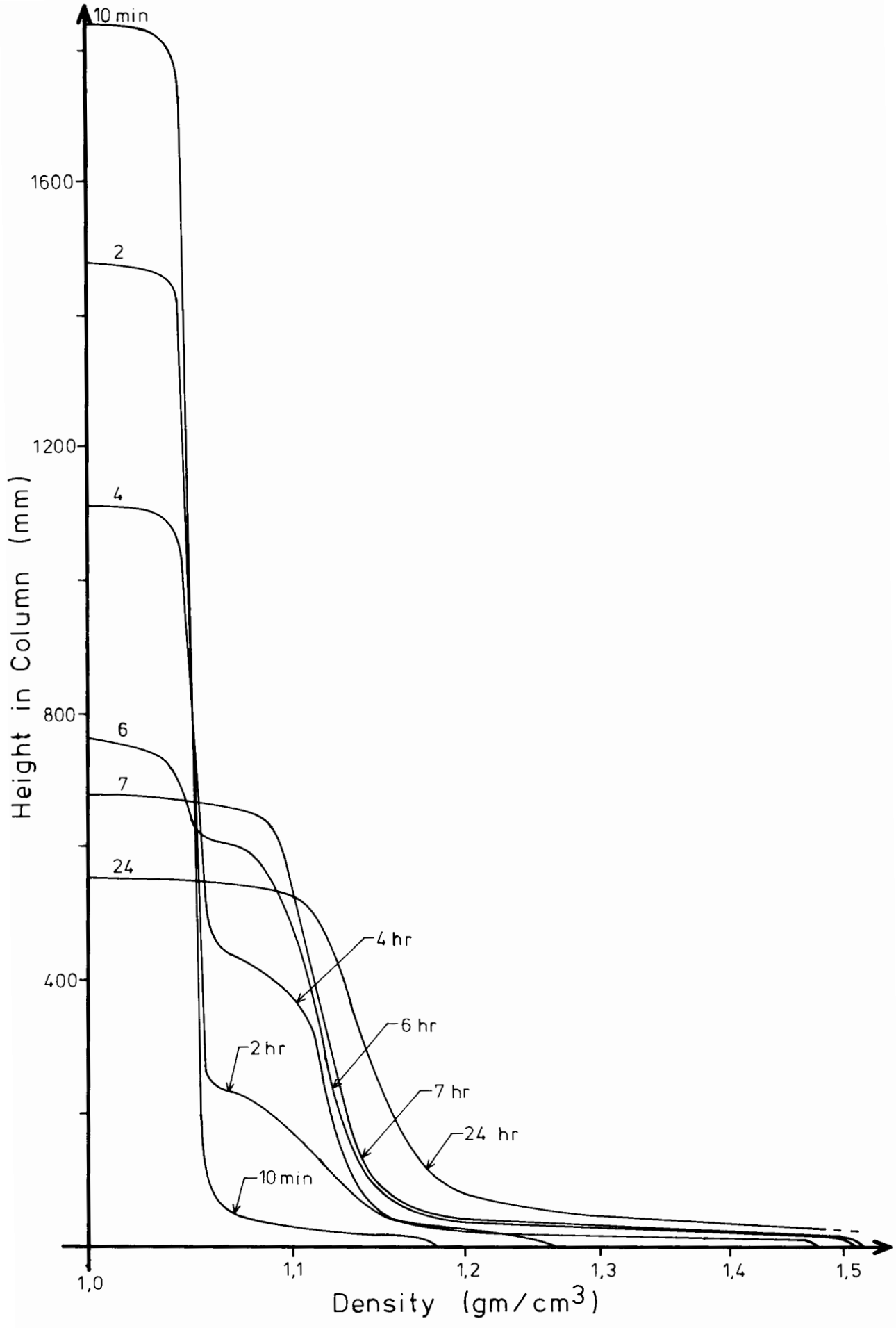


Fig 4.3. Density Profiles. Experiment 6.
Initial Density 1.045 gm/cm^3.

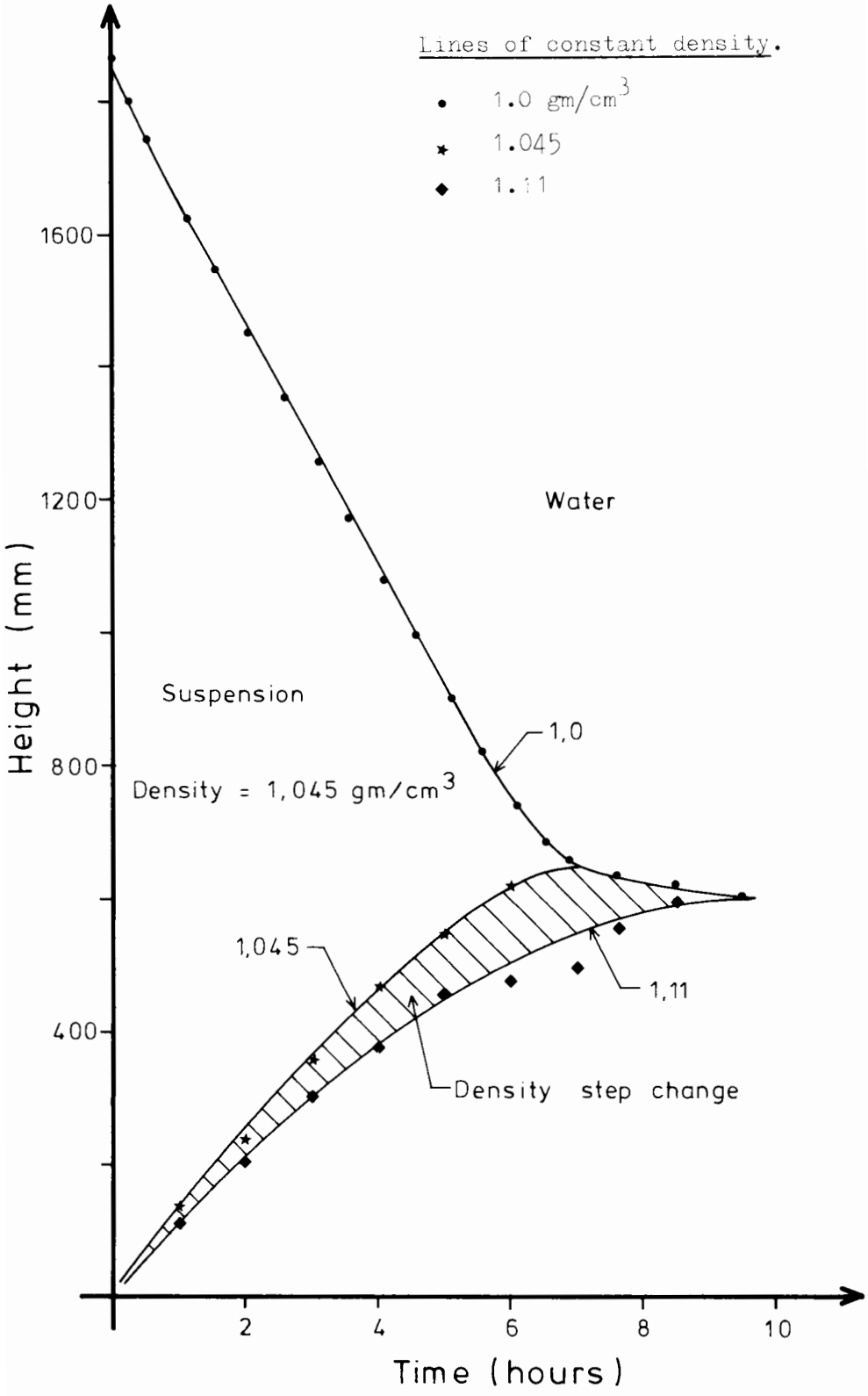


Fig 4.4. Height / Time Plot. Experiment 6.
Initial Density 1.045 gm/cm^3.

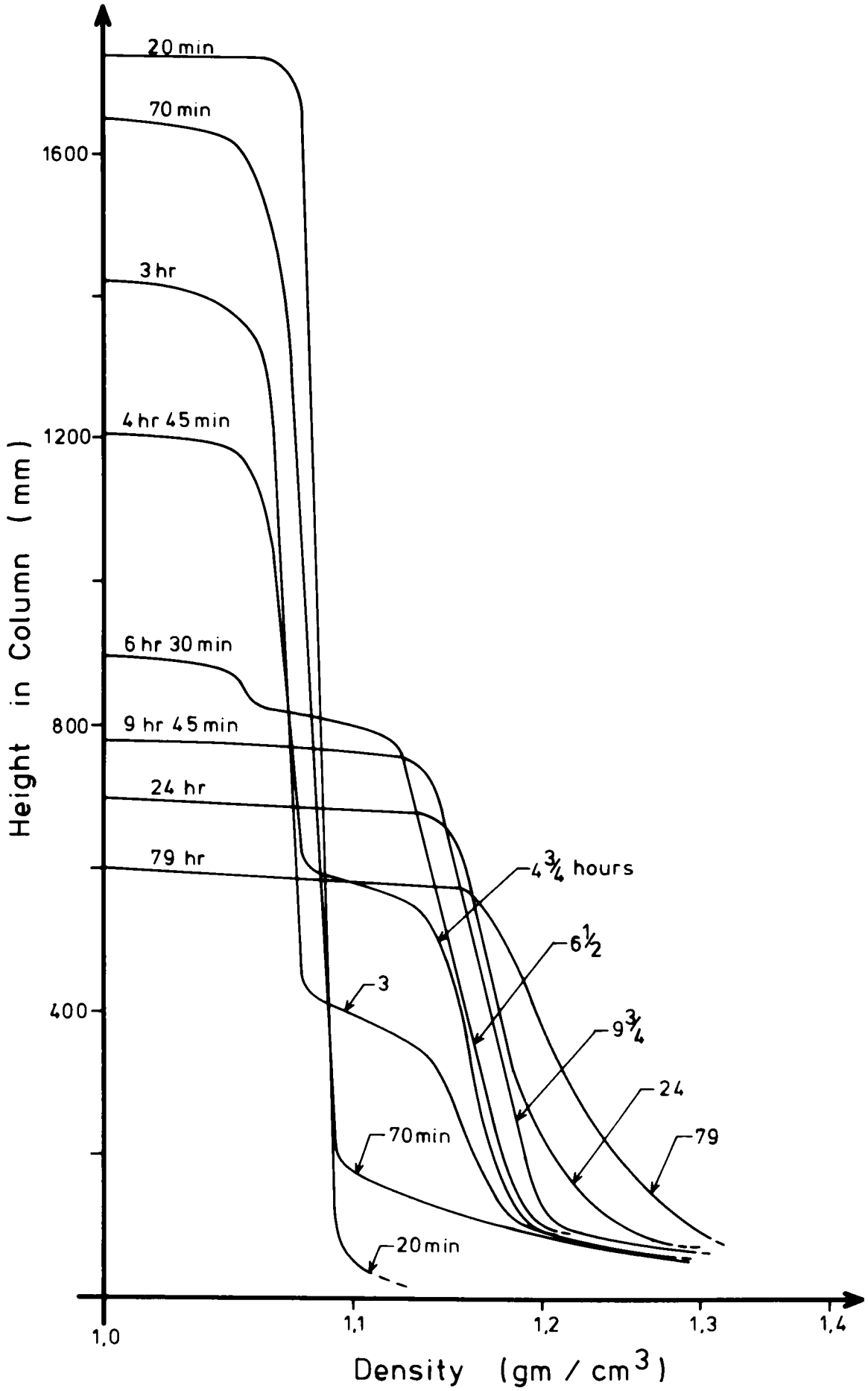


Fig 4.5. Density Profiles. Experiment 7.

Initial Density 1.09 gm/cm^3.

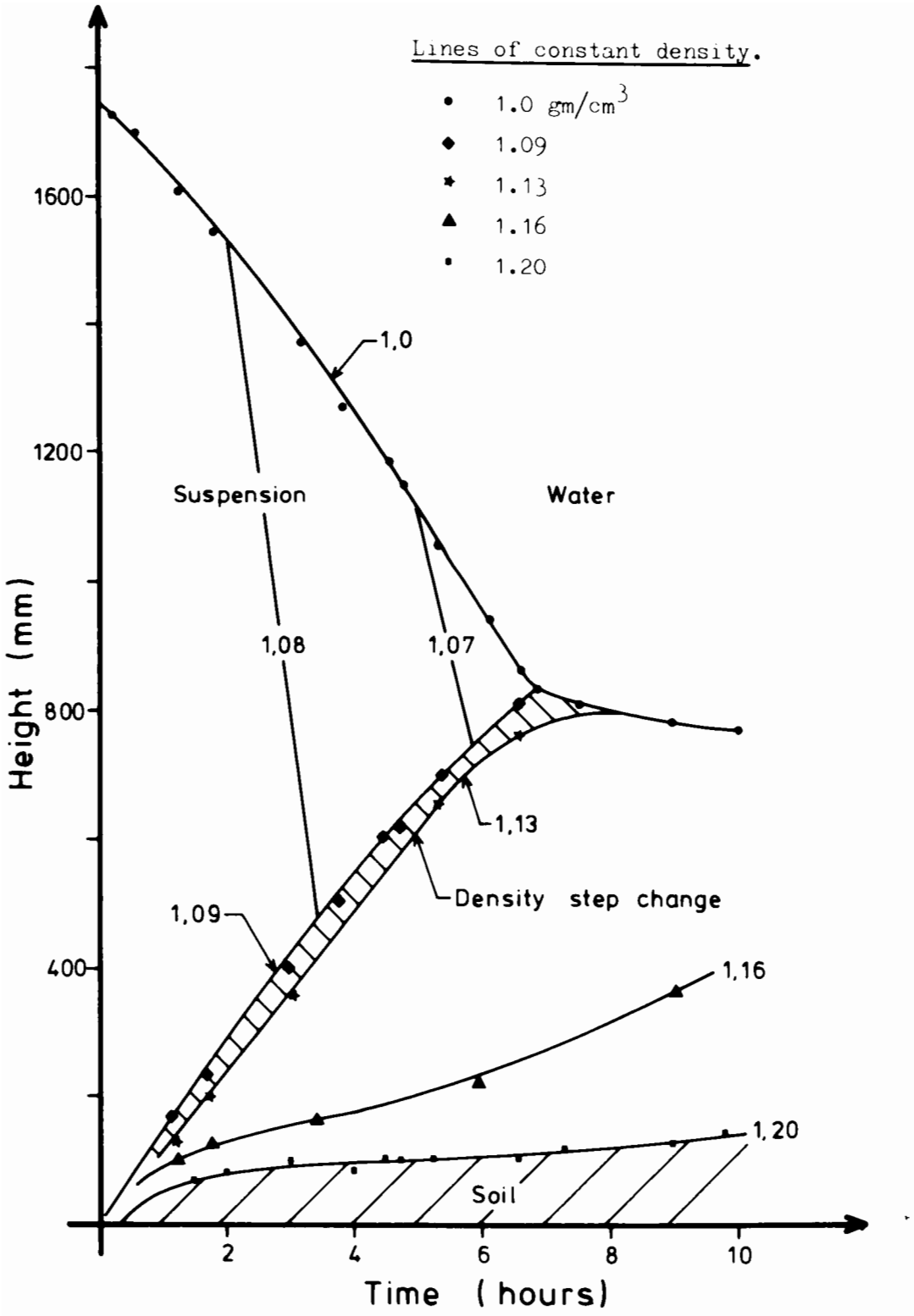


Fig 4.6. Height / Time Plot. Experiment 7.
Initial Density 1.09 gm/cm^3.

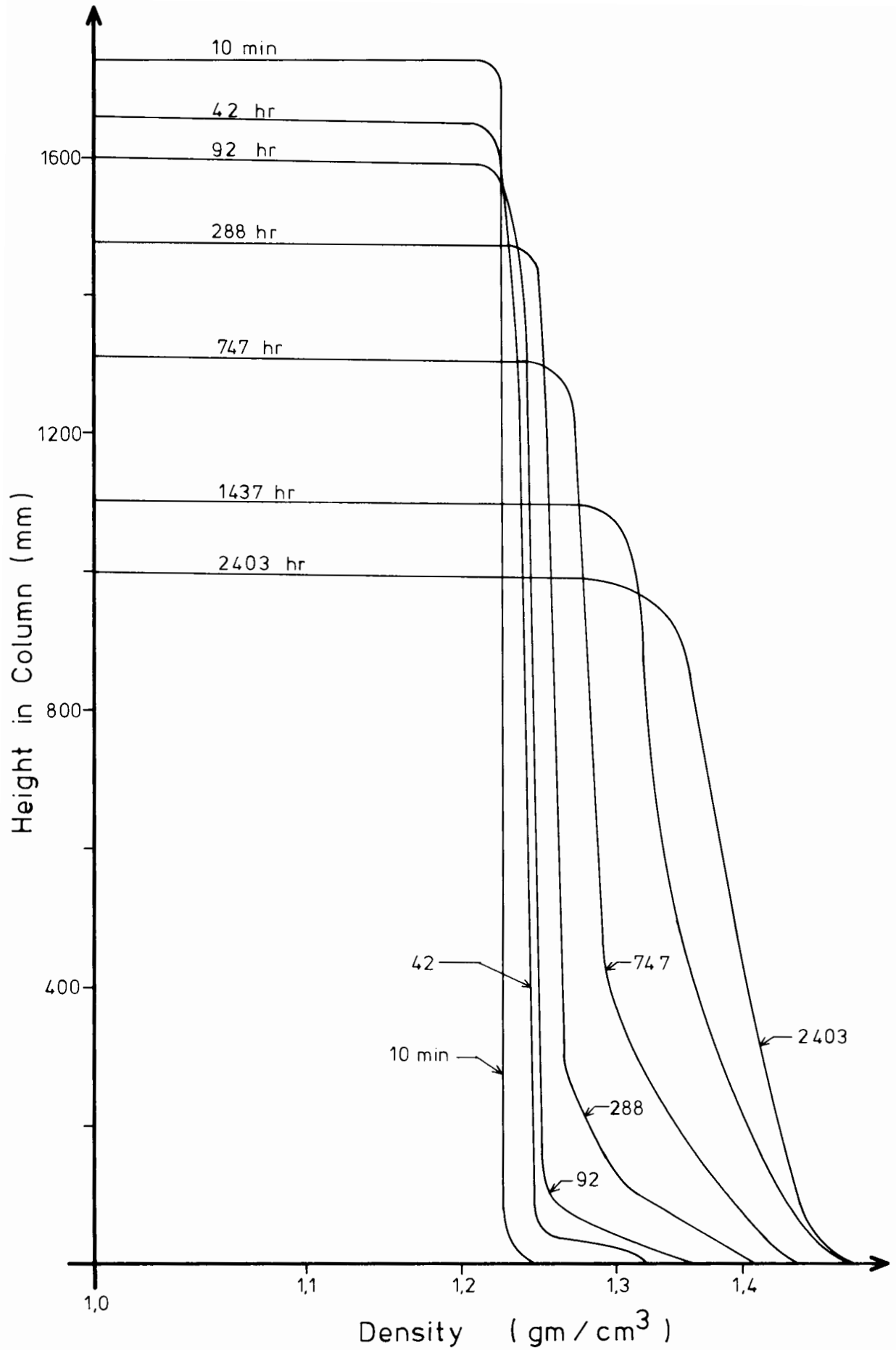


Fig 4.7. Density Profiles. Experiment 8.
Initial Density 1.22 gm/cm^3.

although measurements between 10 and 24 hours were again not performed. A corollary of Kynch's theory is that lines of constant concentration on a plot like this will be straight, so that this form of graph is particularly useful for comparisons with theory in chapter 6. Channelling was again a feature in and below the upper shaded area in this experiment.

In experiment 8 the initial density is 1.22 gm/cm^3, which is comparable to the intermediate region density in experiment 7. Density profiles for this test, fig 4.7, show a completely different behaviour. There are no distinct phases or density changes and settling is a slow continuous process. Channelling did not occur.

4.3 SEGREGATION OF PARTICLES DURING SETTLING

Although the settling behaviour discussed so far in this chapter is that of a flocculated sediment, certain aspects of this behaviour could be the result of segregation of particle sizes by differential settling. Increasing fall rates of suspension surfaces, the decrease in density of the suspension in experiment 7 and the rapid formation of a dense bed at the column base could all be due to segregation.

One way of assessing the extent of differential settling is to compare the particle size distributions of samples taken from different positions in the settled mud bed. This has been done for experiments 7 (initial density 1.09 gm/cm^3), 8 (initial density 1.22 gm/cm^3) and 9. Experiment 9 is a repeat of experiment 6, with an initial density of 1.045 gm/cm^3, but 4 grams of sodium hexametaphosphate per litre of slurry

was added as a dispersant. This test is thus a comparison with undispersed experiments.

Particle size distributions for six samples from the bed in experiment 7 are shown in fig 4.8. The samples from the base and top of the bed are very different from the middle four, but a consistently changing distribution is apparent throughout. A significant proportion of the coarse silt particles have settled through the mud to the base, leaving the top layer with a high percentage of finer material. That this settling of coarse particles through the mud column occurs only in the initial, low density suspension is shown by fig 4.9 where samples from a high initial density test (experiment 8, 1.22 gm/cm^3) all have exactly the same particle size distribution.

Samples taken from the settled bed of the initially dispersed suspension (experiment 9) differ markedly from one another, fig 4.10, showing extensive segregation of particle sizes. Nearly all the coarse and medium silt sizes occur in the two lowest samples respectively and the top sample is 87% clay sizes. Flocculation thus plays an important part in determining the homogeneity of the settled mud as well as the more obvious effects on settling behaviour and speed.

4.4 STRESS DISTRIBUTION IN A SETTLING SEDIMENT

Total vertical stress in a column can be found by graphic integration of the density profile above any point. This method does not include the effect of wall friction on the stress but in suspensions and

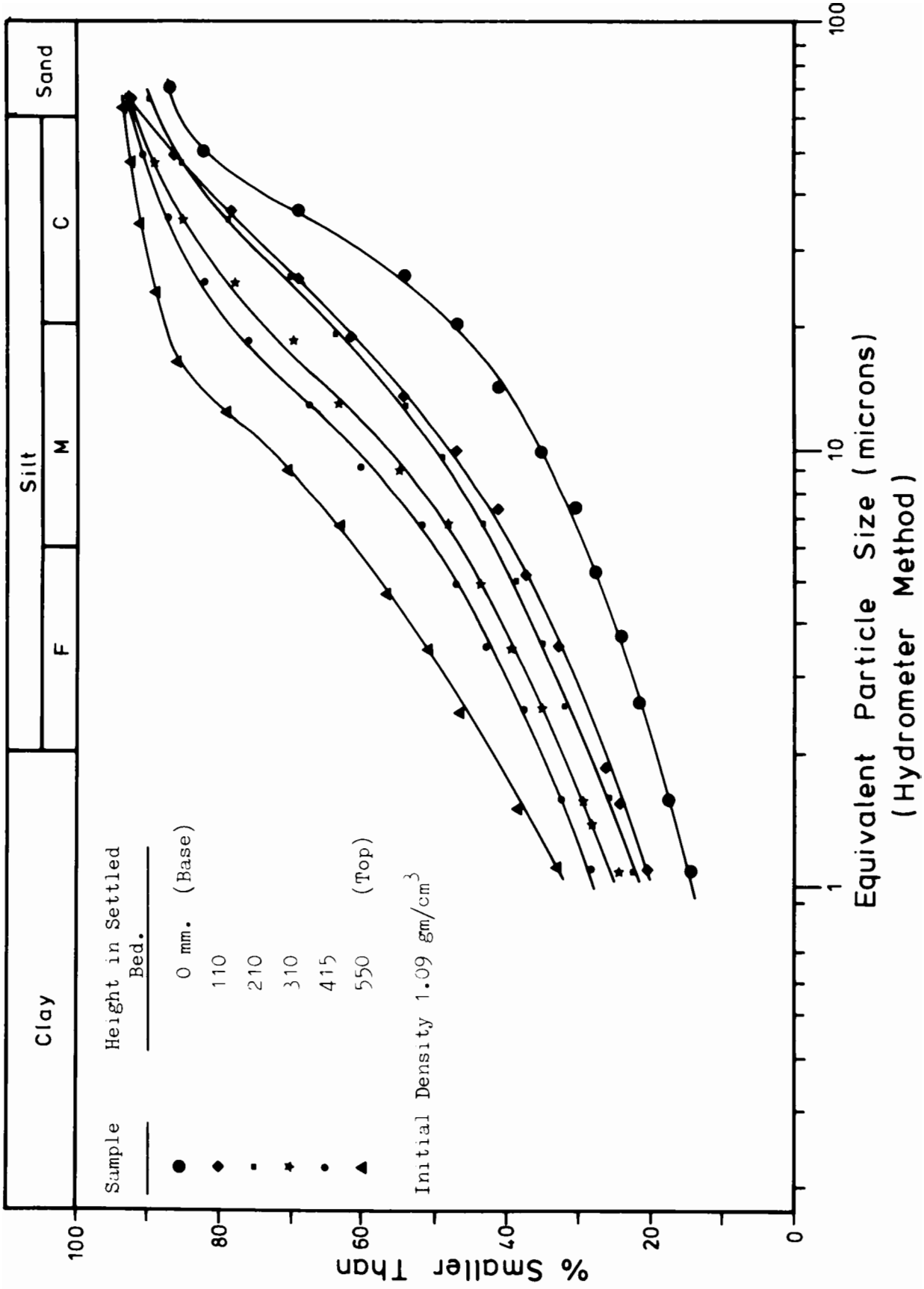


Fig 4.8. Particle Size Distribution at End of Experiment 7. Initial Density 1.09 gm/cm^3, no additive.

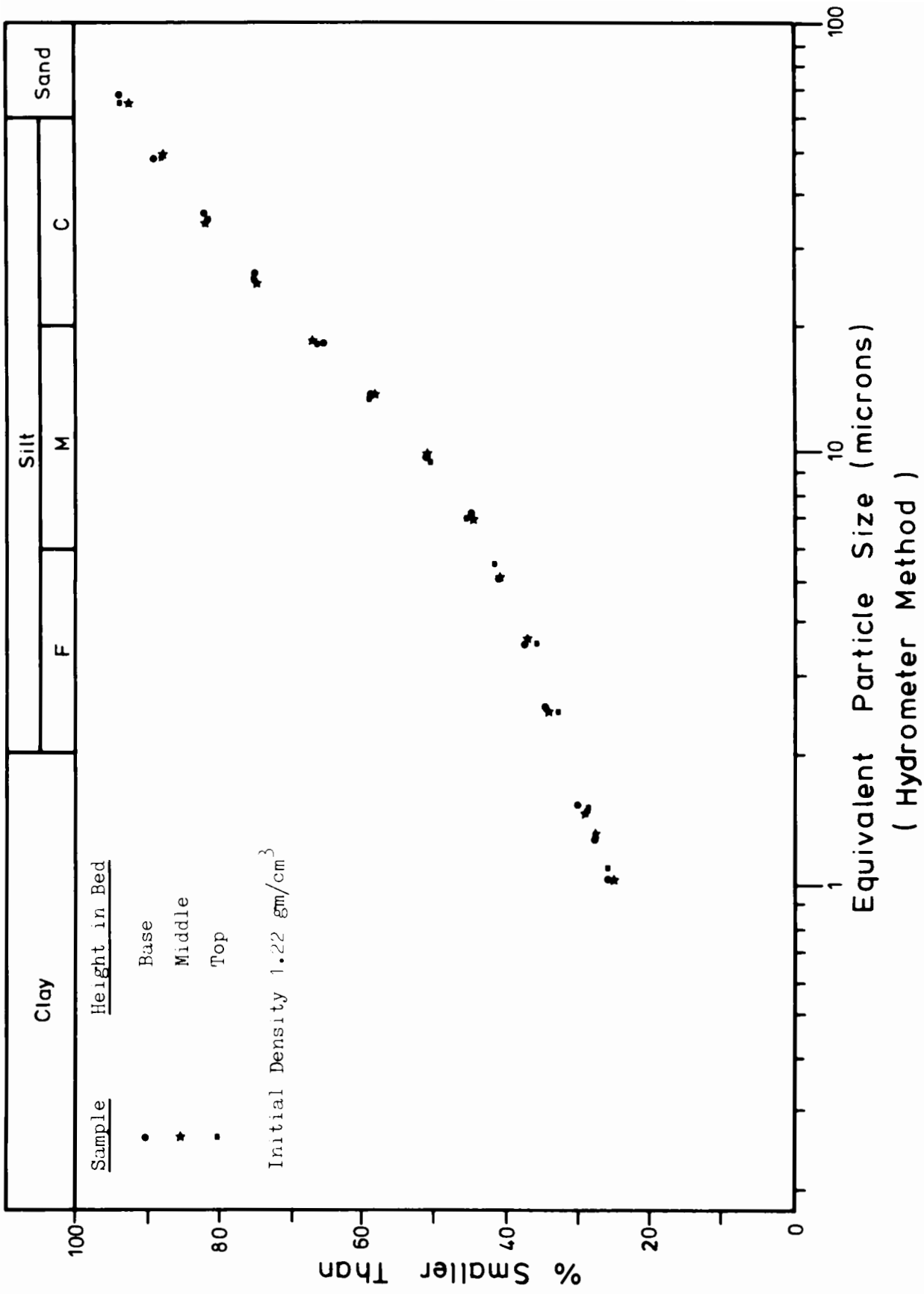


Fig 4.9. Particle Size Distribution at End of Experiment 8.
Initial Density 1.22 gm/cm^3, no additive.

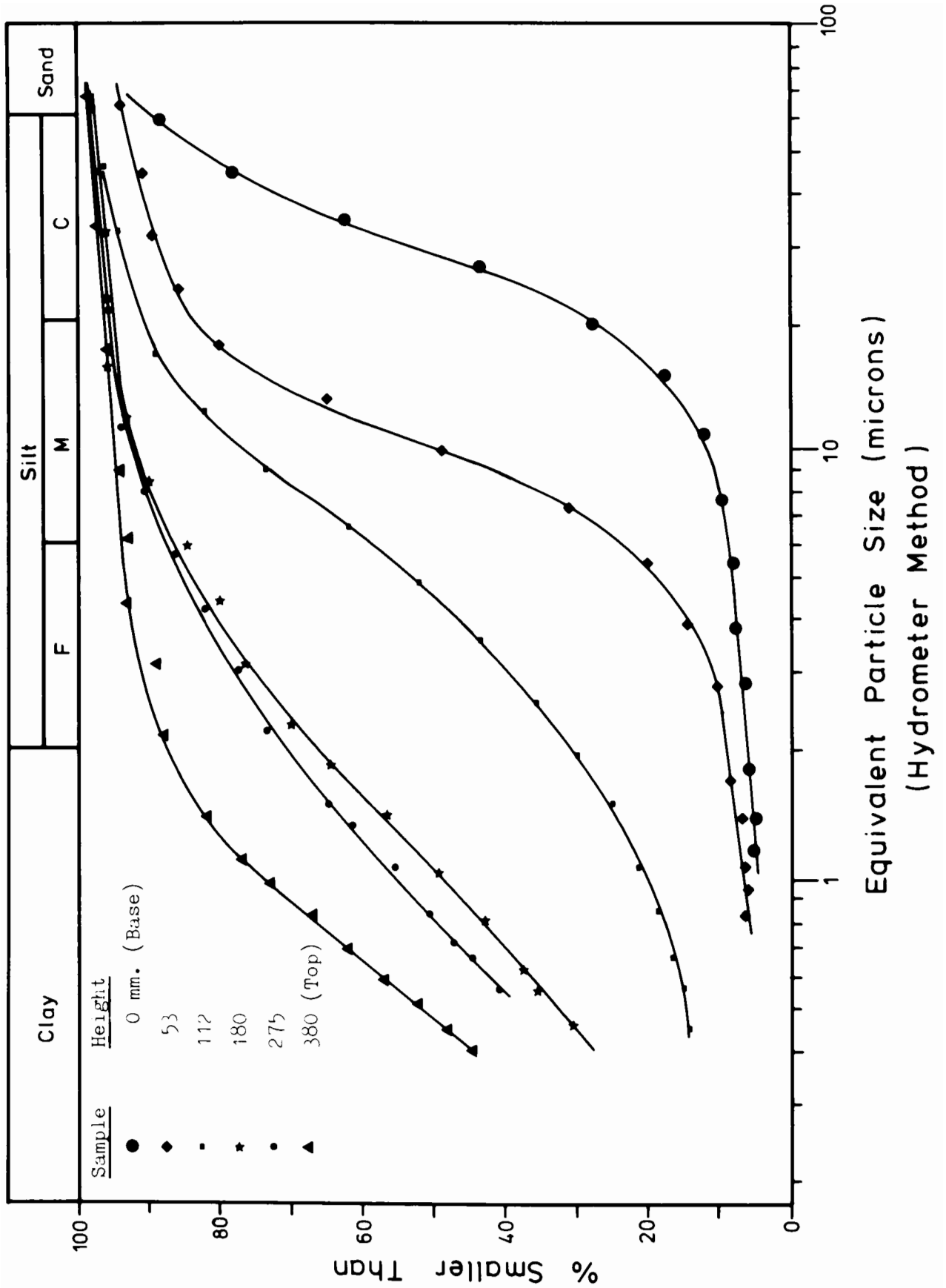


Fig 4.10. Particle Size Distribution at End of Experiment 9. Initial Density 1.045 gm/cm^3, dispersed with Sodium Hexametaphosphate.

nearly fluid mud the effect is very small. Plotting pore water pressures on the same axes gives the effective stress distribution in the column as the difference between the total stress and pore pressure. This is illustrated alongside 3 density profiles for experiment 7 in figures 4.11, 4.12 and 4.13.

Similar behaviour is shown in the 3 and $4\frac{3}{4}$ hour profiles. In the suspension region the measured pore pressures are the same as calculated total stresses, but in the intermediate density zone the two lines diverge and effective stresses exist. The point of divergence corresponds to the step change in suspension density. No suspension phase exists after $9\frac{3}{4}$ hours and the stress distribution shows effective stresses from the mud surface downwards. Below 100 mm, stresses are not shown due to lack of measurements.

Fig 4.14 shows the stress distribution immediately after experiment 8 was started with the density a uniform 1.22 gm/cm^3, which is comparable with the intermediate densities in the previous test. The pore pressure and total stress diverge down the column, indicating an increasing effective stress despite the uniform density. Apparently the suspension cannot exist in a stress free condition at this high density, so that the soil in the column has an effective stress distribution governed by its stress history.

4.5 INTERMEDIATE PHASE AND SOIL BEHAVIOUR

The intermediate density region is of special interest as it is where effective stresses first develop and soil formation begins.

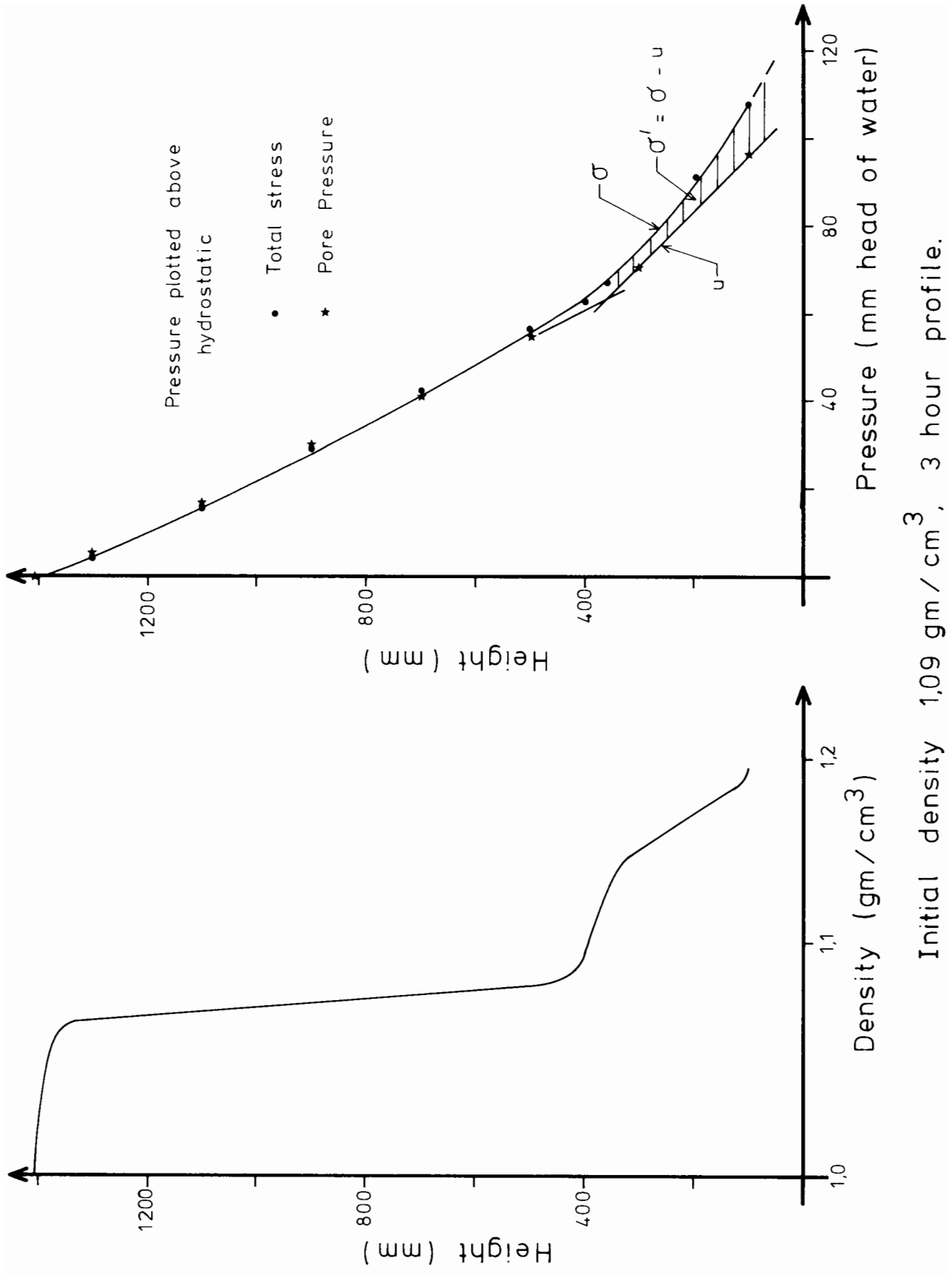


Fig 4.11. Density and Stress Distribution, Experiment 7.
Initial Density 1.09 gm/cm^3, 3 hour Profile.

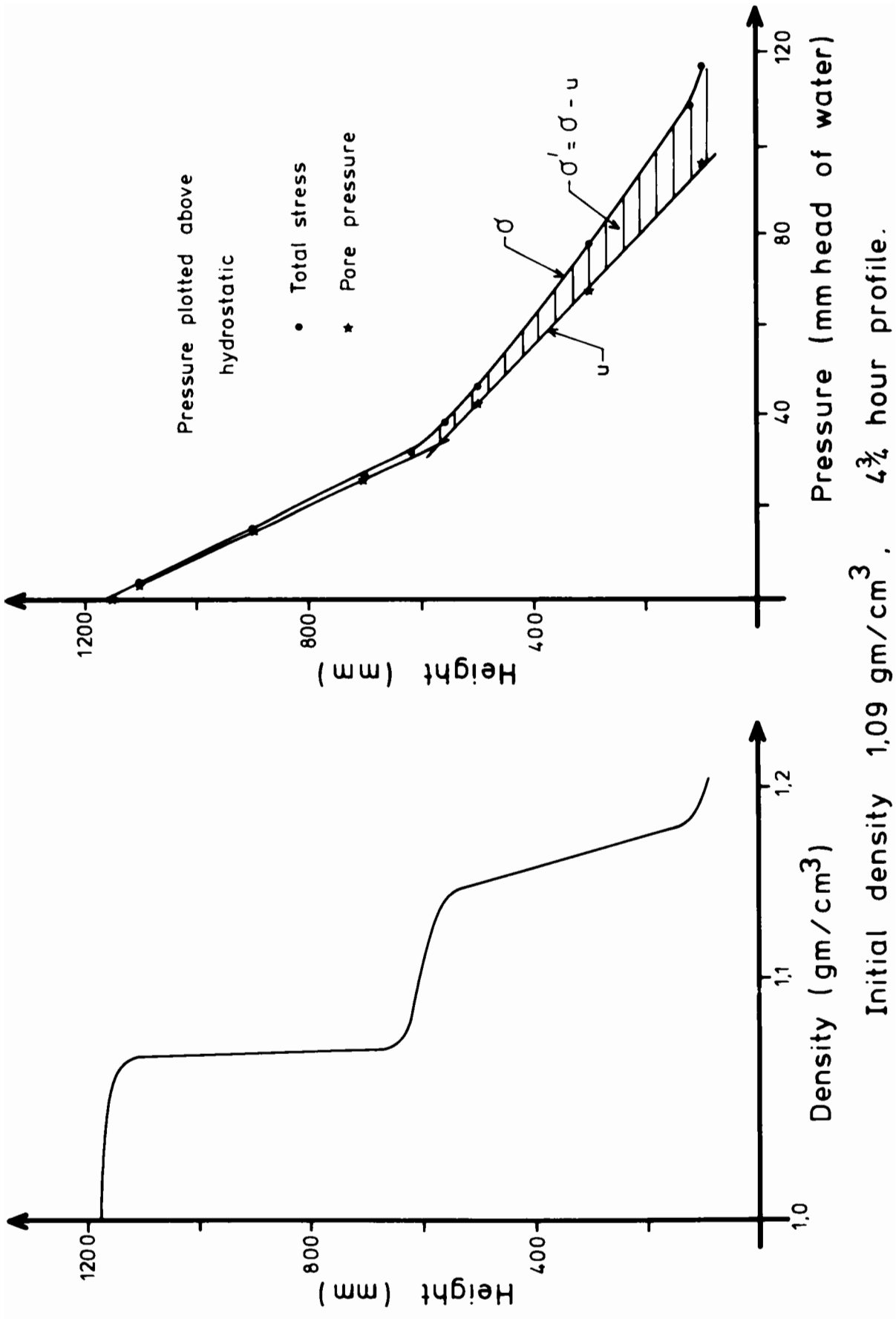


Fig 4.12. Density and Stress Distribution, Experiment 7.
Initial Density 1.09 gm/cm^3, $4\frac{3}{4}$ hour Profile.

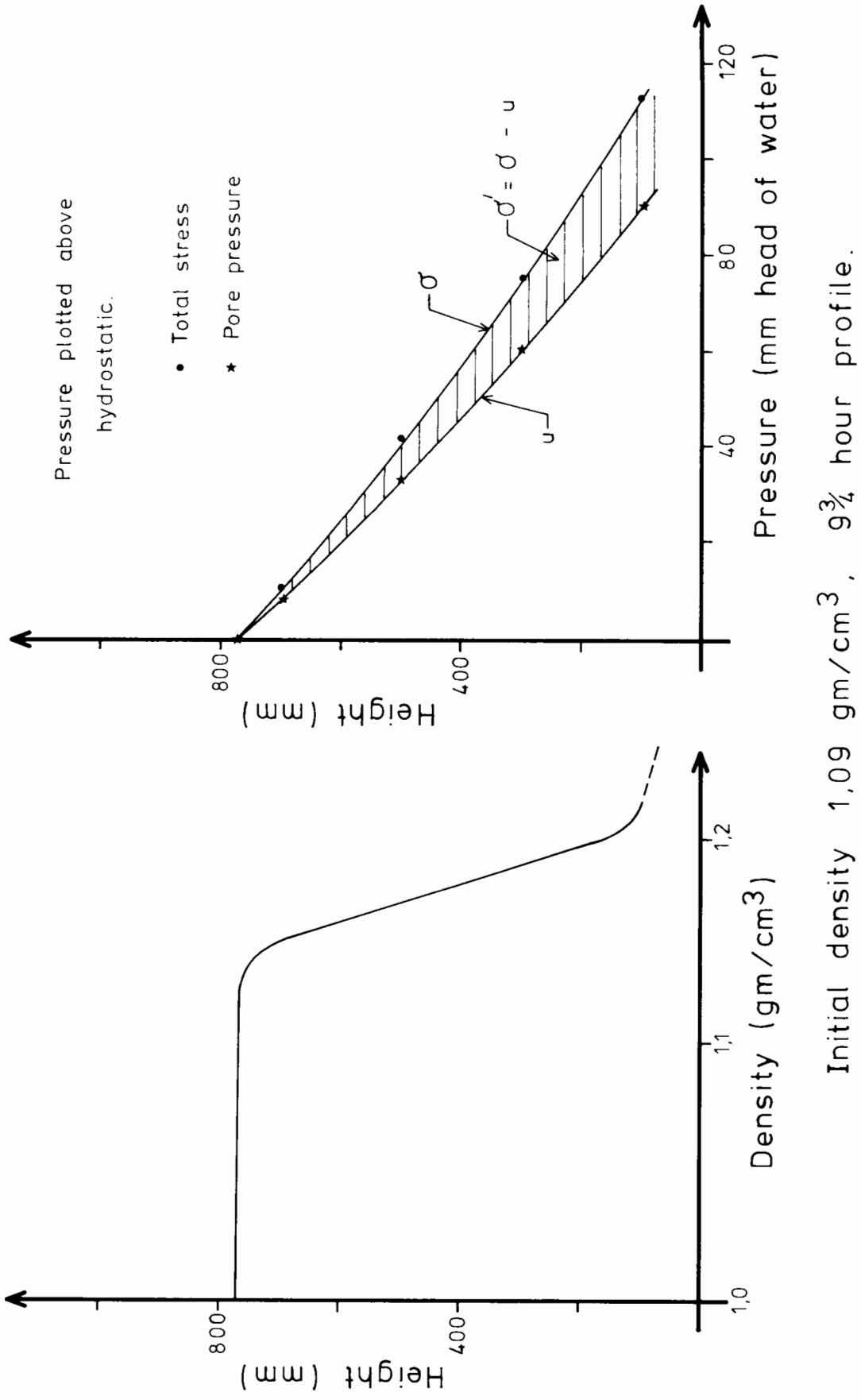


Fig 4.13. Density and Stress Distribution, Experiment 7.
Initial Density 1.09 gm/cm^3, $9\frac{3}{4}$ hour Profile.

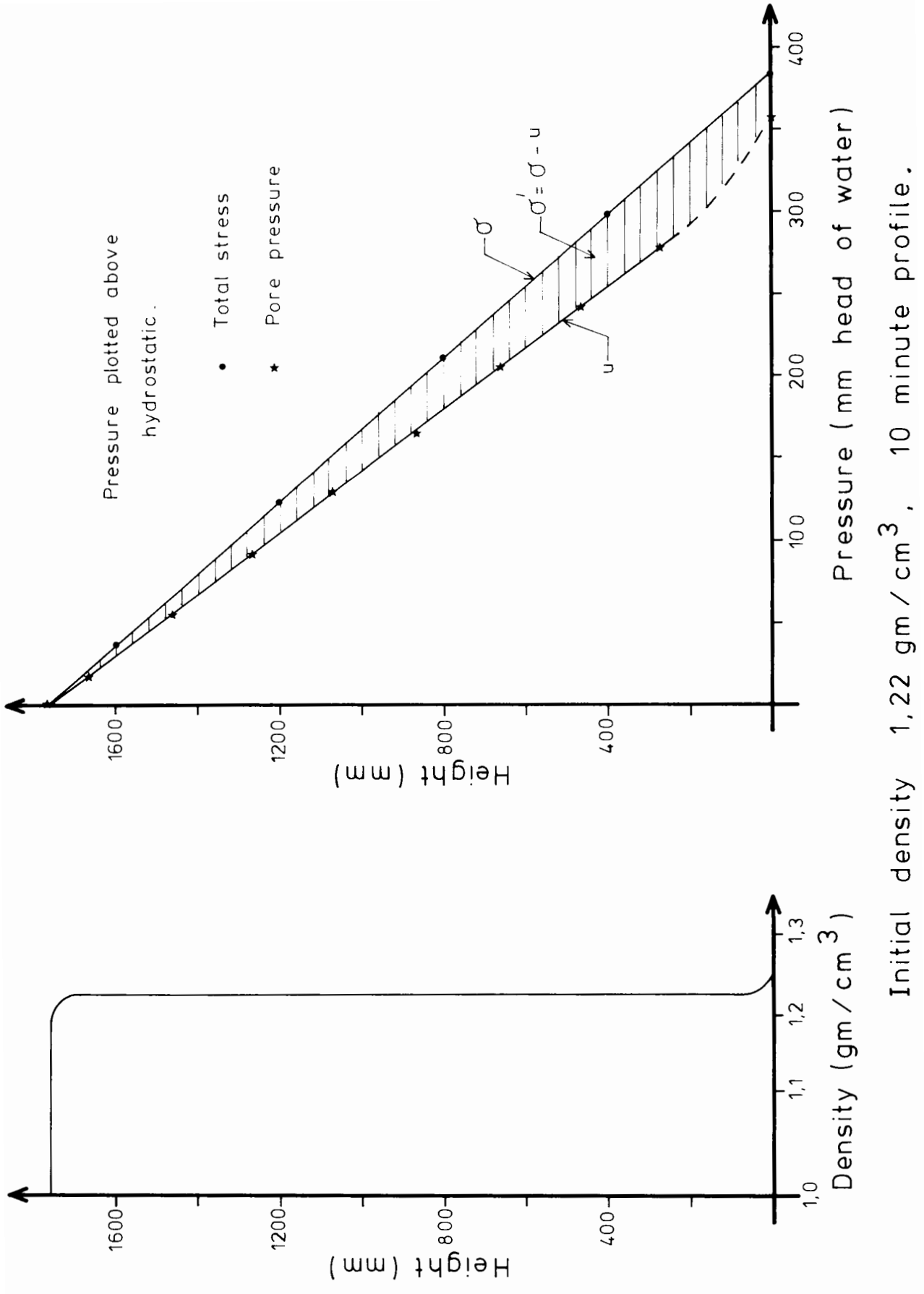


Fig 4.14. Initial Density and Stress Distribution, Experiment 8.
Initial Density 1.22 gm/cm^3.

Experiments 10 to 15 in this section are concerned mainly with examining this intermediate phase and soil formation. A range of initial densities from 1.02 gm/cm^3 to 1.146 gm/cm^3 is covered. (This final figure is quoted to 3 decimal places as measurements showed it to be this, rather than 1.14 gm/cm^3 as intended or 1.15 gm/cm^3. The accuracy of density measurement is in fact somewhere between the 2nd and 3rd decimal places so that 3 figures are justified in instances where quoting to two figures could be misleading).

4.5.1 Surface Settlement

The suspension surface falls relatively quickly at first and slows down significantly after a few hours when the zone of intermediate density reaches the surface (refer to section 4.2). Figure 4.15 shows the settlement curves of the top of the intermediate zone for experiments 10 to 15.

Initially the curves for all but test 15 are steep, corresponding to the period shortly after the intermediate zone reaches the surface. (Suspension surfaces are not plotted in fig 4.15). Thereafter the settling rate decreases steadily as the bed consolidates. Distinction between intermediate and soil behaviour is not apparent from settlement curves. Experiment 15 does not have an initial steep slope as the initial density (1.146 gm/cm^3) is well into the intermediate zone range of densities. Approximately the same mass of soil is present in experiments 11 to 15, which is why all 5 curves approach similar final values.

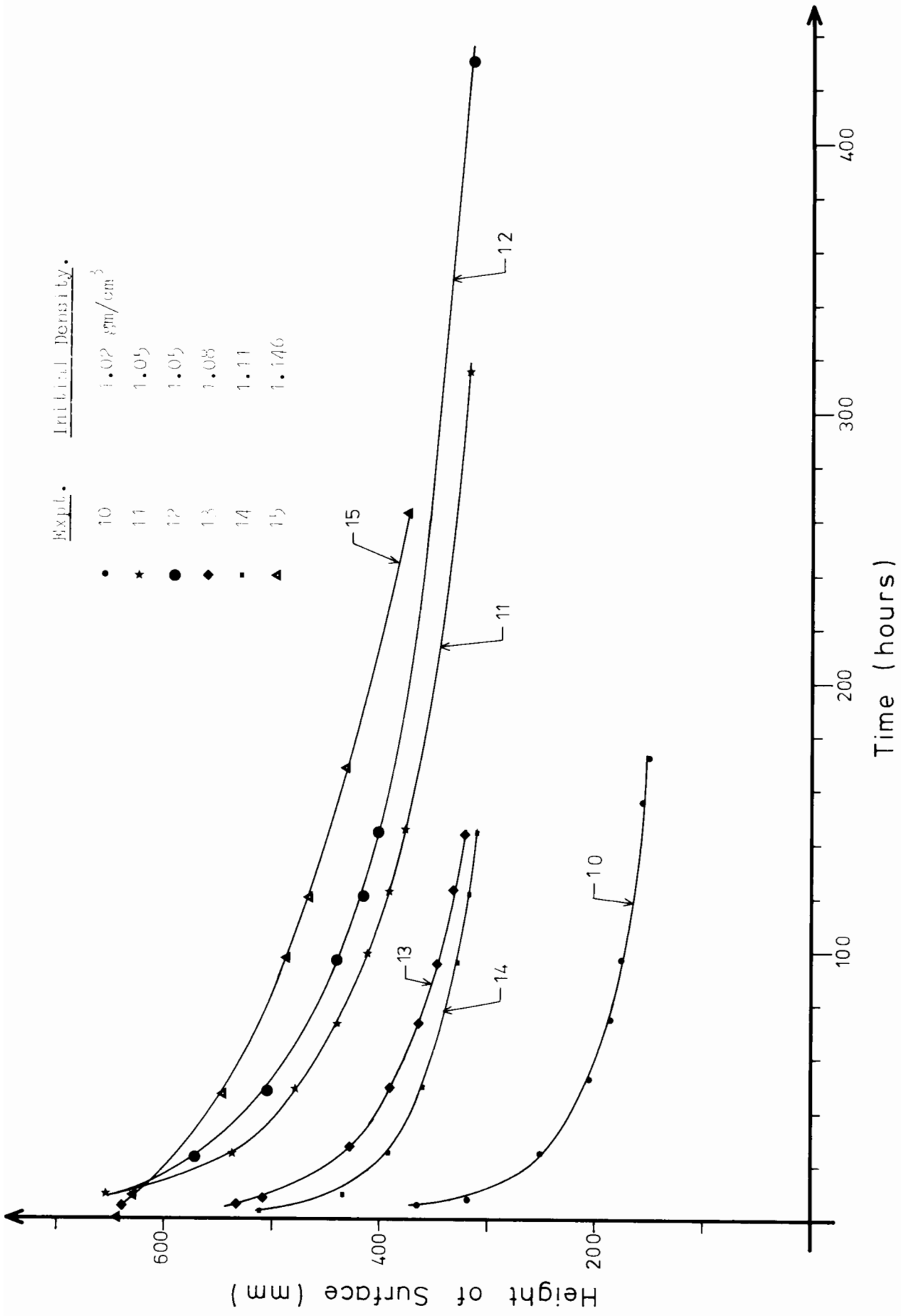


Fig 4.15. Surface Settlement, Experiments 10 - 15.
Duration of Suspension Phase Omitted.

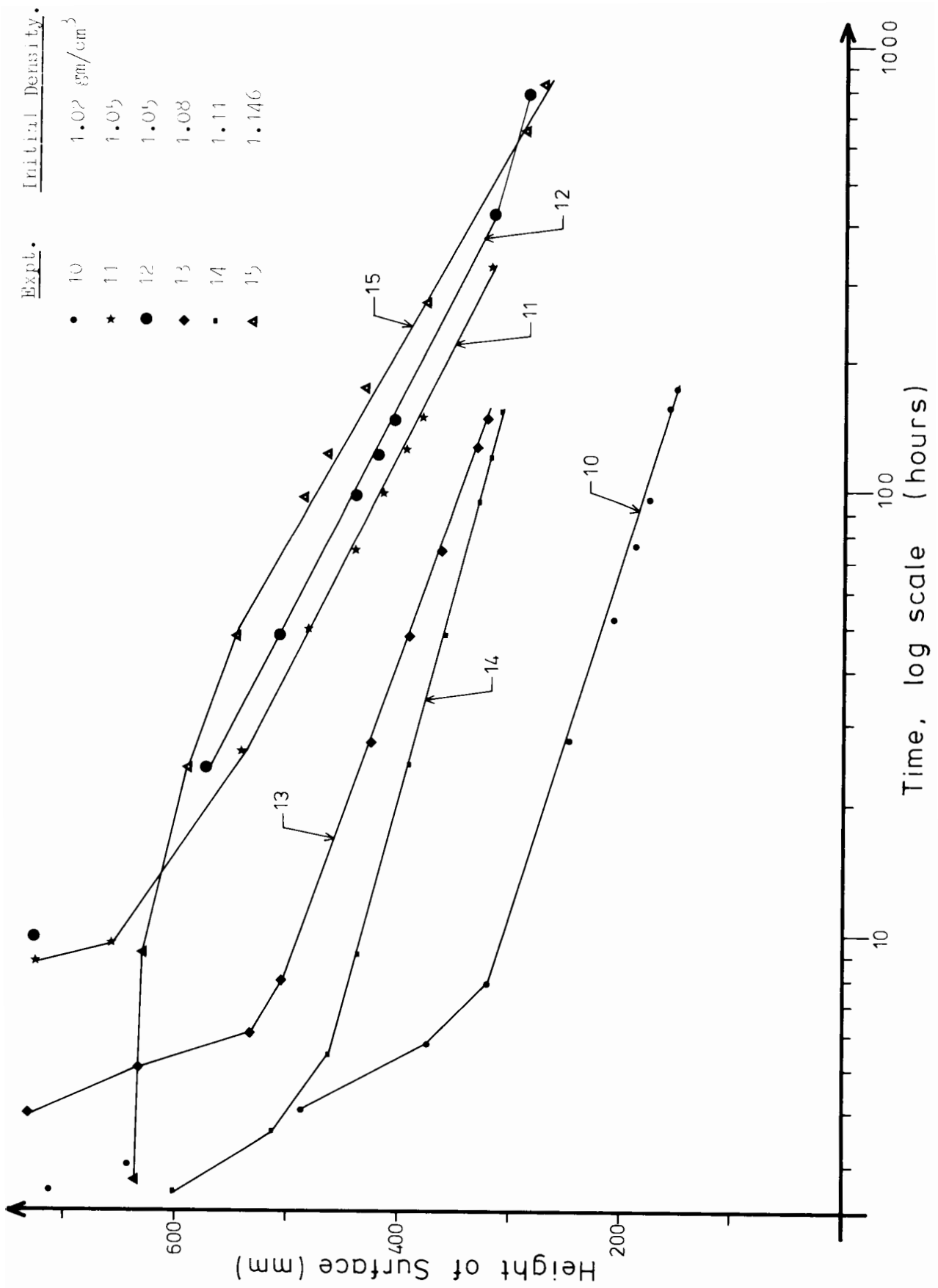


Fig 4.16. Surface Settlement (Log Time), Experiments 10 - 15.
Duration of Suspension Phase Omitted.

Plotted on a logarithm of time scale (fig 4.16), the same curves are linear after 10 hours except for experiment 15 which only becomes linear after about 50 hours. Prior to about 10 hours there is usually still a suspension above the intermediate zone and the curvature of the plots is clearly different as a result.

4.5.2 Density

Several density profiles, excluding those when a suspension still exists, are shown for each of experiments 10 to 15 in figures 4.17 to 4.22 respectively.

The normal trend in all these tests is for the density (excluding the relatively dense layer at the base) to increase gradually and almost uniformly, causing the surface to settle accordingly. Little change occurs in the dense base layer. Only experiments 14 and 15 have slightly outstanding features, as a result of their higher initial densities (1.11 and 1.146 gm/cm^3).

Experiment 15 has more uniform densities in earlier profiles because it has an intermediate zone density that is artificially uniform in the first place. A dense base layer as found in other tests is absent (indicating no particle size segregation) and the curvature of the 848 hour profile is not consistent with other observations. There is a possibility that disturbance of the column during other activities in the laboratory caused this, but effects of creep or real behaviour cannot be disregarded entirely.

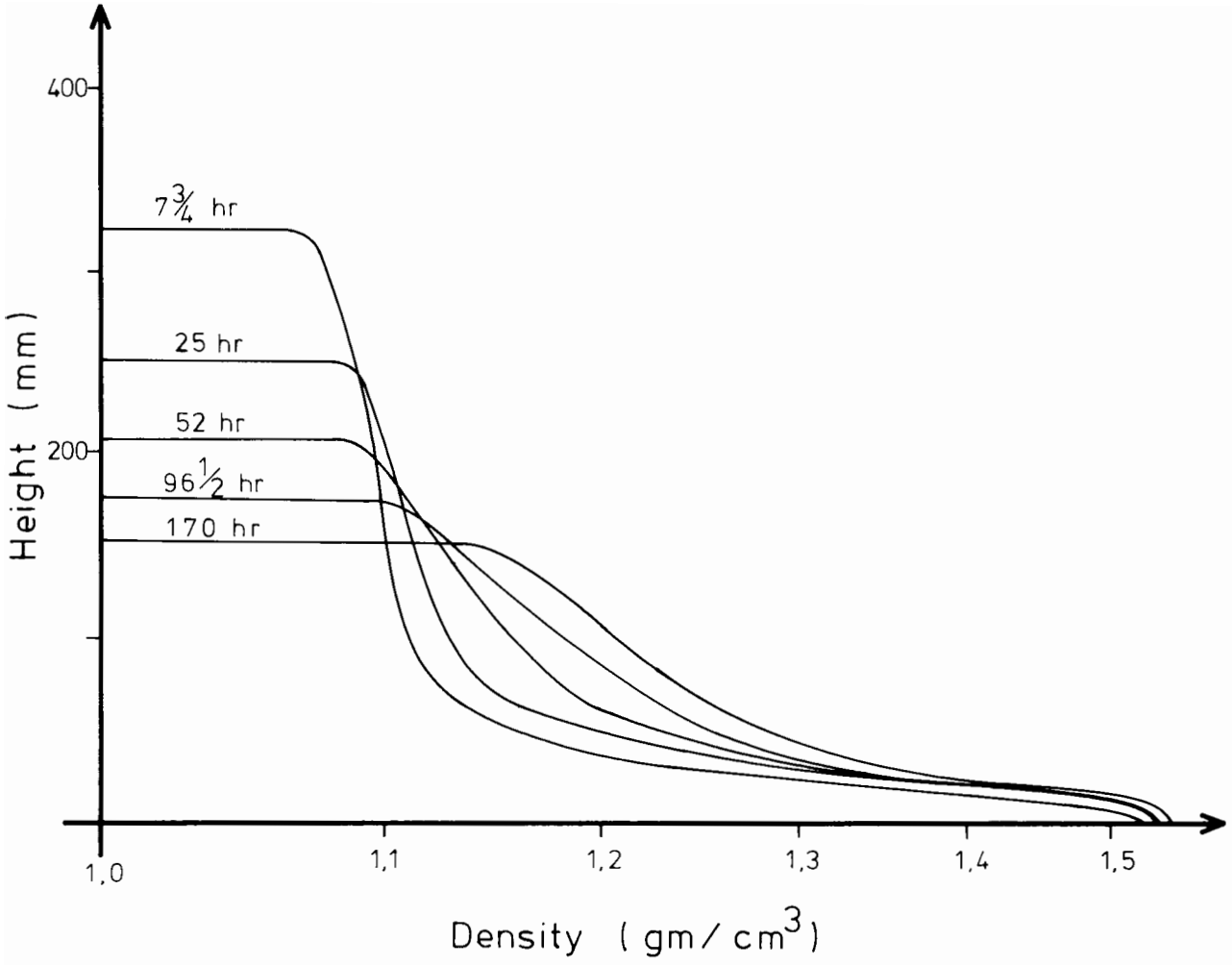


Fig 4.17. Density Profiles, Experiment 10.
Initial Density 1.02 gm/cm^3.

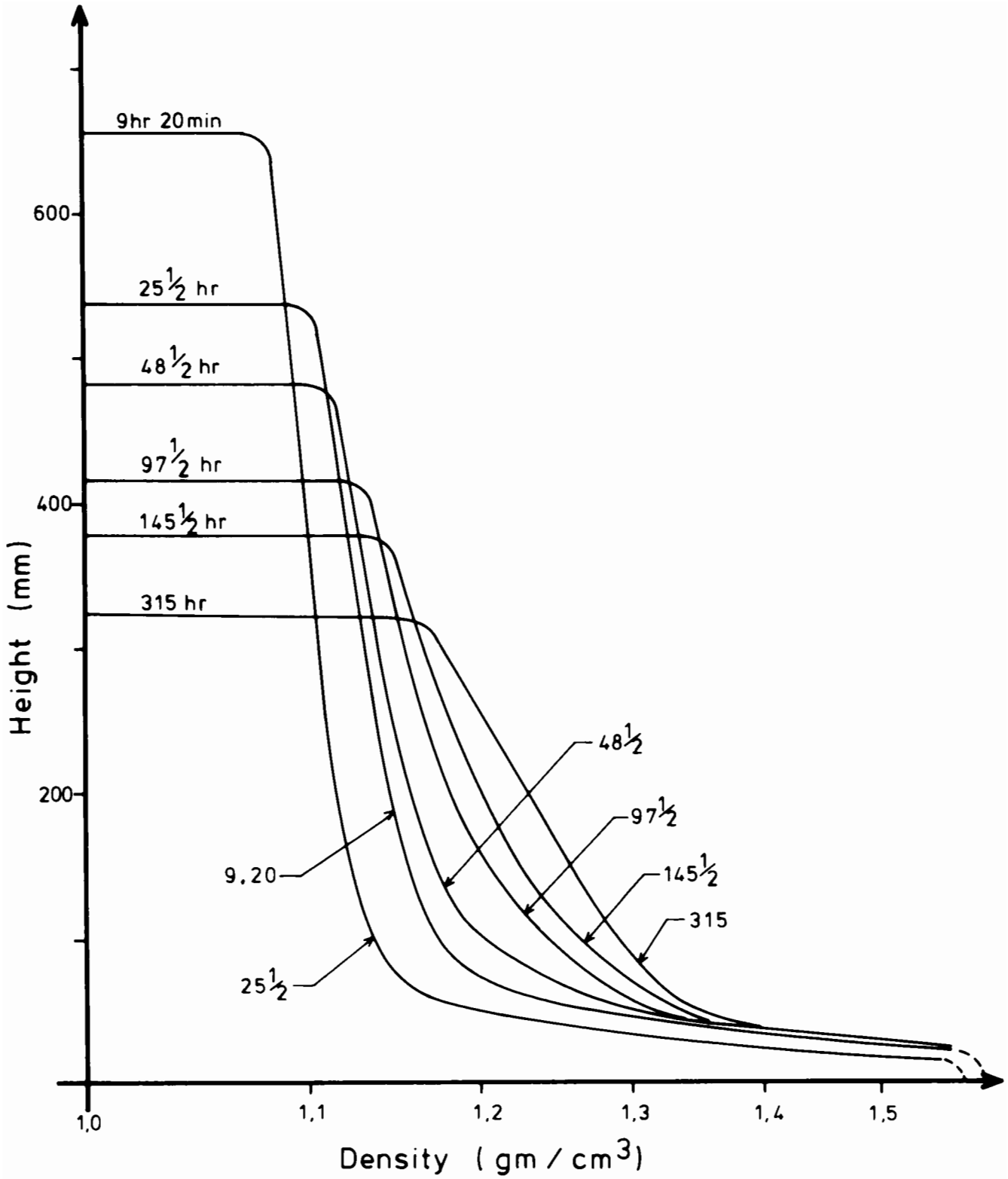


Fig 4.18. Density Profiles, Experiment 11.
Initial Density 1.05 gm/cm^3.

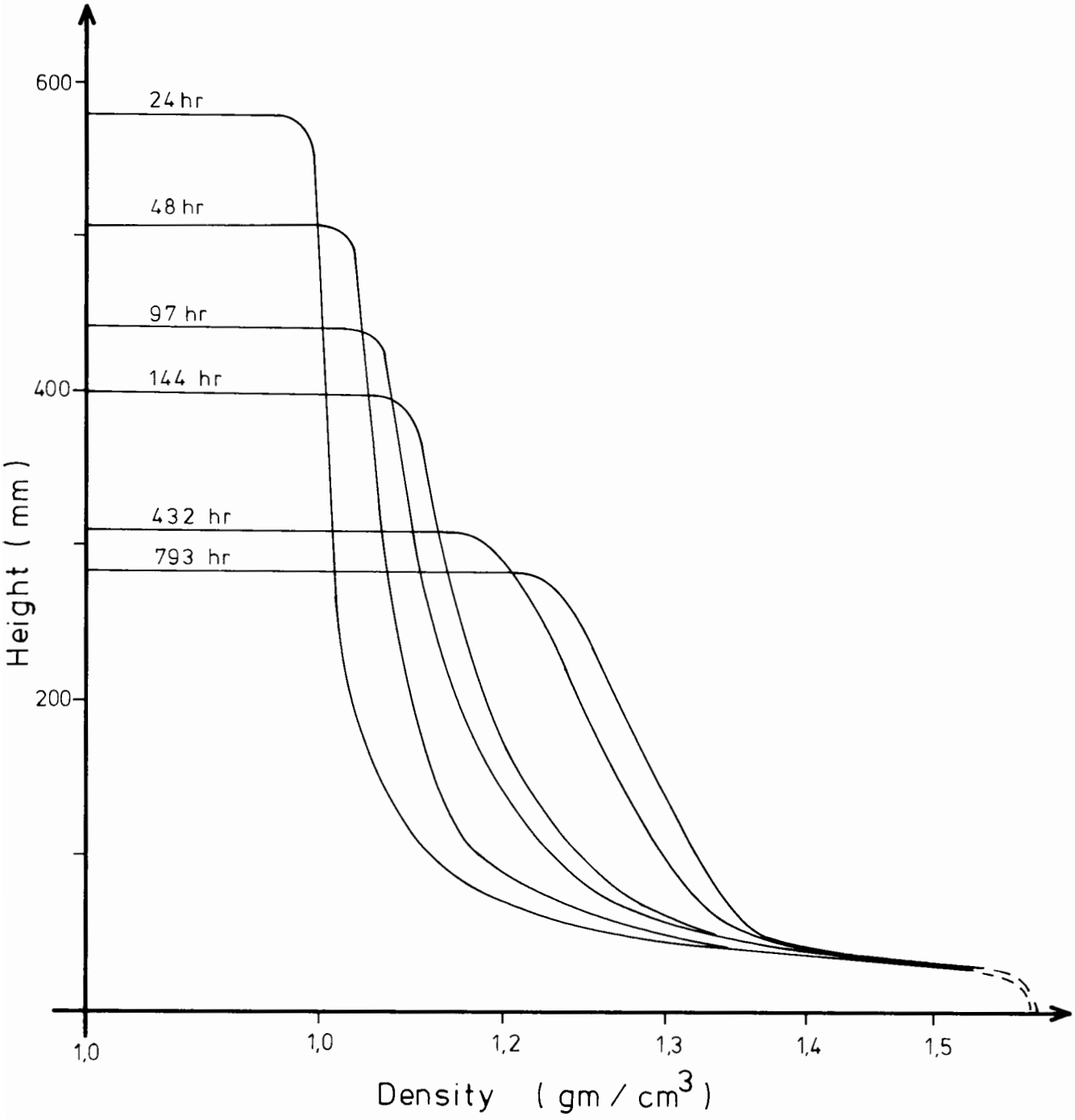


Fig 4.19. Density Profiles, Experiment 12.
Initial Density 1.05 gm/cm^3.

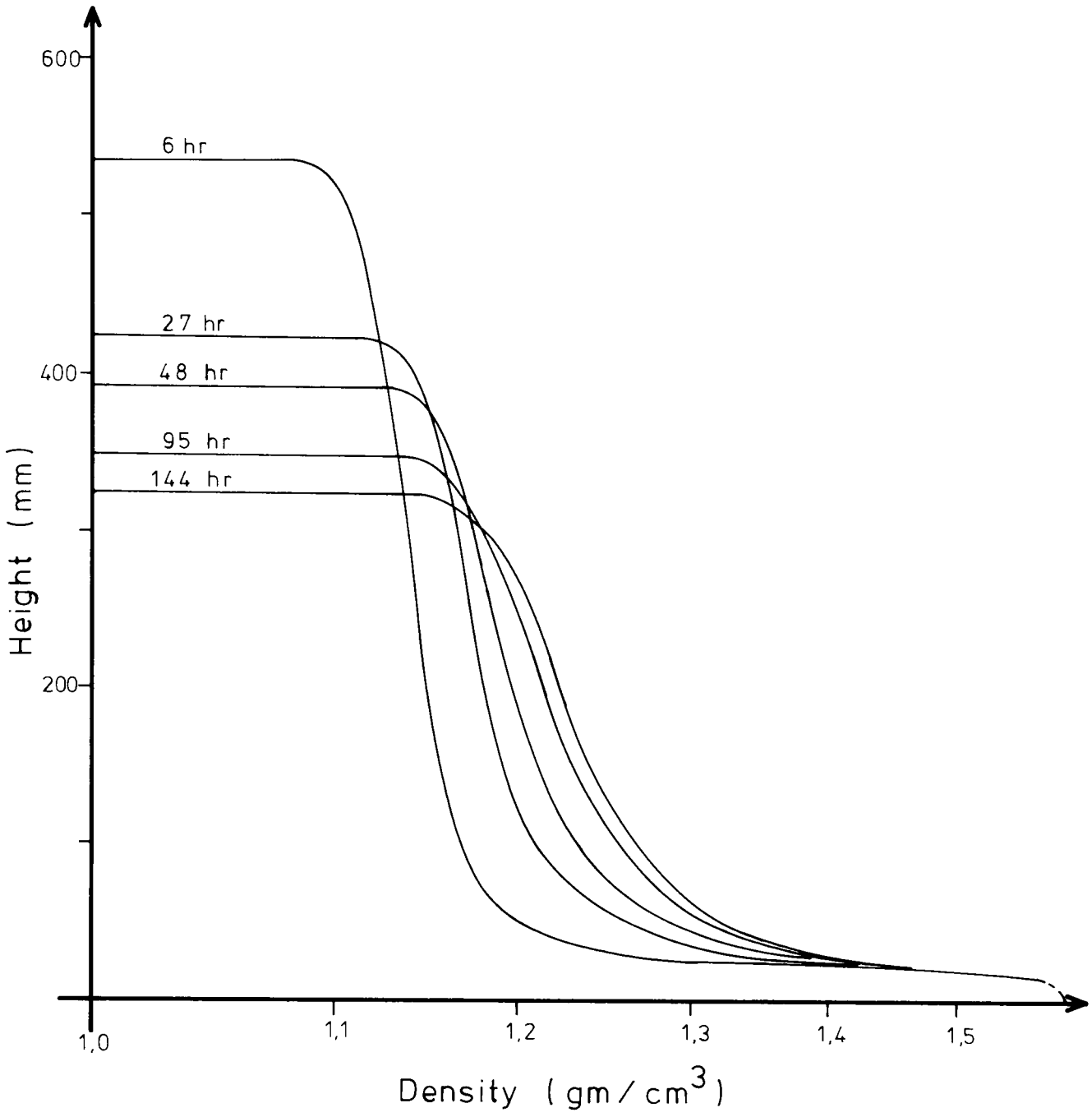


Fig 4.20. Density Profiles, Experiment 13.
Initial Density 1.08 gm/cm^3.

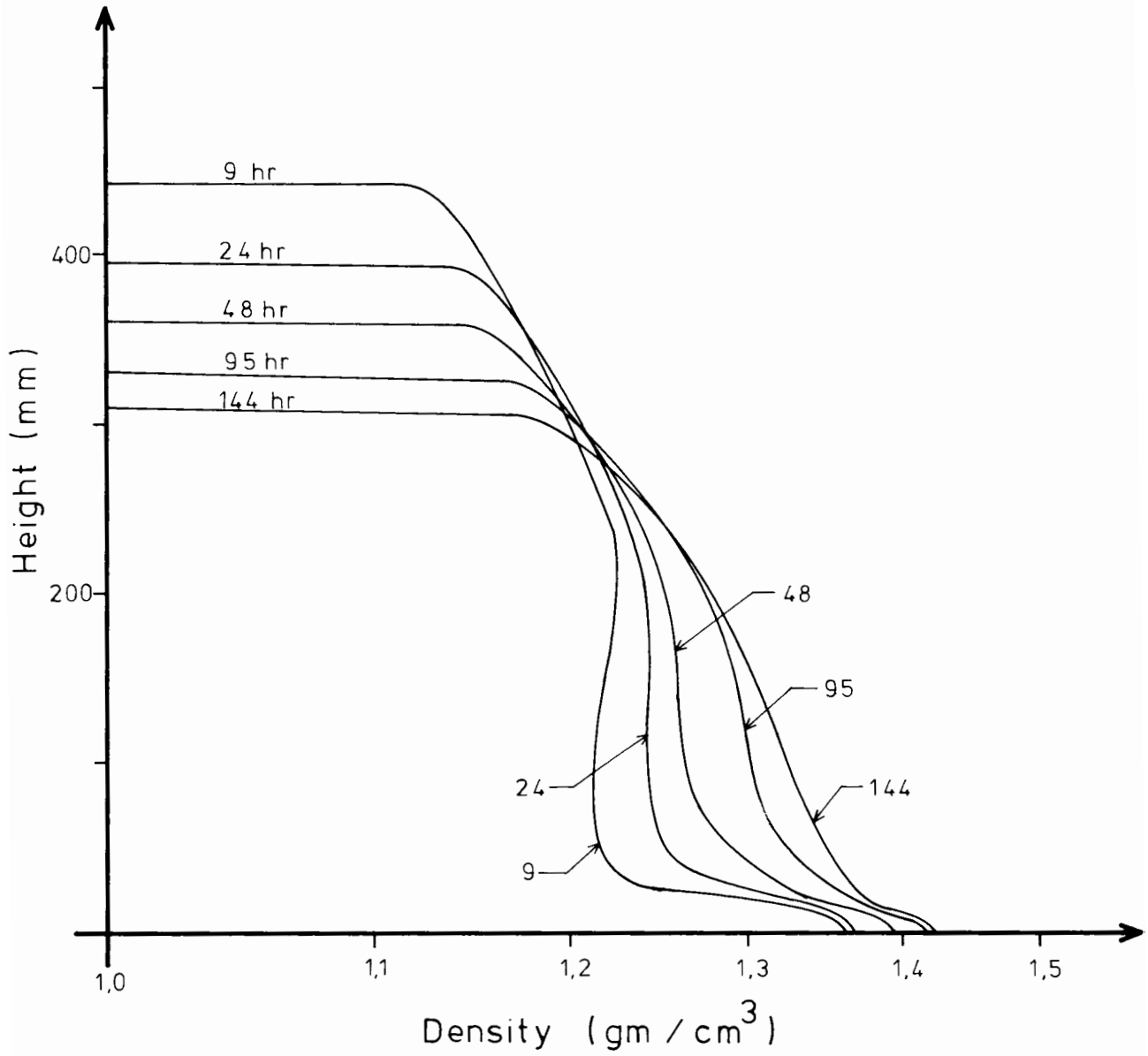


Fig 4.21. Density Profiles, Experiment 14.
Initial Density 1.11 gm/cm^3.

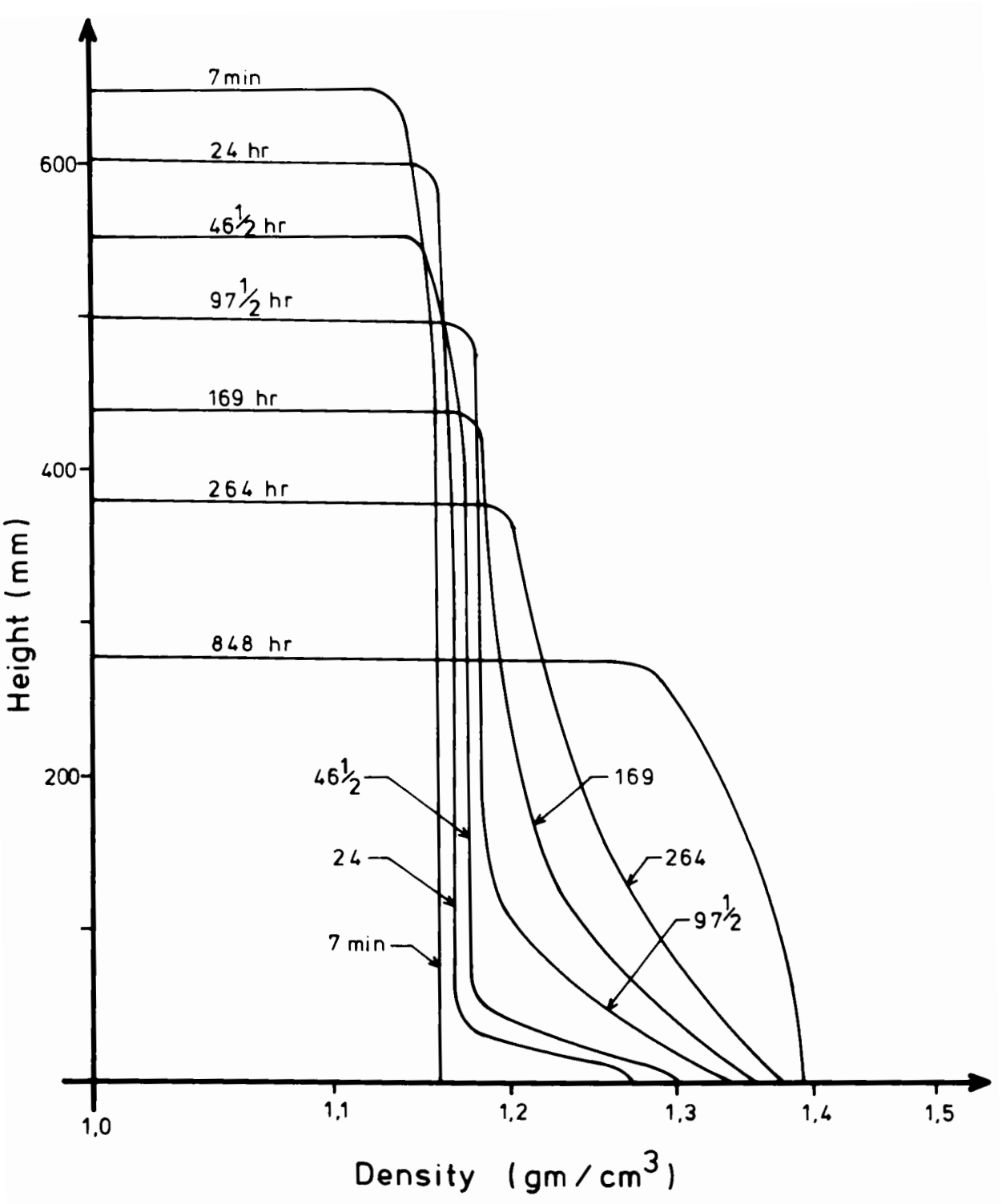


Fig 4.22. Density Profiles, Experiment 15.
Initial Density 1.146 gm/cm^3.

A reversed density gradient occurs in the lower portion of the early profiles in experiment 14 and below the surface the density changes noticeably, rather than remaining nearly uniform. These features appear to be the result of instabilities in settling behaviour, at densities between something that is clearly a suspension and something that is not. Further consideration of this is given in subsequent chapters.

4.5.3 Pore Water Pressure

Excess pore water pressure isochrones are drawn for experiments 10 to 15 in figures 4.23 to 4.28. These have not been normalised so the curves start on the height axis at the level of the mud/water interface at that time. Arrows on the pressure axes indicate the maximum possible values of excess pore water pressure at the base of the column, which will be equal to the total stress (above hydrostatic pressure) when the suspension is first placed, and the effective stress when the soil is fully consolidated.

In general the isochrones reflect conditions in the column indicated by other measurements well. Most early isochrones are concave upwards following the total stress curve (which is concave upwards because density increases with depth) until sufficient pressure is dissipated to reverse the curvature. This is most notable in experiment 10 (figs 4.23 and 4.17) where the density gradient is steep.

There is a relatively rapid dissipation of pore pressure at the base of the column in the first few hours. Water expelled by consolidation near the base has to flow upwards through the soil above,

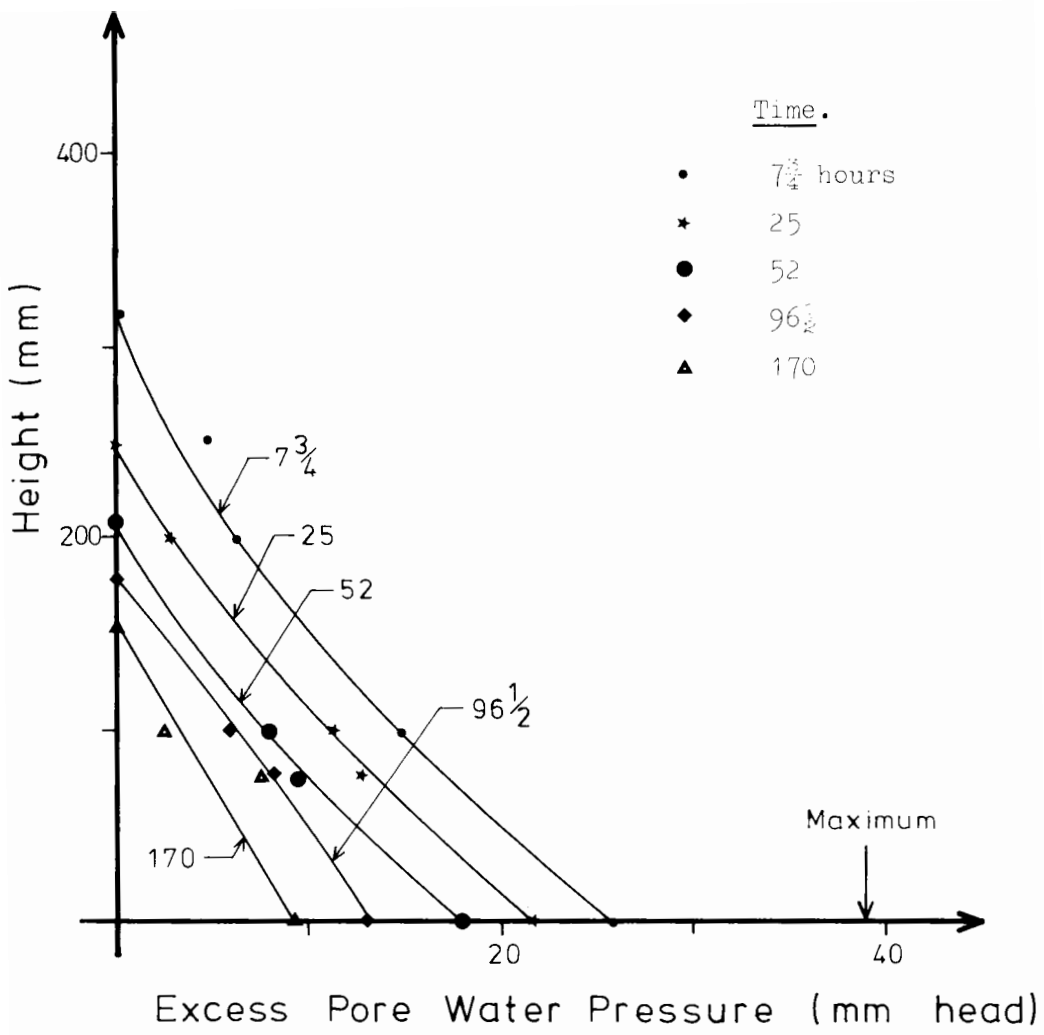


Fig 4.23. Pore Water Pressure, Experiment 10.
Initial Density 1.02 gm/cm^3, 39 mm head Maximum Pressure.

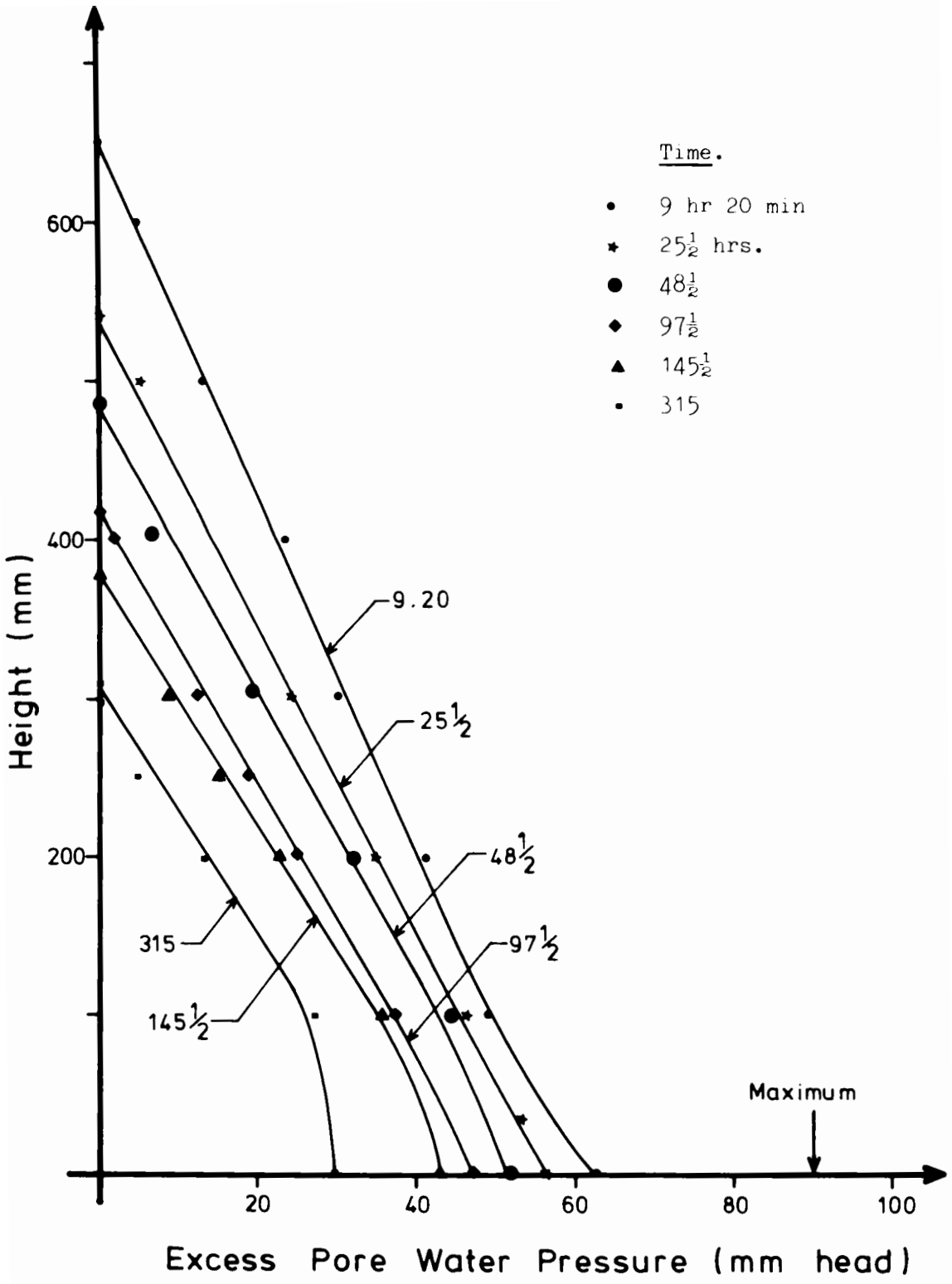


Fig 4.24. Pore Water Pressure, Experiment 11.
Initial Density 1.05 gm/cm^3, 90 mm head Maximum Pressure.

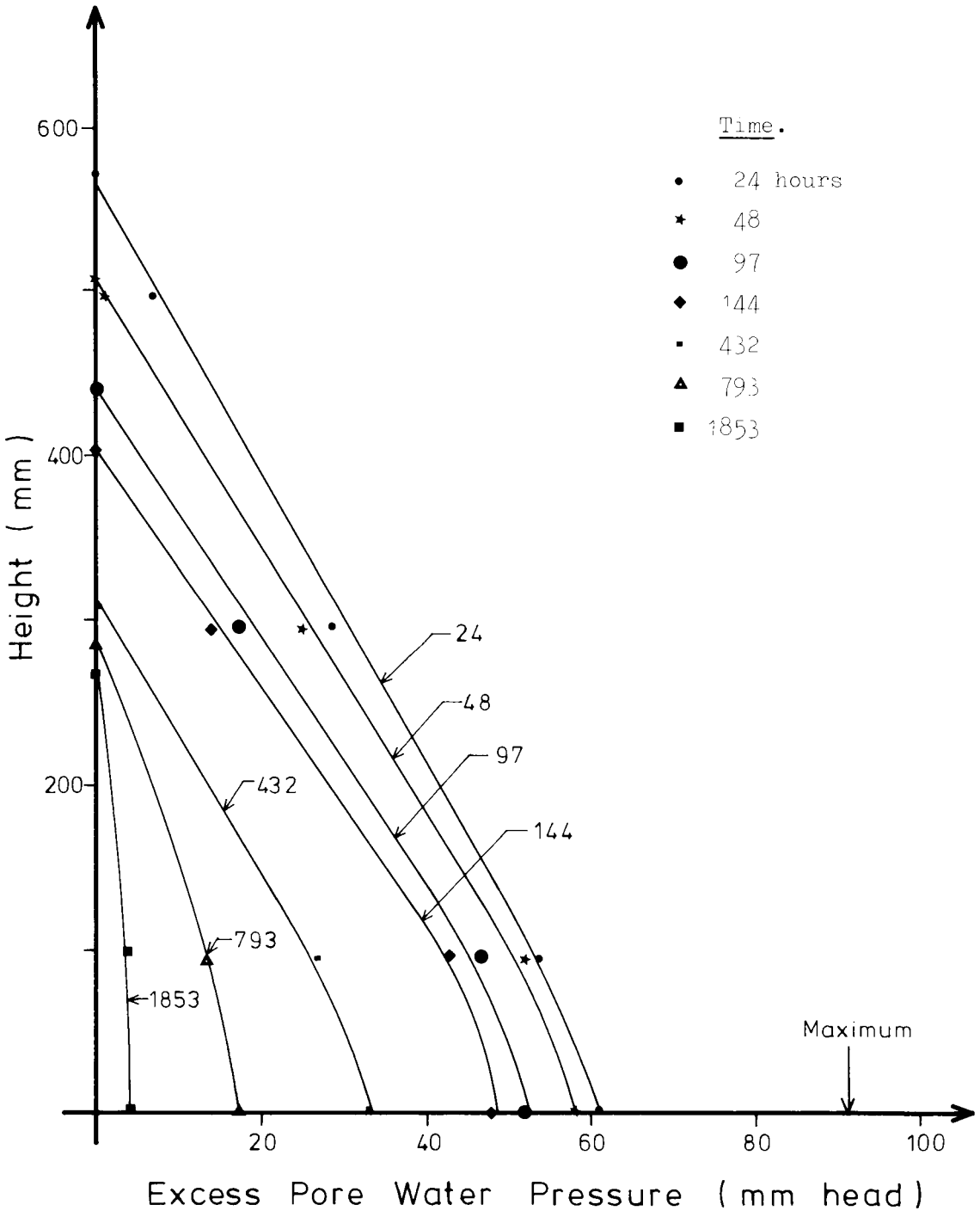


Fig 4.25. Pore Water Pressure, Experiment 12.
Initial Density 1.05 gm/cm^3, 91 mm head Maximum Pressure.

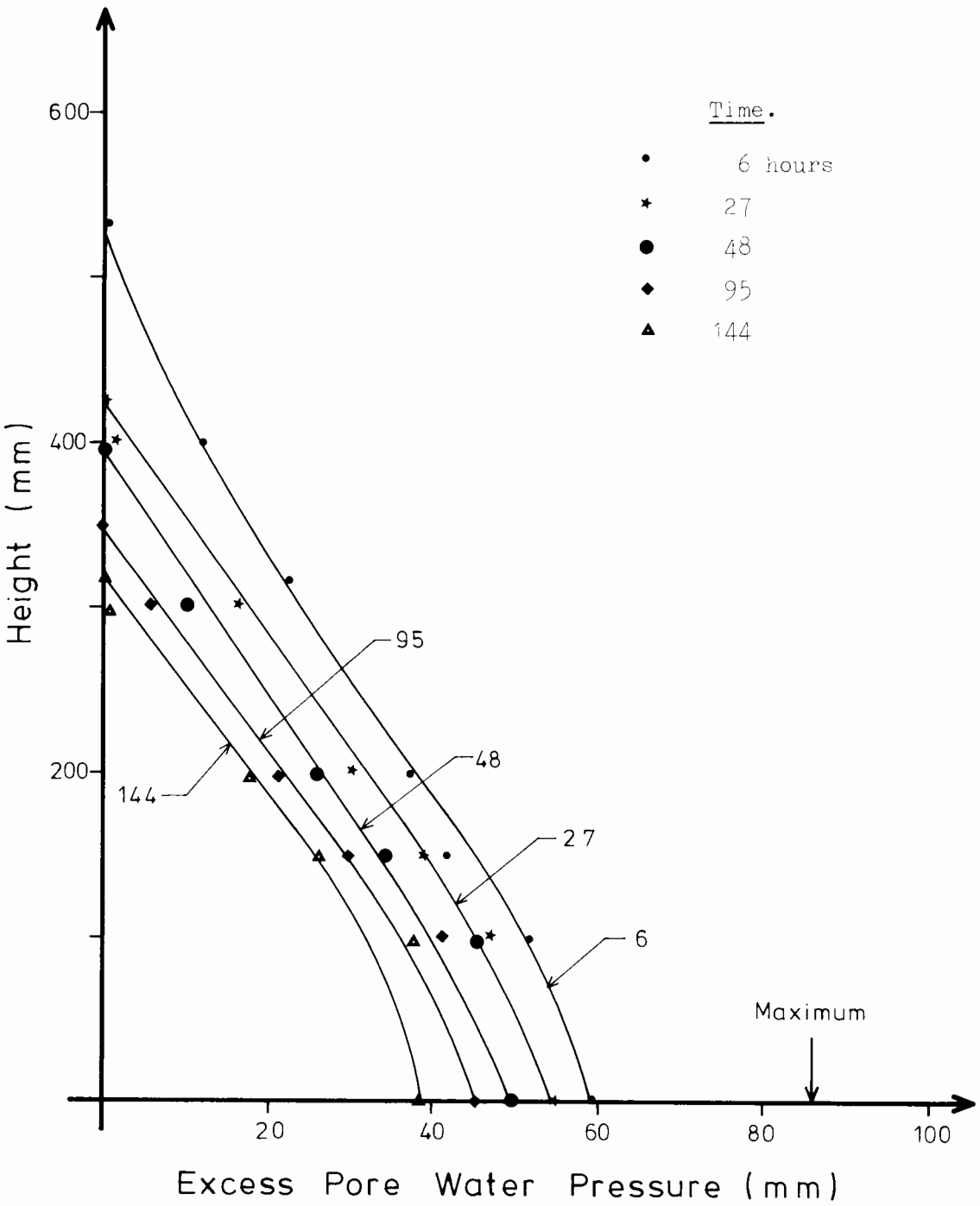


Fig 4.26. Pore Water Pressure, Experiment 13.
Initial Density 1.08 gm/cm^3, 86 mm head Maximum Pressure.

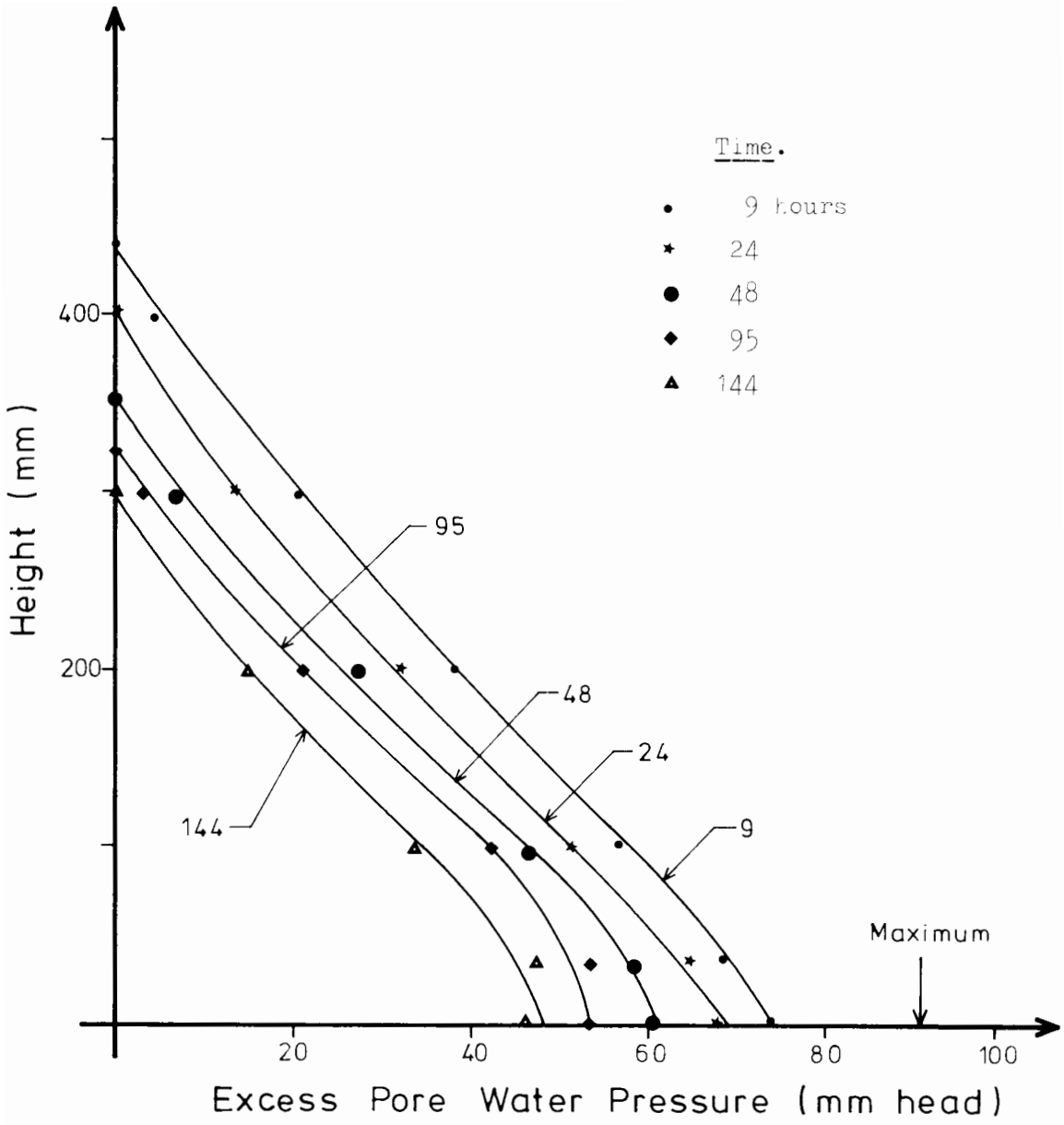


Fig 4.27. Pore Water Pressure, Experiment 14.
Initial Density 1.11 gm/cm^3, 90 mm head Maximum Pressure.

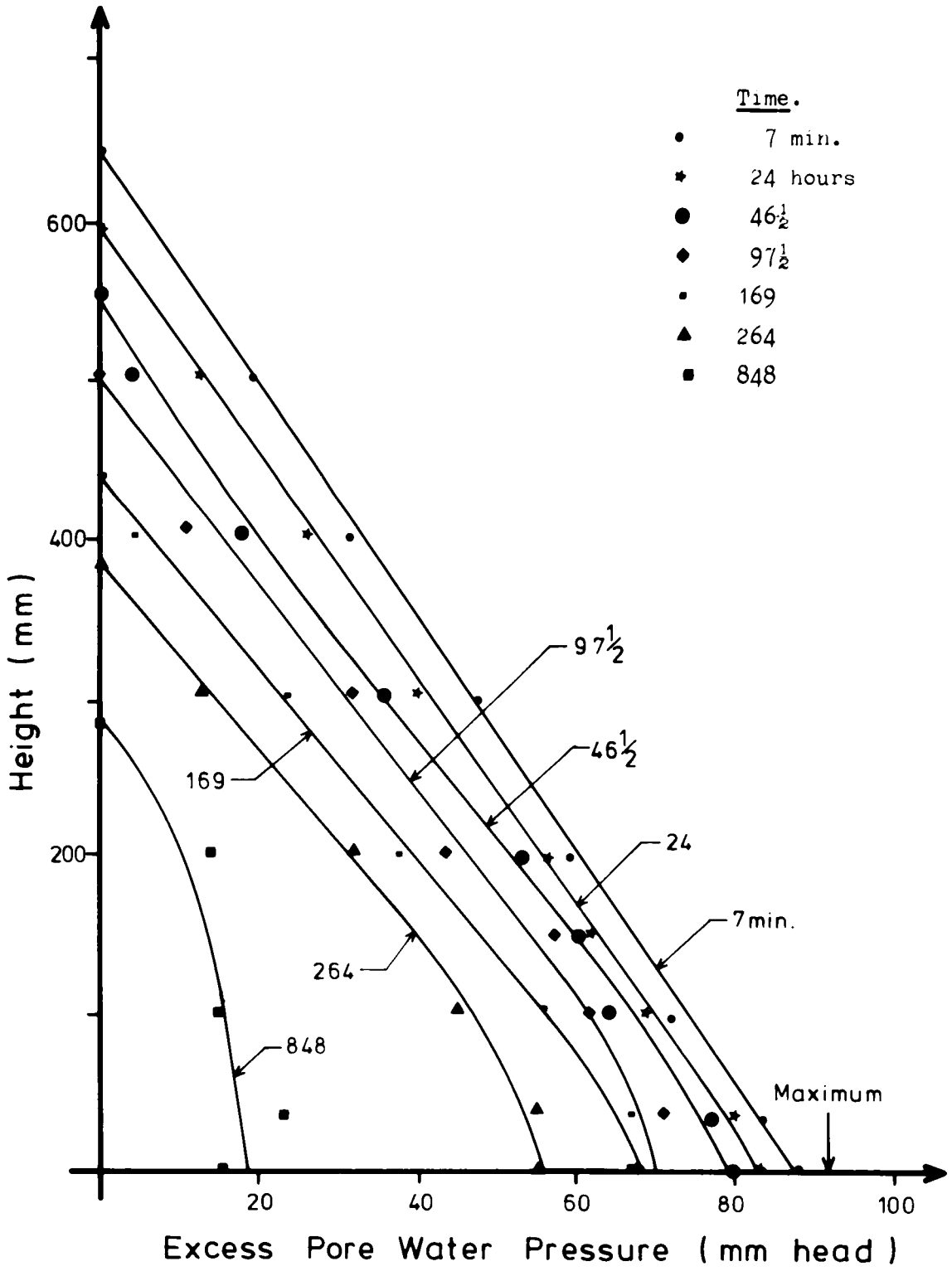


Fig 4.28. Pore Water Pressure, Experiment 15.
Initial Density 1.146 gm/cm^3, 94 mm head Maximum Pressure.

retarding the consolidation of the upper regions. Lee (1979) predicts this more rapid initial consolidation near the base from a theoretical consideration of instantaneously dumped dredged fill. Differential settling and segregation of particle sizes will augment this effect by increasing the relative permeability of the lower layers of soil in the present series of tests.

4.5.4 Effective Stress Development

Integrating the density profile above a point, giving total stress, and subtracting the pore water pressure gives the effective stress. Void ratios can be calculated directly from densities and the void ratio/effective stress relationship plotted as in figures 4.29 to 4.34 for experiments 10 to 15.

Values have been calculated for 5 points in the soil and joined by straight lines to simplify identification. These points are fixed, not in space but in terms of the material coordinates, z, so that the lines join points referring to the same element of soil. Each line is identified by a value of η, the normalized material coordinate, where

$$\eta = \frac{z}{z_c}$$

and z is the solid thickness of material between the point and the base (material coordinate)

z_o is the total solid thickness of the mud

Thus $\eta = 0$ at the base of the column and $\eta = 1$ at the mud surface.

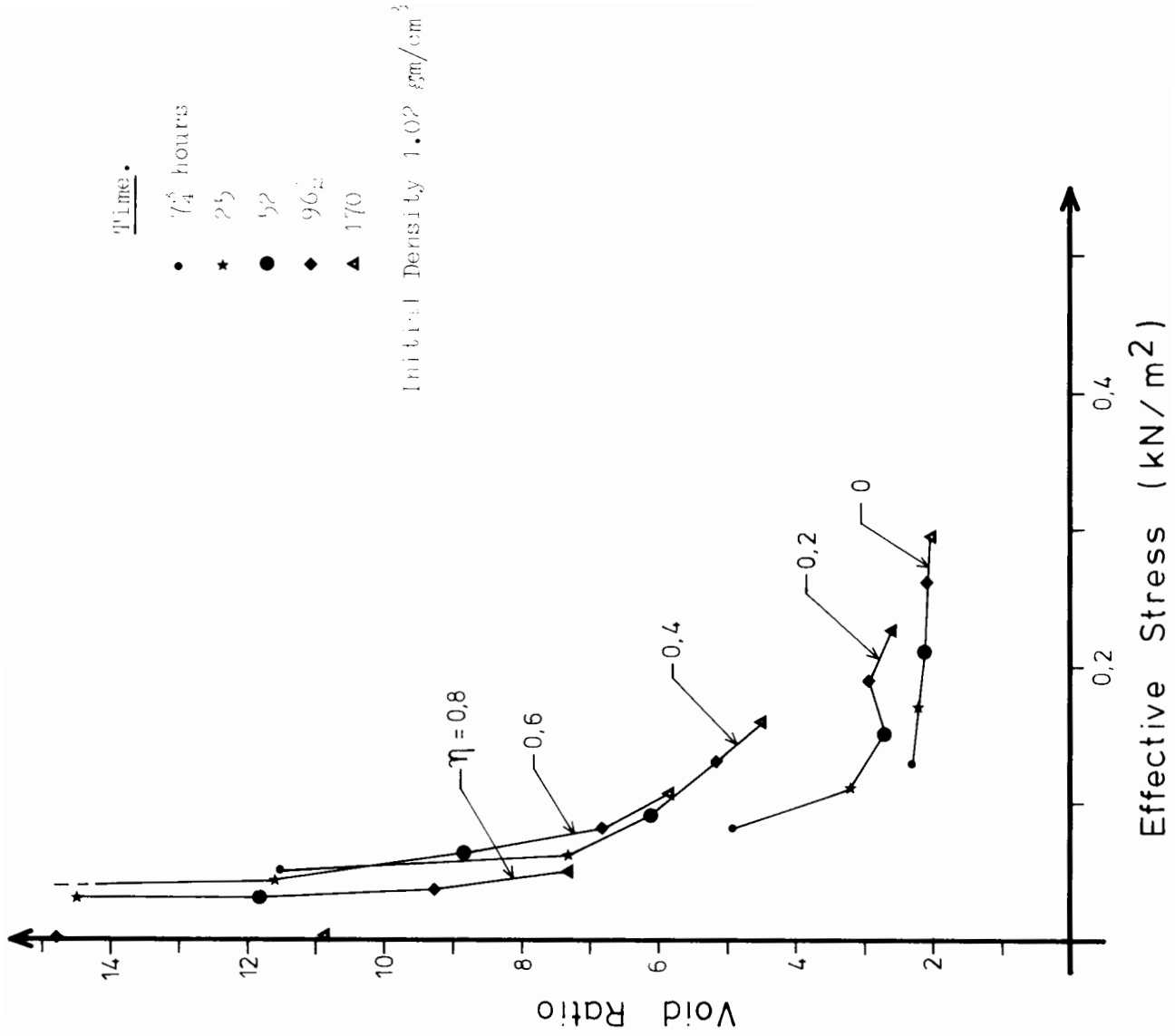


Fig 4.29. Void Ratio / Effective Stress, Experiment 10.
Initial Density 1.02 gm/cm^3.

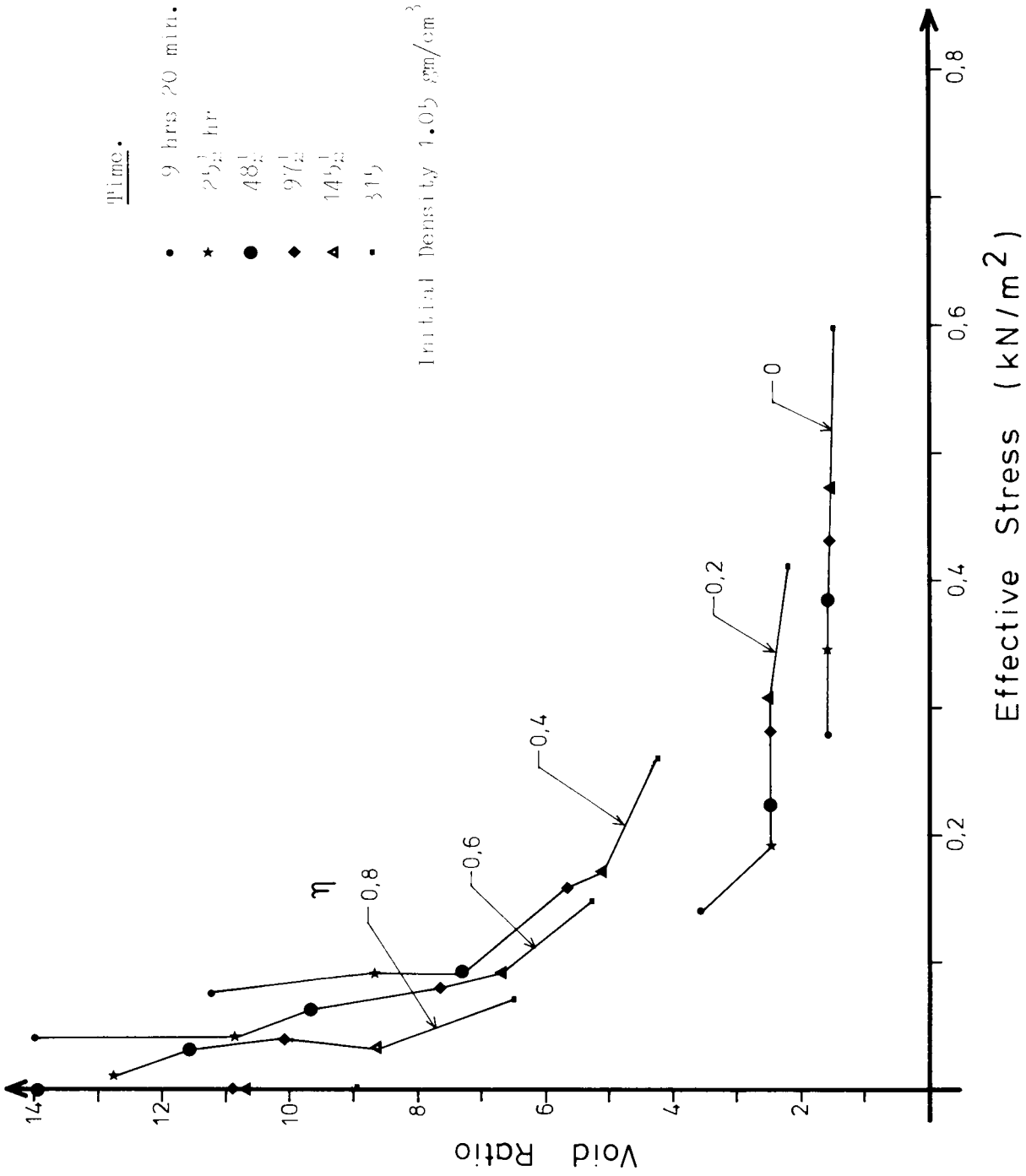


Fig 4.30. Void Ratio / Effective Stress, Experiment 11.
Initial Density 1.05 gm/cm^3.

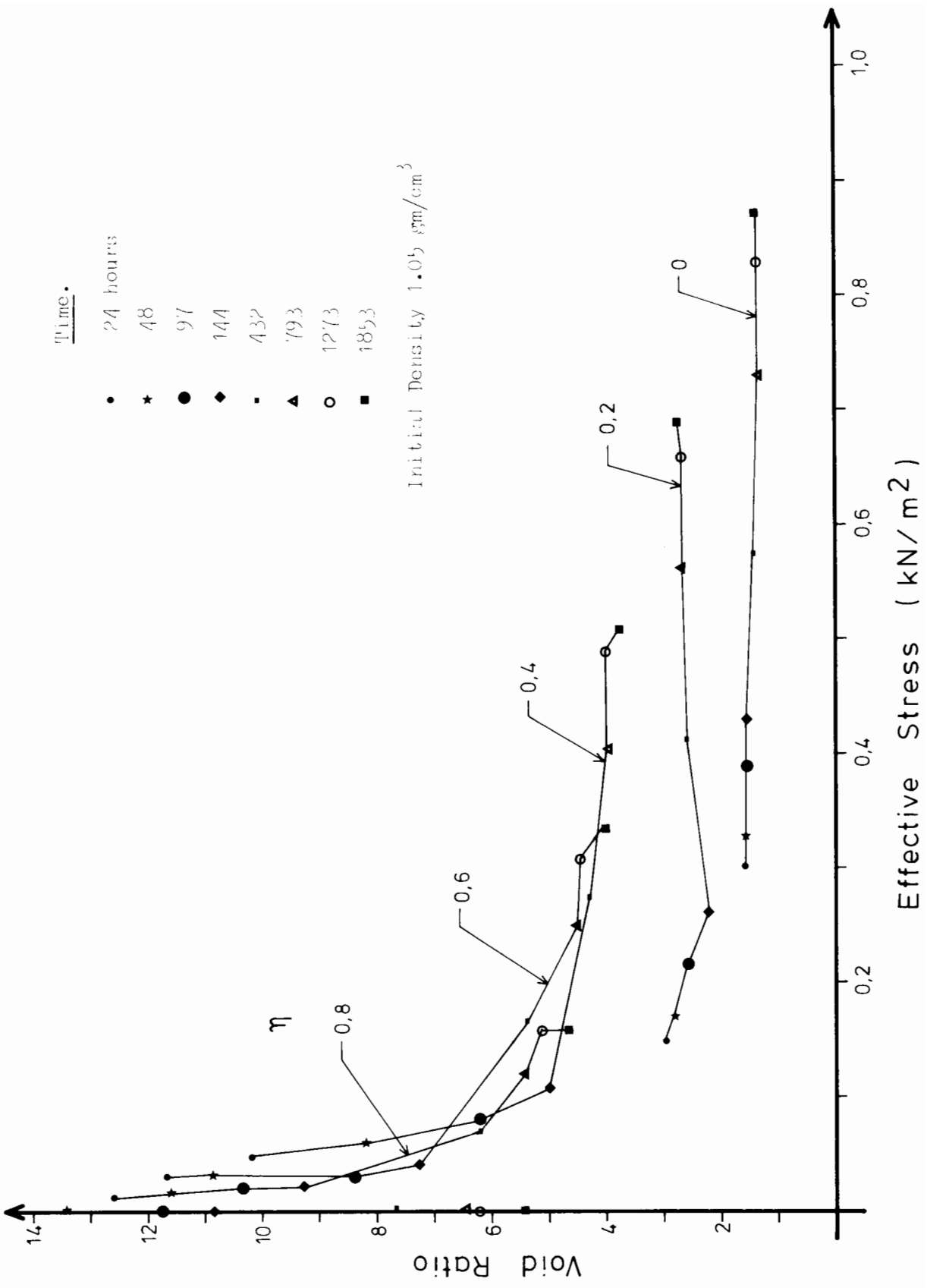


Fig 4.31. Void Ratio / Effective Stress, Experiment 12.
Initial Density 1.05 gm/cm^3.

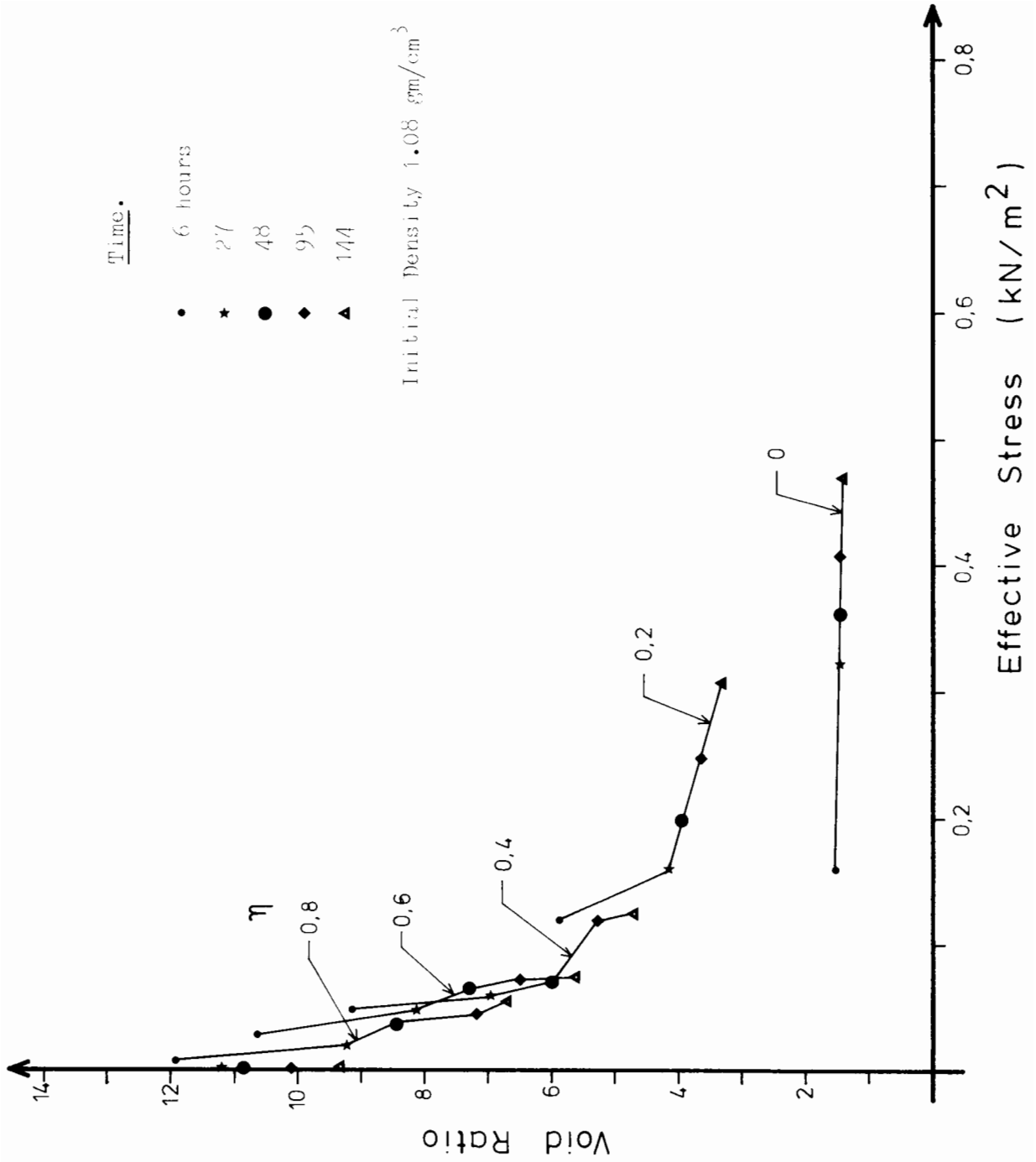


Fig 4.32. Void Ratio / Effective Stress, Experiment 13.
Initial Density 1.08 gm/cm^3.

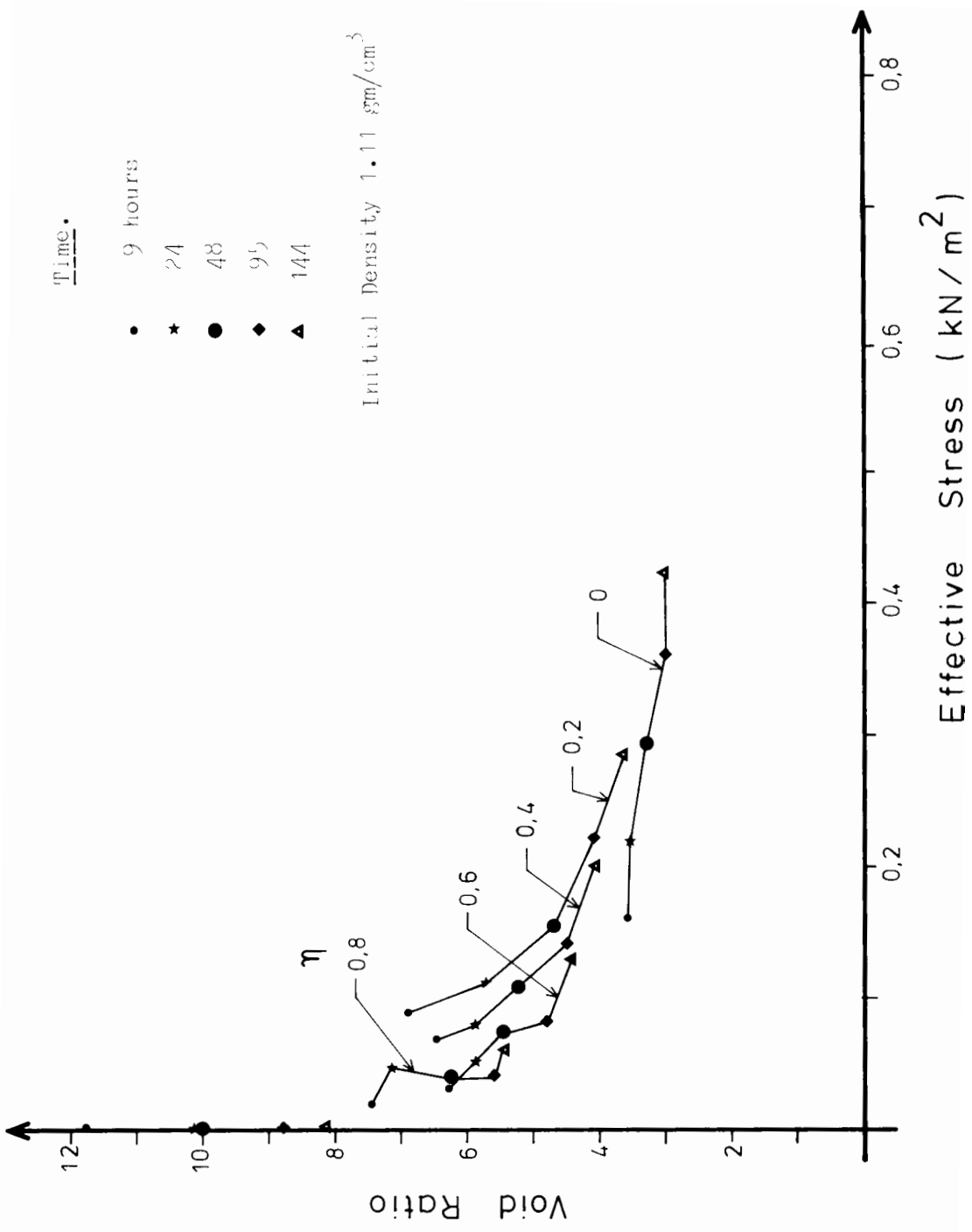


Fig 4.33. Void Ratio / Effective Stress, Experiment 14.
Initial Density 1.11 gm/cm^3.

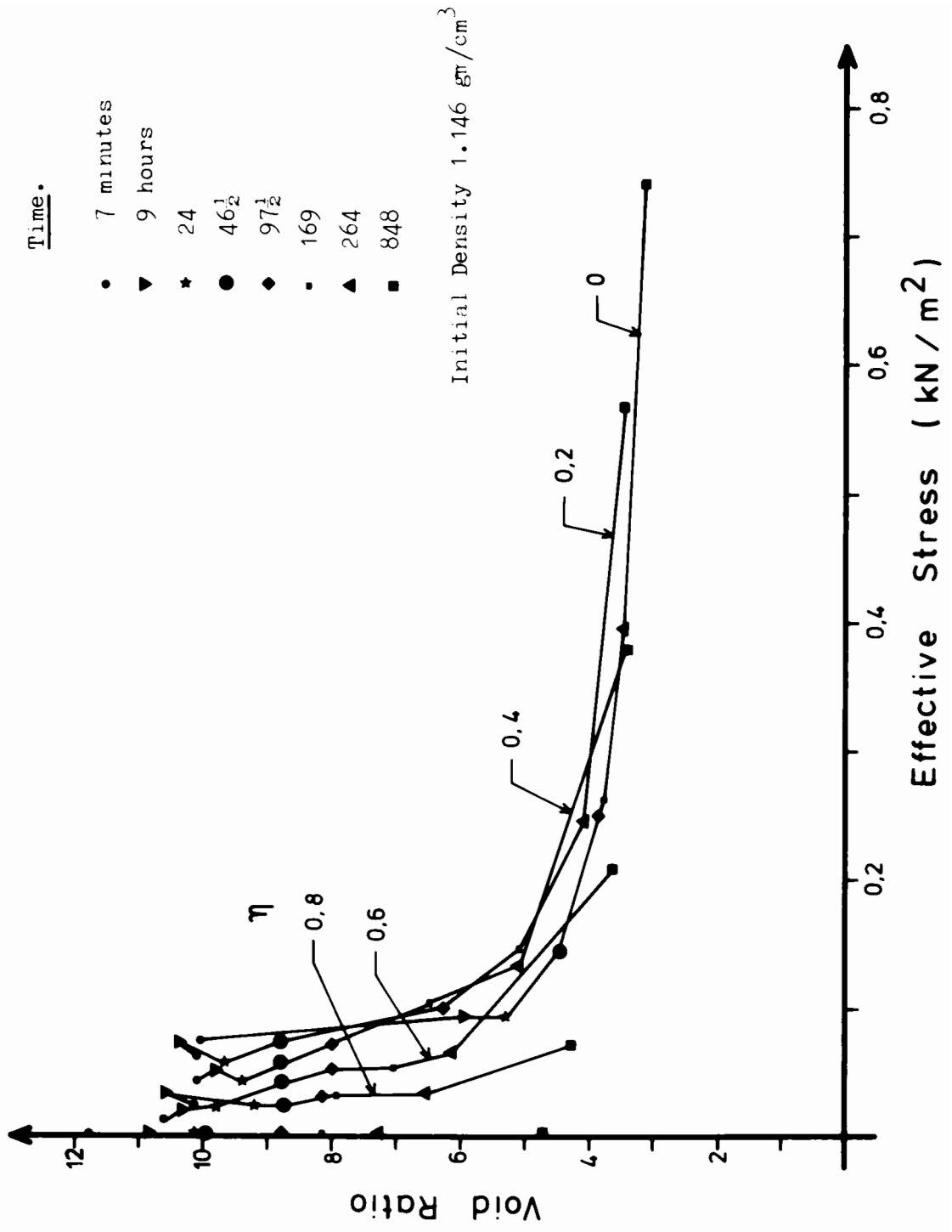


Fig 4.34. Void Ratio / Effective Stress, Experiment 15.
Initial Density 1.146 gm/cm^3.

In the graphs of void ratio against effective stress, values calculated for the bottom of the soil where there are dense layers as a result of particle segregation are slightly different from higher up, and the soil is stiffer. This is not surprising in view of the predominance of coarse silt particles in this region.

Disregarding these points there is still not a unique relationship between void ratio and effective stress in all tests. In other words at a void ratio of approximately 6 the soil could have a range of effective stresses from 0 - 0.1 kN/m^2 even though all parts of the soil are on a virgin consolidation line. Similarly, the zero effective stress element on the soil surface can have a wide range of void ratios. However, as the effective stress increases, the spread of values reduces significantly, reflecting a more soil like behaviour.

4.5.5 Permeability

Permeability can be deduced from density and pore water pressure distributions, assuming Darcy's law in the form

$$v_r = ki \qquad (4.1)$$

where v_r is the relative velocity of the fluid to the solid phase

i is the hydraulic gradient

k is the permeability

The total volume below any fixed section in the column must necessarily remain constant, so that, at the section,

solid flow + fluid flow = 0

Therefore,

$$v_s(1-n) + v_f n = 0 \qquad (4.2)$$

where v_s is velocity of solid phase

v_f is velocity of fluid

n is porosity

and the relative velocity is given by

$$v_r = (v_f - v_s) = \frac{-v_s}{n} \qquad (4.3)$$

where the negative sign indicates the relative velocity is opposite to the direction of the solid velocity. Combining 4.1 and 4.3, the permeability* is found as

$$k = -\frac{v_s}{ni} \qquad (4.4)$$

The average solids velocity for an element of the soil for the time between taking two density profiles is simply the change in height of that soil element divided by the time between the profiles. An average hydraulic gradient and porosity can be calculated directly from the pore pressure curves and density profiles respectively and thus an average permeability for a soil element is found.

Figures 4.35 to 4.40 show plots of permeability calculated in this way versus void ratio for experiments 10 to 15. Lines connect values referring to the same elements of soil for identification as before.

* The more correct form of Darcy's law for eq. 4.1 (used in eq. 6.35) results in eq. 4.4 without the factor n. Since $n \simeq 1$ in this case the calculated permeabilities are approximately correct.

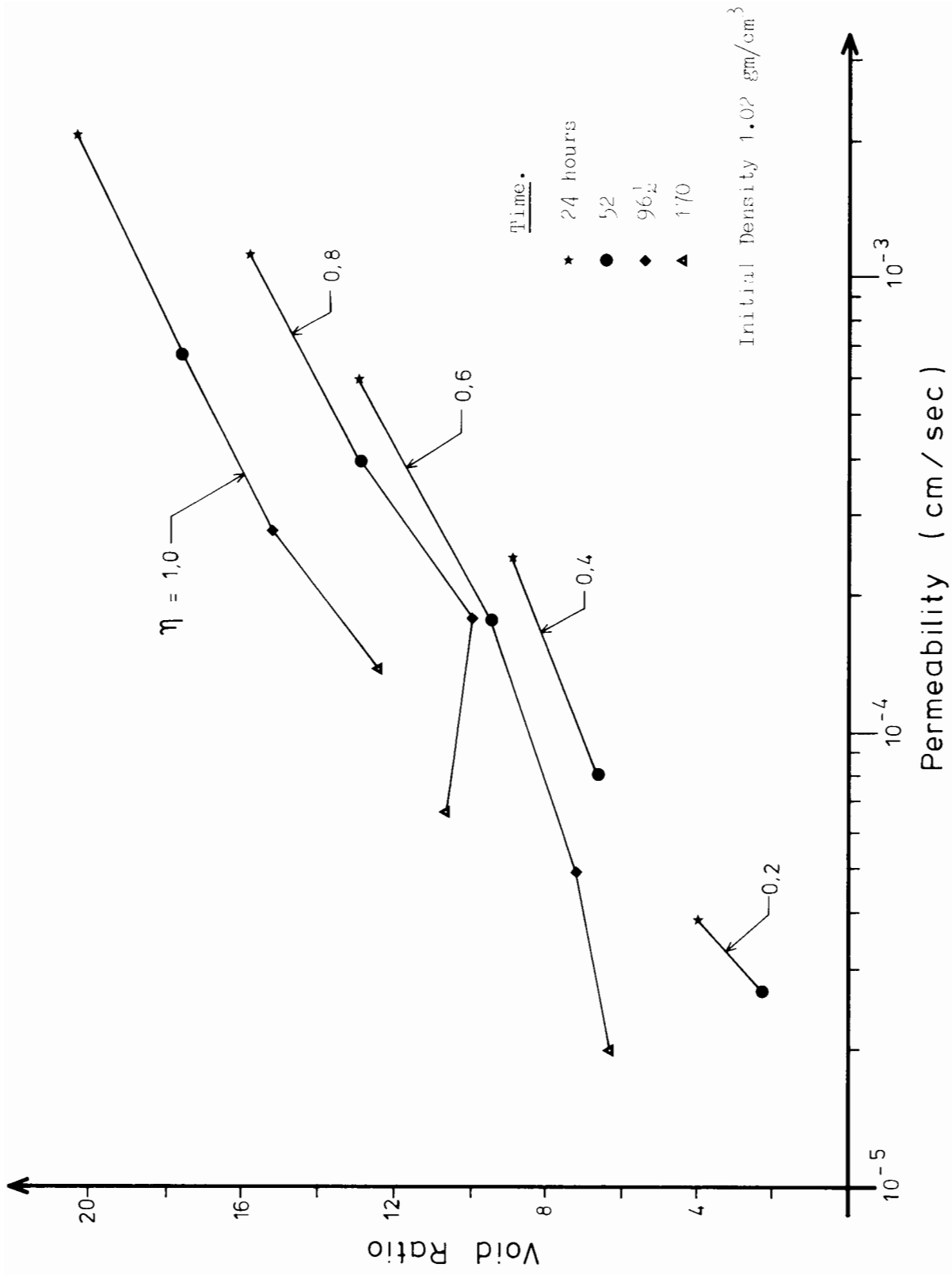


Fig 4.35. Permeability / Void Ratio, Experiment 10.
Initial Density 1.02 gm/cm^3.

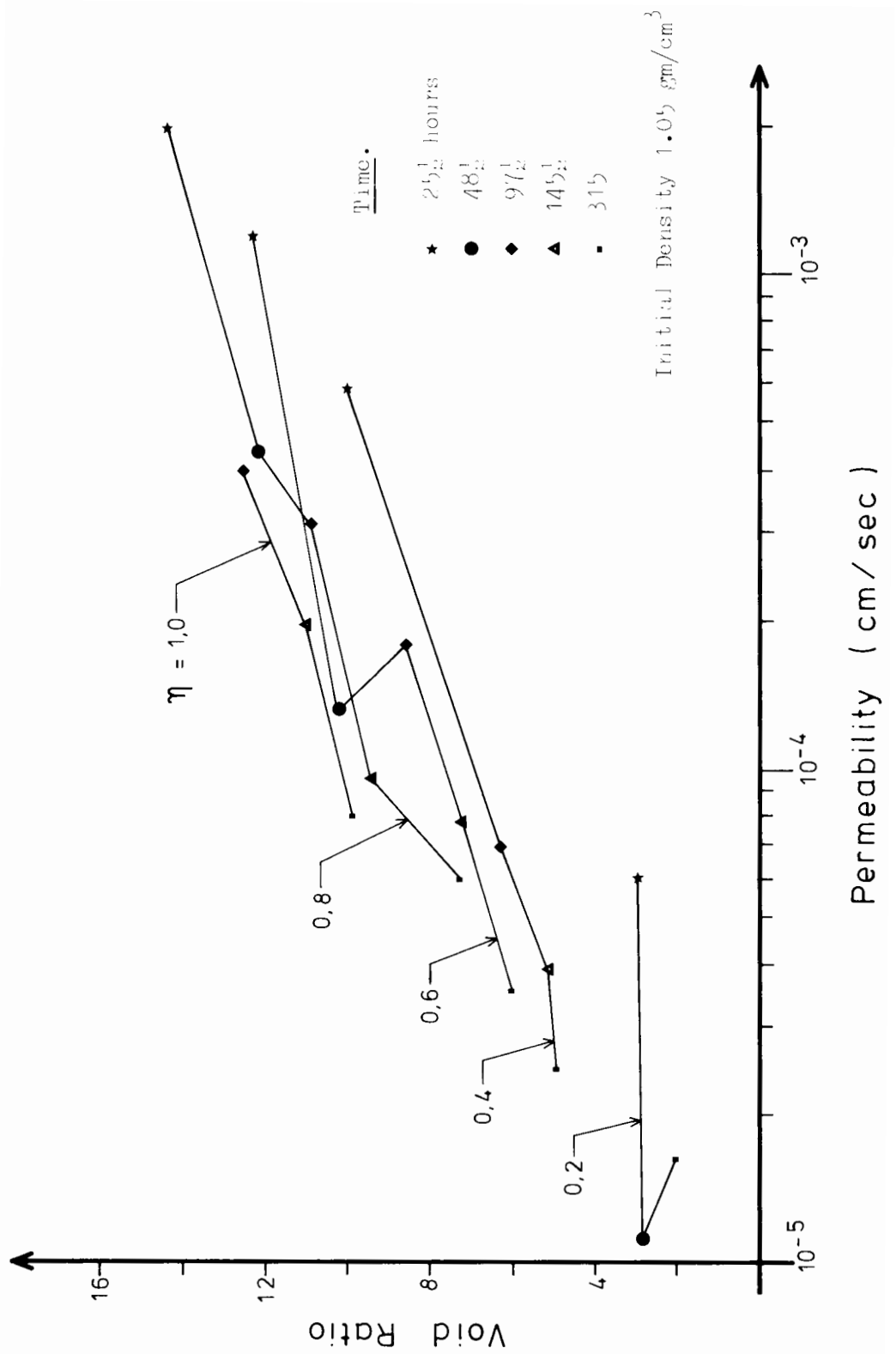


Fig 4.36. Permeability / Void Ratio, Experiment 11.
Initial Density 1.05 gm/cm^3.

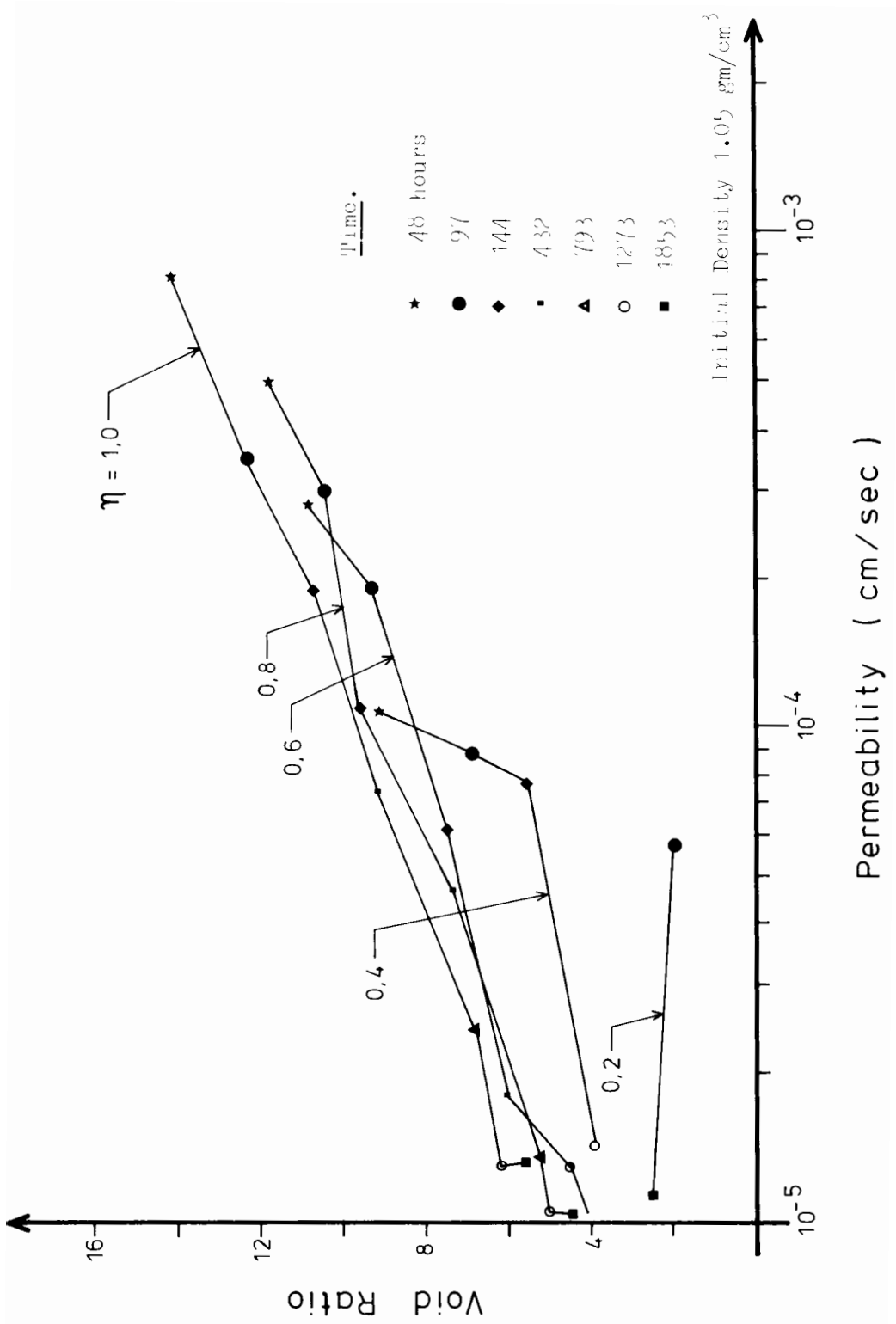


Fig 4.37. Permeability / Void Ratio, Experiment 12.
Initial Density 1.05 gm/cm^3.

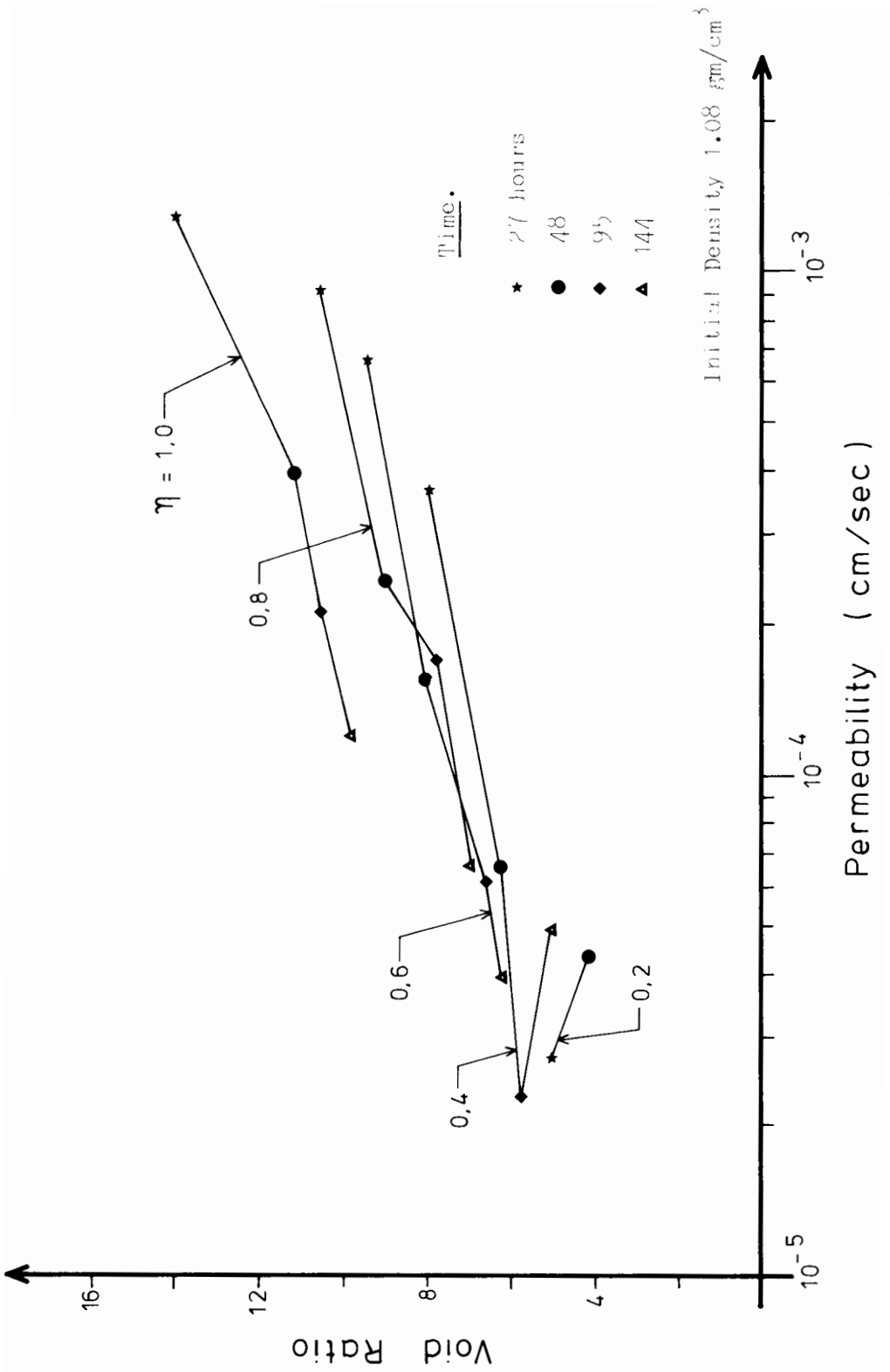


Fig 4.38. Permeability / Void Ratio, Experiment 13.
Initial Density 1.08 gm/cm^3.

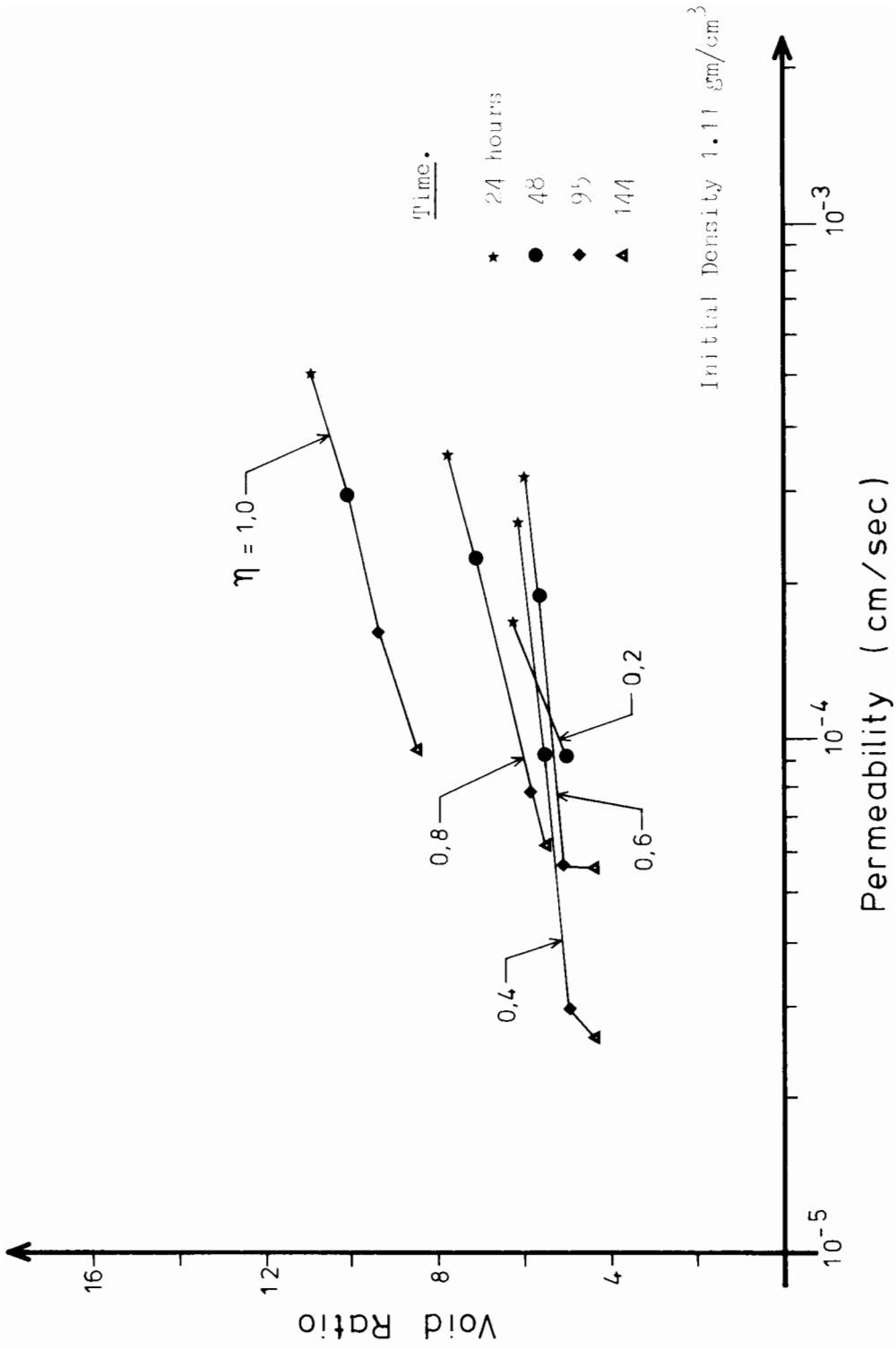


Fig 4.39. Permeability / Void Ratio, Experiment 14.
Initial Density 1.11 gm/cm^3.

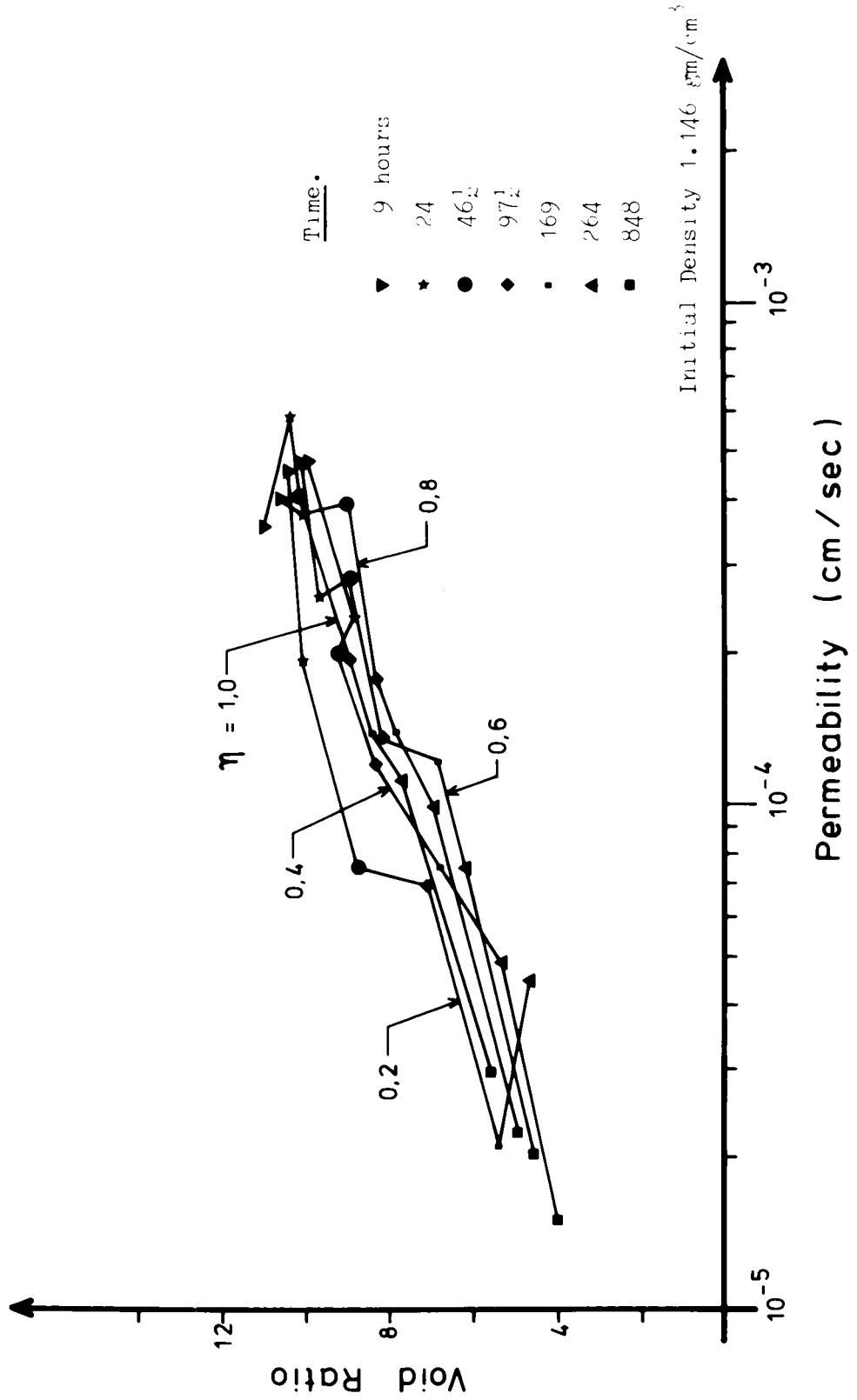


Fig 4.40. Permeability / Void Ratio, Experiment 15.
Initial Density 1.146 gm/cm^3.

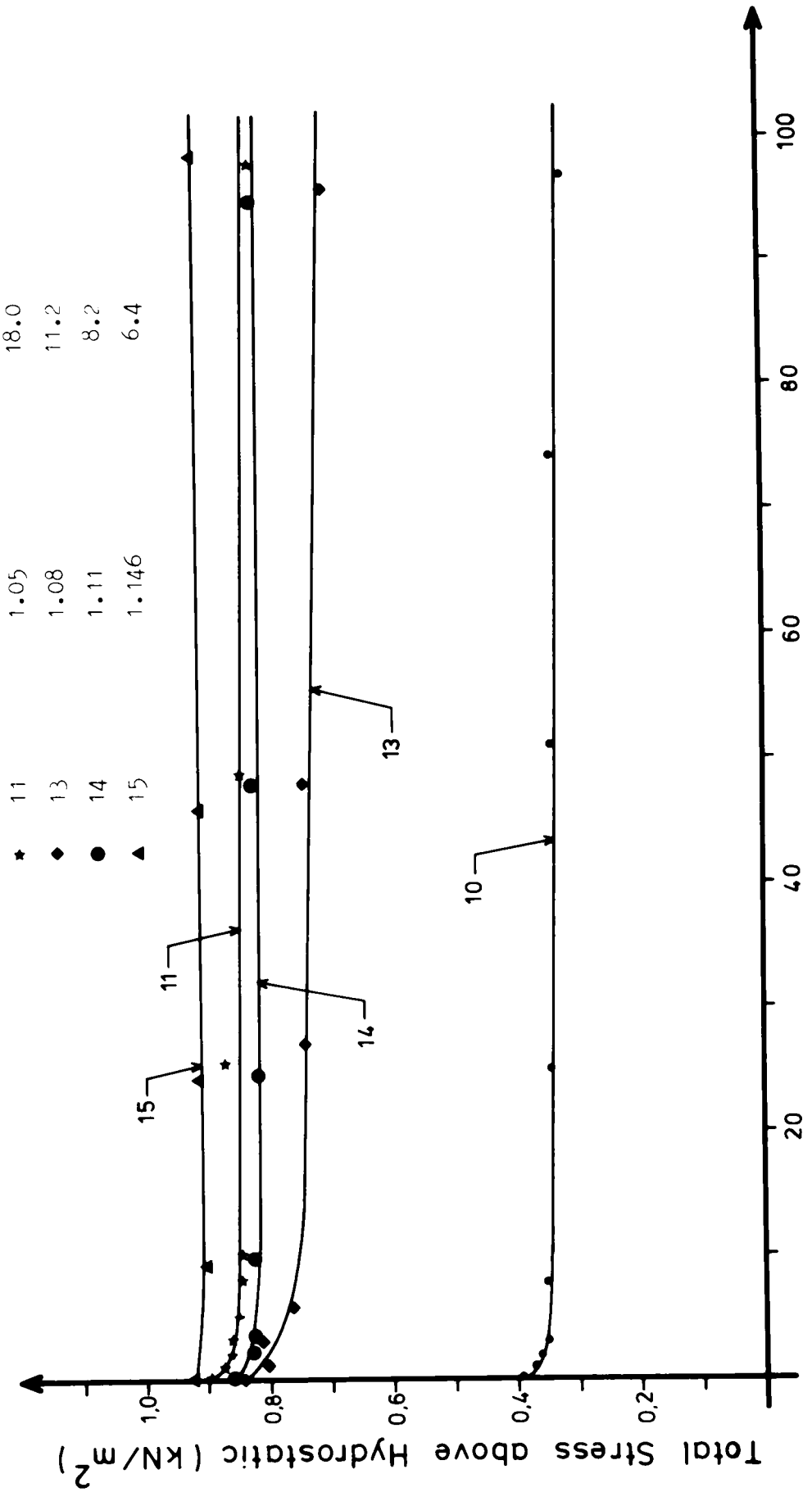
Permeabilities at the base cannot be calculated as the solids are not moving, and in many instances the soil near the base (at $\eta = 0.2$) was also moving too slowly to be measured. Times shown on the graphs refer to the time the profile was taken at the end of the period for which the permeability is calculated.

Scatter in the permeability values is inevitable because measurement of both the hydraulic gradient and the position of a particular soil element is rather inaccurate. Nevertheless the plots are remarkably consistent. Permeabilities range from 10^{-5} to 10^{-3} cm/sec in all six tests and all show approximately the same linear trend of the logarithm of permeability with void ratio.

4.6 TOTAL STRESS MEASUREMENT

The main purpose in measuring the total stress in the base is to assess the friction in the settling column. In fig 4.41 graphs of total stress at the centre of the base with time are shown for experiments 10, 11, 13, 14 and 15. Experiments 10, 11 and 13 have the stress dropping relatively rapidly in the first 5 hours, and a very slow fall thereafter. This initial rapid section is absent for tests 14 and 15 which also have a lower fall over a long period as a result.

These falls in total stress could clearly indicate a significant effect of friction on the consolidation behaviour of the soil as they can be of the order of 10% to 20% of the stress above hydrostatic after 100 hours. However, the relatively dense layer with its preponderance of silt size particles probably makes a large contribution to the friction,



Total Stress as Measured by a 5 mm Square Diaphragm in Centre of Base.

Fig 4.41. Total Stress on Column Base.
Experiments 10, 11, 13, 14, 15.

by being stiffer, and yet has a small effect on the overall settlement for the same reason. This would explain why experiments 14 and 15, without dense base layers, show a much smaller reduction in stress. For this reason most of the analysis in this work has assumed a frictionless column wall and that total stresses from integrated density profiles are true stresses.

Reduction of the total stress as a result of bridging over the diaphragm is likely to be small because the ratio of the diaphragm to particle diameter is large (at least 60 times). This ratio could, however, be considerably reduced if there are large flocs at the base. Evidence suggests that this is not the case as the relatively higher effective stresses would break down flocs near the base.

4.7 HORIZONTAL STRESS

Horizontal total stress was only determined in the column wall 300 mm above the base. This position was generally in the intermediate density zone during the experiments.

Horizontal effective stress is plotted against vertical effective stress for this point in fig 4.42 for four tests. Because the effective stress is only slightly greater than the accuracy of the measurements at this point, the information is inconclusive although it may be pointed out that the horizontal effective stress does tend to be lower than the vertical effective stress.

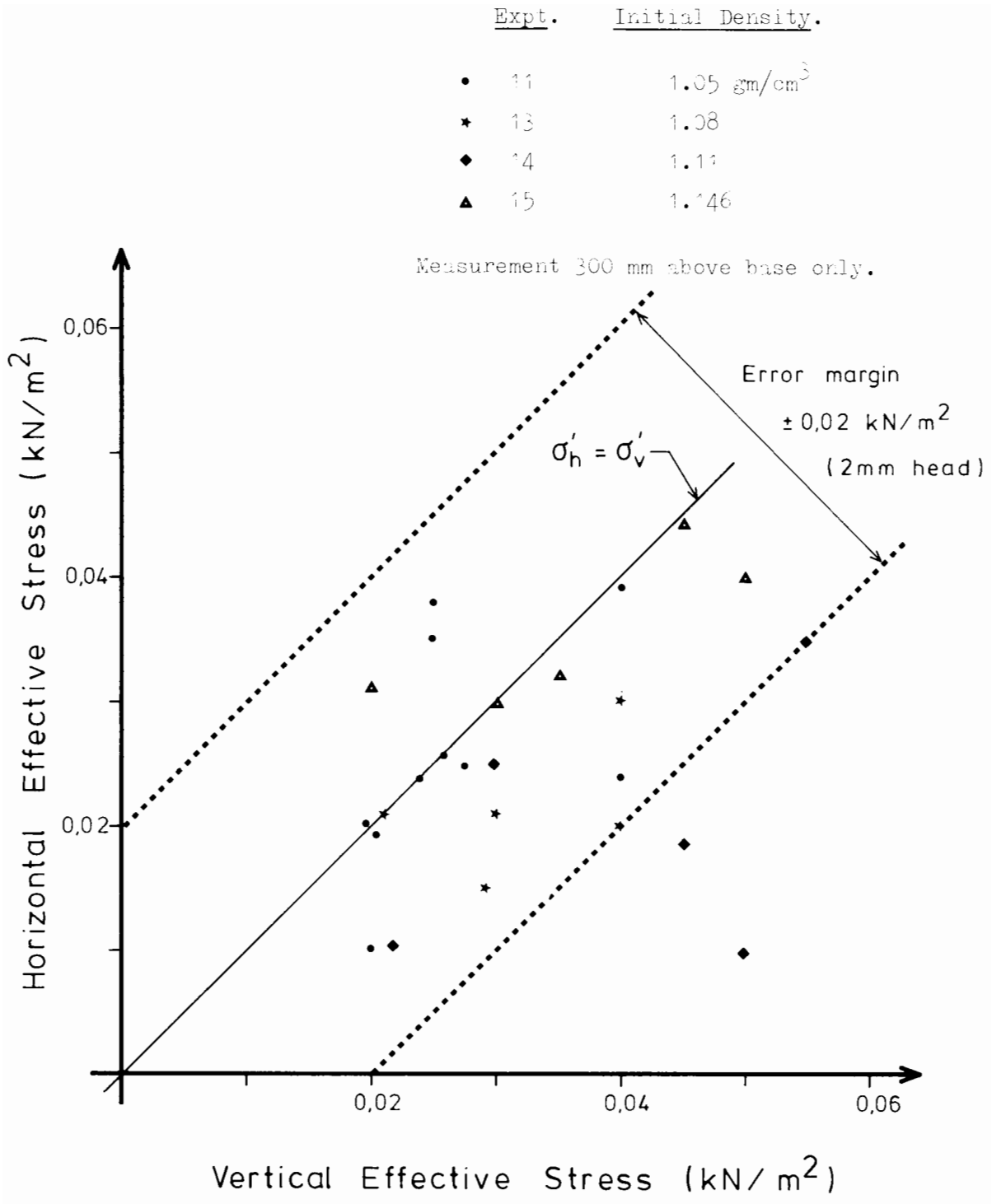


Fig 4.42. Horizontal Stress at 300 mm Height.
Experiments 11, 13, 14, 15.

CHAPTER 5. A QUALITATIVE DISCUSSION OF THE EXPERIMENTAL RESULTS

5.1 Phases of Settling and Consolidation 165

5.1.1 Suspensions 165

5.1.2 Intermediate Phase 167

5.1.3 Soil 168

5.2 A Comparison with Other Studies 169

CHAPTER 5. A QUALITATIVE DISCUSSION OF THE EXPERIMENTAL RESULTS

Existing theories of sedimentation and consolidation, in the context of the experimental observations presented here, are examined in chapter 6. Before this is done the salient features of the results are drawn together in this chapter. In particular the different phases of sedimentation are identified and described.

Because the Parrett silt is classified as a medium plasticity inorganic clay, one might expect the behaviour of this soil to be representative, at least qualitatively, of a large number of other sediments. In other words the discussion in this chapter should be applicable to most naturally occurring clayey sediments.

5.1 PHASES OF SETTLING AND CONSOLIDATION

When a non-dispersed suspension of a clayey silt in water is left to settle under the action of gravity, three sediment phases can be distinguished by their respective properties, based on the density profiles, stress distributions and void ratio/effective stress relationships presented in the previous chapter. The observed characteristics of each, the suspension, intermediate phase and soil, are discussed separately in the following three sub-sections.

5.1.1 Suspensions

Plots of suspension/water interface movement (fig 4.2) indicate that at low densities (1.02 gm/cm^3) settling is relatively fast, at high densities (1.11 gm/cm^3) it becomes much slower, but that at the three densities shown between these the settling rates are similar to one another.

A commonly accepted assumption about suspensions of uniform particles is that the settling rate is a function only of the local density. Extension of this to include non-uniform suspensions has been made by McRoberts and Nixon (1976) on the basis that at "hindered settling" densities particle segregation does not occur readily. Results of the present study, while not repudiating the basic assumption, indicate that the relationship of settling velocity to density is not a simple one. Suspension concentrations often fall during sedimentation, segregation of particles does occur and flocculation behaviour is important. A gradual reduction of the suspension concentration can be explained by particle segregation which is in turn dependent on floc structure.

Environmental conditions and density largely determine flocculation, so that for a given test the initial density has an overriding influence on subsequent sedimentation rates.

Another possible mechanism for changes in concentration is dilation of the suspension at certain densities to increase the downwards flux of solids. As

$$\text{Flux} = \text{velocity} \times \text{concentration} \qquad (5.1)$$

this would increase the flux provided the settling rate increase more than offsets the lowered concentration. The additional water required for this dilation to occur is the pore water expelled from the consolidating material underneath the suspension.

No effective stresses are measureable in dilute suspensions, but there is a certain density (in this instance between 1.11 and 1.14 gm/cm^3) at which a slurry can no longer exist in an effective stress free condition. At this density its properties change and unusual behaviour like channelling occurs. It is now no longer a true suspension but is termed the intermediate phase in this work. Tory and Shannon (1965) also observed that channelling is associated with intermediate densities only, without recognising the intermediate phase/suspension interface because of inadequate density measurement.

Values of density at which the intermediate phase begins will clearly vary widely from soil to soil, fresh to saline water and probably with many other factors.

5.1.2 Intermediate Phase

Distinguished from a suspension by small measured effective stresses, the intermediate phase covers a wide range of void ratios (or densities) while the slurry is still fluid, as opposed to being a soil. Density profiles of columns with initially intermediate slurry densities (figs 4.7 and 4.22) and particle size analysis of a settled bed, indicate that no particle size segregation occurs in intermediate slurries. This is not surprising as the existence of effective stresses implies structure that will support particles or flocs from below. In addition there is the direct retarding effect of a higher density slurry on differential settling of particles. Total stress measurements on the column base suggest there is very little side friction, indicating low shear strengths in intermediate slurries.

At the suspension end of the intermediate phase density range, channelling is an important process. A possible interpretation of this phenomenon is that the soil is in a quick condition at this stage (the effective stress is, to all intents, zero) and any slight weakness or irregularity in the mud column will allow a channel to open up. Water will naturally find the easiest route to the surface so that once a few channels are open, water will continue to flow upwards in them. Permeability is also increased as a result, allowing more rapid consolidation. As effective stresses develop the channels collapse and there is no longer a quick condition, hence new channels are not formed.

The major difference between the intermediate phase and soil is the effective stress/void ratio function, which in a soil is generally unique but is clearly not so in the intermediate zone. Distinguishing

between the soil and the intermediate region in a settling test is not as easy as the transition from a suspension, where channelling and a step change in density are convenient markers.

5.1.3 Soil

A revised concept of the zero effective stress point of a soil is required because of the intermediate zone behaviour. This point will therefore be taken as the void ratio below which there is a unique virgin consolidation line. The surface of a slurry deposit, if left sufficiently long, will tend towards this void ratio.

Void ratio/effective stress relationships (figs 4.29 - 4.34) in the previous chapter indicate that the zero effective stress point of the Parrett mud occurs at a void ratio between 5 and 6. This is not the highest void ratio at which stresses exist, but is the void ratio at which there will be no effective stress in a fully consolidated soil. It is apparent that, in the 0 - 0.2 kN/m^2 effective stress range, there is not a clear distinction between the soil and the intermediate phase. This transition occurs just below the zero effective stress void ratio defined above.

Little more can be said about the soil behaviour from these experimental results because the stress range is small and there are inhomogeneities in the soil bed due to particle size segregation during settling. Permeabilities are only slightly higher in the intermediate phase than in soil and show no other marked change in nature. The void ratio/effective stress relationship for the soil could be approximated quite well by a straight line over this small range of stress.

5.2 A COMPARISON WITH OTHER STUDIES

Experimental results in this study are not readily comparable in a quantitative way with the work of other engineers because the stresses are so low, or of sedimentologists because they do not generally consider effective stresses.

The overall stratified density structure, rather than a smooth profile, has been observed and reported by Parker and Kirby (1977) in field studies of the Severn estuary. They also identify three sediment states; mobile suspensions occuring in turbid water, which settle and evolve into static suspensions, which in turn consolidate to form settled mud. Time scales and density values indicate that static suspensions correspond to the intermediate zone in the present work. Static suspensions are easily eroded (in the tidal cycles, for instance) and this may leave the underlying mud bed very lightly overconsolidated. Combined with some dessication if the mud is in the intertidal zone, this could explain why field compression curves reported by Skempton (1970) for normally consolidated sediments of medium plasticity have lower void ratios (2 to 3.5) at very low overburden pressures than the present results would suggest.

Monte and Krizek (1976) report a void ratio of approximately 7 for the fluid limit of kaolin, where the fluid limit is defined as the water content of the soil/water system at its initial formative state and represents the stress free state of the soil. Results of the present work indicate that stresses exist at high void ratios where the slurry is essentially fluid and cannot be a soil in the conventional sense of the term, so that a stress free soil state is an anomaly.

A further distinct change in the stress/strain curve and the permeability/void ratio line of the kaolin occurred at a void ratio of 4, but details of Monte and Krizek's experimental methods are not adequate to assess their results in the context of the present work.

A more appropriate comparison is with experimental work by Lee (1979), chapter 9, on a very similar soil to the Parrett mud (from Bridgwater Bay). Specimen preparation was by sedimentation directly into the oedometer, so that the initial condition of the thin sample will be very close to the zero effective stress point as defined in section 5.1.3. The few points in the 0 - 5 kN/m^2 range of his void ratio/effective stress curve, interpreted from a restricted drainage consolidation test up to 140 kN/m^2, suggest a zero effective stress point at a void ratio between 5 and 6, the value found in the present study.

The phenomena observed and discussed in this work are not completely new and do compare with other studies. However, the approach based on effective stress behaviour is novel and has resulted in identification of the intermediate zone and a new definition of a soil. A stress free soil as such cannot exist if this definition is used, although a thin sedimented layer is a good approximation. The next step is to examine the applicability of certain theories to the sedimentation process, incorporating these new ideas where necessary.

CHAPTER 6. SOME EXISTING THEORIES OF SEDIMENTATION AND CONSOLIDATION

6.1 Hindered Settling 173

6.2 Soil Consolidation 177

6.2.1 The Governing Equation 177

6.2.2 A Self Weight Consolidation Solution 179

The Linear Soil Model 179

Solution for Dredged Fill, Surface Drain 181

6.3 Comparison Between Hindered Settling Theory and Consolidation Theory 184

6.4 Application to the Present Experimental Work 187

6.4.1 Settling of Suspensions 187

6.4.2 Consolidation Theory 188

CHAPTER 6. SOME EXISTING THEORIES OF SEDIMENTATION AND CONSOLIDATION.

Modifications of Stokes' Law of settling for single, spherical particles are inadequate for describing the sedimentation of natural soils. The diversity of particle shapes, sizes and concentrations cannot be included in the analysis, so that all existing work has been with artificially uniform materials inappropriate for geotechnical applications. Flocculation and inter-particle attractions substantially affect sedimentation and should be included in any analysis for soils.

Some methods of considering hindered settling and settling in compression have been mentioned in section 1.4. In this chapter Kynch's theory, particularly in the form used by McRoberts and Nixon (1976) for soil sedimentation, is examined in some detail. A large strain soil consolidation theory, Gibson et al (1967) and Lee (1979), is also presented and Kynch's theory is shown to be equivalent to the consolidation theory for zero effective stress. Finally the application of these theories to the present experimental results is considered briefly before proceeding to chapter 7.

6.1. HINDERED SETTLING

Hindered settling theory, Kynch (1952), is based on the assumption that at any point in the suspension the velocity of fall of a particle depends only on the local concentration of particles. Wall effects are ignored. The original paper specifies that the particles are of the same size and shape, which is clearly unsatisfactory when soil is considered. Following the argument of McRoberts and Nixon (1976) that the theory is valid only above some minimum concentration such that there is little segregation, the requirement for uniformly sized and shaped particles can be relaxed. Concentration is thus defined as the mass of solids per unit volume (equivalent to dry density) rather than the number of particles per unit volume as per Kynch.

The main assumption of the theory is thus expressed as

$$v_s = v_s(c) \tag{6.1}$$

where v_s is the velocity of fall of particles

c is the suspension concentration.

It is convenient to define the particle flux, or mass of particles crossing a horizontal section per unit time, S where

$$S = v_s c \tag{6.2}$$

The flux, S, is entirely determined by the suspension concentration in this theory. In general the concentration is a function of position in the column and time, so that

$$c = c(x,t) \tag{6.3}$$

where x is the height above the bottom of a column of suspension. Considering a thin horizontal layer, the rate of change of concentration is determined by the particle flux into and out of the layer given by the continuity equation

$$\frac{\partial c}{\partial t} + \frac{\partial S}{\partial x} = 0 \tag{6.4}$$

This equation is different from that of Kynch, which has a negative sign before the $\frac{\partial S}{\partial x}$ term, in order to maintain a consistent positive direction of velocity, flux and the coordinate x. As a result of the relation given by equation 6.2 this is written as

$$\frac{\partial c}{\partial t} + V(c)\frac{\partial c}{\partial x} = 0 \tag{6.5}$$

where

$$V(c) = \frac{dS}{dc} \tag{6.6}$$

Points of equal concentration plotted on a graph of position x against time t are related by the equation

$$c(x+dx,\ t+dt) = c(x,t) \tag{6.7}$$

so that

$$\frac{\partial c}{\partial x}\,dx + \frac{\partial c}{\partial t}\,dt = 0 \tag{6.8}$$

Combining equations 6.5 and 6.8, the slope of a curve of constant concentration is given by

$$\frac{dx}{dt} = V(c) \qquad (6.9)$$

As the concentration, and therefore V(c), is constant along the curve, it must be a straight line of slope V determined by the concentration.

This result forms the basis of Kynch's and McRoberts and Nixon's analysis of the sedimentation process. Since the relationship of flux to concentration is not known, the analysis consists of considering certain forms of flux plots and the resultant characteristics on the (x,t) plot. Propagation of discontinuity (or kinematic) waves largely determines the settling behaviour. One such discontinuity is the falling suspension / water interface and another is the top of the rising intermediate zone in the present work. A typical Kynch plot of a well behaved suspension is illustrated in figure 6.1.

Detailed determination of the real flux / concentration relationship rather than its general form is desirable. McRoberts and Nixon (1976) use the Richardson and Zaki (1954) relationship, equation 1.1, whilst Tory and Shannon (1965) use an exponential height - time relationship for the slurry surface. Both these papers are, however, not entirely satisfactory. McRoberts and Nixon recognise that Kynch's theory cannot be applied when effective stresses exist and particle segregation occurs, but do not make any stress measurements or take bed samples to check on these. The present work indicates that effective stresses develop at relatively low concentrations and that segregation occurs in true

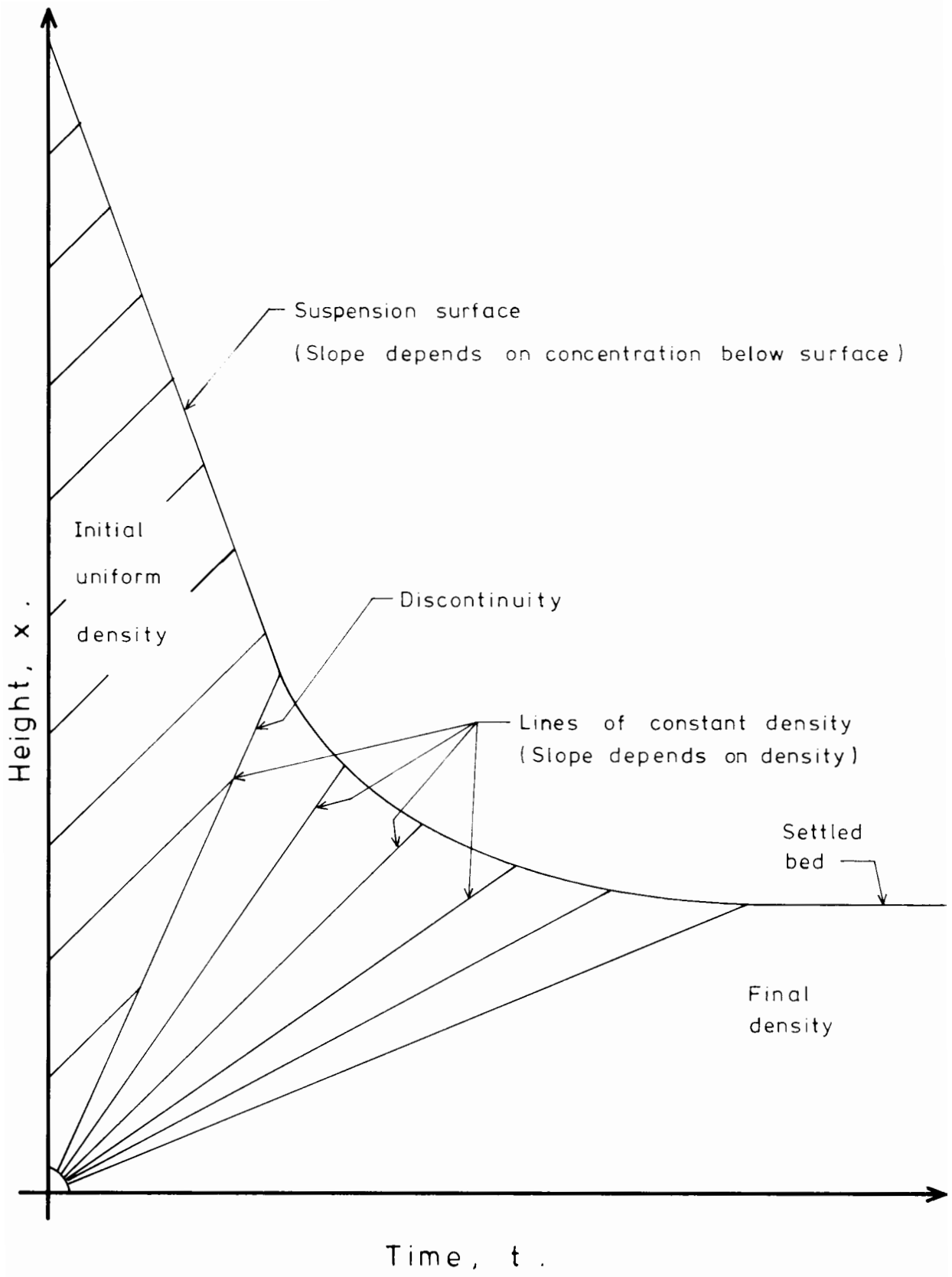


Fig 6.1. Typical Kynch Plot of Constant Concentration Lines.

suspensions (i.e. when the effective stress is zero). On the other hand, Tory and Shannon recognise that slurries "settling in compression" do so because there are mechanical (effective) stresses present, but apply Kynch's theory anyway. The assumption that settling rate is a function of local solids concentration only is clearly a contradiction as any effective stresses imply a structure which will support particles from below. A particle cannot thus settle independently of what is beneath it.

6.2. SOIL CONSOLIDATION

6.2.1. The Governing Equation

Turning to consolidation theory, the principle of effective stress plays an important part. Terzaghi's theory of one-dimensional consolidation, which is so widely used in soil mechanics, is not applicable to the present work, as mentioned in section 1.4.2. Stresses due to self weight and large strains are important in this case but are not part of Terzaghi's theory. Therefore the less restrictive theory of Gibson, England and Hussey (1967) is examined here.

Assuming the pore fluid and the solids are incompressible and that the soil skeleton is homogeneous and possesses no intrinsic time effects (e.g. creep), Gibson et al. give the following equation governing void ratio;

$$\left(\frac{\rho_s}{\rho_f} - 1\right) \frac{d}{de}\left\{\frac{k}{1+e}\right\} \frac{\partial e}{\partial z} + \frac{\partial}{\partial z}\left\{\frac{k}{\rho_f (1+e)} \frac{d\sigma'}{de} \frac{\partial e}{\partial z}\right\} + \frac{\partial e}{\partial t} = 0 \qquad (6.10)$$

where e is the void ratio

z is the material (Lagrangian) coordinate, defined below

k is the permeability, a function of void ratio

ρ_s is the density of solids

ρ_f is the density of the pore fluid

σ' is the effective stress, specified as a function of void ratio alone.

The Lagrangian coordinate, z, of a point in a soil column is the thickness of the solid material occupying the space between the point and the datum plane (in this case the base of the column). This solid thickness is related to the Eulerian or space coordinate, x, by

$$z(x) = \int_o^x \frac{1}{1+\bar{e}}\, dx' \qquad (6.11)$$

(The symbol $\bar{e}$ has been used, where

$$\bar{e} = \bar{e}(x,t)$$

as opposed to

$$e = e(z,t)$$

to avoid confusion later in this chapter.) An advantage of using the material coordinate system is that the boundaries are fixed for a given amount of material, making solution of the governing equation simpler. However, the solution then has to be transformed to real space coordinates for comparison with experimental results. For a formulation of the equivalent equation using the Eulerian coordinate system, the reader is

referred to Lee (1979).

6.2.2. A Self Weight Consolidation Solution

Several solutions to equation 6.10 in the Lagrangian coordinate system, both analytic and numerical, have also been found by Lee (1979). Using a linear effective stress / void ratio and permeability / void ratio relationship simplifies the solution. In particular his solution, page 70, for a dredged fill consolidating under its own weight is presented below because of its relevance to the present experimental results. It is recognised that real soils do not behave linearly as assumed, although it may be a reasonable approximation in some cases.

The Linear Soil Model

The governing equation, 6.10, is

$$\left(\frac{\rho_s}{\rho_f} - 1\right) \frac{d}{de}\left\{\frac{k}{1+e}\right\} \frac{\partial e}{\partial z} + \frac{\partial}{\partial z}\left\{\frac{k}{\rho_f(1+e)} \frac{d\sigma'}{de} \frac{\partial e}{\partial z}\right\} + \frac{\partial e}{\partial t} = 0 \qquad (6.10)$$

Letting $$\frac{k}{\rho_f} = k_o(1+e) \qquad (6.12)$$

and $$\sigma' = A - \alpha e \qquad (6.13)$$

where $$A = \alpha e_o \qquad (6.14)$$

and e_o is the void ratio corresponding to the zero effective stress state of the soil, the coefficient of consolidation, C_f, defined by

$$C_f = -\frac{k}{\rho_f(1+e)}\frac{d\sigma'}{de} = \alpha k_o \qquad (6.15)$$

will be a constant. Using these equations 6.12 to 6.15, the governing equation is simplified to

$$\frac{\partial e}{\partial t} = C_f \frac{\partial^2 e}{\partial z^2} \qquad (6.16)$$

The notation used is that of Lee, with the excention that e_o (instead of e_i) is used for the zero effective stress state so that distinction can be made later between the initial void ratio and the void ratio at zero effective stress as defined in this thesis, section 5.1.3.

As the only loading in the present case is the self weight of the soil, the variation of effective stress with depth in the final equilibrium state of the soil is given by

$$\frac{d\sigma'}{dz} = -(\rho_s - \rho_f) \qquad (6.17)$$

The term $(\rho_s - \rho_f)$ is simply the submerged density of the solids so that the negative sign indicates that the direction of z is opposite to gravity. Now

$$\frac{de}{dz} = \frac{de}{d\sigma'}\frac{d\sigma'}{dz} = \beta \qquad (6.18)$$

where

$$\beta = \frac{1}{\alpha}(\rho_s - \rho_f) \qquad (6.19)$$

The void ratio distribution in the fully consolidated stratum is found by integrating equation 6.18 to give

$$e(z) = e_s - \beta(z_o - z) \tag{6.20}$$

where e_s is the void ratio at the surface

z_o is the solid thickness of the stratum.

Transformation of this linear distribution with solid depth to the space coordinate system is achieved by the relationship

$$x(z) = \int_o^z (1+e)\, dz' \tag{6.21}$$

where x is the real height measured from the datum plane z = 0.

Solution for Dredged Fill, Surface Drain

A dredged fill dumped insitu with a uniform void ratio, e_i, will consolidate according to the governing equation,

$$\frac{\partial e}{\partial t} = C_f \frac{\partial^2 e}{\partial z^2} \qquad 0 \leq z \leq z_o\,, \quad t \geq 0 \tag{6.22}$$

with the initial condition that

$$e(z,0) = e_i \tag{6.23}$$

A further assumption made by Lee is that the void ratio at the surface will remain in this initial state, so that

$$e(z_o,t) = e_i \tag{6.24}$$

At the base of the stratum, an undrained boundary, there is no flow so that the pore pressure gradient must be zero. Transforming this condition to the Lagrangian coordinate in terms of the void ratio gives

$$\frac{\partial e}{\partial z} = \frac{de}{d\sigma'} \frac{\partial \sigma'}{\partial z} = - \frac{de}{d\sigma'} (\rho_s - \rho_f) = \beta \qquad (6.25)$$

the boundary condition at the base thus being

$$\left(\frac{\partial e}{\partial z} \right)_{z=0} = \beta \qquad (6.25)$$

These initial and boundary conditions are illustrated in figure 6.2.

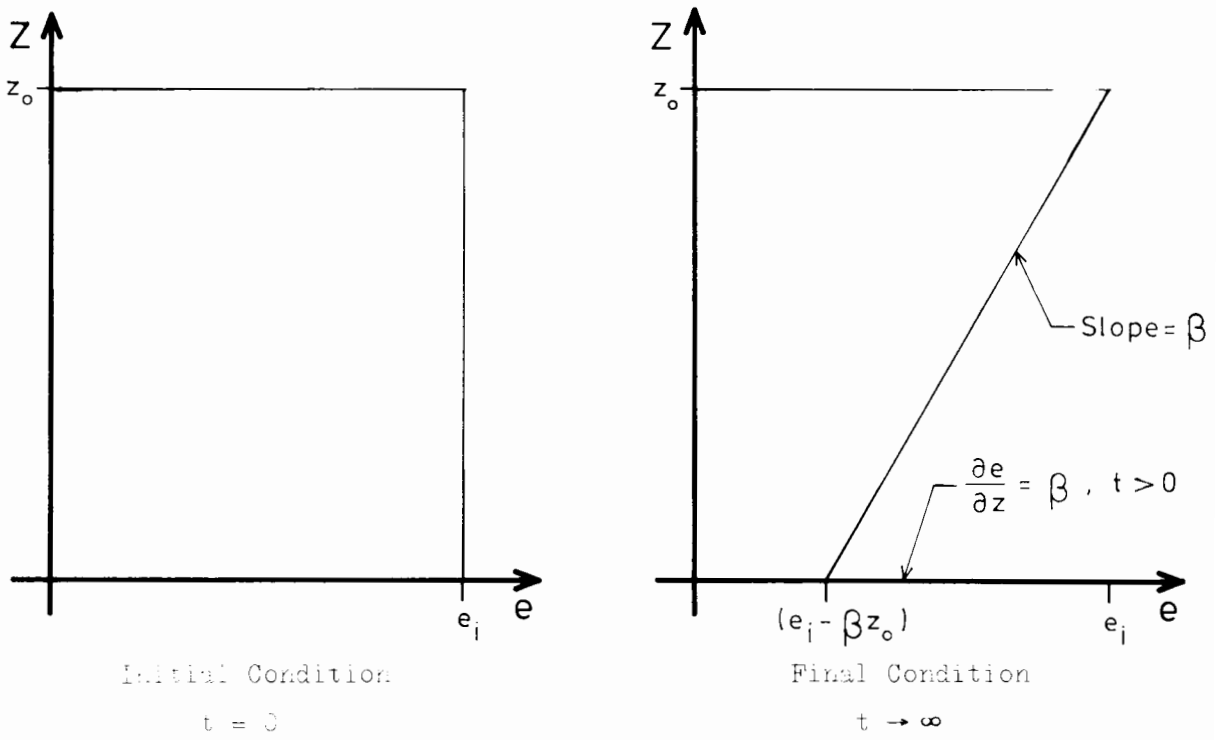


Fig 6.2. Dredged Fill, Boundary Conditions.

Writing the above equations in terms of the normalised material coordinate, η, and the time factor, T, where

$$\eta = \frac{z}{z_o} \tag{6.26}$$

$$T = \frac{C_f\, t}{z_o^2} \tag{6.27}$$

the problem is reduced to solving

$$\frac{\partial e}{\partial T} = \frac{\partial^2 e}{\partial \eta^2} \qquad 0 \leq \eta \leq 1 \;, \quad T \geq 0 \tag{6.28}$$

subject to

$$e(\eta,0) = e_i \tag{6.29}$$

$$e(1,T) = e_i \tag{6.30}$$

$$\frac{\partial e}{\partial \eta}(0,T) = \beta z_o \tag{6.31}$$

Once more these equations differ slightly from Lee (1979) in that the void ratio, rather than change in void ratio, is used for reasons which will be apparent in the next chapter when the theory is modified.

The solution, as per Lee (1979), is then

$$e(\eta,T) = e_i - \beta z_o\{1 - \eta - 2 \sum_n \frac{\cos m\pi\eta}{m^2\pi^2} \exp(-m^2\pi^2 T)\}$$

$$n = 0,\ 1,\ 2,\ \ldots\ ,\quad m = \tfrac{1}{2}(2n+1) \tag{6.32}$$

The degree of surface settlement, S, is

$$S(1,T) = 1 - 4 \sum_{n} \frac{(-1)^n}{m^3\pi^3} \exp(-m^2\pi^2 T) \qquad (6.33)$$

and the excess pore water pressure, u, is

$$u(\eta,T) = 2(\rho_s - \rho_f)z_o \sum_{n} \frac{\cos m\pi\eta}{m^2\pi^2} \exp(-m^2\pi^2 T) \qquad (6.34)$$

Lee plots these solutions in terms of the normalised variables in his figures 4.8 to 4.10, but these are not reproduced here as similar plots are shown in figure 7.3 of this thesis.

6.3. COMPARISON BETWEEN HINDERED SETTLING THEORY AND CONSOLIDATION THEORY

Although equation 6.5 for Kynch's theory and equation 6.10 for that of Gibson et al. are apparently very different, the only intrinsic difference is the use of the effective stress principle in deriving equation 6.10. Both equations describe the relative movement of soil and water by considering continuity and both assume a particular law of flow (Darcy's law in consolidation theory and a velocity of fall / concentration relationship in hindered settling). Different coordinate systems and variables mask any similarities between the two equations. In this section the two theories are shown to be equivalent by relating the velocity of fall of solids (in Kynch's theory) to the permeability and then transforming the soil consolidation theory coordinates to the Eulerian system when the effective stress is zero, yielding the hindered settling equation.

The form of Darcy's law used by Gibson et al. can be written

$$n\,(v_f - v_s) = -\frac{k}{\rho_f}\frac{\partial u}{\partial x} \tag{6.35}$$

where v_f is the real fluid velocity

v_s is the solids velocity (as used by Kynch)

n is the porosity

u is the excess pore water pressure.

When the effective stress is zero, as in a suspension, the excess pore pressure gradient is the submerged density of the solids, hence

$$\frac{\partial u}{\partial x} = -\left(\frac{\rho_s - \rho_f}{1 + \bar{e}}\right) \tag{6.36}$$

the negative sign indicating that the positive x direction opposes gravity. $\bar{e}$ is used as the space coordinate system is being used. Combining 6.36 with 6.35

$$(v_f - v_s) = \frac{k}{\bar{e}}\left(\frac{\rho_s}{\rho_f} - 1\right) \tag{6.37}$$

Considering a fixed plane at a height x, the total volume below the plane is constant so that the net flow of solids and fluid across the plane is zero.

$$v_s\,(1-n) + n\,v_f = 0 \tag{6.38}$$

Eliminating v_f from 6.37 and 6.38 gives

$$v_s = -\frac{k}{1+e}\left(\frac{\rho_s}{\rho_f} - 1\right) \tag{6.39}$$

the desired relationship between permeability and the hindered settling velocity.

Putting the zero effective stress condition into the consolidation equation reduces equation 6.10 to

$$\left(\frac{\rho_s}{\rho_f} - 1 \right) \frac{d}{de}\left\{\frac{k}{1+e}\right\} \frac{\partial e}{\partial z} + \frac{\partial e}{\partial t} = 0 \qquad (6.40)$$

Using the relationships

$$x(z) = \int_0^z (1+e)\, dz' \qquad (6.21)$$

$$c = \frac{\rho_s}{1+e} = \frac{\rho_s}{1+\bar{e}} \qquad (6.41)$$

the function $e(z,t)$ can be transformed to a function $\bar{e}(x,t)$ and then $c(x,t)$ by

$$\frac{\partial e}{\partial z} = \frac{\partial \bar{e}}{\partial x}\frac{\partial x}{\partial z} + \frac{\partial \bar{e}}{\partial t}\frac{\partial t}{\partial z} \qquad (6.42)$$

$$\frac{\partial e}{\partial t} = \frac{\partial \bar{e}}{\partial t} + \frac{\partial \bar{e}}{\partial x}\frac{\partial x}{\partial t} \qquad (6.43)$$

$$\frac{\partial x}{\partial z} = (1+e) = (1+\bar{e}) \qquad (6.44)$$

$$dc = -\frac{c}{1+e}\, de = -\frac{c}{1+\bar{e}}\, d\bar{e} \qquad (6.45)$$

Also $$\frac{\partial t}{\partial z} = 0$$

and $$\frac{\partial x}{\partial t} = v_s \qquad (6.46)$$

since $\frac{\partial x}{\partial t}$ is the rate of movement of the z coordinate in space, which will be the solids falling velocity. Combining equations 6.39 to 6.46 we get

$$\left(v_s + c \frac{dv_s}{dc} \right) \frac{\partial c}{\partial x} + \frac{\partial c}{\partial t} = 0 \qquad (6.47)$$

after some manipulation.

From equation 6.2 the solids flux is

$$S = v_s c$$

hence

$$\frac{dS}{dc} = v_s + c \frac{dv_s}{dc} \qquad (6.48)$$

so that equation 6.47 is in fact exactly Kynch's equation 6.5.

6.4. APPLICATION TO THE PRESENT EXPERIMENTAL WORK

6.4.1. Settling of Suspensions

No theory has been suggested that can take account of all the real processes occurring in a suspension because of the variability of the particles and the complexity of flocculation processes. Kynch's theory, based mainly on the continuity equation, is the most promising one for extension but the alterations to the flux / concentration relationship would have to be more substantial than would permit reasonable numerical analysis of the problem. It would thus still largely be

an empirical correlation for a particular soil.

However, the basic understanding of the sedimentation process arising from Kynch's characteristic solutions is extremely helpful. In figures 4.4 and 4.6, where lines of constant concentration are plotted on height / time axes, the lines are not linear as predicted by Kynch but do reflect a similar general behaviour. That they are not linear is hardly remarkable as the experimental results show that effective stresses occur (except in the true suspension) and this is inconsistent with the assumptions of Kynch. In the suspension, making allowance for differential particle settling, Kynch's theory would predict curved lines and it is only here that the theory should be applied, although this has not been the case in the past.

For the geotechnical engineer the duration of the suspension phase is very short compared to the time scale of soil and, in this instance, intermediate phase consolidation. Also the engineering properties of the settled soil are not very dependent on the flocculation behaviour in suspension, as indicated by the test program of Bishop and Vaughan (1972) and the similar Atterberg limits obtained for the Parrett silt with distilled and saline water.

It thus appears more fruitful for the engineer to turn his attention to the behaviour of the intermediate phase and soil.

6.4.2. Consolidation Theory

In section 6.3 the consolidation equation was reduced to a

settling equation simply by using a zero effective stress condition. Such a condition is implicit in settling theories. As the intermediate phase is associated with effective stress development, consolidation theory should be appropriate in the intermediate region. There are nevertheless some important differences between the assumptions of the theory and the observed intermediate phase behaviour.

A zero effective stress point as used in soil consolidation theories does not exist in the intermediate phase. Void ratios vary from less than 6 to greater than 12 near the surface where effective stresses are very nearly zero. In fact it seems impossible to match the initial condition, figure 6.2 used in the given solution (Lee 1979), of a soil (or even intermediate phase) in a uniform, stress-free state. By allowing the intermediate phase to form by sedimentation a slight density gradient is inevitable and the time taken for settling means that some excess pore pressure is dissipated before the whole bed is deposited. Alternatively, if the bed is initially an intermediate phase material, there will be stress history dependence as in experiment 8 (section 4.4). Although the density (shown in fig. 4.14) is uniform, the effective stress increases with depth in the column immediately after the mud has been pumped into the column. This effect may, however, be small at lower densities within the intermediate phase range, such as experiment 15 (initial density 1.146 gm/cm^3).

A unique void ratio / effective stress relationship is another aspect of the theory which differs from observed intermediate phase behaviour. As the governing equation is in terms of void ratio, the predicted effective stresses, and hence pore pressures, may be inaccurate

even though void ratios are nearly correct. Linearity of the void ratio / effective stress and void ratio / permeability relationships allows simplified analysis, but clearly does not occur in the intermediate zone. This may, however, not be a bad approximation over small ranges of void ratio. Also, the compressibility (void ratio / effective stress relationship) and permeability are combined into the coefficient of consolidation C_f, which may show less variation than either parameter individually.

Finally, relatively minor deviations from the theory will occur as a result of friction with the column wall, creep and the inhomogeneity of the settled mud due to particle size segregation.

CHAPTER 7. COMPARISON OF A MODIFIED LINEAR CONSOLIDATION THEORY WITH EXPERIMENTAL RESULTS

7.1 Derivation and Solution of the Modified Consolidation Equations 193

7.1.1 Void Ratio Distribution 197

7.1.2 Pore Water Pressure Distribution 203

7.1.3 Degree of Settlement 206

7.1.4 Transformation to Space Coordinates 207

7.2 Determination of the Coefficient of Consolidation 209

7.2.1 Choice of Soil Parameters and Initial Conditions 210

Initial Conditions, e_i and z_1 210

Parameters, e_o and Beta 212

Void Ratio / Effective Stress Relationships 214

7.2.2 C_f from Settlement Curves 216

7.2.3 C_f from Pore Pressure Distributions 225

7.2.4 Calculations of C_f from Soil Properties 228

7.2.5 Comparison of C_f Found by Three Methods 230

7.3 Density Profiles Compared 232

7.4 Discussion 240

CHAPTER 7. COMPARISON OF A MODIFIED LINEAR CONSOLIDATION THEORY WITH EXPERIMENTAL RESULTS.

In chapter 6 a theory of consolidation by self-weight was presented. There are several aspects where this theory differs from the observed behaviour. Some of these differences can be accounted for easily, but others require substantial modifications to the theory. In this chapter a modified theory is presented and then assessed by comparing the theoretical results to the experimental observations. As the comparison depends largely on using experimentally derived parameters in the theory, the applicability of the theory must be carefully assessed on the basis of the consistency of its predictions for all aspects of the experiments.

7.1. DERIVATION AND SOLUTION OF THE MODIFIED CONSOLIDATION EQUATIONS

Although the initial condition of an instantaneously dumped fill of uniform initial void ratio and zero effective stress does not occur, it is still a reasonable approximation to make. The duration of the suspension is short compared to the consolidation process and need not be included. Experimental conditions at the end of this period during which a suspension exists (i.e. when deposition is complete) are that there is a non-uniform density profile and some dissipation of excess pore pressure. It therefore seems reasonable that the initial condition can be described by a uniform initial void ratio, e_i, corresponding to the average intermediate phase density when the suspension has disappeared and channelling has ceased. The initial time (t=0), however, is taken to correspond to the start of the whole settling process, including the suspension. Thus in the theoretical model, at the time corresponding to when real deposition is complete, there will also be a non-uniform density profile and some dissipation of excess pore water pressure.

No account can be taken in the theory of the segregation of particle sizes causing the relatively thin, dense layer at the column base. This layer, after complete sedimentation to an intermediate phase, changes very little in thickness or density so that its effect on the total settlement is small. For this reason the application of the theory considers only the mud above this layer of coarser silt, which is assumed to have a constant thickness.

Measured values of the effective stress / void ratio

relationships for experiments 10 to 15, excluding values at the base of experiments 10 to 13 where this layer of silt is present, are shown in figure 7.1. (Points are exactly those plotted in figures 4.29 to 4.34.) A possible linear approximation, estimated by eye, to the relationship is also shown. At the lower effective stresses and higher void ratios there is not a unique relationship, so an approximation is not strictly justified. However, in the early stages of consolidation it is particularly the derivative $\frac{d\sigma'}{de}$ incorporated in the coefficient of consolidation, C_f (eq. 6.15), rather than the actual function, that influences the theoretical mud behaviour. The effect on theoretical predictions of assuming a linear, unique relationship between void ratio and effective stress becomes apparent in later discussion.

Figure 7.2 shows permeabilities for experiments 10 to 15 (taken from figures 4.35 to 4.40). A linear relationship (eq. 6.12),

$$k = k_o \rho_f (1 + e)$$

fitted by eye, that may be used in the theory is plotted. (The line is not straight in the figure as permeability is plotted on a logarithmic scale.) Restricting the compressibility and permeability in figures 7.1 and 7.2 to be linear, results in poorer approximations than may be hoped for. However, at high void ratios the real slope, $\frac{d\sigma'}{de}$, is smaller and the permeability higher than the linear approximations. At relatively low void ratios the opposite is true. Thus the product of the two, appearing in C_f (eq. 6.15) which should be constant, may still give a reasonable approximation.

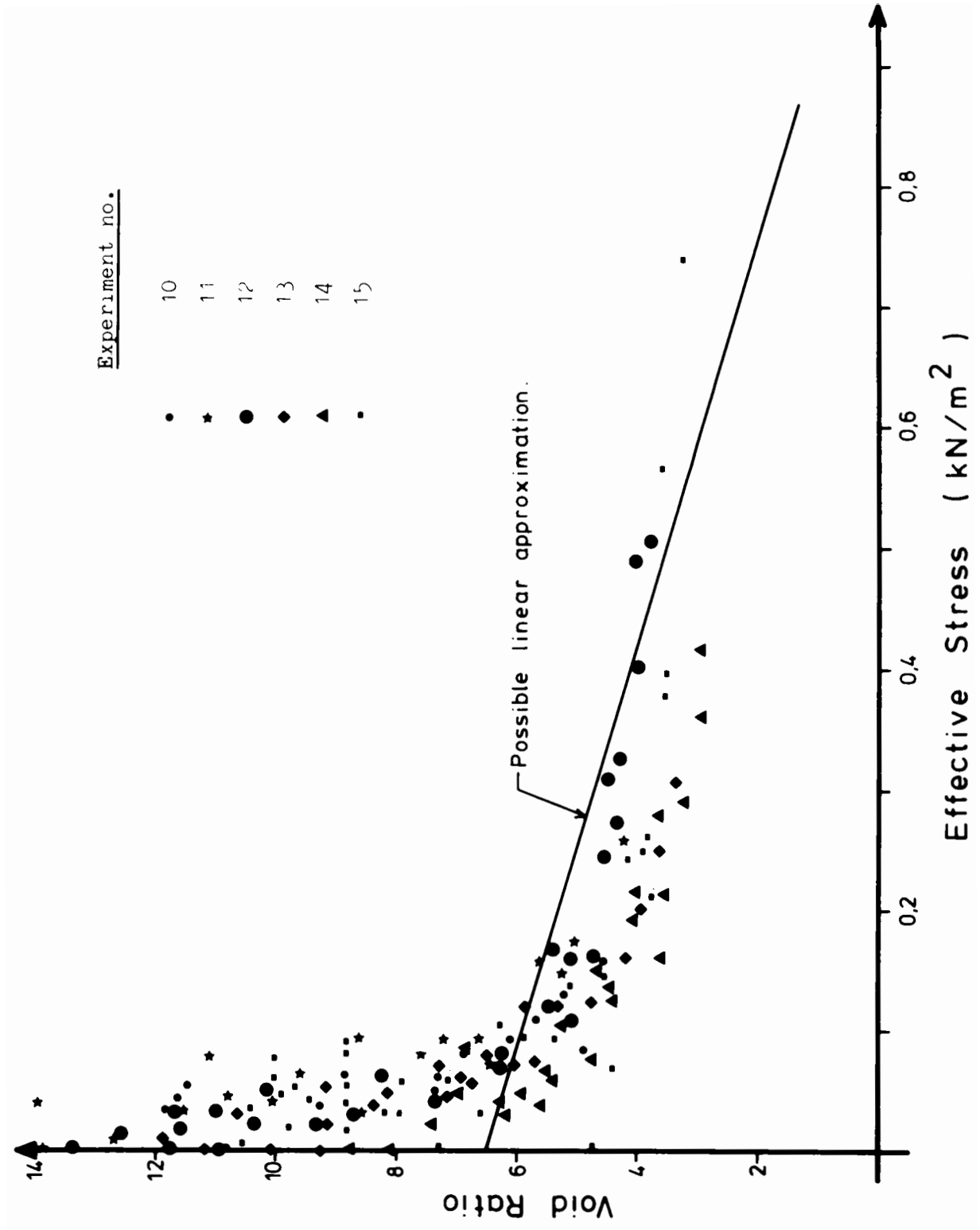


Fig 7.1. Effective Stress / Void Ratio Relationship.

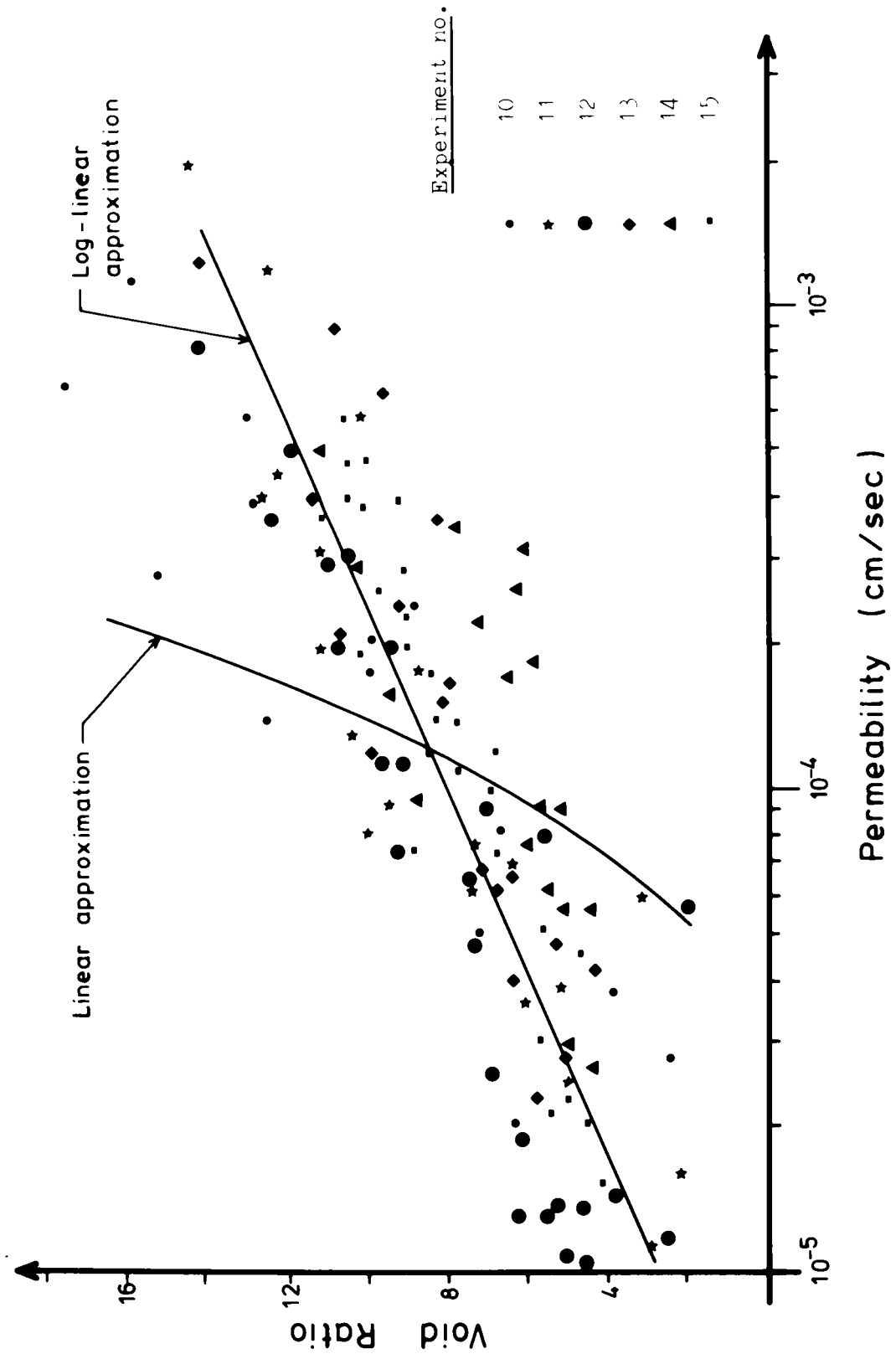


Fig 7.2. Permeability / Void Ratio Relationship.

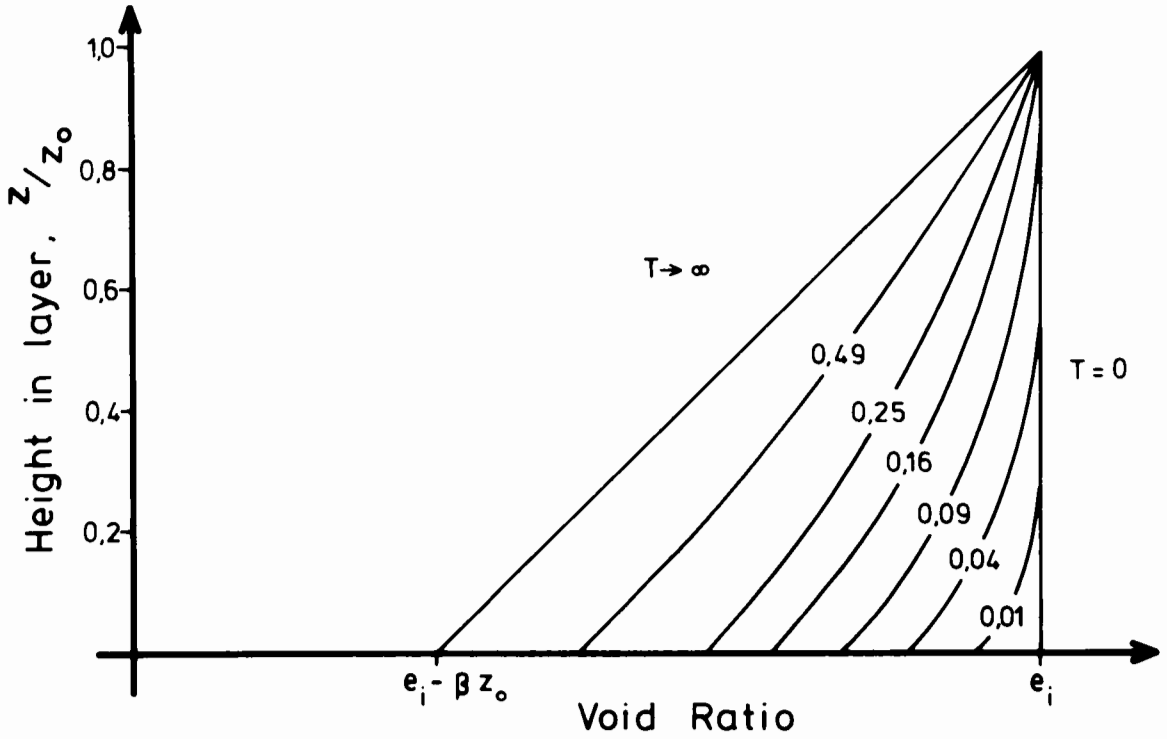
The most serious shortfall of the linear model solution is that an effective stress free soil state is assumed. Thus the surface void ratio remains constant at the value of the initial void ratio. Observations show this does not occur. Figure 7.3(a) shows isochrones of void ratio during consolidation from the linear soil model (after Lee, 1979), whilst figure 7.3(b) shows a set of isochrones that the experimental results indicate may be typical for a real soil. The void ratio e_o is the ultimate zero effective stress point (i.e. for a soil rather than the intermediate zone). In figure 7.3(a) the values e_o and e_i coincide.

In this section a modified solution is given that allows the initial void ratio, e_i, and the ultimate zero effective stress void ratio, e_o, to be different. Expressions are derived for void ratio, pore pressure and degree of settlement.

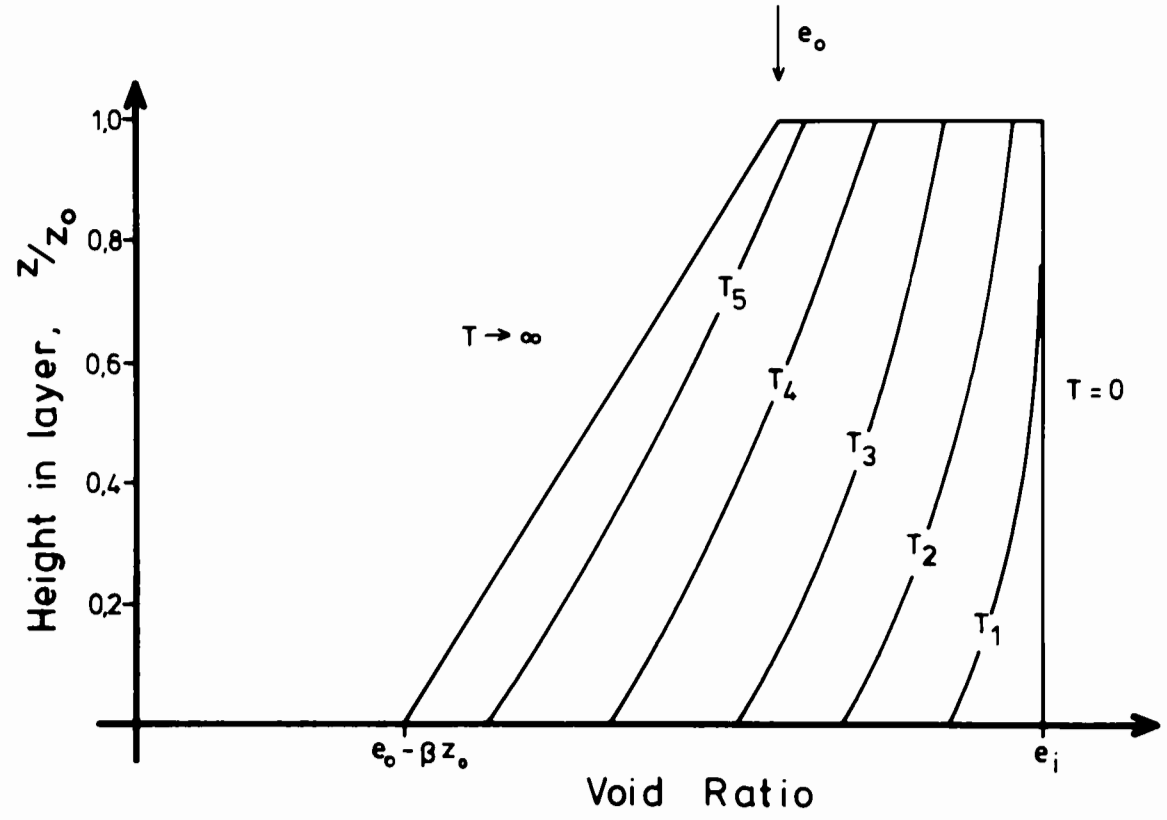
7.1.1. Void Ratio Distribution

Inspection of figures 7.3(a) and (b) reveals a similarity between the lower portion of (a) and the whole of (b). Thus a portion of the solution for (a) could be used to generate a modified solution (b). This is equivalent to assuming that a thicker layer of soil has been deposited and that the actual stratum of soil behaves like the equivalent lower portion of the thicker layer. In other words the soil behaves as if it has an overburden of similar, consolidating material.

A solution to the governing equation is required in terms of the normalised coordinates for the actual layer. Figure 7.4 shows



(a) After Lee (1979) or Equation 6.32.



(b) Form Expected from Experiments.

Fig 7.3. Isochrones of Void Ratio.

the boundary conditions to be satisfied, letting the solid thickness of the mud be z_1, the assumed initial void ratio e_i and the ultimate zero effective stress void ratio e_o. β is the slope of the final void ratio distribution. Normalised coordinates are now defined as

$$\eta' = \frac{z}{z_1} \tag{7.1}$$

$$T' = \frac{C_f\ t}{z_1^2} \tag{7.2}$$

and C_f is, as per equation 6.15, given by

$$C_f = -\frac{k}{\rho_f(1+e)} \frac{d\sigma'}{de}$$

Extending the line of the final void ratio distribution upwards to the value of the initial void ratio, figure 7.5, the new problem with an imaginary overburden is defined. The imaginary solids thickness, z_o, is given by

$$\beta\ (z_o - z_1) = e_i - e_o \tag{7.3}$$

and the normalised coordinates are

$$\eta = \frac{z}{z_o} \tag{7.4}$$

$$T = \frac{C_f\ t}{z_o^2} \tag{7.5}$$

Thus

$$\eta' = \frac{z_o}{z_1}\ \eta \tag{7.6}$$

and

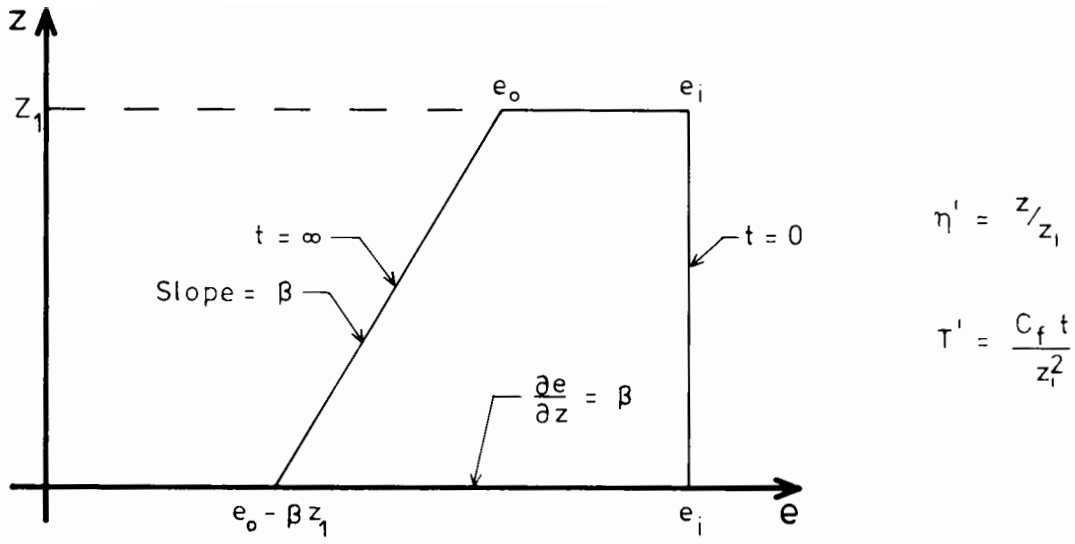


Fig 7.4. Boundary Conditions Solution Must Satisfy.

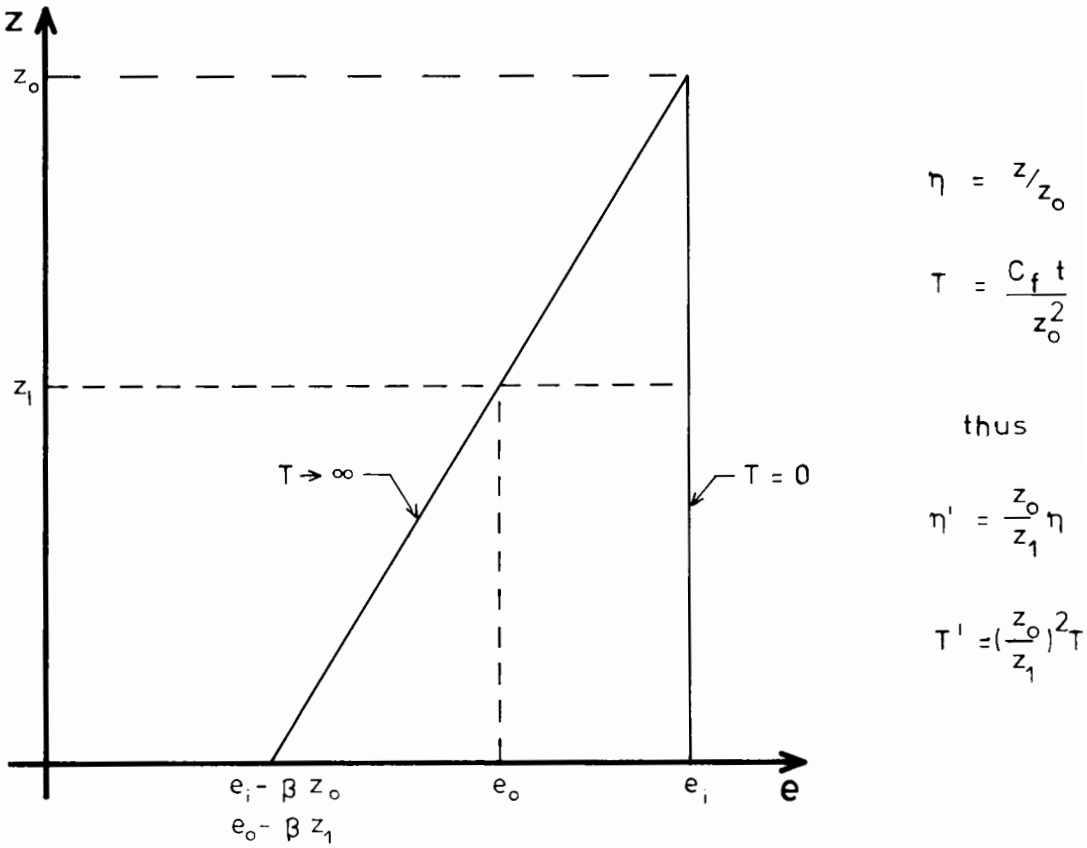


Fig 7.5. Definition of the Modified Problem.

$$T' = \left(\frac{z_o}{z_1}\right)^2 T \qquad (7.7)$$

Equations 6.28 to 6.31 define the problem in figure 7.5 as

$$\frac{\partial e}{\partial T} = \frac{\partial^2 e}{\partial \eta^2} \qquad 0 \leq \eta \leq 1 \ , \quad T \geq 0 \qquad (6.28)$$

$$e(\eta,0) = e_i \qquad (6.29)$$

$$e(1,T) = e_i \qquad (6.30)$$

$$\frac{\partial e}{\partial \eta}(0,T) = \beta z_o \qquad (6.31)$$

having the solution

$$e(\eta,T) = e_i - \beta z_o \{ 1 - \eta - 2 \sum_n \frac{\cos m\pi\eta}{m^2\pi^2} \exp(-m^2\pi^2 T) \}$$

$$n = 0, 1, 2, \ldots . \ , \quad m = \tfrac{1}{2}(2n+1) \qquad (6.32)$$

The modified solution for the problem in figure 7.4 is found by substituting equations 7.6 and 7.7 into 6.32, giving

$$e(\eta',T') = e_i - \beta z_o \{1 - \frac{z_1}{z_o}\eta' - 2 \sum_n \frac{\cos m\pi\frac{z_1}{z_o}\eta'}{m^2\pi^2} \exp(-m^2\pi^2(\frac{z_1}{z_o})^2 T')\}$$

$$\text{for} \quad 0 \leq \eta' \leq 1 \ , \quad T' \geq 0 \qquad (7.8)$$

where z_o is given by equation 7.3. This solution is illustrated in figure 7.6 for the case $z_o = 1.5\, z_1$.

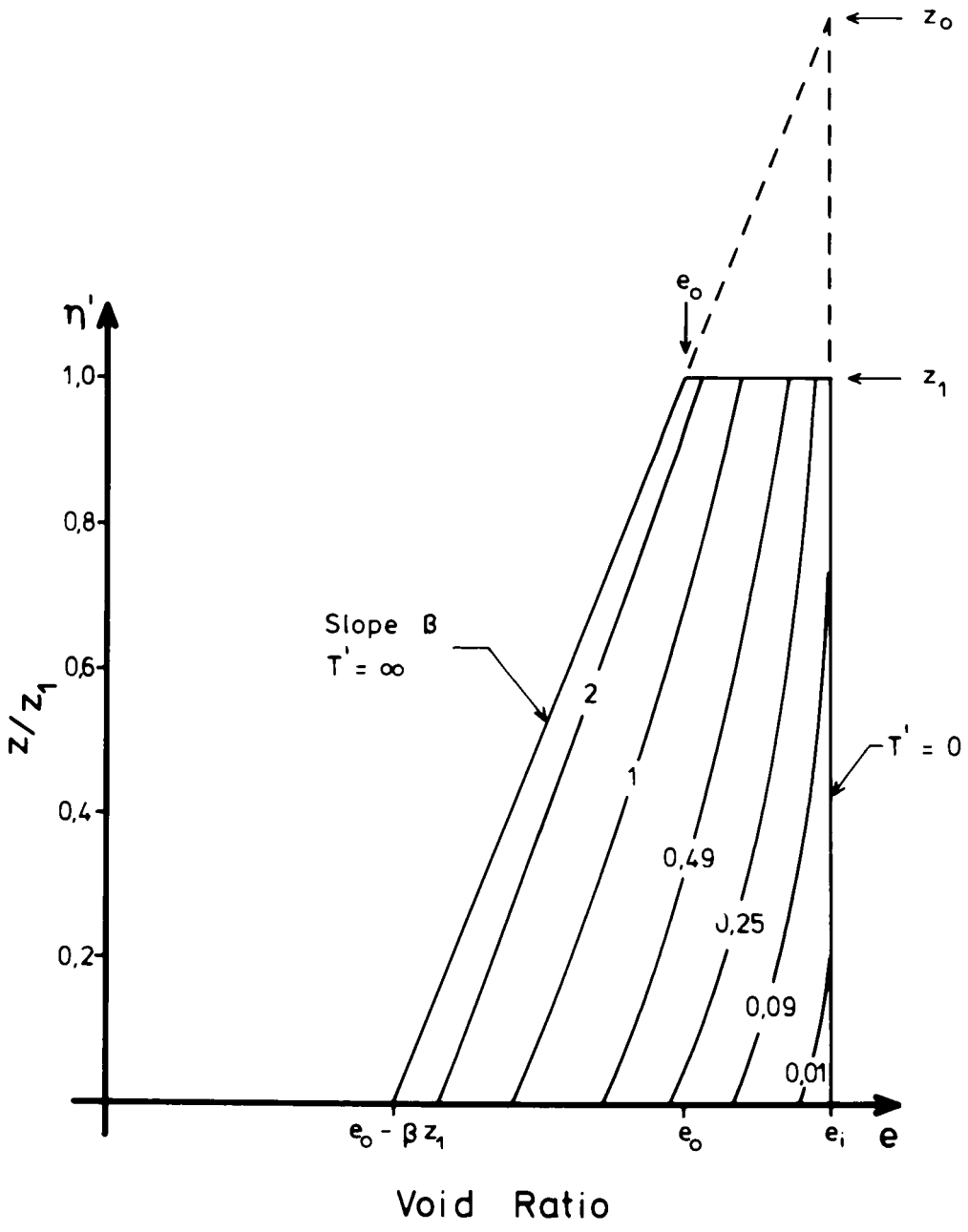


Fig 7.6. Isochrones of Void Ratio, $z_o = 1.5\ z_1$.

7.1.2. Pore Water Pressure Distribution

Considering the excess pore pressure distribution for the stratum plus imaginary overburden, given by equation 6.34 as

$$u(\eta,T) = 2(\rho_s - \rho_f)z_o \sum_n \frac{\cos m\pi\eta}{m^2\pi^2} \exp(-m^2\pi^2 T)$$

$$n = 0, 1, 2, \ldots , \quad m = \tfrac{1}{2}(2n+1) \qquad (6.34)$$

the excess pore pressure at $z = z_1$, the top of the real layer, is non-zero. At the top of the real soil, however, there is clearly no excess pore pressure so that the required solution is given as the excess pressure above the value at $z = z_1$. Referring to figure 7.7(a) where a pore pressure isochrone is plotted,

$$u' = u(\eta,T) - u(\frac{z_1}{z_o},T) \quad , \quad 0 \leq \eta \leq \frac{z_1}{z_o} \qquad (7.9)$$

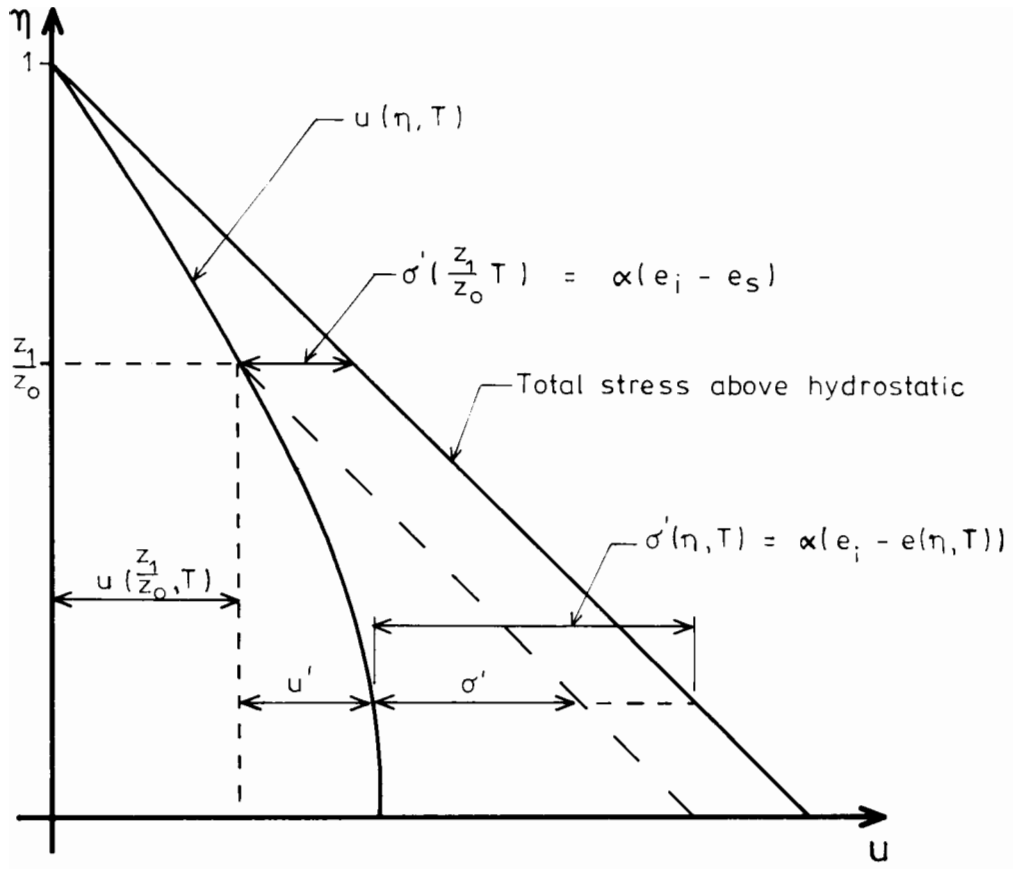
Thus

$$u(\eta',T') = 2(\rho_s - \rho_f)z_o \sum_n \frac{\cos m\pi \frac{z_1}{z_o}\eta' - \cos m\pi \frac{z_1}{z_o}}{m^2\pi^2} \exp(-m^2\pi^2(\frac{z_1}{z_o})^2 T')$$

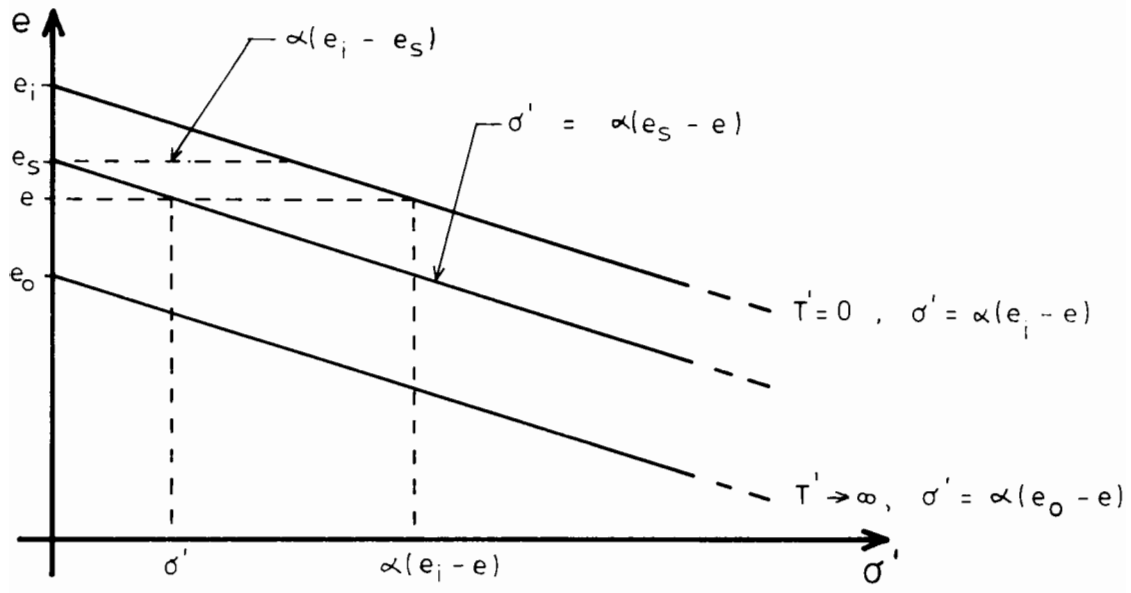
$$n = 0, 1, 2, \ldots , \quad m = \tfrac{1}{2}(2n+1) \qquad (7.10)$$

where $u(\eta',T')$ is the excess pore pressure distribution in the actual soil layer. Figure 7.8 shows isochrones of excess pore water pressure for the case $z_o = 1.5\ z_1$.

Equation 7.9 used to derive this solution is the equivalent,



(a) In Terms of Pore Water Pressure.



(b) In Terms of Effective Stress.

Fig 7.7. Modified Excess Pore Pressures.

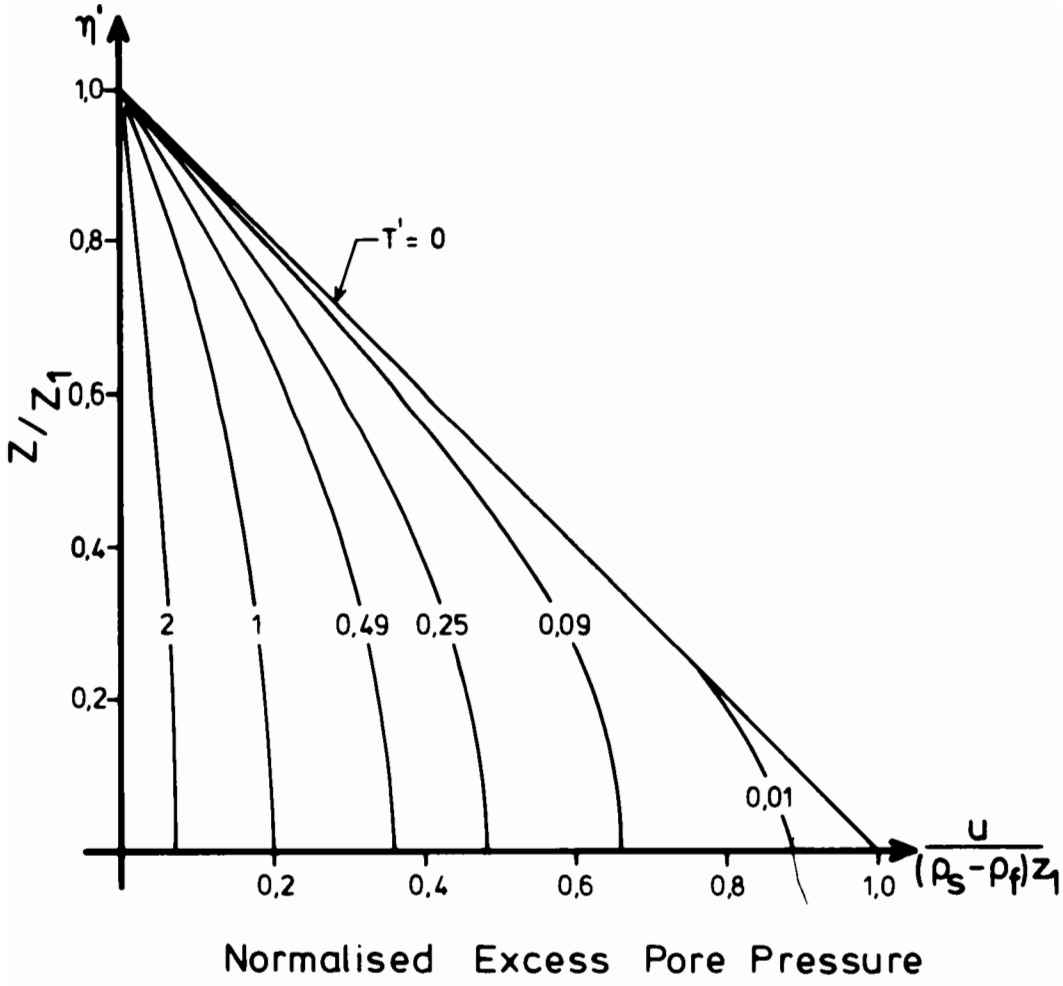


Fig 7.8. Isochrones of Pore Water Pressure, $z_o = 1.5\ z_1$.

in terms of the void ratio / effective stress relationship, of having

$$\sigma' = A - \alpha e \tag{6.13}$$

as in equation 6.13, but with (in place of eq. 6.14)

$$A = \alpha e_s \tag{7.11}$$

where, e_s, the void ratio at the surface is

$$e_s = e(1,T') = e\left(\frac{z_1}{z_o}, T\right) \tag{7.12}$$

Figure 7.7(b), along with (a), illustrates this. A non-unique void ratio / effective stress relationship is thus being used, but the slope ($\frac{d\sigma'}{de}$) is constant.

7.1.3. Degree of Settlement

The stratum plus overburden has a degree of surface settlement given by equation 6.33. In a similar way, defining the local degree of settlement within the stratum as

$$S(\eta,T) = \frac{x(\eta,0) - x(\eta,T)}{x(\eta,0) - x(\eta,\infty)} \tag{7.13}$$

where x is the space coordinate given by substitution into eq. 6.21 as

$$x(\eta) = z_o \int_0^{\eta} (1 + e)\, d\eta' \tag{7.14}$$

the local degree of settlement is calculated.

$$S(\eta,T) = 1 - \frac{4}{(2-\eta)\eta} \sum_{n} \frac{\sin m\pi\eta}{m^3\pi^3} \exp(-m^2\pi^2 T)$$

$$n = 0,\ 1,\ 2,\ \ldots\ ,\quad m = \tfrac{1}{2}(2n+1) \qquad (7.15)$$

Substitution of equations 7.6 and 7.7 for η' and T' and putting $\eta' = 1$ gives the degree of surface settlement of the real layer. (Fig. 7.9)

$$S(1,T') = 1 - \frac{4}{(2-\frac{z_1}{z_o})\frac{z_1}{z_o}} \sum_{n} \frac{\sin m\pi \frac{z_1}{z_o}}{m^3\pi^3} \exp(-m^2\pi^2(\frac{z_1}{z_o})^2 T')$$

$$n = 0,\ 1,\ 2,\ \ldots\ ,\quad m = \tfrac{1}{2}(2n+1) \qquad (7.16)$$

7.1.4 Transformation to Space Coordinates

Comparison of calculated values with experimental results requires knowledge of the position in space, x, of any soil element. Integrating equation 6.21 gives

$$x(\eta',T') = (1+e_i-\beta z_o)z_1\eta' + \frac{\beta}{2}(z_1\eta')^2 + 2\beta z_o^2 \sum_{n} \frac{\sin m\pi \frac{z_1}{z_o}\eta'}{m^3\pi^3} \exp(-m^2\pi^2(\frac{z_1}{z_o})^2 T')$$

$$n = 0,\ 1,\ 2,\ \ldots\ ,\quad m = \tfrac{1}{2}(2n+1) \qquad (7.17)$$

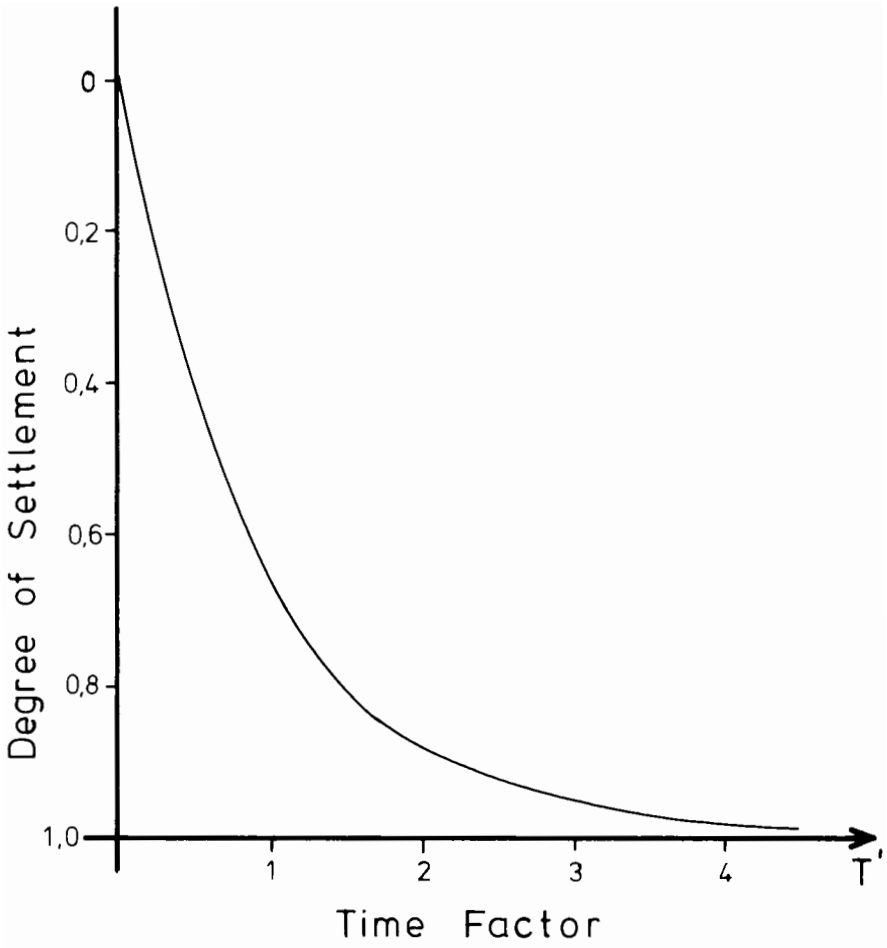


Fig 7.9. Degree of Surface Settlement, $z_o = 1.5\ z_1$.

7.2. DETERMINATION OF THE COEFFICIENT OF CONSOLIDATION

Three soil parameters are embodied in the solutions derived in the previous section;

e_o , the ultimate zero effective stress point of the soil

β , the slope of the final void ratio distribution, which is determined (eq. 6.19) by the effective stress / void ratio relationship

$k_o = \frac{k}{\rho_f(1+e)}$, the permeability relationship.

In order to generate a solution to the equations a value of e_i, the assumed initial uniform void ratio, and z_1, the solid thickness of the mud, must also be specified.

Once these values have been chosen from the experimental observations, the coefficient of consolidation can be found in three ways;

(a) Direct calculation.

From

$$C_f = -\frac{k}{\rho_f(1+e)} \frac{d\sigma'}{de} \tag{6.15}$$

or

$$C_f = k_o \frac{(\rho_s - \rho_f)}{\beta} \tag{7.18}$$

Use of the constants k_o and β in equation 7.18 will yield a constant C_f value, but putting values of $\frac{d\sigma'}{de}$ and k at different void ratios estimated from the experiments into equation 6.15 may give a range of C_f values.

(b) Comparison of settlement curves.

Calculated settlements plotted as a function of time factor, T', and real surface settlements plotted in terms of real time t are compared, allowing C_f to be found from equation 7.2

$$T' = \frac{C_f \, t}{z_1^2} \tag{7.2}$$

when the real points fit the calculated curve best.

(c) Pore water pressure dissipation.

Instead of comparing settlement curves, isochrones of excess pore water pressure calculated for T' are plotted. Real pore pressure measurements at a particular time are used to find the best corresponding value of time factor T' and C_f is calculated using equation 7.2 as before.

Method (a) requires measurements of stress, deformation and pore pressures, while (b) relies only on deformation and (c) only on pore pressures. An assessment of the theoretical model can therefore be made by comparing the coefficient of consolidation found in these three different ways.

7.2.1. Choice of Soil Parameters and Initial Conditions

Relevant values taken from the experimental data for experiments 10 to 15 (figs. 4.15 to 4.42) are tabulated in table 7.1.

Initial conditions, e_1 and z_1

The solid thickness of mud in a column is calculated directly

Experiment no.	10	11	12	13	14	15
Initial Density (Void Ratio)	82	32	32	19	14	10.3
Solid Thickness in Column (cm)	2.35	5.42	5.48	5.18	5.42	5.66
Allowance for Particle Segregation	18%	13%	13%	10%	-	-
z_1 (cm)	1.93	4.70	4.76	4.64	5.42	5.66
Height of Dense Bottom Layer (cm)	1.6	2.0	2.0	1.6	-	-
Assumed Initial Average Void Ratio (e_i)	16.0	11.9	11.9	9.6	7.5	10.3
β (cm^{-1}) (Estimated)	2.5	1.27	0.98	1.14	0.76	0.72
Zero Effective Stress Void Ratio (e_o)	8.3	7.3	6.7	6.9	6.3	6.0
β (cm^{-1}) (Adjusted)	1.98	1.12	1.12	0.91	0.82	0.76
e_o (adjusted)	7.4	7.0	7.0	6.4	6.3	6.1

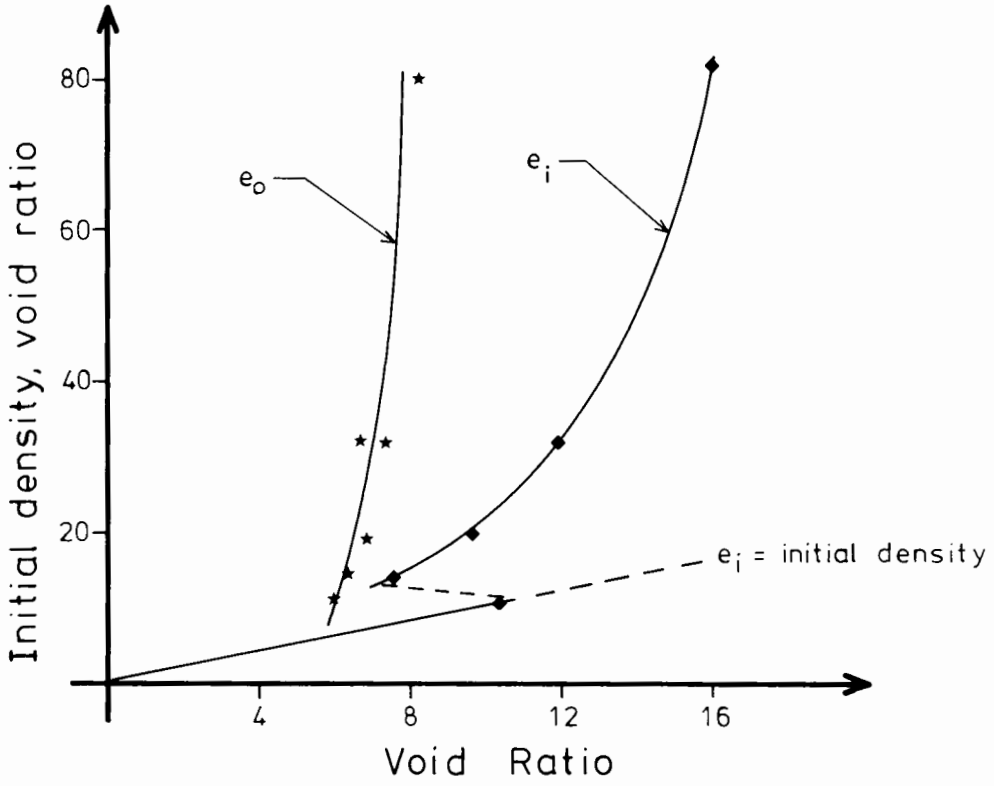
Table 7.1. Experimental Data for Calculations.

from the known mass of soil present, the cross-sectional area of the column, and the solids density. A revised solid thickness for the calculations, z_1, is estimated by subtraction of the solid thickness of the dense layer at the column base caused by particle segregation. No such allowance is necessary for tests 14 and 15. An important effect of this particle segregation is that the mud left above the dense layer is depleted of coarser silt particles to varying degrees in each test. Some variation in soil parameters for each experiment is thus to be expected.

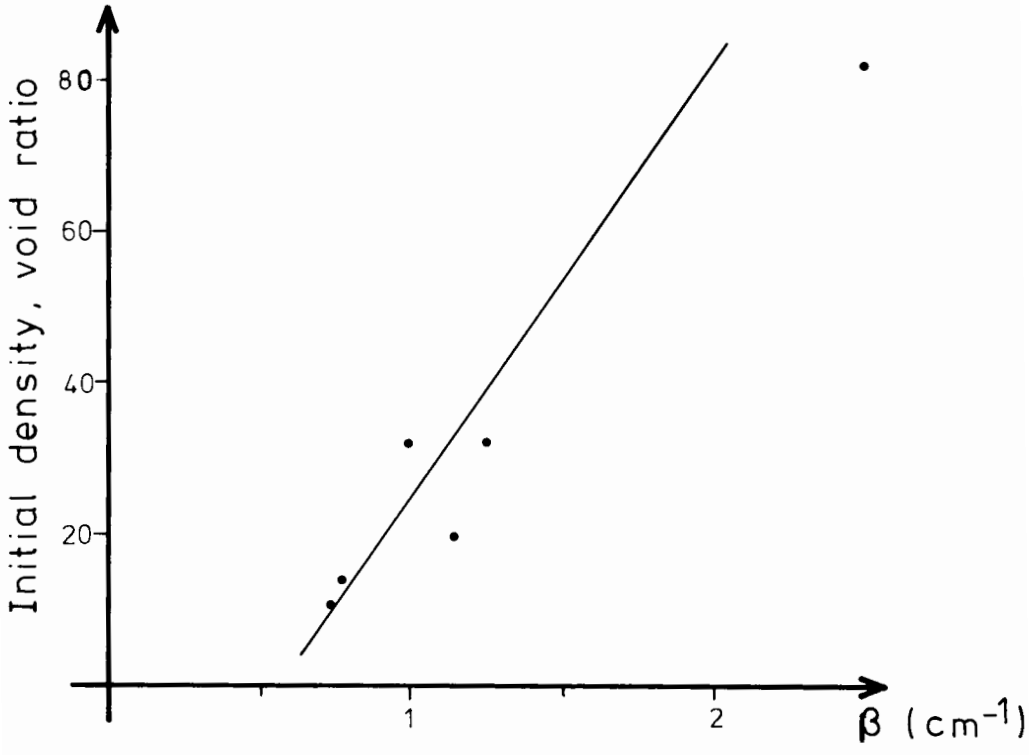
An average initial void ratio is calculated from the height of mud when a true suspension no longer exists, based on the value of z_1. Figure 7.10(a) shows this value of initial void ratio e_i plotted against the suspension initial void ratio (calculated directly from the initial density). Tests 10 to 14 lie on a smooth curve but there is then a jump to the "e_i = initial suspension density" line for experiment 15. This occurs because experiment 15 has an initial density in the intermediate phase range. There is a marked difference between the density profiles during the early parts of a test with an initial density in the intermediate range (experiments 8 and 15) and those during a test that is initially a true suspension. Although one might expect the curve to join the straight line without the discontinuity, it seems that the instability at the transition density prevents this happening. Channelling and the unusual density profiles seen in experiment 14 (where the initial density is just within the suspension range, fig. 4.21), also reflect this instability.

Parameters e_o and β

Values of the ultimate zero effective stress point are shown



(a) Zero Effective Stress Point, e_o, and Assumed Initial Void Ratio, e_i.



(b) Beta.

Fig 7.10. Soil Parameter Trends.

on fig 7.10(a) and fig 7.10(b) shows the values of β against the initial suspension void ratio. Both e_o and β are estimated from density profiles in the more advanced state of consolidation. A small adjustment of the values is sometimes necessary to obtain agreement between the final calculated bed height and the real bed height, because accurate determinations from the density profiles are difficult. Curvature of the density profile at the surface makes the choice of e_o rather subjective and similarly β can only be a guessed approximation to the average slope of the density profile.

For the theoretical calculations in this chapter the values of e_o and β actually used are those that lie on the lines indicating the trends in figure 7.10. It is arguable that constant values should be used as the same soil sample is involved in all cases. However, as mentioned earlier, particle segregation could largely account for these trends so that constants have not been used, although the use of $e_o = 6.5$ and $\beta = 1\ cm^{-1}$ as constants would probably not affect the accuracy of predictions for initial void ratios under 30.

Void Ratio/Effective Stress Relationships

Combining equations 6.13, 6.14 and 6.19, the void ratio effective stress relationship is defined by e_o and β.

$$\sigma' = (\rho_s - \rho_f) \frac{(e_o - e)}{\beta} \qquad (7.19)$$

This relationship is shown for the six tests (10 to 15) in figure 7.11 and compared to the linear approximation proposed in figure 7.1 (which

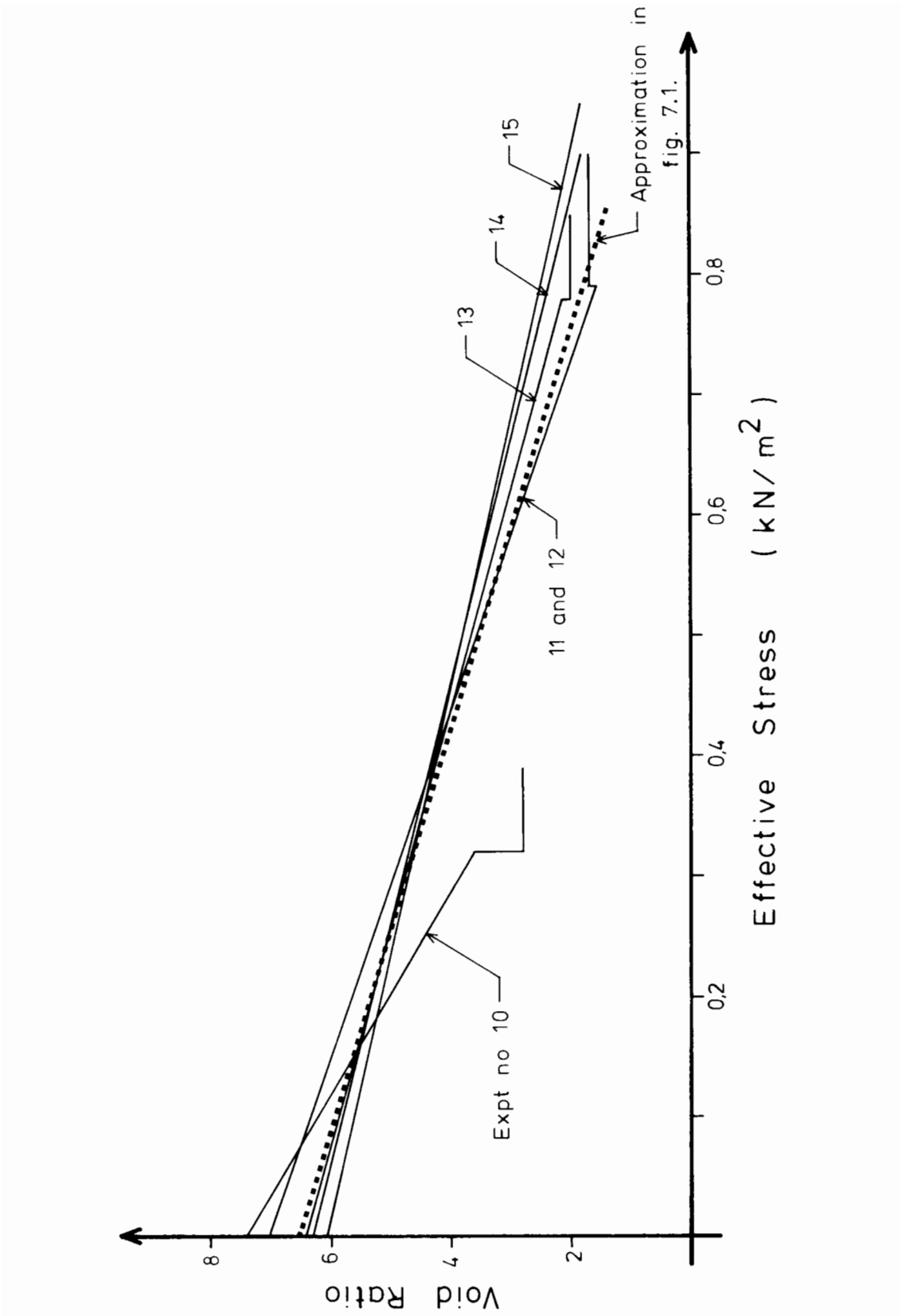


Fig 7.11. Assumed Final Effective Stress / Void Ratio Relationships.

has e_o = 6.5, β = 1.0 cm^{-1}). Discontinuities at the ends of the lines for experiments 10 to 13 show the effect of the allowance made for the dense base layer formed by particle segregation.

Each relationship is a slightly better linear approximation to the relevant experiment than the single line could provide.

7.2.2 C_f from Settlement Curves

Calculated surface settlements for experiments 10 to 15 (assuming the initial theoretical conditions outlined at the beginning of section 7.1) are shown as full lines in figures 7.12 to 7.17. Real surface heights in the first few hours are suspension surfaces and will be very different, as these calculated values represent the top of the intermediate phase. The calculations are therefore not applicable before the time the intermediate zone reaches the surface. Measured settlements of the intermediate phase surface, plotted as stars on the same axes, fit the calculated lines best when values of the coefficient of consolidation (C_f) are as given in each figure and tabulated in Table 7.2. Each test has approximately the same value of C_f for the best fit.

In general the measured points lie quite close to the calculated lines but the trend is for real settlements to be faster initially, and slower at later stages, than calculated settlements. Although the shape of the real effective stress/void ratio curve and a build up of friction as the effective stress increases lead one to expect this trend,

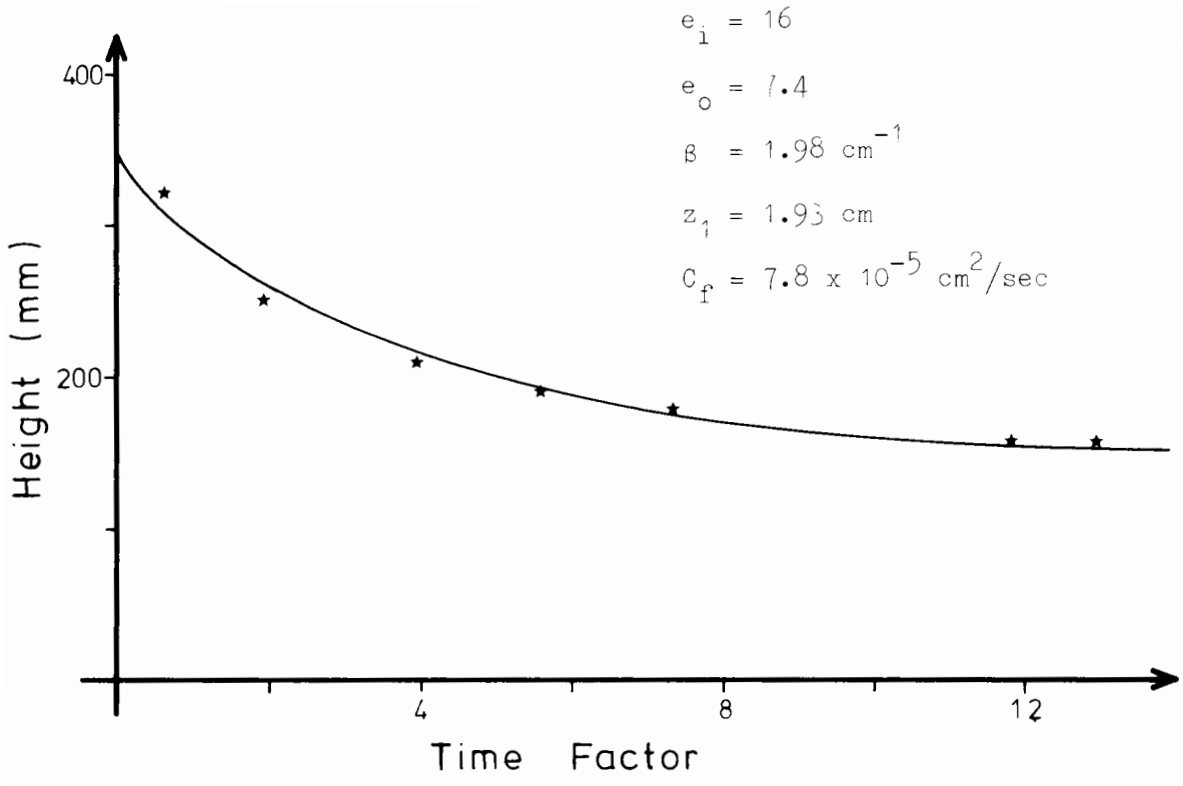


Fig 7.12. Settlement Curve, Experiment 10.

Initial Density 1.02 gm/cm^3

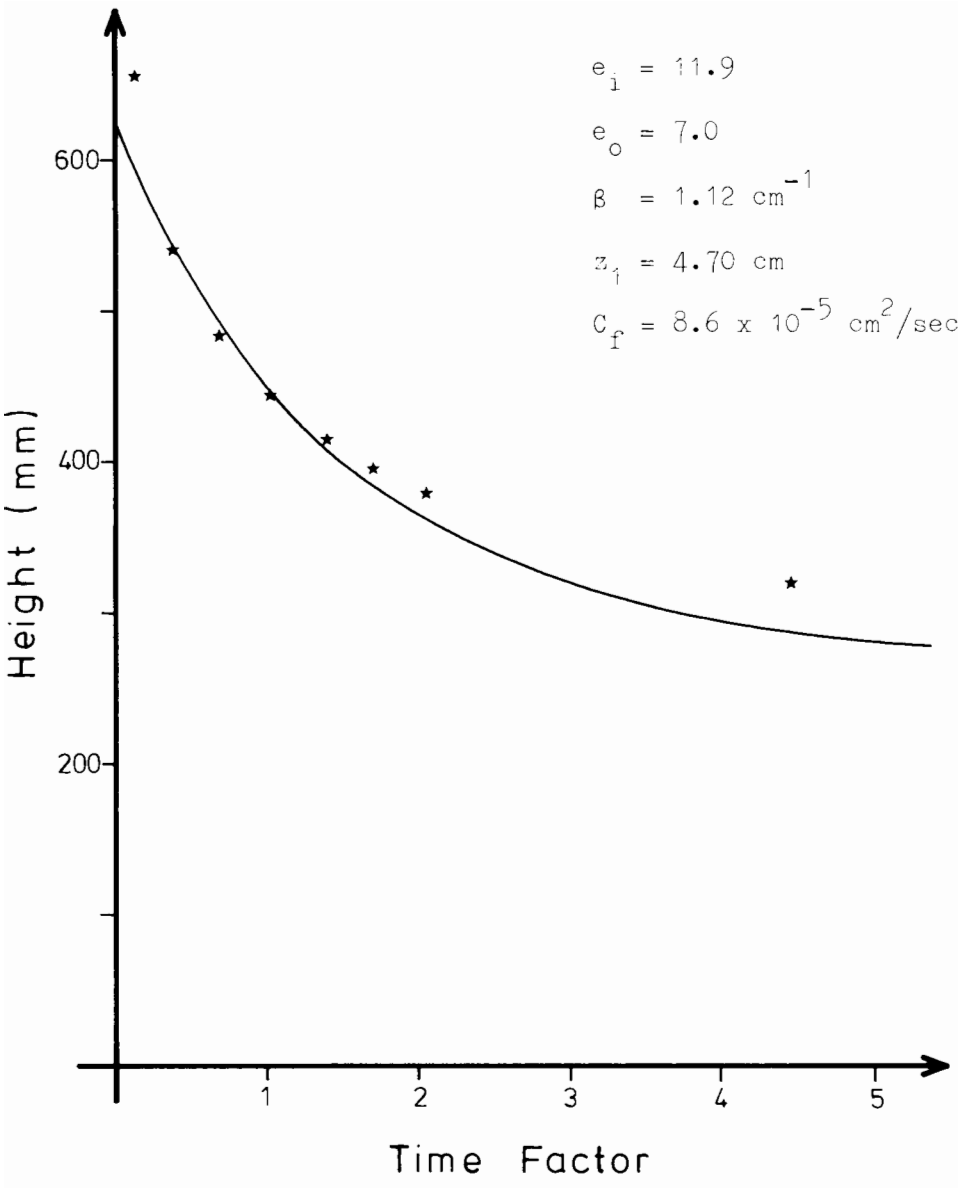


Fig 7.13. Settlement Curve, Experiment 11.

Initial Density 1.05 gm/cm^3

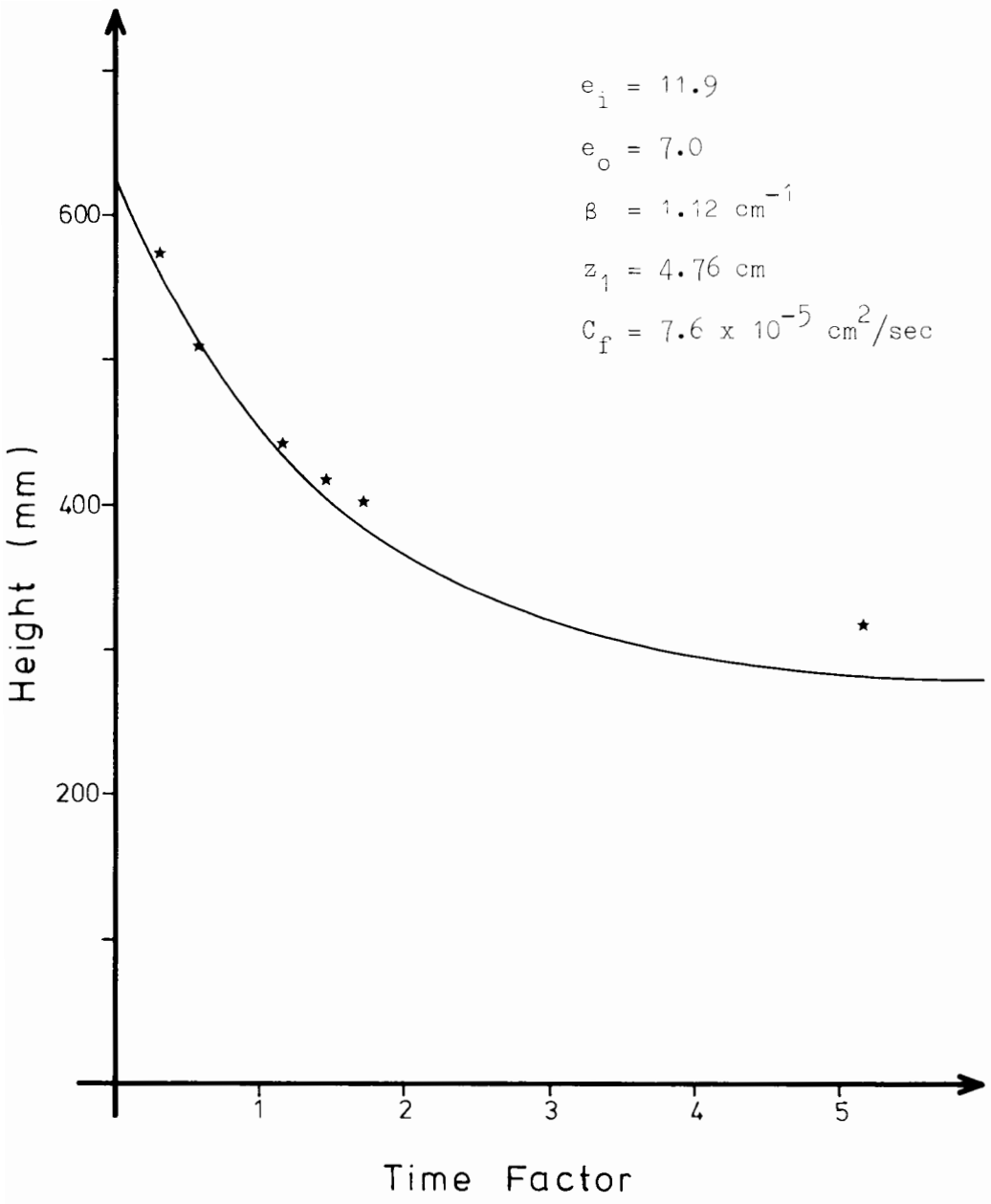


Fig 7.14. Settlement Curve, Experiment 12.

Initial Density 1.05 gm/cm^3

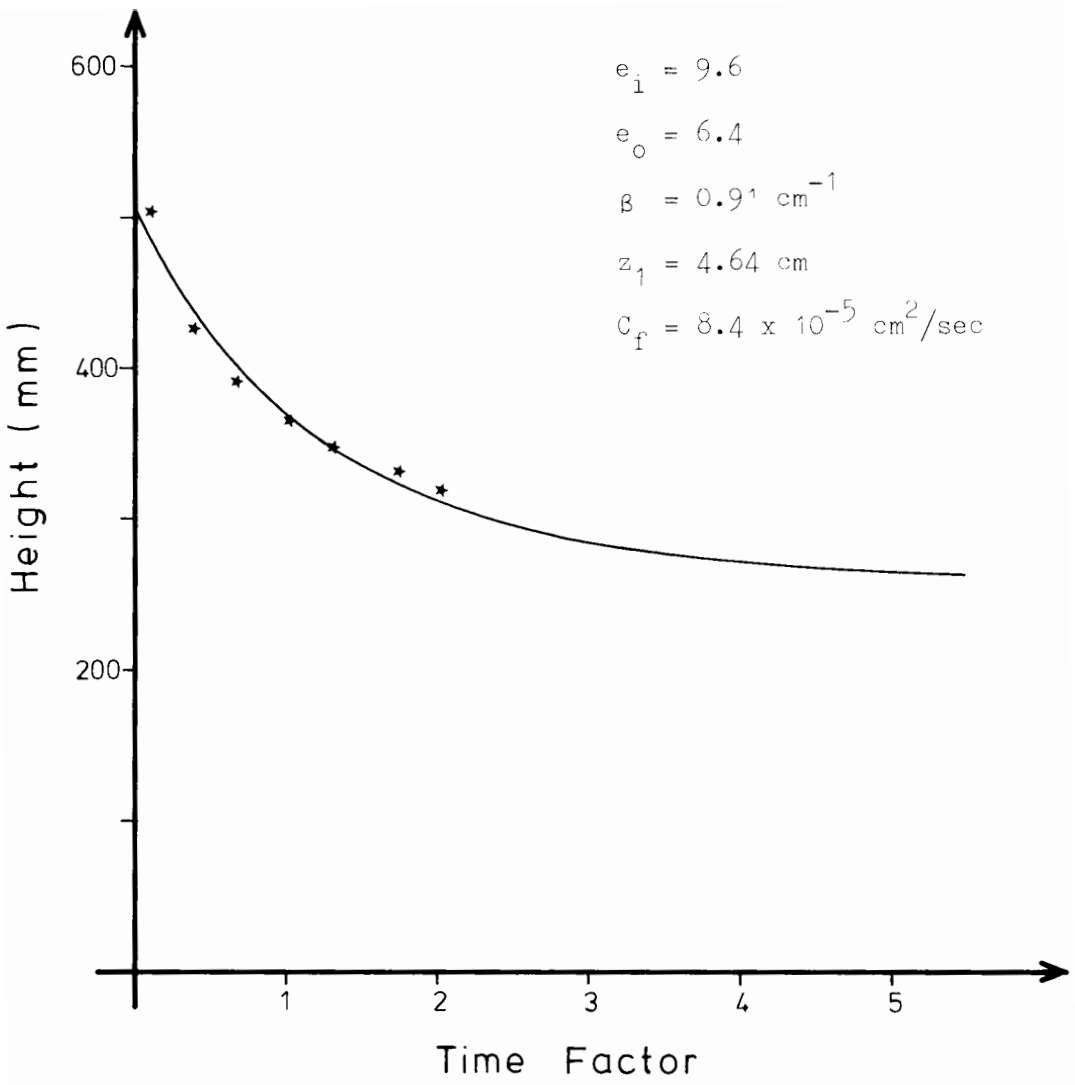


Fig 7.15. Settlement Curve, Experiment 13.

Initial Density 1.08 gm/cm^3

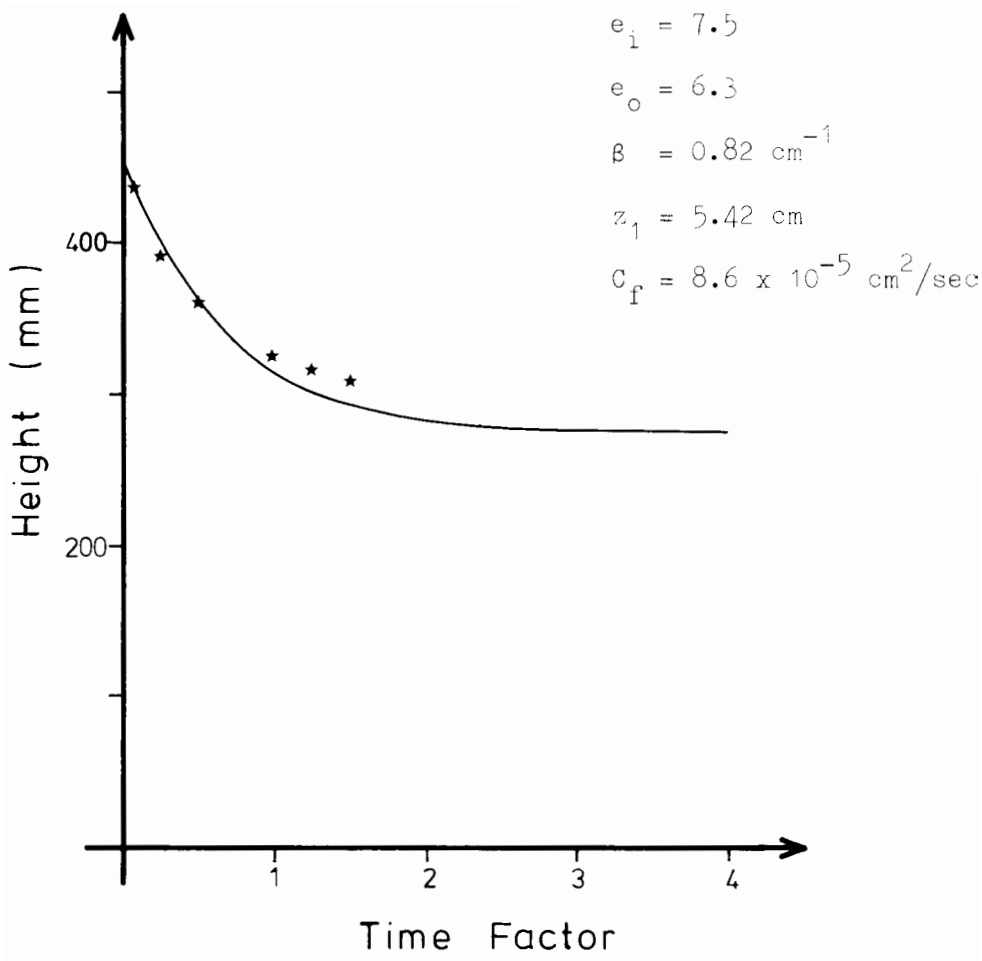


Fig 7.16. Settlement Curve, Experiment 14.

Initial Density 1.11 gm/cm^3

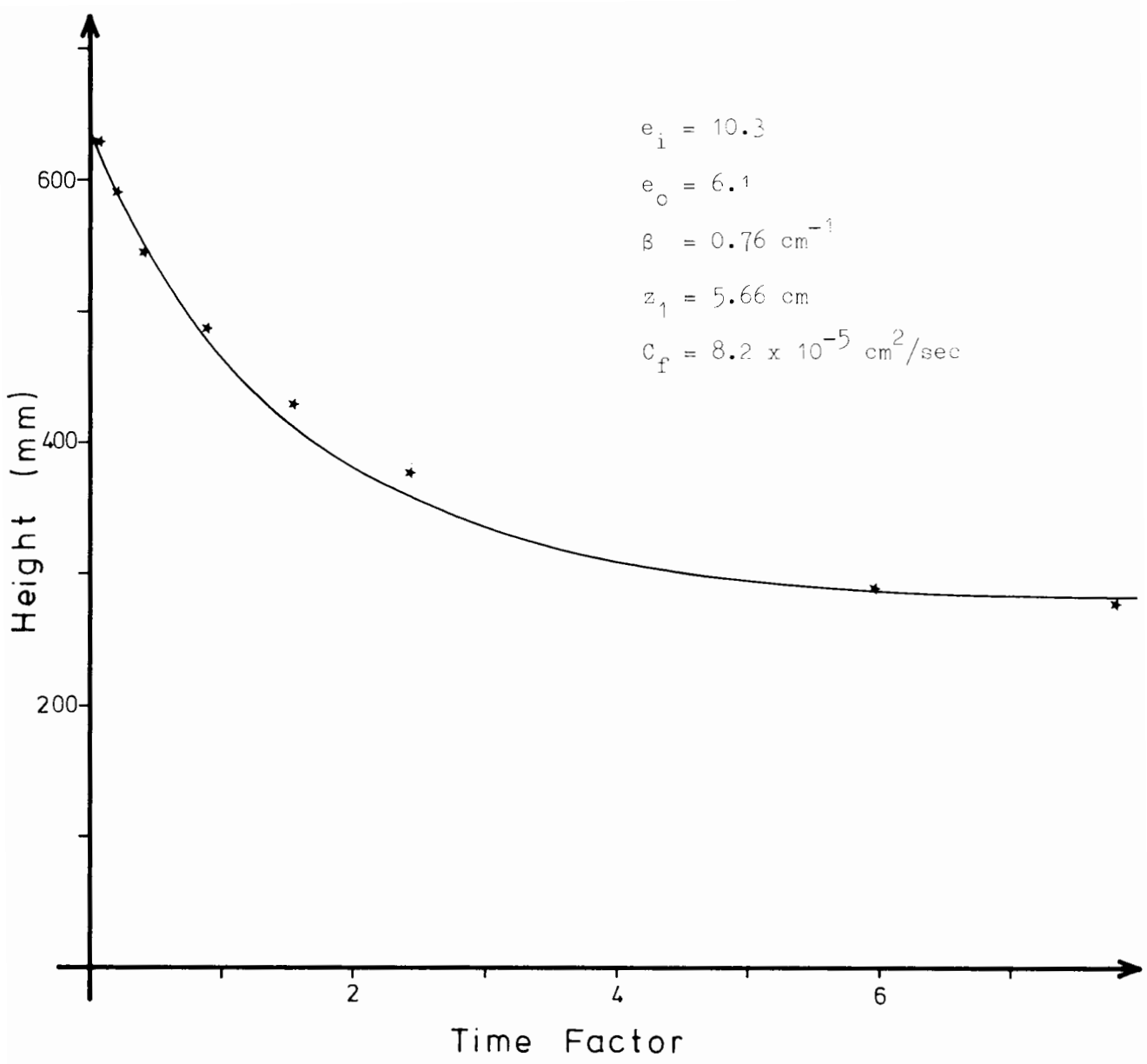


Fig 7.17. Settlement Curve, Experiment 15.

Initial Density 1.146 gm/cm^3

Experiment no.	Coefficient of Consolidation (Best Fit C_f, cm^2/sec)	β cm^{-1}	$\frac{k}{1+e}$ cm/sec
10	7.8×10^{-5}	1.98	9.3×10^{-5}
11	8.6×10^{-5}	1.12	5.8×10^{-5}
12	7.6×10^{-5}	1.12	5.1×10^{-5}
13	8.4×10^{-5}	0.91	4.6×10^{-5}
14	8.6×10^{-5}	0.82	4.2×10^{-5}
15	8.2×10^{-5}	0.76	3.8×10^{-5}

Table 7.2. Coefficient of Consolidation from Settlement Curves.

Experiment no.	Highest C_f cm^2/sec	Lowest C_f cm^2/sec	Mean C_f cm^2/sec
10	2.4×10^{-5}	1.0×10^{-5}	1.4×10^{-5}
11	7.3×10^{-5}	1.5×10^{-5}	3.1×10^{-5}
12	2.8×10^{-5}	9.5×10^{-6}	1.5×10^{-5}
13	7.5×10^{-5}	1.6×10^{-5}	3.2×10^{-5}
14	2.7×10^{-5}	1.3×10^{-5}	1.8×10^{-5}
15	2.0×10^{-5}	3.7×10^{-6}	9.0×10^{-6}

Table 7.3. Coefficient of Consolidation from Pore Pressures.

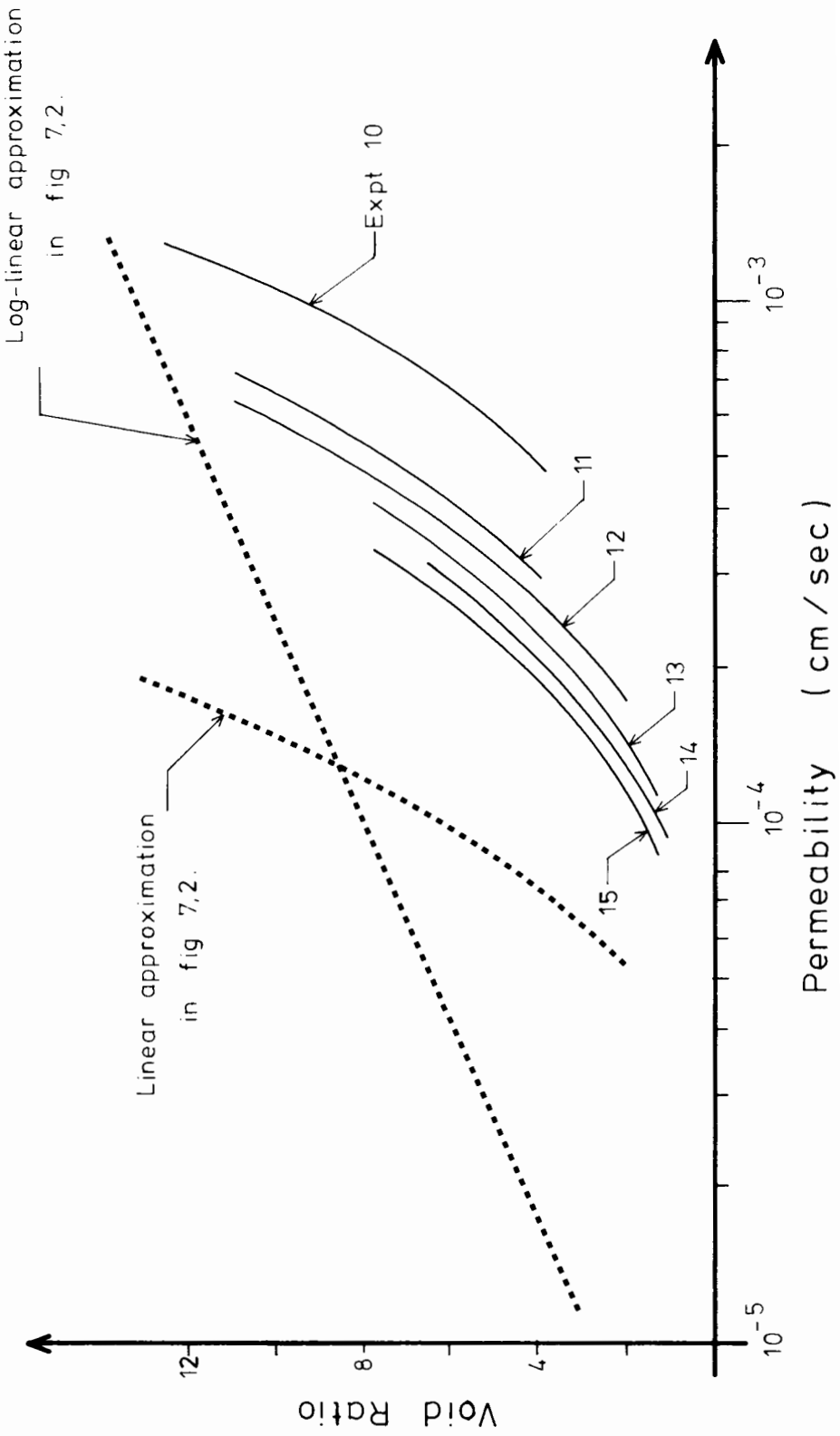


Fig 7.18. Permeability, Back Analysed from Settlement C_f.

(Refer to Table 7.2)

it is mainly an effect of the linearised permeability function.

In table 7.2 permeability / void ratio relationships back analysed from values of C_f and β using equation 7.18 are given. These are then plotted in figure 7.18 for each test and compared to the trend shown by measured permeabilities in figure 7.2. The back analysed permeabilities all lie in the range 10^{-4} to 10^{-3} cm/sec, which is comparable with measured values only during the early stages of consolidation when higher void ratios exist (and most of the settlement occurs). Thus the real settlements that are governed by permeabilities between 10^{-5} and 10^{-4} cm/sec in the later stages, occur more slowly than the calculations predict.

7.2.3. C_f from Pore Water Pressure Distributions

Normalised excess pore water pressures from figure 4.24 for experiment 11 have been plotted in figure 7.19(a) as isochrones in real time. Calculated isochrones in terms of the time factor T' are shown in figure 7.19(b). By comparing the isochrones, a value of T' can be estimated corresponding to each real time isochrone and C_f calculated by

$$C_f = \frac{T' \, z_1^2}{t} \qquad (7.2)$$

This has been done for each of experiments 10 to 15 and the results appear in table 7.3.

The range of values covered by these coefficients is not

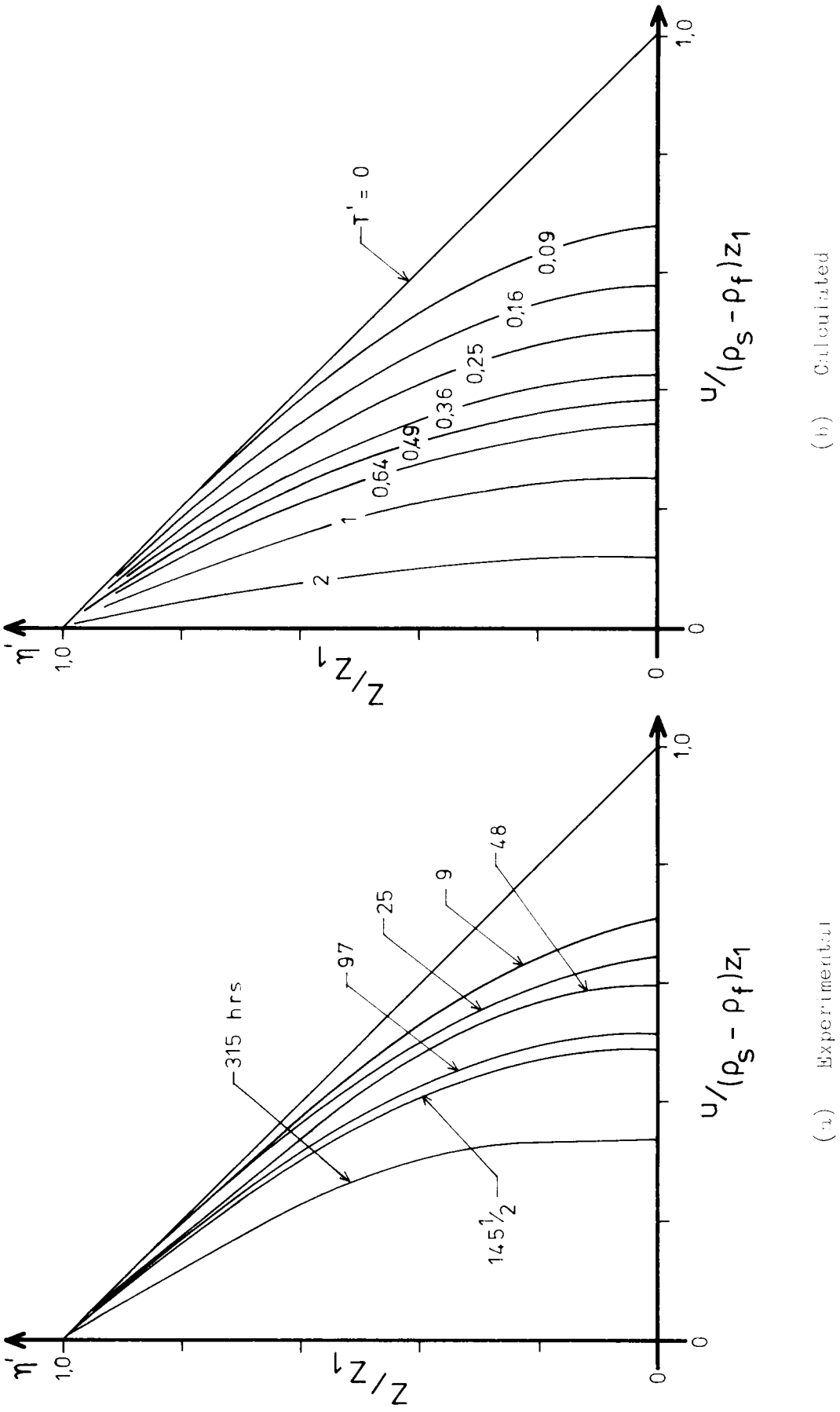


Fig 7.19. Normalised Excess Pore Pressure Isochrones.

Experiment 11, Initial Density 1.05 gm/cm^3.

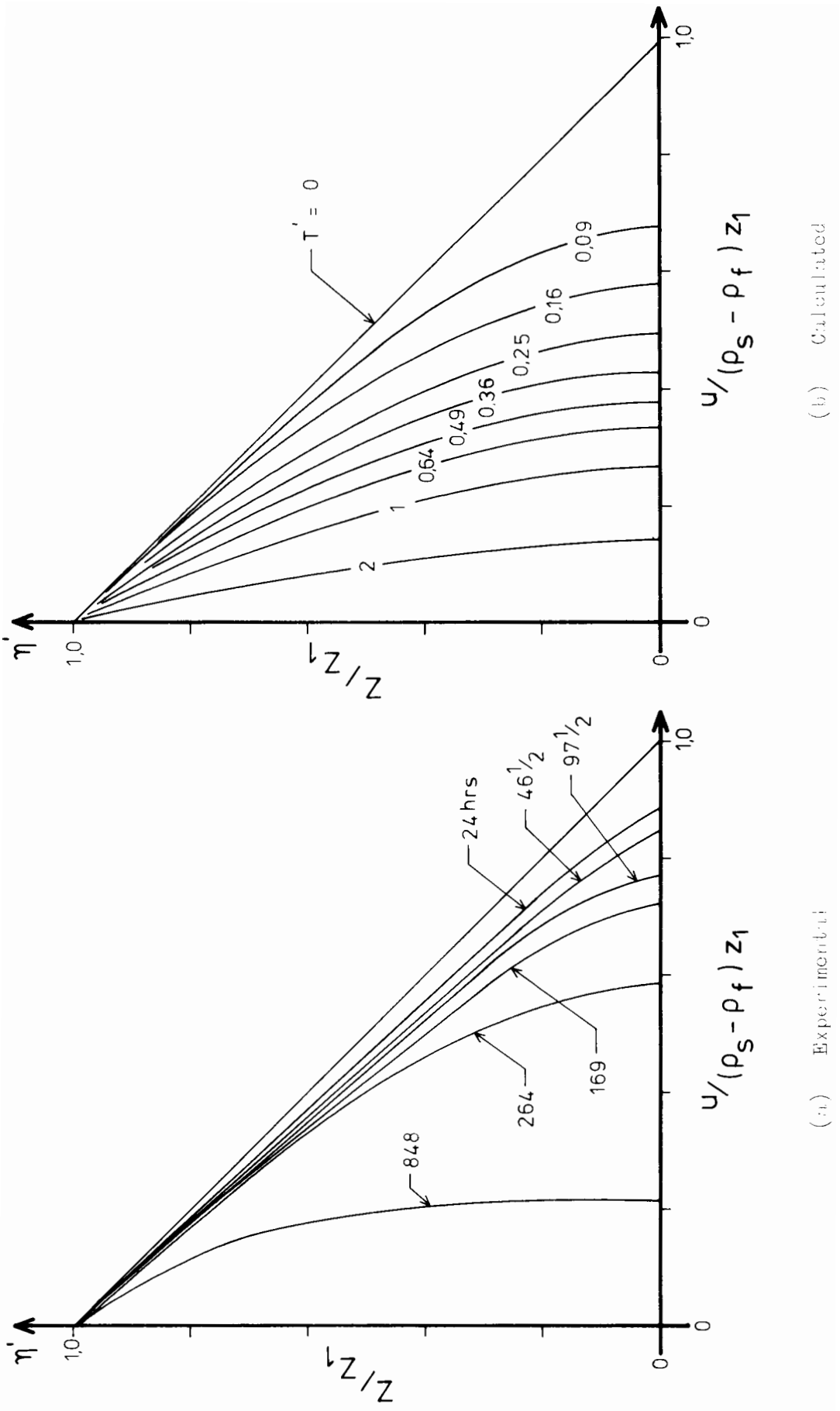


Fig 7.20. Normalised Excess Pore Pressure Isochrones.

Experiment 15, Initial Density 1.146 gm/cm^3.

excessive, especially as the second highest values for test 11 and 13 are 3.9 $\times 10^{-5}$ cm^2/sec and 3 $\times 10^{-5}$ cm^2/sec respectively. (Figure 7.21 is possibly more informative.) A constant C_f of about 1.8 $\times 10^{-5}$ cm^2/sec to predict pore pressures seems a reasonable assumption to make.

Experiment 15 has a slightly different general form to its normalised excess pore pressure isochrones from the other experiments, shown in figure 7.20. It was thus more difficult to compare isochrones to find the C_f value in this case. A good reason for this is not obvious, but it may be noted that the initial density in this experiment was in the intermediate phase range.

7.2.4. Calculation of C_f from Soil Properties

Equation 6.15 gives the coefficient of consolidation as

$$C_f = - \frac{k}{\rho_f (1+e)} \frac{d\sigma'}{de} \qquad (6.15)$$

Because of the difficulty of estimating $\frac{d\sigma'}{de}$ from a typical void ratio / effective stress plot in the present work, a constant value has been used for each experiment as in figure 7.11. In other words the best linear void ratio / effective stress function is used. From figures 4.35 to 4.40 for each experiment 10 to 15 a value of permeability at a certain void ratio is found and C_f is then calculated, table 7.4.

The effect of assuming a constant value of $\frac{d\sigma'}{de}$ is to increase the spread of values in the table. At low void ratios the soil is

Experiment no.	Void Ratio	Permeability k, cm/sec	C_f cm^2/sec	Mean C_f cm^2/sec
10	4	1.8×10^{-5}	3.8×10^{-6}	
	6	3.5×10^{-5}	4.2×10^{-6}	
$\beta = 1.98$	8	7.0×10^{-5}	6.5×10^{-6}	8.5×10^{-6}
	10	1.4×10^{-4}	1.1×10^{-5}	
	12	2.7×10^{-4}	1.7×10^{-5}	
11	4	2.4×10^{-5}	7.1×10^{-6}	
	6	5.4×10^{-5}	1.1×10^{-5}	1.8×10^{-5}
$\beta = 1.12$	8	1.2×10^{-4}	2.0×10^{-5}	
	10	2.5×10^{-4}	3.4×10^{-5}	
12	4	1.7×10^{-5}	5.0×10^{-6}	
	6	3.5×10^{-5}	7.4×10^{-6}	1.2×10^{-5}
$\beta = 1.12$	8	7.5×10^{-5}	1.2×10^{-5}	
	10	1.6×10^{-4}	2.2×10^{-5}	
13	4	2.2×10^{-5}	8.0×10^{-6}	
	6	5.2×10^{-5}	1.4×10^{-5}	2.4×10^{-5}
$\beta = 0.91$	8	1.2×10^{-4}	2.4×10^{-5}	
	10	2.9×10^{-4}	4.8×10^{-5}	
14	4	3.1×10^{-5}	1.3×10^{-5}	
	6	1.4×10^{-4}	4.0×10^{-5}	4.1×10^{-5}
$\beta = 0.82$	8	2.5×10^{-4}	5.6×10^{-5}	
15	4	1.2×10^{-5}	5.2×10^{-6}	
	6	3.6×10^{-5}	1.1×10^{-5}	2.5×10^{-5}
$\beta = 0.76$	8	1.0×10^{-4}	2.4×10^{-5}	
	10	3.0×10^{-4}	6.0×10^{-5}	

Table 7.4. Calculated Coefficient of Consolidation.

stiffer than the average, so the real $\frac{d\sigma'}{de}$ is greater than used in the calculations. Thus the lower values in the table should be increased and, by the same argument, the higher values decreased. Void ratios of 10 in experiments 13 and 15, and 8 in experiment 14, should be given less weight in determining a mean value of C_f as these void ratios exist only for a relatively short period of time in the early stages of consolidation.

Bearing the above factors in mind the range of C_f found in this way is not inconsistent with the constant C_f assumption.

7.2.5. Comparison of C_f Found by Three Methods

Figure 7.21 shows the data from tables 7.2, 7.3, and 7.4 graphically so that they may be compared. Values that refer to early stages of settling only (under 10 hours) or to void ratios that in fact exist only near the surface for a short period are plotted, but joined to other points only by dotted lines to indicate their reduced significance.

All three methods give a reasonably small variation in C_f. C_f found from settlement curves, however, is significantly higher than the other two methods, which are similar. Both the calculated and the pore pressure C_f depend on pore pressure measurements but the settlement C_f is purely an average deformation quantity. Since the link is thus a theoretical one, the difference is due to an inconsistency between the theory and real intermediate phase behaviour.

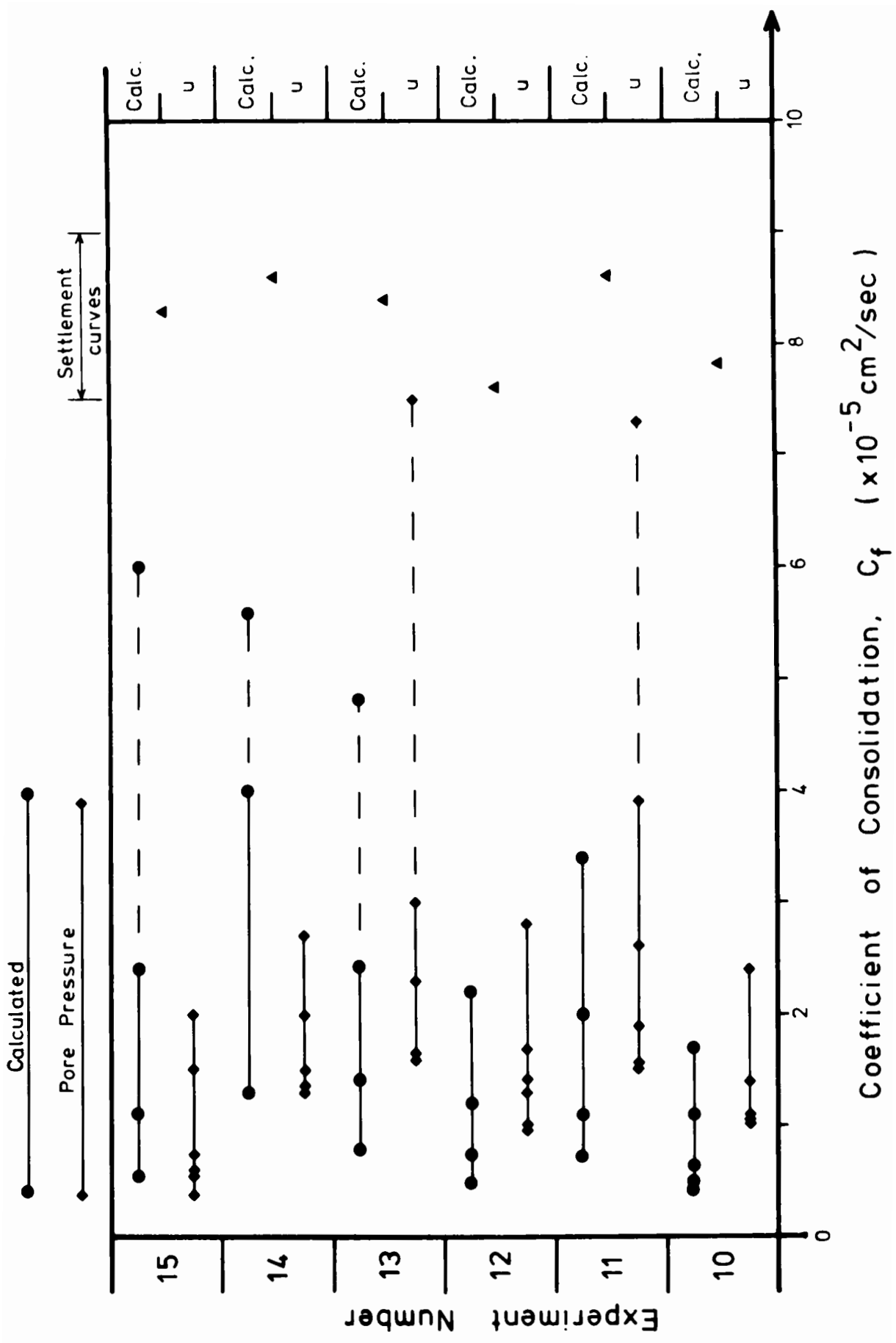


Fig 7.21. Comparison of Coefficients of Consolidation.

(Tables 7.2 to 7.4)

In the unmodified theory (chapter 6) pore pressures are found from the void ratio distribution. Given a void ratio value, the effective stress is determined from the unique void ratio / effective stress relationship and subtracted from the total stress to give the pore pressure. (Total stress is simply a function of depth in the soil stratum.) As there is not a unique relationship in the intermediate phase, the modified theory of this chapter uses the void ratio at the surface to determine the void ratio / effective stress function. There is no reason why this relationship should occur in a real soil and indeed the above C_f values indicate it is not a very good approximation to use.

Comparison of the pore pressure values of C_f with the calculated values shows they are very similar despite the inclusion of stress-strain behaviour in the calculated values. This suggests that consolidation in the intermediate phase is governed largely by the expulsion of pore water and that effective stress / strain behaviour (or compressibility) has a much smaller effect than in true soils.

7.3 DENSITY PROFILES COMPARED

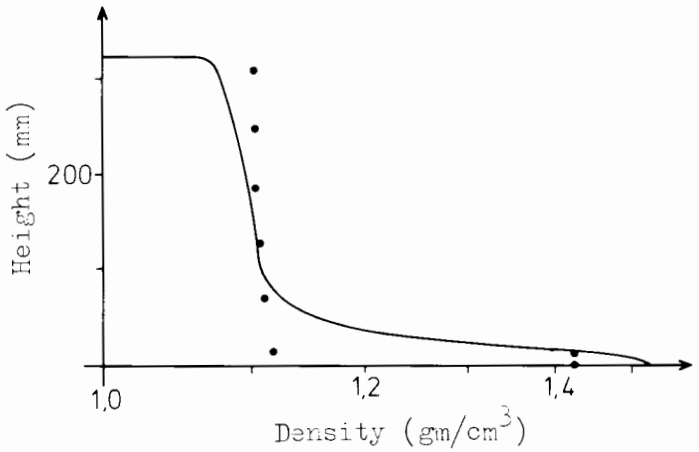
Although the coefficient of consolidation derived from the settlement plots is nearly constant, it does not compare closely with otherwise calculated values, revealing the (probably) inadequate method of predicting pore pressures from the void ratio distribution. The settlement curve is, however, only a measure of the average void ratio changes in the soil bed. In this section the C_f value found from settlement plots is therefore used in the theory to compare predicted

void ratio distributions within the layer to actual density profiles. Since pore water pressure measurements are not used at all, this provides an assessment of the solution in terms of void ratio alone.

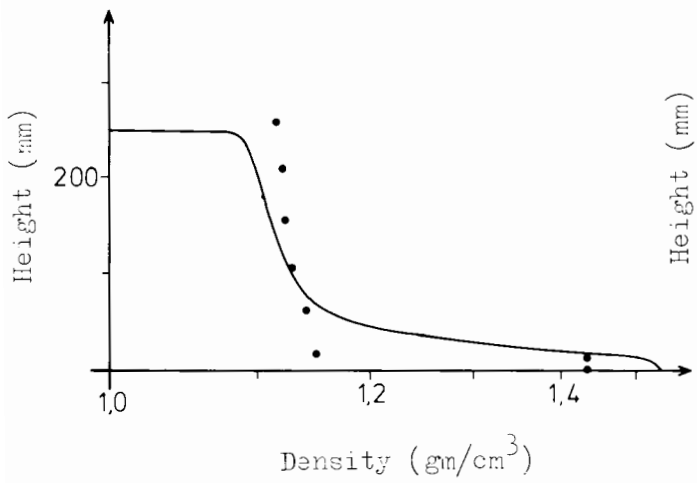
Figures 7.22 to 7.27 show measured density profiles for experiments 10 to 15 (as per figs. 4.17 to 4.22) as full lines with calculated predictions as dots plotted on the same axes. Calculations are based on the modified theory, equation 7.8 (converted to space coordinates by equation 7.17), using the C_f values in table 7.2 that give the best fit to the settlement curves. Allowance has been made for the coarser particles settling quickly to the base where applicable.

In general the theory fits the real profiles well in the later stages shown. A good fit is expected here as the β and e_o values chosen for the calculations are partly based on the profiles between 144 and 200 hours. In the earlier profiles the effect of assuming a uniform initial density (instead of the real gradient after deposition) is to keep the calculated profiles more nearly uniform than the real ones. In experiments 14, and especially 15, where the higher initial densities result in more uniform real profiles, a good fit is maintained throughout the consolidation.

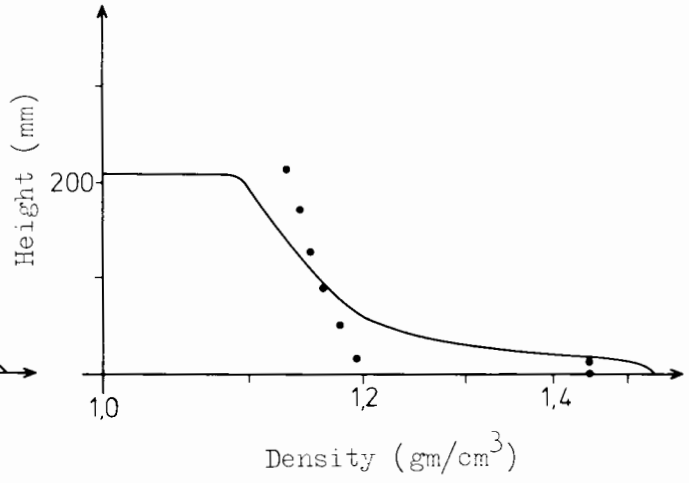
Reasonable success, with certain limitations, could thus be expected if the modified theory is used to estimate void ratio or density distributions, provided the appropriate coefficient of consolidation is used.



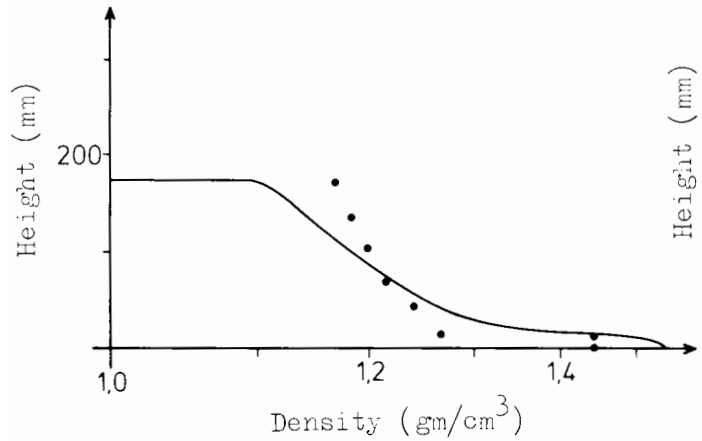
7 hours 45 minutes



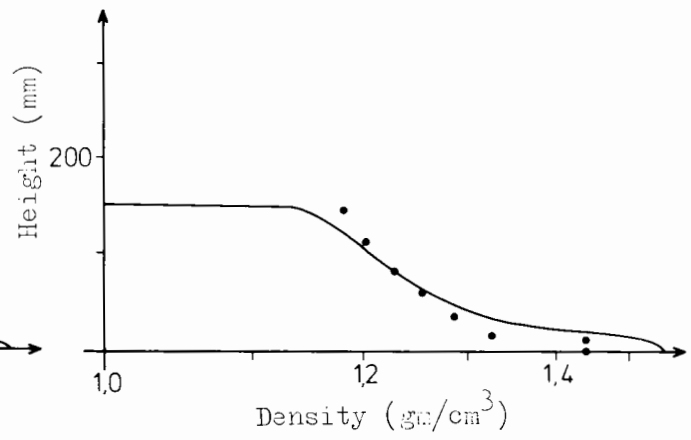
25 hours



52 hours



$96\frac{1}{2}$ hours



170 hours

Fig 7.22. Comparison of Density Profiles.

Experiment 10, Initial Density 1.02 gm/cm^3

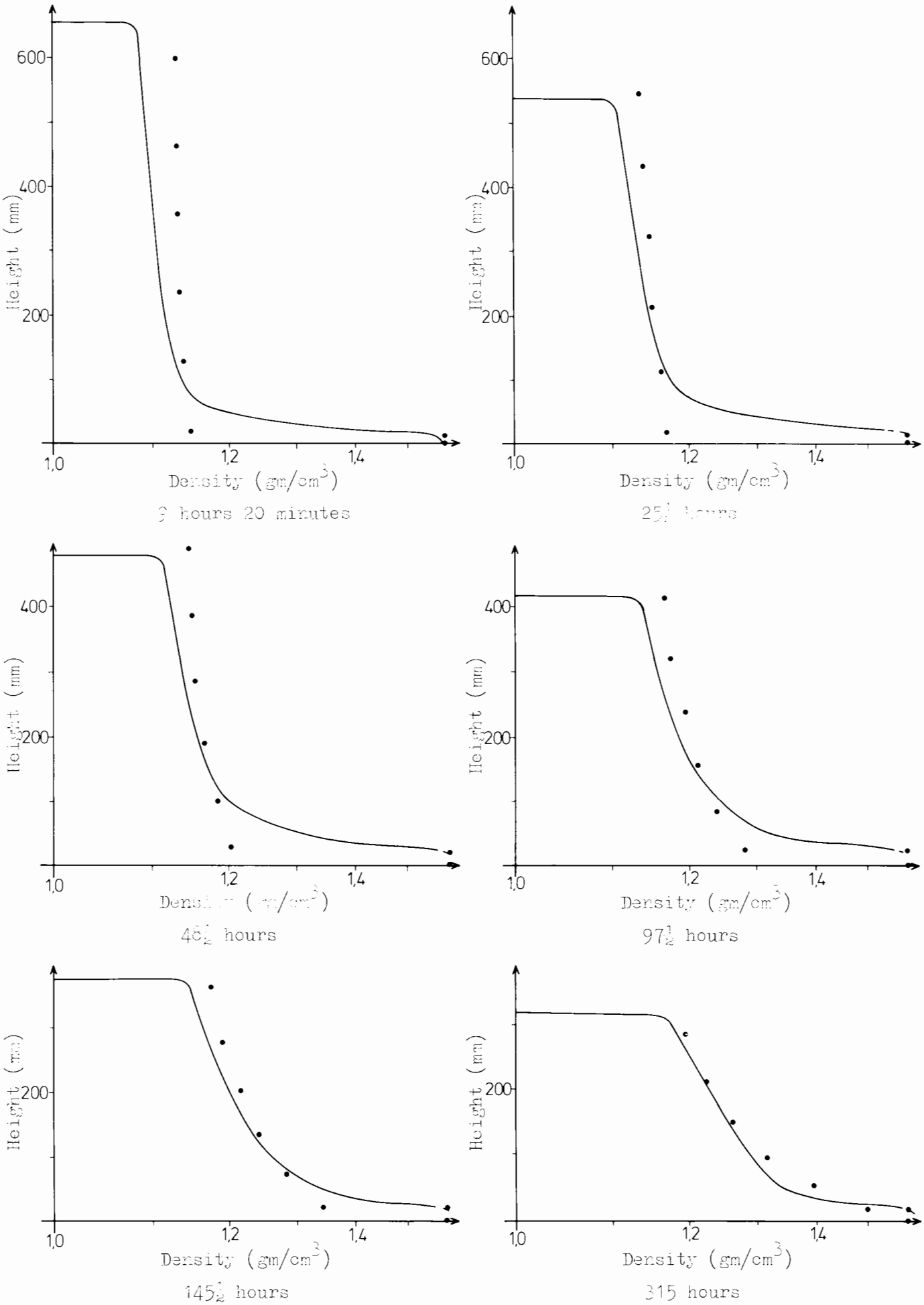


Fig 7.23. Comparison of Density Profiles.
Experiment 11, Initial Density 1.05 gm/cm^3

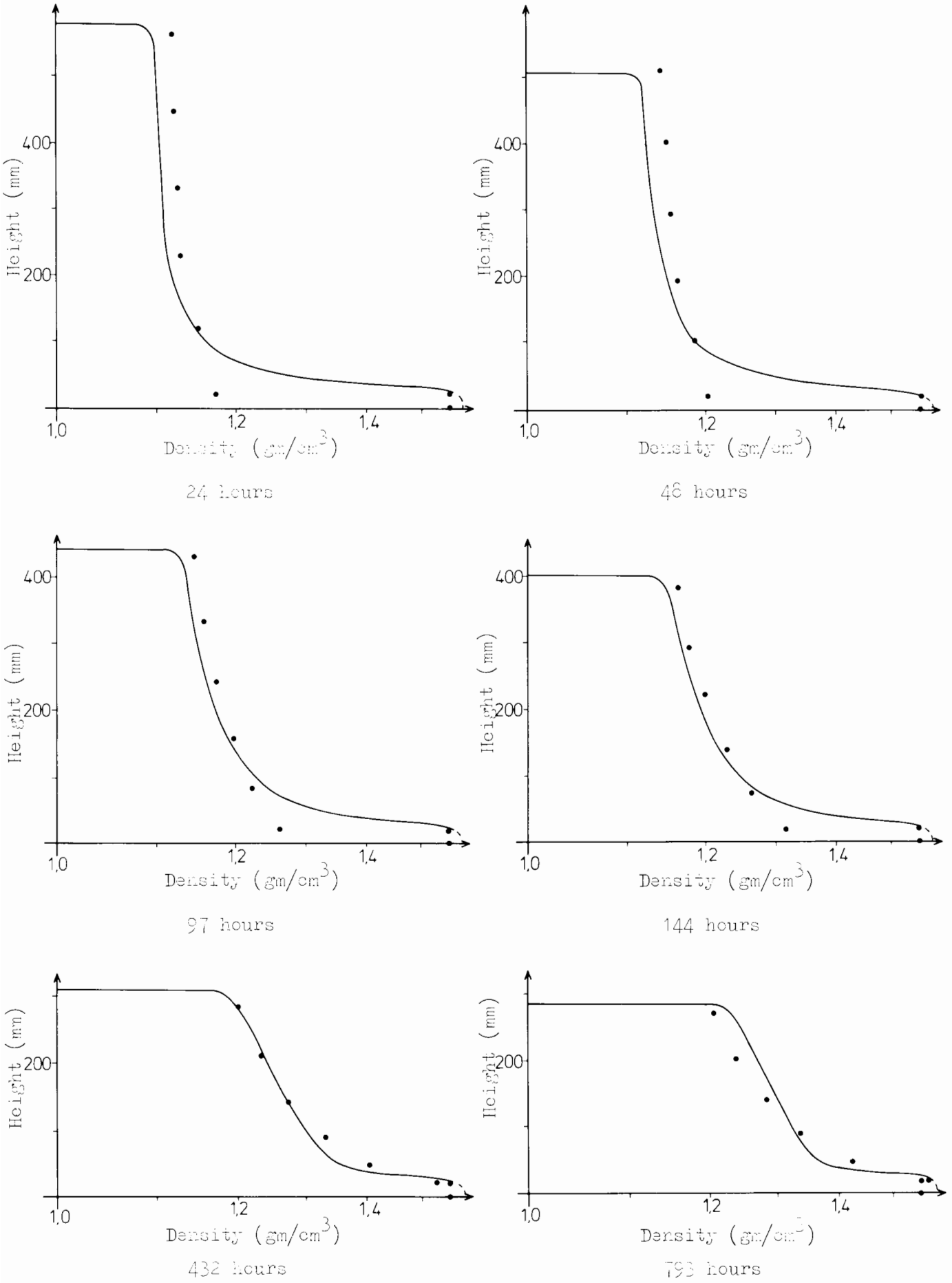
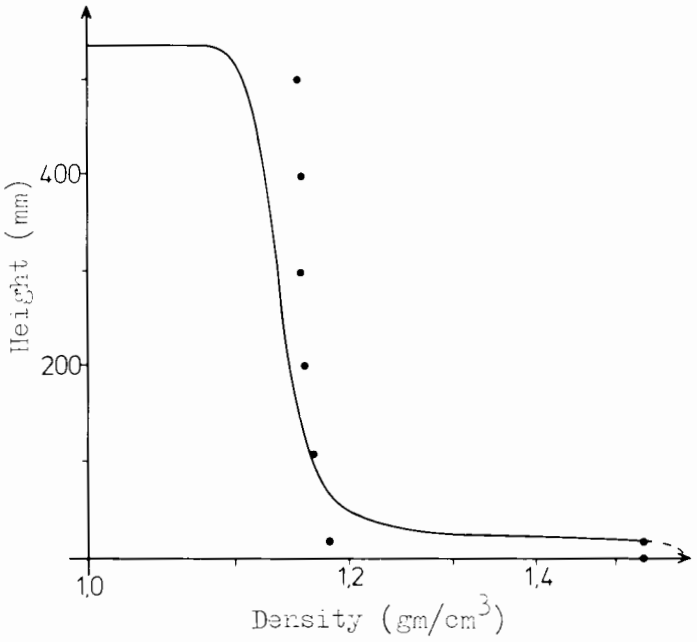
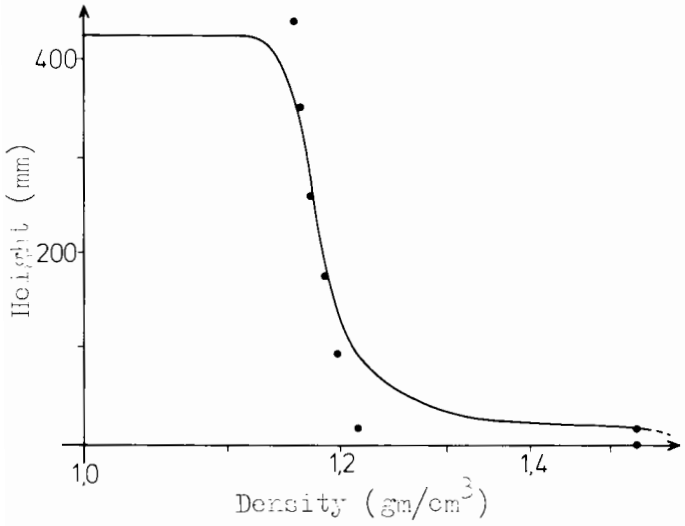


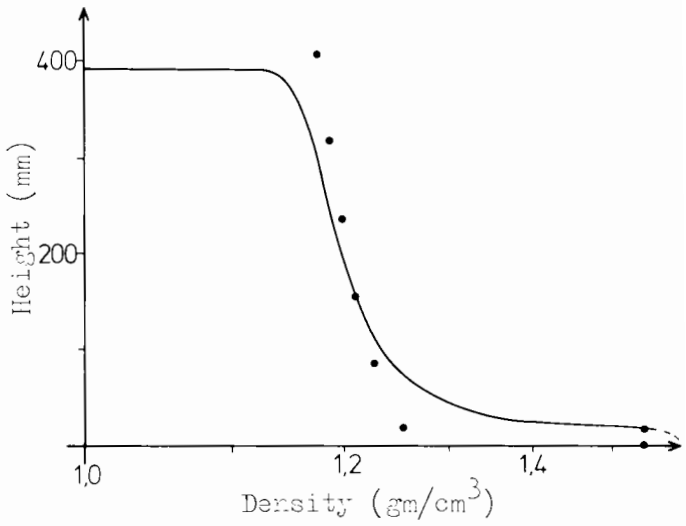
Fig 7.24. Comparison of Density Profiles.
Experiment 12, Initial Density 1.05 gm/cm^3



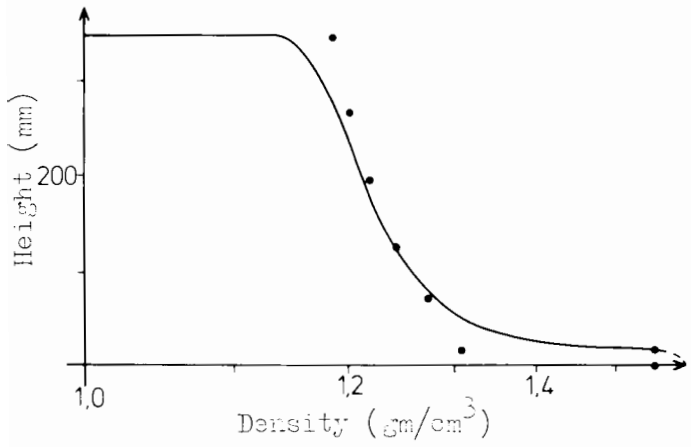
6 hours



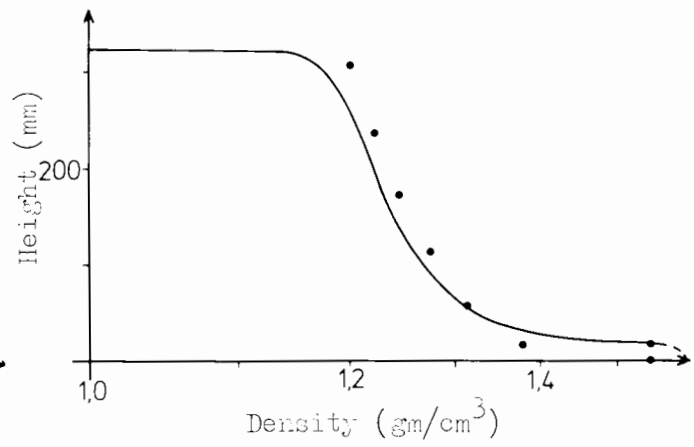
27 hours



48 hours

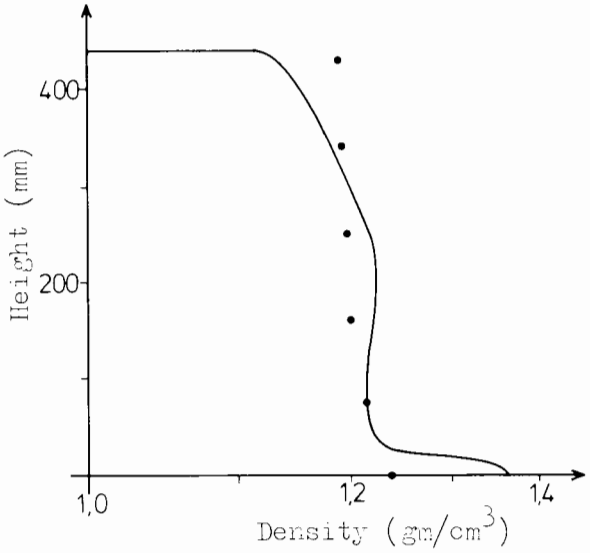


95 hours

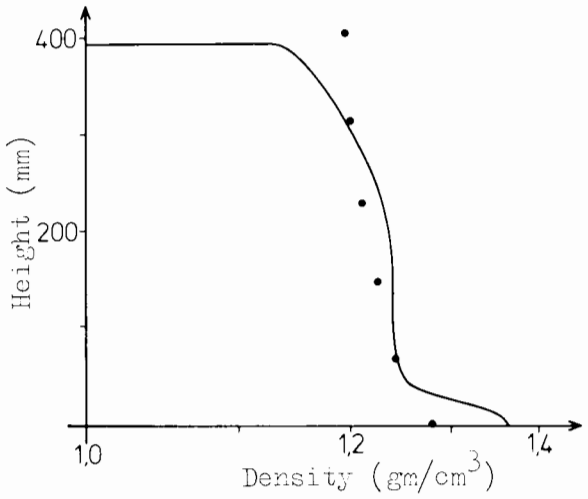


144 hours

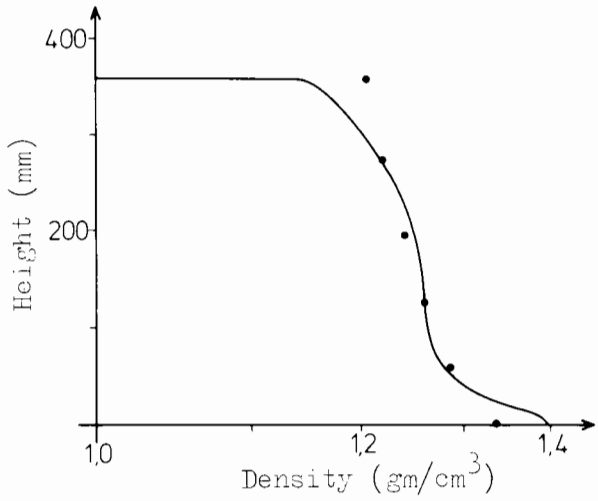
Fig 7.25. Comparison of Density Profiles.
Experiment 13, Initial Density 1.08 gm/cm^3



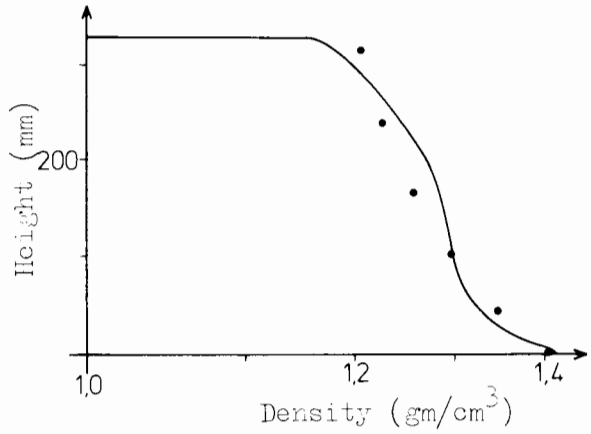
9 hours



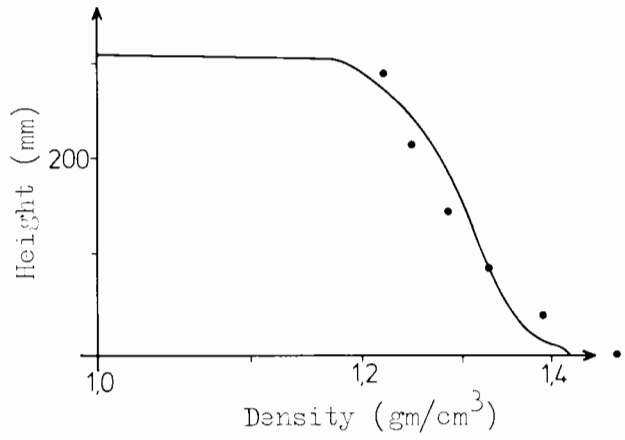
24 hours



48 hours



95 hours



144 hours

Fig 7.23. Comparison of Density Profiles.
Experiment 14, Initial Density 1.11 gm/cm^3

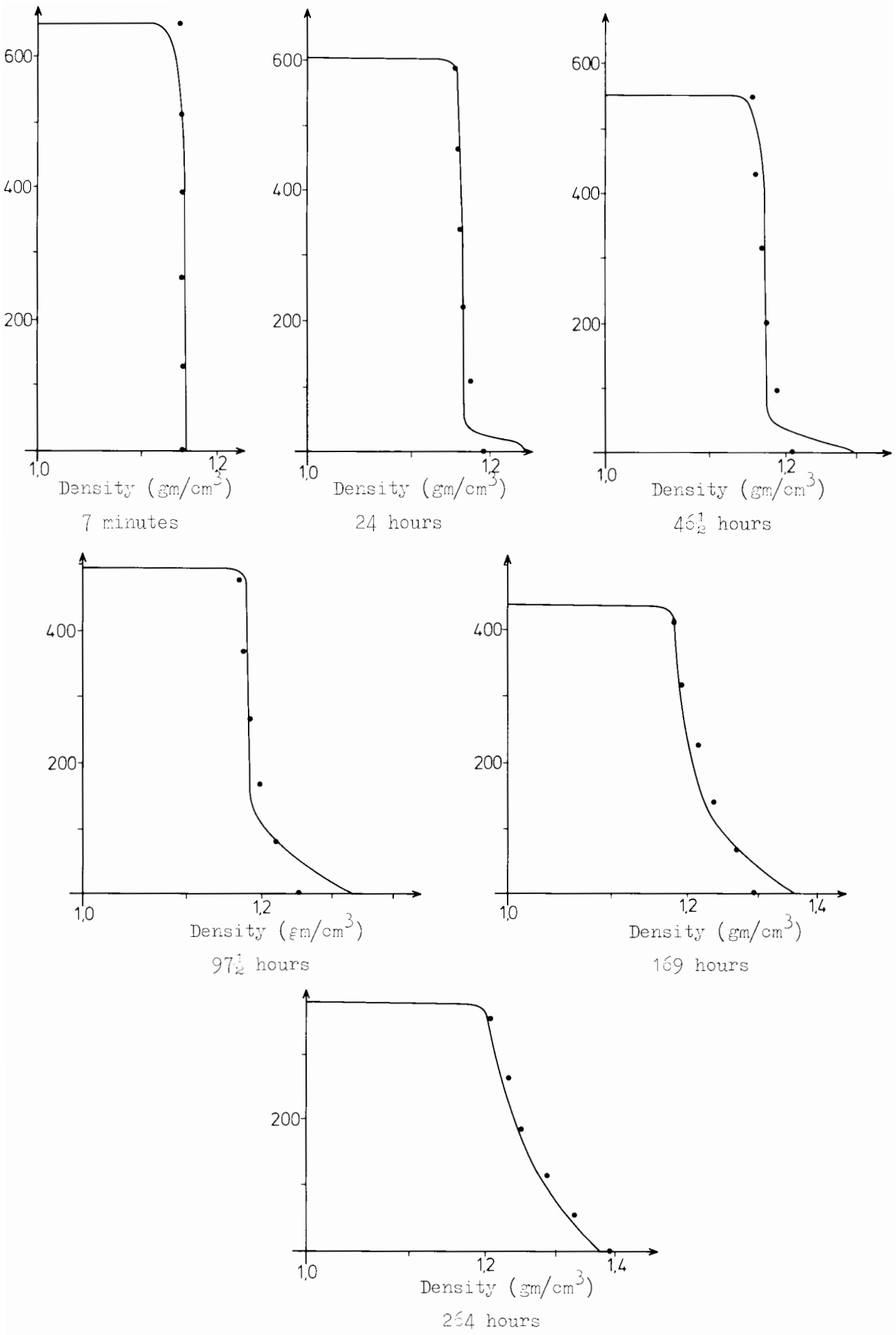


Fig 7.27. Comparison of Density Profiles.
Experiment 15, Initial Density 1.146 gm/cm^3

7.4. DISCUSSION

In deriving the modified consolidation theory and solutions, several simplifications are necessary. Much more sophisticated solutions are possible but not justified by the level of physical understanding of the intermediate phase. Several minor differences between the real behaviour and the theoretical predictions occur and largely reflect these simplifying approximations.

Variation in the coefficient of consolidation between different methods (despite nearly constant values within each method)shows up the major drawback of the modified theory. Proper account is not taken of the non-unique void ratio / effective stress relationship in the intermediate zone, which is clearly important when relating void ratios to pore water pressures during consolidation. Non-linearity of the permeability / void ratio function is also significant. Experimental results suggest a log - linear function would be more appropriate for this particular soil.

A further indication from the compared coefficients of consolidation is that the expulsion of pore fluid (hence also permeability) is the most important process in the intermediate phase and that effective stress and compressibility has a smaller effect. This concept is consistent with qualitative observations of the intermediate phase behaviour.

Despite the obvious faults in the theory, predictions of sedimentation behaviour of the same soil under slightly different

conditions could be made on the basis of this model, provided the correct value of C_f is used. This value can sensibly be constant but will be different for pore pressure predictions and settlement or density predictions. A constant β, or linear void ratio / effective stress function, can also be used within a reasonable range of initial densities.

CHAPTER 8. IN CONCLUSION

8.1 Conclusions 243

8.1.1 Experimental Techniques and Procedures 243

8.1.2 Stages of Soil Sedimentation 243

8.1.3 Theoretical Considerations 246

8.2 Contribution of This Thesis 247

8.3 Application of the Results to Practical Problems 248

8.4 Recommendations for Further Work 249

CHAPTER 8. IN CONCLUSION

8.1. CONCLUSIONS

8.1.1. Experimental Techniques and Procedures

The X-ray density measurement apparatus, combined with appropriate pressure measurements, has proved to be a very powerful tool in this study. Extremely careful preparation and use of the equipment is necessary to produce sufficiently reliable results and has allowed certain aspects of soil behaviour to be studied for the first time.

Although only one specific soil was used throughout, the qualitative results and conclusions of this work should be applicable to a wide range of flocculated soil / water mixtures. Quantitive differences between soils may, however, be large.

8.1.2. Stages of Soil Sedimentation

Both a suspension and an unconsolidated soil may be considered as a soil / water mixture with relative movement between the solid and liquid parts. During sedimentation a transition, or intermediate, phase has been identified.

This intermediate phase is distinguished from a suspension by the presence of effective stresses (or more correctly the pore water

and total pressures differ). Channelling usually occurs at the transition from a suspension to the intermediate phase, indicating the very different behaviour of the two phases. A more subtle difference separates the intermediate phase from a soil. In the intermediate zone there is not a unique void ratio / effective stress relationship as is implied by the virgin consolidation line commonly accepted in soil mechanics.

A stress free soil state, or a zero effective stress void ratio for a soil, is thus an anomaly. Two void ratios are important in describing the soil formation process. Firstly there is the void ratio, e_1, below which an effective stress will always exist. Secondly there is the void ratio, e_2, below which a unique virgin consolidation line exists. It would be convenient to say that a suspension always has a higher void ratio than e_1, the intermediate phase lies strictly between the two values and a soil has a void ratio below e_2. The soil formation process is not this simple.

A slurry deposited at a higher void ratio than e_1 will have no effective stresses initially. Sedimentation rates will be high, particle segregation may occur and the density profiles will have a step as a denser region rises from the base. Kynch's theory may be applied to the suspension above the step. Below the step pore pressures differ from total stresses so that effective stresses exist.

Deposition at a void ratio between e_1 and e_2 results in a slurry, with effective stresses, which does not show density steps, particle segregation or rapid sedimentation. This characterises the

intermediate phase. Similar behaviour occurs in the intermediate phase when it is deposited by sedimentation from a true suspension to when the initial density is intermediate. Any small differences in behaviour after deposition appear to be the result of stress history dependence.

There is not a single effective stress / void ratio curve in the intermediate phase. Consolidation increases the density and with time the intermediate phase slurry will become a soil, with a unique consolidation curve. The void ratio e_2 will occur at the top of such a soil. Although this void ratio is a simple way to distinguish the intermediate phase from a soil, the diagram in figure 8.1 shows how, at earlier times of intermediate phase consolidation, a unique curve may not exist, even below e_2.

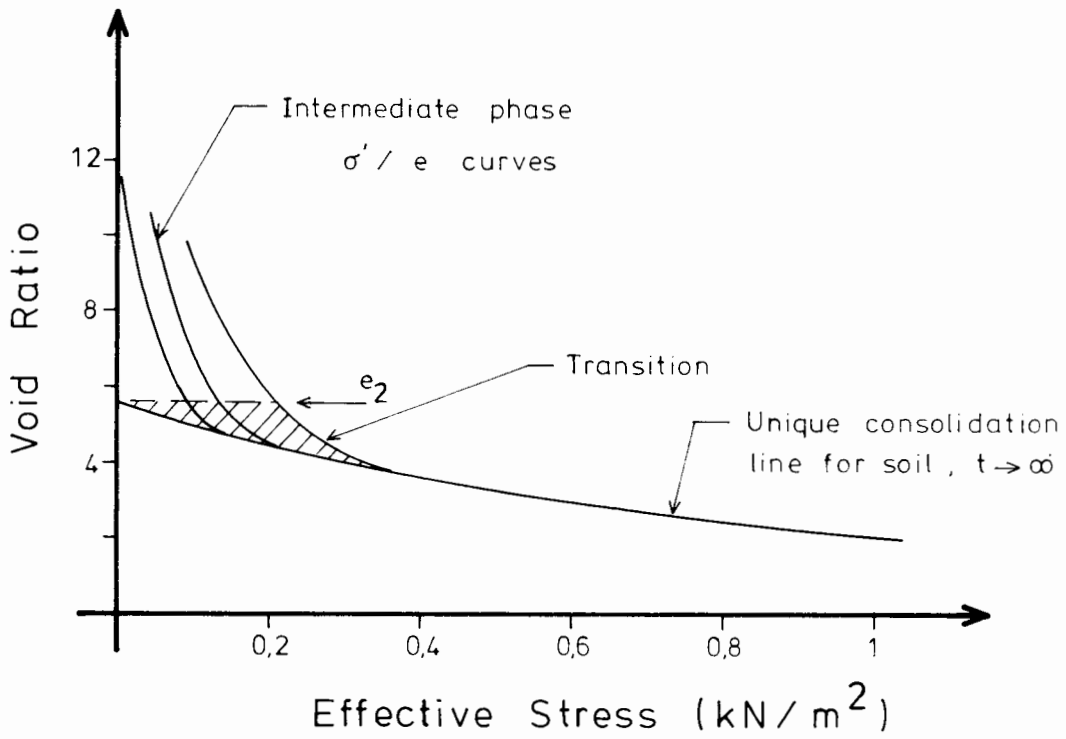


Fig 8.1. The Intermediate Phase and Soil.

A distinction between the intermediate phase and a soil, that does not have this apparent time dependence, may be possible on the basis of shear stresses. If the horizontal and vertical effective stresses are equal, the Mohr's circle of stress for the mud in the column reduces to a point. Thus the shear stress is zero. The present results are not adequate to investigate this, but it could be possible to define the intermediate phase as a soil with no shear strength, rather than using the void ratio / effective stress curve as a criterion.

8.1.3. Theoretical Considerations

Some simple modifications to a large strain soil consolidation theory can be useful in interpreting experimental data from the intermediate phase.

Using an appropriate coefficient of consolidation, C_f, a reasonable agreement between calculated and real settlements and density distributions can be found. A linear permeability / void ratio function is not, however, a good approximation. A log-linear function would be better.

Comparison of C_f values found independently from settlement and pore pressure measurements indicates the basic flaw in the modified theory - an inadequate method of dealing with the void ratio / effective stress relationship in the intermediate phase. The modified consolidation theory is clearly a better description of the intermediate phase the closer it becomes to being a soil in the traditional sense.

Further comparison of C_f values shows that the expulsion of pore fluid and dissipation of excess pore water pressure is much more important than the compressibility of the solid skeleton in the intermediate phase.

8.2. CONTRIBUTION OF THIS THESIS

A significant part of this work is devoted to describing the X-ray density measurement technique that has been developed. It is a valuable tool, giving accurate density measurements faster than has previously been possible. In addition the measurements are non-destructive and are made throughout the sample, rather than at boundaries only.

By identifying the intermediate phase a new insight into sedimentation has been achieved. The principle of effective stress is apparently peculiar to soil mechanics, so that its use in studying dense "suspensions" is a large step from the more traditional sedimentation theory.

For the geotechnical engineer a start has been made at describing what happens during soil formation when the stresses are very small. A better understanding of effective stresses during soil formation could lead to a fuller understanding of subsequent soil behaviour. The revised definition of the zero effective stress point for a soil is a novel concept, although it is probably not important on a practical engineering level where much higher stresses are involved. The application of a self weight consolidation theory to

experimental results is also an innovation in that analytic solutions to large strain theories have not previously been available.

A large gap exists between the philosophy of the soil engineer, the sedimentologist and the chemical engineer in dealing with similar materials (i.e. flocculated solid/water mixtures). The present work is a step towards narrowing this gap.

8.3 APPLICATION OF THE RESULTS TO PRACTICAL PROBLEMS

Using the results of the previous chapter with a suitable experimental program, one could estimate the state of the seabed after a period of sedimentation. Particularly important would be the stiffness and strength of the upper layers of the bed. If they are strong enough to resist erosion at the maximum water velocities, a stable seabed will have been formed. On the other hand erosion may disperse the upper seabed into suspension once more. Either way it would be helpful to know which was more likely to occur in certain areas when considering dredging, pollution and navigation.

Knowing the settlements and strength of hydraulic spoil material would be essential in planning the use of such spoil areas at a later date. From the point of view of pollution studies it might be necessary to know the settlement times and details of water movement through recent mud deposits.

The present study has been purely a laboratory study and there

is still much to be done in relating the results and principles to field behaviour of soils. Some suggestions are put forward in the next section.

8.4. RECOMMENDATIONS FOR FURTHER WORK

The next step in this study should be to examine the effect of different environmental conditions, such as salinity and temperature variations, on one-dimensional settling. A wider variety of natural soils should also be used to broaden the scope of the work.

A method of continuous introduction of soil into a settling column should be developed. In nature sedimentation is often a relatively slow, continuous process so that the present system of starting a test is not entirely satisfactory for some applications. Figure 8.2 shows a possible device for achieving a constant rate of introduction. A similar system (simpler, but unsatisfactory for the present application) is mentioned by Einsele et al. (1974).

A header tank is used so that the slurry is fed into the column under a constant head through a fixed pipe. A servo-system controls the level in the reservoir to maintain a constant head in the header tank. It may be possible to use a single tank with the slurry level held constant, but there would be two problems to overcome. Firstly the feed line to the column would be moving as the tank is moved to maintain the head. This may affect the flow. Secondly, there would be the practical problem of supporting a sufficiently

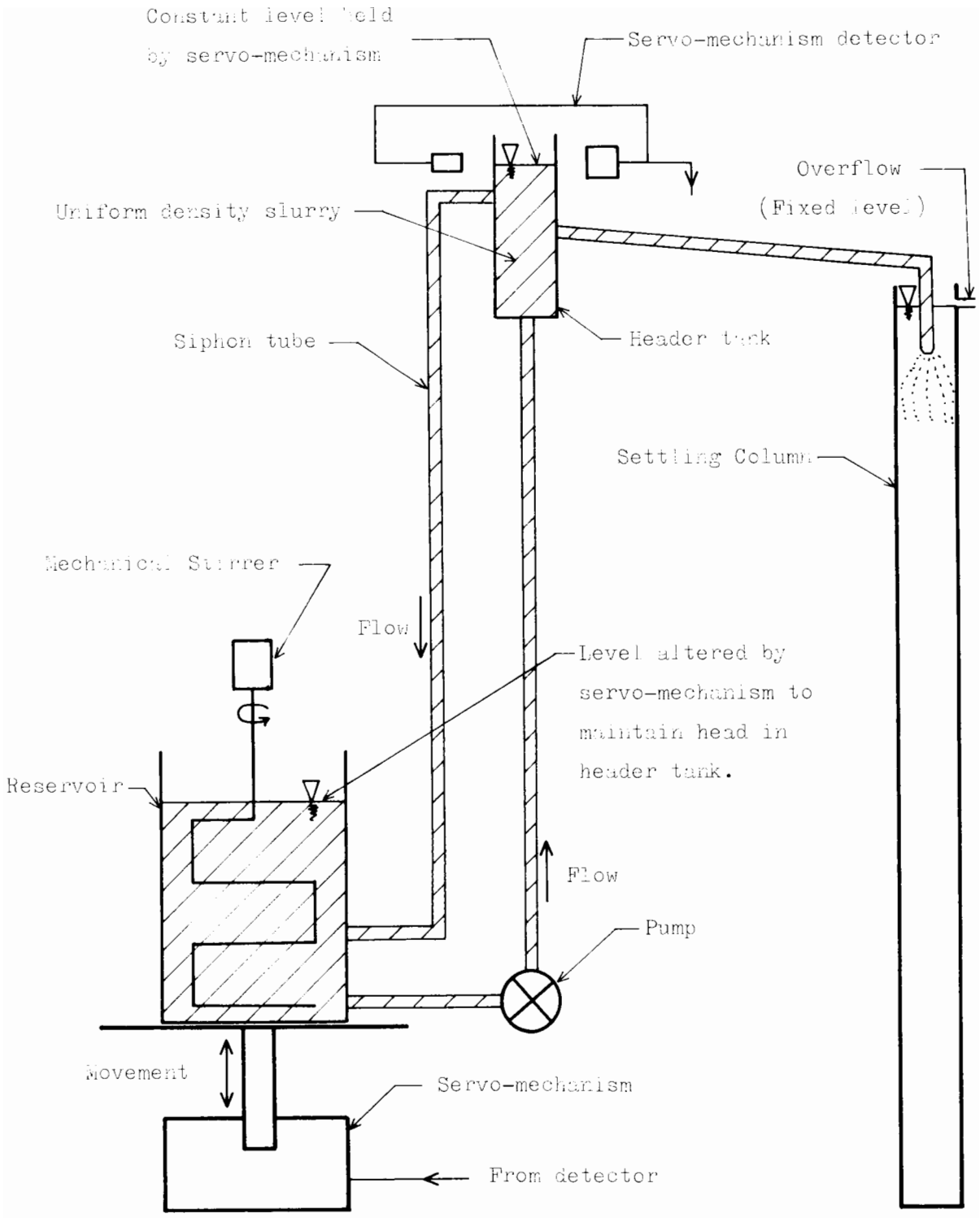


Fig 8.2. Constant Rate of Sedimentation Device.

large reservoir tank and servo-mechanism at a height of 2 metres. Another method may be to apply a servo-controlled pressure head to a reservoir tank at ground level.

A rather more difficult extension should be to remove the restriction to one dimension so that account may be taken of real lateral phenomena like currents and salinity, temperature or density gradients. Tests in a flume are a possibility.

Shear strengths are widely used in field surveys. Thus an extensive program of shear strength measurements in the laboratory tests should be done to correlate laboratory and field data. Direct shear strength measurements of soft soils using a vane or similar device may present difficulties. Shear strengths are very low and a sensitive instrument is necessary. Thixotropy and pore water viscosity may also be significant factors. Determination of shear stresses by comparison of vertical and horizontal effective stresses could be carried out, but this would not necessarily give a good measure of shear strength.

There is still much scope for development of numerical and analytic solutions to the governing equations for soil consolidation. More representative approximations to the soil properties in the intermediate phase (or soils at low stresses and high void ratios) should be used. Lee (1979) has found solutions when the soil stratum thickness is increasing due to sedimentation, which could be modified to include intermediate phase behaviour and thus model the experimental conditions more accurately. This can only be achieved at the expense of simplicity of the mathematics, and care should be taken that the theoretical

development does not outstrip the more important aspects of measurement and understanding of the real physical behaviour of soils.

REFERENCES

Bishop A.W. and Vaughan P.R. (1972)

'Consolidation of a Fine Grained Dredged Material after Hydraulic Deposition.' Report to National Ports Council, Imperial College of Science and Technology, London. August.

Coumoulos D.G. (1967)

'A Radiographic Study of Soils.' Ph.D. Thesis, Cambridge University.

De Wit C.T. and Arens P.L. (1950)

'Moisture Content and Density of Some Clay Minerals and Some Remarks on the Hydration Pattern of Clay.' Trans. 4th Int. Congress of Soil Science, 2, 59 - 62.

Einsele G., Overbeck R., Schwarz H.U. and Unsöld G. (1974)

'Mass Physical Properties, Sliding and Erodibility of Experimentally Deposited and Differently Consolidated Clayey Muds.' Sedimentology, 21, 339 - 372.

EMI Electronics

Photomultiplier Catalogue, P001/fP70. EMI Electronics.

Fitch B. (1966)

'A Mechanism of Sedimentation.' Industrial and Engineering Chemistry Fundamentals, 5, 129.

Gibson R.E., England G.L. and Hussey M.J.L. (1967)
'The Theory of One-Dimensional Consolidation of Saturated Clays. 1. Finite Non-Linear Consolidation of Thin Homogeneous Layers.' Geotechnique, 17, 261 - 273.

Halmshaw R. (1966)
'Physics of Industrial Radiology.' Heywood.

Iredale P. (1961)
'Non-Proportional Response of NaI(Tl) Crystals to Gamma-rays.' Nuclear Instruments and Methods, 11, 336.

Kirby R. and Parker W.R. (1977)
'The Physical Characteristics and Environmental Significance of Fine Sediment Suspensions in Estuaries.' National Academy of Sciences, Washington D.C. Symposium on Estuaries, Geophysics and the Environment. Paper 11.

Kohl J., Zentner R.D. and Lukens H.R. (1961)
'Radioisotope Applications Engineering.' Van Nostrand.

Krinitsky E.L. (1972)
'X-ray Measurement of Soil Densities in Models.' U.S. Army Waterways Experiment Station, Paper S - 72 - 1, January.

Kynch G.J. (1952)
'A Theory of Sedimentation.' Trans. of the Faraday Society, 48, 166 - 176.

Lee K. (1979)

'An Analytical and Experimental Study of Large Strain Soil Consolidation.' D. Phil. Thesis, Oxford University.

McRoberts E.C. and Nixon J.F. (1976)

'A Theory of Soil Sedimentation.' Canadian Geotechnical Journal, 13, 294.

Makower B., Shaw T.M. and Alexander L.T. (1937)

'The Specific Surface and Density of Some Soils and Their Colloids.' Soil Science Society of America Proceedings, 2, 101 - 109.

Maus L.D., Rose V.C. and Nacci V.A. (1973)

'Gamma-ray Monitoring of Sediment Consolidation Tests.' Ocean Engineering, 2, 195 - 205. Pergamon Press.

Michaels A.S. and Bolger J.C. (1962)

'Settling Rates and Sedimentation Volumes of Flocculated Kaolin Suspensions.' Industrial and Engineering Chemistry Fundamentals, 1, 24 - 33. February.

Monte J.L. and Krizek R.J. (1976)

'One-Dimensional Mathematical Model for Large Strain Consolidation.' Geotechnique, 26, 495 - 510.

O'Loughlin M.W.B. (1964)

'Radiological Examination of Granular Materials.' Ph.D. Thesis, Cambridge University.

Owen M.W. (1970)

'Properties of a Consolidating Mud.' Hydraulics Research Station, Wallingford, England, Int 83, December.

Parker W.R. and Kirby R. (1977)

'Fine Sediment Studies Relevant to Dredging Practice and Control.' 2nd Int. Symp. on Dredging Technology, BHRA Fluid Engineering / Texas A & M University. Paper B2, pp 15 - 26.

Parker W.R., Sills G.C. and Paske R.E.A. (1975)

'In Situ Nuclear Density Measurements in Dredging Practice and Control.' 1st Int. Symp. on Dredging Technology, Kent, England.

Preiss K. (1968)

'Non Destructive Laboratory Measurement of Marine Sediment Density in a Core Barrel using Gamma Radiation.' Deep Sea Research, 15, 401 - 407.

Pringle R.W. (1950)

'The Scintillation Counter.' Nature, 166, 4209. July.

Rockley J.C. (1964)

'An Introduction to Industrial Radiology.' Butterworths.

Roscoe K.H., Arthur J.R.F. and James R.G. (1963)

'Strains in Soils by an X-ray Method.' Civil Engineering and Public Works Review, 873 - 876 & 1009 - 1012, July & Aug.

Richardson J.F. and Zaki W.N. (1954)

'Sedimentation and Fluidisation.' Trans. Institution of Chemical Engineers, 32, 35 - 53.

Sharpe J. (1964)

'Nuclear Radiation Detectors.' Methuen.

Sirwan K.Z. (1964)

'Deformation of Soil Specimens.' Ph.D. Thesis, Cambridge University.

Skempton A.W. (1970)

'The Consolidation of Clays by Gravitational Compaction.' Quarterly Journal of the Geological Society London, 125, 373 - 411.

Tory E.M. and Shannon P.T. (1965)

'Reappraisal of the Concept of Settling in Compression.' Industrial and Engineering Chemistry Fundamentals, 4, 194 - 203.